Modeling, Analysis, and Optimization of Random Wireless Networks: Stochastic Geometry Approach

by

Hesham Mahmoud Medhat Mahmoud Elsawy

A Thesis submitted to The Faculty of Graduate Studies of

The University of Manitoba

in partial fulfillment of the requirements for the degree of

Doctor of Philosophy

Department of Electrical and Computer Engineering

University of Manitoba

Winnipeg

February 2014

Abstract

Recently, stochastic geometry has been shown to be a very powerful tool to model, analyze, and design networks with random topologies such as wireless ad hoc and sensor networks as well as multi-tier cellular networks. In stochastic geometry analysis, point processes are used to model the positions and the channel access behaviors of the nodes. The thesis develops analytical frameworks to characterize the performance of large-scale wireless networks with random topologies. In particular, I use stochastic geometry tools to model, analyze, and design ad hoc networks, star-connected sensor networks, and infrastructure-based two-tier cellular networks. I have optimized the tradeoff between outage probability and spatial frequency reuse efficiency in carrier-sensing-multiple-access based ad hoc networks. I have developed a novel spectrum-efficient design paradigm for star-connected wireless sensor networks. For downlink transmission in cellular networks with cognitive femto access points (FAPs), I have quantified the performance gain imposed by cognition and developed a paradigm to optimize the spectrum sensing threshold for cognitive FAPs. Finally, I have developed a novel modeling paradigm for uplink transmission in cellular networks and obtained simple expressions for network performance metrics including the outage probability and average rate. Furthermore, I have revealed a transition point in the behavior of uplink transmission in cellular networks that depends on the relative values of the network parameters.

Acknowledgements

After thanking Almighty "ALLAH" for his blessing and guidance to complete this work, I would like to thank my advisor Prof. Ekram Hossain for the amazing opportunity he provided me with. His flexibility, dedication, and encouragement have pushed me far beyond my expectations.

I would like to thank my committee members and examiners, Prof. Pradeepa Yahampath, Prof. Pourang Irani, and Prof. Mohamed-Slim Alouini. I would like to express my gratitude to Prof. Attahiru Alfa for his interesting discussions and sincere advice. I acknowledge the financial support from NSERC and TRTech. I would like to thank the staff at the Department of Electrical and Computer Engineering. Special thanks to Amy Dario for her kind help. I thank all my group members and lab colleagues, specially Ahmed Sakr, it was fun working with all of you.

I would like to acknowledge the three most impactful persons in my life, my parents and my wife. Starting from my mother, I don't know what to say, I would have never been in this position without your love, care, and support. My father, you have always been my mentor, you trained me well for the struggle of life. My sincere, beautiful, supporting, and loving wife, without you, nothing is complete.

Finally, I would like to acknowledge a lot of sincere and loving people, I have been blessed with, that have strongly contributed to this success. Starting with my brother Mostafa ElSawy, for taking care of everything back home on my behalf, my father and mother in law, what can I say to express my gratitude to you, and my little son and daughter, you added a great value for everything.

Table of Contents

List of Figures

List of Tables

List of Abbreviations

AP	Access point
BCU	Body control unit
BI	Beacon interval
BO	Superframe order
BPP	Binomial point process
BS	Base station
CAP	Contention access period
Ch	Chapter
CF	Characteristic function
CFP	Contention free period
cdf	Cumulative distribution function
CDMA	Code division multiple access
CHCPP	Classical hard core point process (Matérn HCPP type II)
cmf	Cumulative mass function
CN	Coordinator node
CSMA	Carrier sense multiple access
ED	Energy detection
FAP	Femto-access point
FDMA	Frequency division multiple access

FT	Fourier Transform
GTS	Guaranteed time slot
HCPP	Hard core point process
i.i.d.	Independent and identically distributed
ISM	Industrial scientific and medical
KPI	Key performance indicator
LT	Laplace transform
MAC	Medium access control
MBS	Macro base station
MGF	Moment generation function
MHCPP	Modified Hard core point process
OFDMA	Orthogonal frequency division multiple access
PCP	Poisson cluster process
pdf	Probability density function
pmf	Probability mass function
PPP	Poisson point process
SCN	Star-connected network
SD	Superframe duration
SINR	Signal to interference plus noise ratio
SIR	Signal to interference ratio
SN	Slave node
SNR	Signal to noise ratio
SO	Superframe order
SON	Self-organizing networks
SSR	Spectrum sensing region

TDMA	Time division multiple access
UE	User Equipment
WLAN	Wireless local area network
WPAN	Wireless personal area network
w.r.t.	With respect to

List of Symbols

$\mathbb{1}\{.\}$	The indicator function
A	Frequency dependent propagation constant
$\mathcal{A}$	Intensity of femto-access points
$\mathcal{B}$	Intensity of BSs in a cellular network
$\mathbf{B}_x(r)$	Set of points bounded by the disc centered at x and having a radius r
BO	Beacon order
C	Link capacity
$\mathbb{E}_X[.]$	Expectation with respect to the random variable X
$\mathcal{G}(m)$	Coexistence gain offered by the m^{th} channel
$f_X(.)$	*pdf* of the random variable X
$F_X(.)$	*cdf* of the random variable X
$G\{V, E\}$	Graph constituted by the set of vertices V and the set of edges E
$h(x, y)$	The random channel power gain between the two location x and y
h	Random variable representing the channel power gain
$\mathcal{I}$	Aggregate interference
K_f	Number of free channels
K_u	Number of used channels
$L(.)$	The Lebesgue measure

$\mathcal{L}_X(.)$	The Laplace transform of the *pdf* of the random variable X
$\mathbf{N}_x$	Set containing the neighbors of a node located at x
$\mathcal{N}(v_s)$	Mean number of CNs in the contention domain
$\mathcal{O}$	Outage probability
$\mathbb{P}\{.\}$	The probability of the event (.)
$P(x, y)$	The power received at y from the transmitter located at x
$\mathcal{P}_{ac}(v_s, m)$	Spectrum access probability in an m channel scenario for a given γ
P_a	Transmit power of a femto-access point
P_b	Transmit power of a base station
P_t	Transmit power of a generic transmitter
P_u	Transmit power of a user
$\mathcal{R}$	Average rate
$\mathbb{R}$	The set of all real numbers
$\mathbf{S}$	Set of available channels
SO	Superframe order
$\mathcal{T}$	Transmission capacity
$\mathcal{U}$	Intensity of Users
$\mathbb{Z}^+$	The set of all positive integers
Δ	Degree of a vertex
$\Gamma(.)$	The gamma function
$\Gamma(s, x)$	The upper incomplete gamma function defined as $\Gamma(s, x) = \int_x^\infty t^{s-1}e^{-1}dt$
$\mathbf{\Psi}$	A point process (usually PPP)
β	SINR threshold defined for correct reception
δ	Data rate requirement for the supported application
η	Path-loss exponent

$\gamma(s,x)$	The lower incomplete gamma function defined as $\gamma(s,x) = \int_0^x t^{s-1}e^{-1}dt$
λ_T	Intensity of transmitters
ψ	Self-admission failure probability threshold
μ^{-1}	Mean channel gain
σ^2	Noise variance
υ_s	Spectrum sensing threshold
ξ_a	The probability that a generic user us served be a femto-access point
ξ_b	The probability that a generic user us served be a base station
$\|.\|$	Euclidean norm
$\|.\|$	Set cardinality
$\forall$	for all
$\exists$	There exist

Publications

- Journal Publications:

1. **H. ElSawy** and E. Hossain, "Analytical modeling of mode selection and power control for underlay D2D communication in cellular networks" submitted to the *IEEE Transactions on Communications*.
2. **H. ElSawy** and E. Hossain, "A tractable uplink modeling paradigm for single and multi-tier multi-channel cellular wireless networks" to be submitted to *IEEE Transactions on Wireless Communications*.
3. **H. ElSawy**, E. Hossain, and S. Camorlinga, "Spectrum-efficient multi-channel design for coexisting IEEE 802.15.4 networks: A stochastic geometry approach," *IEEE Transactions on Mobile Computing*, to appear.
4. **H. ElSawy** and E. Hossain, "Two-tier HetNets with cognitive femtocells: Downlink performance modeling and analysis in a multi-channel environment," *IEEE Transactions on Mobile Computing*, vol.13, no.3, pp.649–663, March 2014.
5. **H. ElSawy**, E. Hossain, and M. Haenggi, "Stochastic geometry for modeling, analysis, and design of multi-tier and cognitive cellular wireless networks: A survey," *IEEE Communication Surveys and Tutorials*, vol. 15,

pp. 996–1019, July 2013..

6. **H. ElSawy** and E. Hossain, "A modified hard core point process for analysis of random CSMA wireless networks in general fading environments," *IEEE Transactions on Communications*, vol. 61, no. 4, pp.1520–1534, April 2013.

7. **H. ElSawy**, E. Hossain, and D. I. Kim, "HetNets with cognitive small cells: User offloading and resource allocation techniques," *IEEE Communications Magazine Special Issue on "Heterogeneous and Small Cell Networks (HetSNets)"*, vol. 51, no. 6, June 2013.

- Conference Publications:

1. **H. ElSawy** and E. Hossain, "Analysis of uplink transmissions in cellular networks: A stochastic geometry approach" to be presented in Proc. of *IEEE Int. Conf. on Communications (ICC 2014)*, Sydney, Australia, 10-14 June 2014.

2. **H. ElSawy** and E. Hossain, "Channel assignment and opportunistic spectrum access in two-tier cellular networks with cognitive small cells" in Proc. of *IEEE Global Communications Conference (Globecom 2013)*, Atlanta, GA, December 2013.

3. **H. ElSawy** and E. Hossain, "On cognitive small cells in two-tier heterogeneous networks," in the 9*th int. Workshop on Spatial Stochastic Models for Wireless Networks (SpaSWiN 2013)*, in conjunction with *11th Intl. Symposium on Modeling and Optimization in Mobile, Ad Hoc, and Wireless Networks (WiOpt 2013)*, Tsukuba Science City, Japan, May 13-17, 2013.

4. **H. ElSawy**, E. Hossain, and S. Camorlinga, "Multi-channel design for random CSMA wireless networks: Stochastic geometry approach," in Proc. of *IEEE Int. Conf. on Communications (ICC'13)*, Budapest, Hungary, 9-13 June, 2013.

5. **H. ElSawy**, E. Hossain, and S. Camorlinga, "Traffic offloading techniques in two-tier femtocell networks," in Proc. of *IEEE Int. Conf. on Communications (ICC'13)*, Budapest, Hungary, 9-13 June, 2013.

6. **H. ElSawy** and E. Hossain, "Modeling random CSMA wireless networks in general fading environments," in Proc. of *IEEE Int. Conf. on Communications (ICC 2012)*, Ottawa, Canada, 10-15 June 2012.

7. **H. ElSawy**, E. Hossain, and S. Camorlinga, "Characterizing random CSMA wireless networks: A stochastic geometry approach," in Proc. of *IEEE Int. Conf. on Communications (ICC 2012)*, Ottawa, Canada, 10-15 June 2012.

8. **H. ElSawy**, E. Hossain, and S. Camorlinga, "A distributed spectrum sharing method for improving coexistence of IEEE 802.15.4 networks," in Proc. of *IEEE Global Communications Conference (Globecom 2011)*, 5-9 December, Houston, TX, USA, 2011.

Chapter 1

Introduction

1.1 Introduction

A basic wireless communication system consists of a transmitter (source of information), receiver (destination), and a communication channel. The transmitter modulates an electromagnetic carrier signal based on the information and sends the modulated carrier signal through the propagation medium. In case of free space propagation (i.e., with no obstacle between the transmitter and the receiver), the power of the electromagnetic signal[1] decays with the propagation distance according to the power law $r^{-\eta}$, where r is the distance between the transmitter and receiver and η is the path-loss exponent. Note that for correct data recovery from the carrier, the signal power received at the receiver should exceed the thermal noise power with a certain threshold. That is, the signal-to-noise power ratio (SNR) should be greater than a certain threshold defined for correct information recovery. Therefore, the transmitter is required to transmit the signal with a sufficient power to compensate for the path-loss attenuation such that the signal power is received at the receiver with

[1]For brevity, electromagnetic signal is denoted hereafter as signal.

the required SNR. Hence, the transmit power is an important design parameter in wireless communication.

In wireless communications, the available spectrum is divided into frequency channels. Each frequency channel is specified by two parameters, the centre frequency and the bandwidth. Non-overlapping frequency channels represent independent communication links. That is, if different transmitters transmit their data over non-overlapping channels, the data transmitted from each transmitter can be recovered at its intended receiver if the SNR threshold is satisfied. Therefore, the higher the number of channels, the higher the number of independent wireless communication links that can be established. The data rate (also referred to as link capacity) is given by Shannon's formula as follows:

$$C = W \log_2(1 + \text{SNR}) \quad \text{bits/sec} \tag{1.1}$$

where W is the bandwidth of a channel. Shannon's formula shows the relationship between the bandwidth, the SNR and maximum data rate supported by each channel.

Shannon's formula defines an important tradeoff, namely, tradeoff between the number of channels and the data rate supported on each channel. To accommodate the increasing number of wireless devices and technologies, the tradeoff between the number of channels and the channel bandwidth should be designed carefully and the channels should be shared and reused by multiple wireless links. In that case, if multiple signals from more than one transmitter are transmitted on the same channel, the signals interfere with each other which may lead to the loss of all of the transmitted data. From a receiver's perspective, if multiple signals are received on the same channel, the data from the signal with dominating power can be recovered. That is, on a channel shared by several signals, only one signal can be recovered at a

given receiver if that signal power is sufficiently greater than the interfering signals powers plus the thermal noise power. In other words, a receiver can recover the data transmitted from its intended transmitter on a shared wireless channel if the received signal-to-interference-plus-noise (SINR) ratio is above the threshold defined for correct signal recovery. Wireless networks where multiple links sharing the same frequency spectrum are called multi-access networks. For a multi-access network, when the interference is treated as noise, the Shannon's formula for a generic link can be written as

$$C = W \log_2(1 + \text{SINR}) \quad \text{bits/sec.} \tag{1.2}$$

In a wireless system with a single link, the required signal-to-noise ratio (SNR) can be maintained through a proper transmission power to compensate for the signal attenuation with distance. In a shared spectrum scenario, increasing the power of all transmitters increases the desired signal level as well as the interference level, which may degrade the SINR, and hence link capacity. Therefore, in a multi-access network, the SINR cannot be maintained above the required threshold by simply increasing the transmission powers of the coexisting transmitters. Instead, a design paradigm that accounts for the network characteristics can be developed to balance the tradeoffs among the different network parameter and achieve the required SINR performance. In the next two subsections, I discuss two fundamental network parameters that highly affect the SINR.

1.1.1 Network Geometry

The first network parameter that highly affects the SINR is the network geometry. In wireless communications systems, the transmitter-receiver pairs (i.e., network nodes) are distributed over the spatial domain. The pattern formed by the network nodes

over the spatial domain is called the network geometry (also denoted as network topology). That is, the network geometry defines the positions of the network nodes with respect to (w.r.t.) each other. The network geometry is highly affected by the network characteristics such as the network type, application, and infrastructure. For instance, sensor networks often have a random network topology. On the other hand, cellular networks with base stations carefully planned and deployed by a service provider often have a regular network topology.

In a wireless network where multiple links share the same radio spectrum, the SINR at any receiver is a function of the locations of the transmitting nodes (i.e., network geometry) and the transmit powers of the transmitters using the same channel. Therefore, the network geometry has a fundamental impact on the performance of wireless networks. Note that, although the rapid signal power attenuation with the distance is a limiting factor for any communication link, it also creates more opportunities to reuse the spectrum by other communication links over the spatial domain.

1.1.2 Medium Access Control

In a wireless network, the locations of the simultaneously active (interfering) nodes can be controlled and manipulated via network design parameters (e.g., those related to medium access control techniques, frequency planning, cognition[2] and coordination techniques). Therefore, in a multi-access network, it is very important to coordinate the access of the transmitters to the shared wireless spectrum in order to maintain sufficient SINRs at the network receivers. The medium access is coordinated via a

[2]A cognitive network node is an intelligent transmitter which is able to monitor the spectrum, identify spectrum access opportunities, learn from its past experience, and adapt its parameters to opportunistically access the spectrum without harming other network receivers.

medium access control (MAC) protocol. The main function of the MAC protocol is to select the links that can simultaneously share the same channel. A MAC protocol can select relatively dispersed links in the spatial domain to share the same channel in order to maintain a sufficient SINR at each link. Another important objective of the MAC protocol is to ensure fair access of all links to the shared wireless spectrum. That is, each transmitter having data to transmit should have a guaranteed access to the shared spectrum at some point in time. Depending on the network type and application, the MAC protocol can be implemented via a centralized or distributed scheme. A centralized MAC protocol has a coordinator entity that controls the spectrum access of all the network nodes. On the other hand, in a distributed MAC protocol, the network nodes contend for the spectrum access or coordinate with each other (e.g., through message passing) for spectrum access.

1.1.3 Key Performance Indicators (KPIs)

SINR is one of the main performance metrics in multiple-access wireless networks. Many KPIs are related to the SINR at the receiver. In the following I define some fundamental KPIs in wireless networks and their relation with the SINR.

- **Outage Probability:** is the probability that the SINR at the receiver goes below the threshold (β) defined for correct signal recovery. The outage probability is a function of the SINR defined as $\mathcal{O} = \mathbb{P}\{\text{SINR} \leq \beta\}$.

- **Spectral Efficiency:** is the average data rate supported per channel per hertz. The spectral efficiency is a function of the SINR defined as $\mathcal{R} = \log_2(1+\text{SINR})$.

- **Spatial Frequency Reuse Efficiency:** is a KPI that reflects how often the same frequency is reused over the spatial domain. If the required SINR thresh-

old β for correct data recovery is high, the same frequency channel should be reused over a larger spatial interval which degrades the spatial frequency reuse efficiency, and vice versa.

- **Delay:** determine the number of retransmissions required to successfully transmit a massage to its destination. The average delay can be defined as $\mathcal{O}^{-1}$.

- **Energy Efficiency:** is defined as the data rate delivered per unit power. Reducing interference without increasing the power of the intended signal increases energy efficiency. This is because low interference implies high SINR, high data rate, and low outage probability which increases the data rate delivered with the same transmit power.

From the previous definition of the KPIs, the effect of SINR on the network performance can be clearly observed. In the next sections, I will discuss how to develop a design paradigm to engineer the SINR in large-scale wireless networks.

1.2 Modeling, Analysis, and Design of Wireless Networks

As mentioned before, in a multi access network, the SINR cannot be simply increased by increasing the transmit powers of the transmitters. Instead, the network parameters (e.g., MAC protocol, transmit powers, etc.) should be carefully engineered via a design paradigm. A design paradigm for wireless networks is developed in three steps, namely, modeling, analysis, and design, which are three related processes for the practical implementation, maintenance, or expansion of wireless networks. The modeling phase aims at obtaining some expressions that govern the network behavior. The inputs for the modeling expressions are the network parameters (i.e., network geometry, MAC protocol, propagation environment, etc.) and the outputs are the

KPIs (e.g., outage probability, spectral efficiency, etc.). The modeling expressions should capture the network type, characteristics, MAC protocol, and network geometry. After modeling the network and obtaining the expressions that govern the network behavior, the analysis phase starts. In the analysis phase, the system response to different network parameters is analyzed, via the expression obtained from the modeling phase, to understand the system behavior. Hence, the performance tradeoffs can be highlighted and the design insights are obtained. Note that with simpler expressions obtained from the analysis, insights can be obtained for the network design. Finally, in the design phase, the network parameters that balance the tradeoffs among the different KPIs are determined. The tradeoffs among the different KPIs are determined based on the operator policy, regulator constraints, customer expectations, application requirements, or a combination of all. In the next section, I discuss different approaches used in the literature to model and analyze the SINR performance in wireless networks.

1.3 Different Approaches for Modeling and Analysis of Wireless Networks

In the literature, researchers either ignore the effects of network topology by incorporating the distance-dependent path-loss into the channel fading (e.g., Wyner model) or assume simple and deterministic network topology (e.g., specific coexistence model and grid-based models). Wyner model completely ignores the network geometry and uses very simplistic assumptions which lead to disputable results and insights for the network performance [11]. For a known network topology, a specific coexistence model can be developed and analyzed, however, the analysis is only limited to the developed coexistence model and cannot be generalized to large-scale network de-

ployments. The grid models are widely accepted and used in large-scale wireless networks. However, grid-based models highly complicate the analytical modeling and analysis for the network and do not capture the actual topology for emerging large-scale wireless networks (e.g., multi-tier cellular networks) as will be discussed in this section.

1.3.1 Infrastructure-based Networks

Infrastructure-based networks are networks constituted from access points and nodes such that a link between any two nodes must be established via the access point. Grid-based models (e.g., hexagonal grid, square grid, triangular lattice) have been extensively used and are widely accepted to model infrastructure-based networks. For instance, the hexagonal grid model for the cellular networks. In the network shown Fig. 1.1, if each user associates in the downlink to the nearest BS, the hexagons determine the service range of each BS. Hence, a user cannot be further than the hexagon radius from her serving BS. Furthermore, the association scheme guarantees that none of the interfering BSs can be closer to the intended user than her serving BS. Moreover, if a frequency reuse scheme of 3 is adapted to the network model, no user receives interference from her adjacent hexagon cells, which significantly reduce interference.

Grid-based models for modern cellular networks are considered too idealistic and do not capture actual network topology. Fig. 1.2 shows an actual BSs' deployment for the same cellular operator in Nottingham downtown, UK[3]. Another studies on actual BSs' deployments were conducted in [12, 13] which confirm that the cellular topology significantly deviates from the grid-based model. Instead, it was shown that

[3]This data is obtained via the open source website of Ofcom available at http://sitender.ofcom.org.uk/search

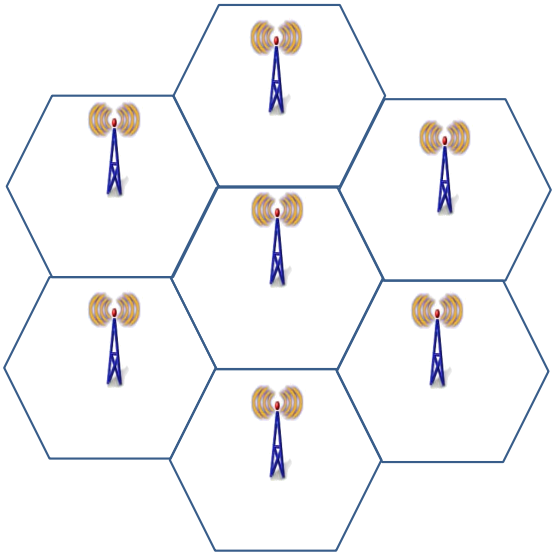

Figure 1.1: Grid-based network models.

the BSs' locations form random patterns which change from one location to another. The main reason for this deviation is the capacity variation across the service area and the infeasibility to exactly follow a gird model for the BSs' deployment. Furthermore, the deployment of multi-tier cellular networks with different types of BSs (e.g., macro, micro, pico, and femto) will impose more uncertainties to the network topological structure. Therefore, a grid-based model represents a very idealistic network deployment for cellular networks and cannot capture the multi-tier network deployments. Moreover, the grid-based modeling for cellular networks highly complicates the analysis and result in complicated expressions with multiple integrals which necessitate computationally complex Monte Carlo evaluations [11]. Note that complex expressions for the performance metrics significantly decrease the insights that can be obtained via the model.

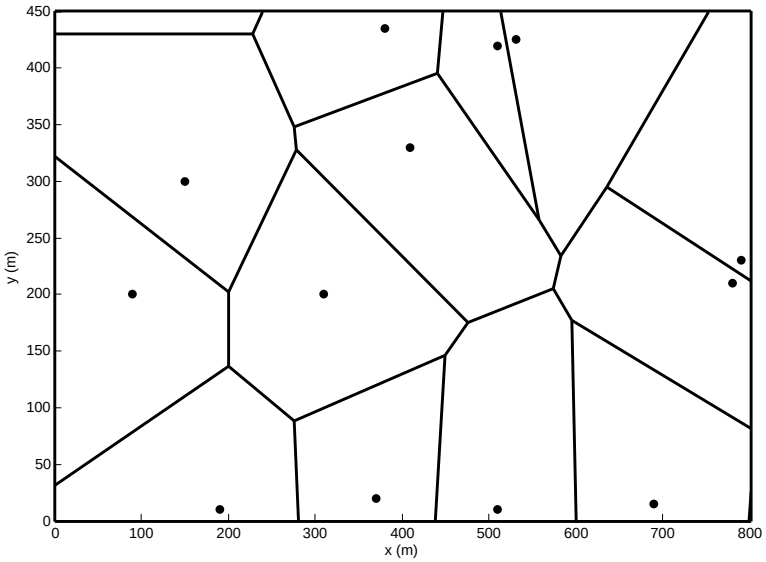

Figure 1.2: Actual deployment of BSs in a 800 m × 450 m in Nottingham downtown, UK.

1.3.2 Infrastructure-less Networks

In contrast to the infrastructure-based networks, any two nodes can directly communicate together in the infrastructure-less based network (also denoted by ad hoc network). Although ad hoc network topologies are inherently random, the grid-based models have been widely used in ad hoc networks with coordinated spectrum access to reflect the worst-case interference [14–16]. For instance, in a carrier sensing multiple access (CSMA) network, the sensing threshold for the CSMA protocol guarantees a minimum distance between any two simultaneously active transmitters. Therefore, the triangular lattice shown in Fig. 1.3 represents the worst-case packing density for CSMA networks with deterministic channel gains. The grid-based models in this case can be only used to model the worst-case performance which may lead to a very pessimistic and conservative network design.

Therefore, in addition to the complicated analysis, the grid-based model does not

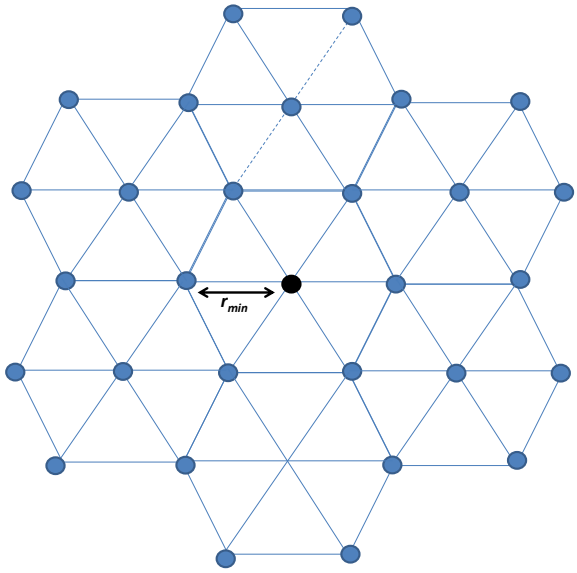

Figure 1.3: Worst-case interference for the centre node (black node) in a CSMA network with deterministic channel gain.

capture the actual topology of either the infrastructure-based networks or the ad hoc networks. That is, both the infrastructure-based networks and the ad hoc networks have uncertainties in their node locations. Given the impact of the network geometry on the network performance, the modeling expressions should be able to capture the actual network topology more precisely. Furthermore, the modeling expressions should be simple enough to facilitate the analysis and design phases. That is, simple expressions clearly characterize the network performance and highlight the tradeoffs, which facilitate the network design. In the next section, I will discuss the challenges to model random wireless networks.

1.4 Challenges in Modeling Random Wireless Networks

Given the impact of distance on the received signal power, the modeling expressions for the SINR should explicitly account for the network geometry. It is straightfor-

ward to incorporate location information for networks with deterministic topology (e.g., grid-based models). However, in random wireless networks, the SINR of a generic receiver may change form one time instant to another and from one location to another, therefore, it is required to average the modeling expressions over all possible network realizations, each weighted by its probability of occurrence. Note that averaging the modeling expressions over all possible network realizations cannot be done via elementary probability theory. The modeling expressions that explicitly account for the random geometry is necessary for a design that is robust to the network's topological variations.

For random networks with dynamic topology, static design parameters averaged over all network topologies may lead to a very conservative network operation. Therefore, sophisticated and adaptive multi-access schemes for interference coordination and mitigation are required to improve the network performance. These techniques aims at developing a new generation of networks denoted as self-organizing networks (SONs), which are able to self-optimize, self-maintain, and self-recover their operation. The randomized topology of the SON necessitates the development of rigorous, general, topology-aware analytical tools for its modeling, design, analysis, and performance assessment.

1.5 Motivation and Objective

Motivated by the impact of network geometry on the network performance, I aim at developing rigorous topology-aware models for wireless networks which can be used to optimize the network performance. Note that the topology-awareness cannot be obtained via any of the techniques discussed in Sec. 1.3. That is, the Wyner model completely ignores the network geometry effect. A coexistence model with arbitrary

locations of nodes cannot be generalized to large-scale deployments. The grid-based models are not analytically tractable and also fail to capture realistic network topologies. Therefore, I adopt the stochastic geometry approach for modeling, analysis, and design for large-scale wireless networks. Stochastic geometry is the only[4] analytical tool that can capture the uncertainties in the locations of network elements and average over all network realizations [1–10]. Furthermore, stochastic geometry has proven to be very powerful to deal with large-scale networks with randomized topologies leading to simple expressions for the performance metrics which help understanding the network behavior with variations in the network design parameters.

The main objective of this thesis is to develop a general framework that accounts for the network geometry in the design and analysis of large-scale wireless networks. Stochastic geometry is a powerful tool that will be used throughout this work to model, analyze, design, and obtain the performance metrics for different types of wireless networks, all characterized with their randomized topologies. Particularly, in this work, I address a broad range of large-scale wireless networks such as ad hoc networks, star-connected sensor networks, and multi-tier cellular networks.

For more than three decades, stochastic geometry has been used to model large-scale ad hoc wireless networks, and it has succeeded to develop tractable models to characterize and better understand the performance of these networks. Recently, stochastic geometry models have been shown to provide tractable yet accurate performance bounds for multi-tier and cognitive cellular wireless networks. Using stochastic geometry for ad hoc networks analysis can be traced back to the late 70's [17], since then, it has been used to model and analyze ad hoc systems with random chan-

[4]Note that stochastic geometry is not necessarily the best tool to model wireless networks because each modeling tool has its merits and limitations. However, as long as capturing the topological randomness in the analysis is required, stochastic geometry is the only analytical tool that could be used.

nel access (e.g., ALOHA [17–39] and CSMA [40–51]), single- and multi-tier cellular networks [11, 12, 52–79], and networks with cognitive elements [75–85].

For the sake of an organized presentation, I postpone the detailed discussion of the related work to the analysis chapters. That is, for each type of network addressed in this thesis, the related work is presented and the novelty is highlighted.

1.6 Scope and Contribution of the Thesis

In this thesis, I will exploit tools from stochastic geometry to model, analyze, and design a wide-range of wireless networks. More specifically, I adapt and extend stochastic geometry models to practical networks and scenarios that have not been addressed in the literature, and thereby increase the applications of the stochastic geometry models to wireless communications. For ad hoc networks, most of the stochastic geometry models existing in the literature address networks without coordinated spectrum access. Only very little efforts have been invested in ad hoc networks with coordinated spectrum access. For infrastructure-based networks, most of the literature addresses downlink systems without cognitive elements. The uplink and cognitive networks are not sufficiently addressed in the literature. Furthermore, for both infrastructure-based and ad hoc networks, all of the existing stochastic geometry models are for a single-channel environment. In this thesis I extend the stochastic geometry analysis for coordinated spectrum access ad hoc networks, networks with cognitive elements, uplink systems, and multi-channel environments. I have also shown how stochastic geometry modeling approach can be incorporated into a unified network design for a practical sensor networks scenario.

The main contribution of this thesis is the development of general, flexible, and rigorous modeling paradigms for different types of large-scale wireless networks. The

developed paradigms are used for understanding the system behavior with variations to the system design parameters. Hence, many design insights and tradeoffs for the considered wireless networks are obtained and the network performance can be optimized via the proposed models. In the following I present a detailed discussion about the contributions of the work done in this thesis for each type of the considered networks:

1.6.1 Ad hoc and Sensor Networks

Chapters 2 and 3 present a design framework for large scale CSMA wireless networks. In Chapter 2, I show that the conventional stochastic geometry analysis (i.e., using the Matérn hard core point process type II[5]) for CSMA networks results in underestimating the probability of spectrum access and the intensity of active transmitters, hereafter referred as the underestimation error. Note that the underestimation error of the Matérn hard core point process type II is a well known open problem [86, 87]. In Chapter 2, I provide a thorough discussion for the underestimation error, quantify it, show its dependence of the system parameters, and provide a solution to mitigating it, namely, the modified hard core point process. Although, the provided solution does not completely solve the underestimation error, it broadens the application of the hard core process to a wider range of system parameters values.

In Chapter 3, I exploit stochastic geometry to engineer a large scale random star-connected sensor networks (SNCs). The design aims at maximizing the spatial frequency reuse efficiency subject to constraints on the data rates and outage probability per SCN. The design paradigm developed in Chapter 3 was proposed as a potential solution to design large scale body area networks used for e-Health application.

[5]The Matérn hard core point process type II is defined later in Sec. 2.1.5

1.6.2 Cellular Networks

Chapters 4 and 5 present a design paradigm for distributed interference management in multi-tier cellular networks. While centralized interference management in multi-tier cellular networks is infeasible due to complexity and signaling issues, cognition is envisioned as a potential solution for distributed interference management. Note that, different from legacy cognitive networks with primary and secondary spectrum users, cognition is mainly implemented in multi-tier cellular networks for interference management. Hence, there is no notion of priority in the spectrum access and there should be some performance guarantee for all network elements (i.e., the cognitive and non-cognitive). Chapters 4 and 5 quantify the performance gain imposed by cognition capabilities and optimize the design tradeoffs for cognitive downlink cellular networks.

Finally, Chapter 7 provides a rigorous paradigm for modeling, analysis, and design of uplink cellular networks. The main contribution in Chapter 7 is that the outage probability and mean achievable rate for a generic user in uplink transmission have been obtained in simple closed forms. The simple closed forms enabled a complete characterizations for the uplink behavior in response to the network parameters. To the best of my knowledge this is the first modeling paradigm for uplink transmission that can obtain the outage probability and mean achievable rate for a generic user in a simple form with one integral and an incomplete gamma function in the general case, and in closed form for some special cases.

1.6.3 Summary of Contributions

The contributions of the thesis are shown in Fig. 1.4 and summarized in the following points:

- CSMA-based wireless ad hoc networks

Figure 1.4: Thesis contributions.

- Quantify the intensity underestimation problem of the traditional stochastic geometry models when applied to CSMA-based wireless networks.
- Propose a novel technique to mitigate the intensity underestimation problem.
- Model the tradeoff imposed by the spectrum sensing threshold on the outage probability and the spatial frequency reuse efficiency.
- Optimize the spectrum sensing threshold (or equivalently the spectrum sensing region [SSR]) that maximizes transmission capacity.

• Large-scale star-connected wireless sensor networks

- Propose a complete topology-aware and spectrum-efficient design paradigm for large-scale star-connected wireless sensor network.
- Reveal the conservativeness of the IEEE 802.15.4-based wireless sensor

networks and the resulting spectrum under-utilization.

  - Optimize the long term superframe scheduling and the spectrum sensing threshold (or equivalently the SSR) for the IEEE 802.15.4 standard-based beacon enabled mode to maximize the coexistence capability of the IEEE 802.15.4-based networks in the congested ISM band.
  - Reveal the nonlinear relationship between the number of channels and the intensity of coexisting nodes that can be accommodated by the system.

- Downlink transmissions in two-tier macrocell-femtocell networks
  - Provide a framework for the design and analysis of cellular networks with cognitive small cells.
  - Quantify the performance gain, in terms of outage probability, for cellular networks with cognitive femto access points (FAP).
  - Optimize the spectrum sensing threshold (or equivalently the SSR) for the cognitive femto-access points that maximizes the spatial frequency reuse.
  - Highlight the tradeoffs between the resource allocation in cellular networks and opportunistic spectrum access in FAPs.
  - Extend the downlink modeling to the multi-channel environment.

- Uplink transmissions in multi-tier cellular networks
  - Provide a novel framework for modeling uplink transmission with truncated channel inversion power control in multi-tier cellular networks.
  - Characterize the uplink transmission for multi-tier cellular networks and show that there exists a transfer point in the system behavior that depends on the relative values of the design parameters.

1.7 Organization of the Thesis

In Chapter 2, I present a high level overview on stochastic geometry analysis and the different modeling/analysis techniques used in the literature. In Chapter 3, I present the stochastic geometry analysis for ad hoc CSMA wireless networks. In Chapter 4, I present the modeling paradigm for large-scale star-connected wireless sensor networks using the IEEE 802.15.4 technology. Chapter 5 and Chapter 6 present the downlink modeling framework for multi-tier cellular networks with cognitive small cells. Chapter 7 presents the uplink modeling framework for multi-tier cellular networks. Finally, in Chapter 8 I summarize and conclude the work done in this thesis and point out some directions for future research.

It is worth noting that, tuning the spectrum sensing threshold to optimize the tradeoff between the spatial frequency reuse efficiency and the SINR outage probability is a common theme in Chapters 3, 4, 5, 6 but for different types of networks (cf. Fig 1.4). Chapter 7 complements Chapters 5, 6 and highlights the difference between the uplink and downlink transmission performances in cellular networks.

Chapter 2

Overview on Stochastic Geometry Analysis

2.1 Stochastic Geometry Analysis

As discussed in Chapter 1, the network geometry has a significant impact on the interference experienced by the network receivers. According to the network model, the aggregate interference $\mathcal{I}$, seen from a generic receiver perspective, can be either resulting from a finite or infinite number of interferers, and the locations and the intensity of the interferers (i.e., the number of interferers per unit area) depend on the network characteristics (e.g., network topology, number of channels, association criterion, etc.) and medium access control (MAC) layer protocol (e.g., ALOHA, CSMA, TDMA, CDMA, etc.). In the following, I give two examples to elaborate the effect of user association and spectrum access method (i.e., MAC protocol) on the locations and/or intensities of the interferers.

- In a cellular network, a user may select the BS providing the highest signal power to be her serving BS. Therefore, when all the BSs have the same transmit powers

(i.e., single-tier cellular network), the distance between a generic user and her nearest interfering BS will be greater than the distance between that user and her serving BS. In a multi-tier cellular network, different network entities have different transmit powers. Therefore, as shown in Fig. 2.1(a), given that the distance between a macro-cell user and her serving MBS is r and the transmit power of the serving MBS is P_m, the nearest interfering MBS transmitting with the same power P_m will be located at a distance $r_m > r$. On the other hand, assuming the same path-loss exponent η for macro and small cell tiers, the nearest interfering small base station (SBS) with transmit power P_s will be located at a distance $r_s > r\left(\frac{P_s}{P_m}\right)^{\frac{1}{\eta}}$. Similarly, Fig. 2.1(b) shows the relation between the desired link distance for a small cell user (i.e., the distance between the small cell user and her serving SBS) and the nearest interference sources.

- A cognitive spectrum access method affects both the locations of the interference sources as well as their intensity. In a cognitive network, each network element performs spectrum sensing and accesses a channel if and only if the received power on that channel is less than a given threshold (υ_s). If deterministic channel gains are assumed, the spectrum sensing threshold (υ_s) translates to a minimum exclusion distance $r_e = \left(\frac{P_t A}{\upsilon_s}\right)^{\frac{1}{\eta}}$ between the network elements using the same channel, where P_t is the transmit power and A is a propagation constant. Fig. 2.2(a) shows the locations of the cognitive network elements and Fig. 2.2(b) shows the potential locations of the simultaneously transmitting network elements on the same channel. Fig. 2.2(b) shows that there is a minimum distance between any two network elements using the same channel which controls both the minimum distance between a receiver and her interference sources as well as the intensity of the interference sources.

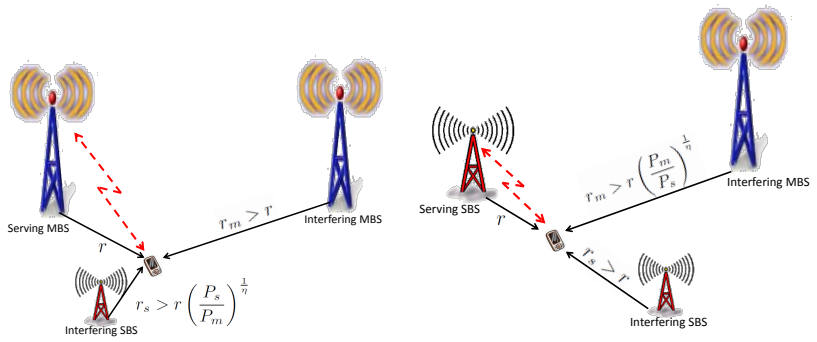

Figure 2.1: The relation between the desired link distance and the nearest interference sources: (a) macro-cell user, (b) small-cell user.

At a generic time instant, the SINR experienced by each receiver depends on its location, the positions of the interference sources as well as the instantaneous channel gains. Hence, given the effect of network geometry on interference, the SINR is a random variable that strongly depends on the network geometry and significantly varies from one receiver to another and from one time instant to another.

Stochastic geometry is a mathematical tool that provides spatial averages, i.e., averages taken over large number of nodes at different locations or[1] over many network realizations, for the quantities of interest (e.g., interference, SINR, outage probability, and achieved data rate) [3]. In other words, the stochastic geometry averages over all network topologies seen from a generic node weighted by their probability of occurrence [8, 82]. Fig. 2.3 shows a schematic diagram for stochastic geometry analysis. Point process is a branch of the stochastic geometry used to statistically describe patterns produced by points in the D-dimensional space. In my models, point process will be used to model the spatial distribution of the network elements. In this section, I will overview some basics of the point process and introduce the

[1]If the point process is ergodic, the spatial averages (across points) equal the ensemble averages (across realizations) [8, Ch. 2].

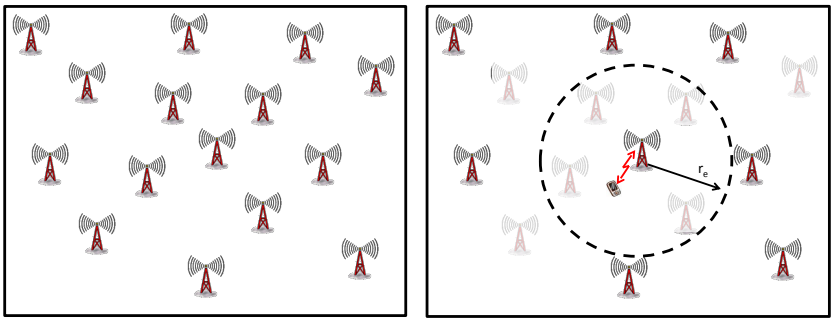

(a) (b)

Figure 2.2: (a) The locations of the cognitive network elements, (b) the potential locations of the simultaneously transmitting network elements on the same channel (the shaded network elements cannot simultaneously transmit on the same channel due to the cognitive nature of the spectrum access).

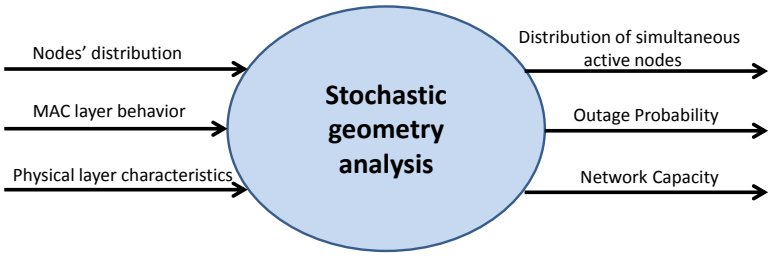

Figure 2.3: Schematic diagram for stochastic geometry analysis.

most commonly users point processes in wireless communication, namely, Poisson point process (PPP), the Binomial point process (BPP), the Poisson cluster process (PCP), and the Matérn hard core point process (HCPP).

2.1.1 Point Process

Point process is a tool used to statistically describe the patterns produced by points existing in a d-dimensional space $\mathbb{R}^d$. These points can represent trees in a forest, stars in the space, or wireless nodes in a network. For instance, the call arrival times to a network can be represented using a 1-D point process, where the location of each

point on the time axis represents the call request time. If the type of call was also of interest, and each call type can be represented by a unique mark form the space M, then a new dimension is added to the model and a 2-D point process ($\mathbb{R} \times M$) can be used to model this stochastic process. In this point process, each point on the time access will have a mark ($m \in M$) to determine its type. If the call location rather than the call arrival time and type was the parameter of interest, then a point process on a $\mathbb{R}^2$ map can be used to model this stochastic process. If the type of call is added to the model, then the 3-D point process ($\mathbb{R}^2 \times M$) can be used. These simple examples show the relation between a stochastic process and its modeling using a point process with the proper dimensions. For more applications of point processes see [1, 2].

2.1.2 Poisson Point Process

Poisson point process (PPP) is the simplest and most widely used point process. The simplicity of the PPP is due to the independence between the points of the process. For a PPP, the number points existing in any bounded area is a Poisson random variable, and the numbers of points in disjoint areas are independent. A point process is defined using a random set $\mathbf{\Psi} = \{x_i; i = 1, 2, 3, ...\}$, where x_i is the location of the i^{th} node in the $\mathbb{R}^d$ space. For a PPP in $\mathbb{R}^2$ plane, $N(\mathbf{A}) = |\mathbf{\Psi} \cap \mathbf{A}| \sim Poisson(\lambda)$. That is, for any $\mathbf{A} \subset \mathbb{R}^2$ the number of point $N(\mathbf{A})$ has the *pmf*:

$$\mathbb{P}\{N(\mathbf{A}) = k\} = \frac{(\lambda L(\mathbf{A}))^k e^{-\lambda L(\mathbf{A})}}{k!} \tag{2.1}$$

where $L(.)$ denotes the Lebesgue measure[2], and λ is the intensity of the point process and has the units $\frac{points}{m^2}$.

The independence between the points of the PPP simplifies its analysis. For example, the reduced Palm probability $P^{!x}$ of the PPP is the distribution of the PPP itself (Slivnyak's theorem) [1–3]. This means that the point process seen from an arbitrary location $u \in \mathbb{R}^2$ is the same whether a condition on having a point at that location is present or not (i.e., $P^{!x} = P$).

2.1.3 Binomial Point Process

The Binomial Point Process (BPP) models the random patterns produced by a fixed number of points (N) in a set $\mathbf{A} \subset \mathbb{R}^d$ with a finite Lebesgue measure $L(\mathbf{A}) < \infty$. Let $\mathbf{\Psi} = \{x_i; i = 1, 2, 3, \ldots\}$ and $\mathbf{\Psi} \subset \mathbf{A}$, then $\mathbf{\Psi}$ is a BPP if the number of points inside a compact set $\mathbf{b} \subseteq \mathbf{A}$ is a binomial random variable with the parameters $\left(N, p = \frac{L(\mathbf{b})}{L(\mathbf{A})}\right)$, and the numbers of points in disjoint sets are related via a multinomial distribution.

A BPP can be obtained by conditioning on the number of points in a PPP over a finite area. That is, each realization of the PPP over a finite area gives a different BPP realization.

2.1.4 Poisson Cluster Process

The Poisson Cluster Process (PCP) models the random patterns produced by random clusters. The Poisson cluster process is constructed from a parent PPP $\mathbf{\Psi} = \{x_i; i = 1, 2, 3, \ldots\}$ by replacing each point $x_i \in \mathbf{\Psi}$ with a cluster of points M_i, $\forall x_i \in \mathbf{\Psi}$, where the points in M_i are independently and identically distributed in the spatial

[2]In measure theory, the Lebesgue measure is the standard way of assigning a measure to subsets of an n-dimensional Euclidean space. For $n = 1$, 2, or 3, it coincides with the standard measure of length, area, or volume.

domain. There are two type of PCP, namely, the Matérn cluster process and the Thomas cluster processes. In the Matérn cluster process, each point $x \in \mathbf{\Psi}$ from the parent PPP is replaced by a cluster of point uniformly distributed in a disc with fixed radius centered at the parent point location $x \in \mathbb{R}^2$. On the other hand, in the Thomas cluster processes, each point $x \in \mathbf{\Psi}$ from the parent PPP is replaced by a cluster of points normally distributed over the plane $\mathbb{R}^2$ around the parent point x.

2.1.5 Matérn Hard Core Process

The hard core point process (HCPP), is a repulsive point process which models the pattern of points that are prohibited to coexist with a distance less than a predetermined value r_{min}. Conditioning on having a minimum distance between the points of the process, correlates their positions. The HCPP is constructed from a parent PPP $\mathbf{\Psi} = \{x_i; i = 1, 2, 3, \ldots\}$ by dependent thinning. Matérn has introduced two approaches to construct an HCPP from a PPP, namely, the Matérn hard core process type I and type II. Both the Matérn hard core processes (i.e., type I and type II) provide a legitimate HCPP but with different packing density. Since the HCPP is an essential point process for wireless communication that will be extensively used in my work, I will give more elaborations for the two types of the HCPP.

Matérn Hard Core Process Type I

Matérn hard core process type I models the pattern of points that are prohibited to coexist with a distance less than a certain value r_{min}. In this section, I show how to construct the Matérn hard core process type I for a parent PPP. Let $\mathbf{\Psi}$ be a PPP in $\mathbb{R}^2$ with intensity λ. The Matérn hard core process type I ($\mathbf{\Psi}_H^I$) is constructed from $\mathbf{\Psi}$ by deleting all points that coexist with a distance less than the minimum distance

r_{min}. For a generic point $x_i \in \mathbf{\Psi}$, the retaining probability for that point in $\mathbf{\Psi}_H^I$ is given by the probability that x_i exists alone in the disc with a radius r_{min} centered at x_i. Hereafter, I will denote that disc by $\mathbf{B}_{x_i}(r_{min})$. Using the Palm probability, $P^{!x_i}(dist(x_i, \mathbf{\Psi}') \geq r_{min}) = P(dist(x_i, \mathbf{\Psi}') \geq r_{min})$, where $\mathbf{\Psi}' = \mathbf{\Psi} \setminus x_i$ and $dist(x_i, \mathbf{\Psi}')$ is the distance between x_i and the closest point in $\mathbf{\Psi}'$. Then, the retaining probability is given by:

$$P_I = \mathbb{P}\left\{x_i \in \mathbf{\Psi}_H^I | x_i \in \mathbf{\Psi}\right\} = e^{-\lambda\pi r_{min}^2}. \tag{2.2}$$

Having the retaining probability (P_I), the HCPP type I intensity is given by $\lambda_I = P_I\lambda = \lambda e^{-\lambda\pi r_{min}^2}$ [1, 2]. It can be seen that $\lim_{\lambda\to\infty} \lambda e^{-\lambda\pi r_{min}^2} = 0$, which means that at high intensity of the PPP all the points will be coexisting with a distance less than r_{min}. Hence, all the points will be deleted and $\mathbf{\Psi}_H^I = \phi$. Therefore, Matérn hard core process type I is too conservative and results in a point process with a very low intensity. Matérn hard core process type II overcomes this flaw and results in a point process with much higher intensity.

Matérn Hard Core Process Type II

The Matérn hard core process type II also models the pattern of points that are prohibited to coexist with a distance less than a certain value r_{min}. In this section I show how to construct the Matérn hard core process type II from a parent PPP. Let $\mathbf{\Psi}$ be a PPP in $\mathbb{R}^2$ with intensity λ. Matérn hard core point process type II is derived from $\mathbf{\Psi}$ in two steps. At first, the marked point process $\mathbf{\Psi}^m$ is constructed by applying an independent mark uniformly distributed from $[0, 1]$ to $\mathbf{\Psi}$. Then, a point $(x_i, m_i) \in \mathbf{\Psi}^m$ is selected to be in $\mathbf{\Psi}_H^{II}$ (retained in $\mathbf{\Psi}_H^{II}$) if and only if it has the lowest mark m_i in the ball of radius r_{min} centered at x_i ($\mathbf{B}_{x_i}(r_{min})$). That is,

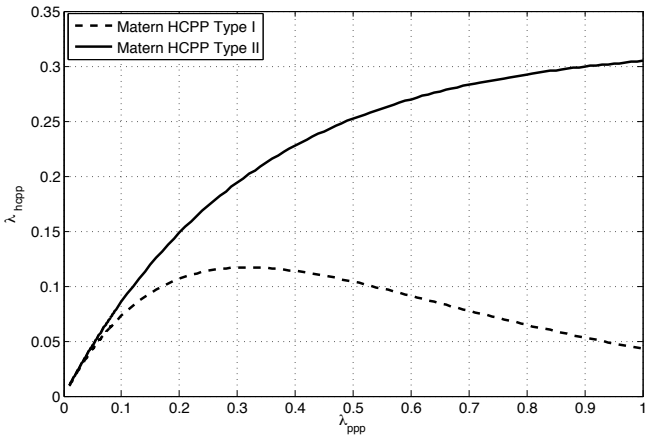

Figure 2.4: Comparing the Matérn HCPP Type I and Type II.

$(m_i > m_j \forall j | x_j \in \mathbf{B}_{x_i}(r_{min}) \cap \mathbf{\Psi})$. Conditioning on that x_i coexist with n points in $\mathbf{B}_{x_i}(r_{min})$, due to the independent marking and the uniform distribution of the marks, the probability that x_i has the lowest mark is $1/(n+1)$. Hence, averaging over all possible probabilities (law of total probability), the probability of retaining a generic point $x_i \in \mathbf{\Psi}$ in $\mathbf{\Psi}_H^{II}$ is given by:

$$\begin{aligned} P_{II} = \mathbb{P}\left\{x_i \in \mathbf{\Psi}_H^{II} | x_i \in \mathbf{\Psi}\right\} &= \sum_{n=1}^{\infty} \frac{1}{n+1} \frac{(\lambda \pi r_{min}^2)^n e^{-\lambda \pi r_{min}^2}}{n!} \\ &= \frac{1 - e^{-\lambda \pi r_{min}^2}}{\lambda \pi r_{min}^2}. \end{aligned} \tag{2.3}$$

Having the retaining probability (P_{II}), the HCPP type II intensity is given by $\lambda_{II} = P_{II}\lambda = \frac{1-e^{-\lambda \pi r_{min}^2}}{\pi r_{min}^2}$. It can be seen that $\lim_{\lambda \to \infty} \frac{1-e^{-\lambda \pi r_{min}^2}}{\pi r_{min}^2} = \frac{1}{\pi r_{min}^2}$, which means that at high intensity of the PPP, the intensity of the HCPP type II converges to a constant (one point every $\mathbf{B}_{x_i}(r_{min})$). Hence, Matérn hard core process type II overcomes the conservativeness flaw of type I and results in a HCPP with much higher intensity as shown in Fig. 2.4.

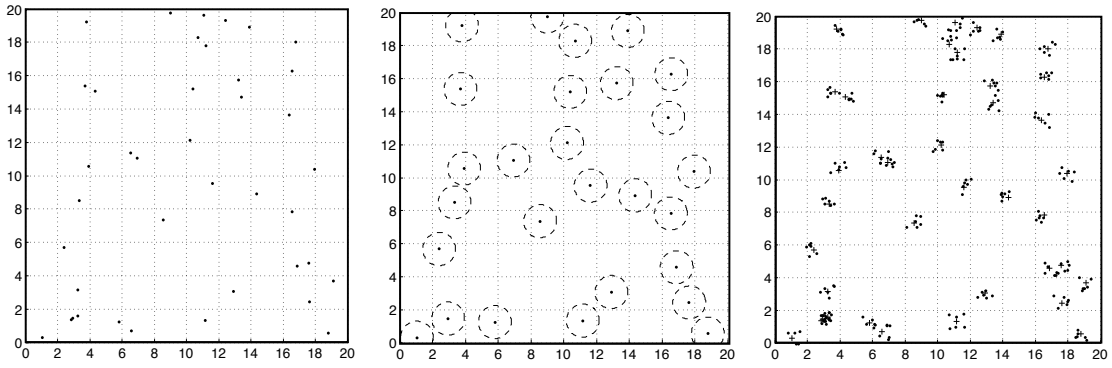

(a) (b) (c)

Figure 2.5: (a) PPP in a 20m × 20m region with intensity 0.1 points/m^2, (b) the corresponding HCPP type II with r_{min} = 2m, each point of the HCPP lies at the center of a non-overlapping circles with radius $r_{min}/2$ represented by the dashed circles, (c) the corresponding Matérn cluster process where the clusters have a Poisson distributed number of points with mean 2, the parent PPP points are plotted in crosses"+" while the added cluster points are plotted in dots.

From the previous definitions of the point processes, it can be seen that the PPP is a fundamental point process for two reasons. The first is that all point processes which are commonly used in wireless communication are somehow related to the PPP. The second is that the PPP is the only point process with uncorrelated points' location which highly simplifies its analysis. Fig. 2.5 shows a realization for a PPP and its corresponding HCPP and PCP.

2.2 Performance Metrics & Analysis

Interference is one of the main network parameters to characterize using the stochastic geometry analysis. The aggregate interference can be considered as a function of the point processes. That is, given that the signal power decays with distance at the rate $r^{-\eta}$, where η is the path loss exponent, the aggregate interference seen by a generic node located at $x \in \mathbb{R}^2$ is given by $\mathcal{I} = \sum_{y \in \mathbf{\Psi}_{\mathcal{I}}} P_{\mathrm{t}}(y) A h(x,y) \left\| x - y \right\|^{-\eta}$, where $\mathbf{\Psi}_{\mathcal{I}}$ is the

point processes constituted by the set of interfering network elements, $P_{\mathrm{t}}(y)$ is the transmit power of the network element located at $y \in \mathbb{R}^2$, A is a frequency dependent propagation constant, $h(x, y)$ is the random channel gain between the two locations x and y, and $\|.\|$ is the Euclidean norm. The aggregate interference is a stochastic process that depends on the time variant locations of the interfering network elements captured by the point process $\mathbf{\Psi}_{\mathcal{I}} = \{x_i\}$ and the time variant random channel gains $h(x, y)$. Note that point processes of the interfering network elements' locations $\mathbf{\Psi}_{\mathcal{I}}$ is defined by the network properties and the medium access control (MAC) layer as discussed in Sec. 2.1.

While the aggregate interference is a stochastic process which varies according to the test location and time, stochastic geometry analysis gives the statistics of the interference (averaged w.r.t. the spatial domain) behavior experienced by the nodes existing in the network. Interference can be completely characterized by its *pdf* (or equivalently, its cumulative distribution function (*cdf*)). Generally, there is no known expression for the *pdf* of the aggregate interference in large-scale wireless networks. Hence, the aggregate interference is usually characterized by using the Laplace transform (LT) of the *pdf* (or equivalently its characteristic function [CF] or moment generation function [MGF])[3]. The Laplace transform of the aggregate interference is given by

$$\mathcal{L}_{\mathcal{I}}(s) = \mathbb{E}[e^{-s\mathcal{I}}]. \tag{2.4}$$

Since the aggregate interference is a strictly positive random variable, its Laplace transform always exists. Stochastic geometry provides a systematic way to obtain the LT, CF, or MGF for the aggregate interference associated with the PP of interest. At this point, I have not yet introduced enough preliminaries that allow delving into the

[3]Hereafter, I will use "the Laplace transform of the random variable" to denote the Laplace transform of its *pdf*.

details of how to derive the LT, CF, or MGF for the aggregate interference associated with the PP of interest. Therefore, the derivation details of the LT, CF, or MGF for the aggregate interference will be postponed to the analysis chapters. However, to give a broad overview on the stochastic geometry modeling, it is important to highlight how the LT, CF, or MGF for the aggregate interference can be used to characterize some performance metrics in wireless networks. Since the expressions for the LT, CF, or MGF, cannot be inverted in general, the LT, CF, or MGF, can only be used to generate the moments (if they exist) of the aggregate interference as $\mathbb{E}[\mathcal{I}^n] = (-1)^n \, \mathcal{L}_{\mathcal{I}}^{(n)}(s)\Big|_{s=0}$, where $\mathcal{L}_{\mathcal{I}}^{(n)}(s)$ is the n^{th} derivative of $\mathcal{L}_{\mathcal{I}}(s)$. Consequently, in the general case, it is not possible to derive the exact performance metrics (e.g., outage probability, transmission capacity, average achievable rate) from the LT, CF, or the MGF. In the next section, I will show the different techniques used in the literature to utilize the LT, CF, or the MGF and go beyond the moments of the aggregate interference to evaluate the performance of large-scale wireless networks.

2.3 Techniques to Analyze Network Performance

In the literature, there are five main techniques to utilize the LT, CF, or the MGF and go beyond the moments of interference and model the network performance metrics. In the following, I will discuss the techniques which were used in the literature to overcome the obstacle imposed by the non-existence of any useful closed-form expression for the *pdf* of the interference.

2.3.1 ***Technique*** *#1: Resort to the Rayleigh Fading Assumption*

Because of its analytical tractability, the Rayleigh fading assumption is the most popular assumption in the literature to overcome the obstacle imposed by the non-

existence of any closed-form expression for the *pdf* of the aggregate interference [25,27]. Although the interference statistics cannot be obtained, *by assuming Rayleigh fading on the desired link* (i.e., the link between the test receiver and its serving transmitter), the exact distribution for the SINR can be obtained. That is, if the desired link is impaired by Rayleigh fading, the expression for the *cdf* of the SINR can be obtained from the LT of the aggregate interference evaluated at some value.

Without loss of generality, let $r = \|x_0 - y\|$ be the constant distance between the transmitter and the test receiver, $h_0 \sim \exp(\mu)$ be the channel power gain of the desired link, then I have

$$\begin{aligned}
F_{\text{SINR}}(\beta) &= \mathbb{P}\left\{\text{SINR} \leq \beta\right\} \\
&= \mathbb{P}\left\{\frac{P_{\text{t}} A h_0 r^{-\eta}}{\sigma^2 + \mathcal{I}} \leq \beta\right\} \\
&= \mathbb{P}\left\{h_0 \leq \frac{(\sigma^2 + \mathcal{I})\beta r^{\eta}}{P_{\text{t}} A}\right\} \\
&= \int_u F_{h_0}\left(\frac{(\sigma^2 + u)\beta r^{\eta}}{P_{\text{t}} A}\right) f_{\mathcal{I}}(u) du \\
&\overset{(i)}{=} 1 - \mathbb{E}_{I_{\text{agg}}}\left[\exp\left(-\frac{(\sigma^2 + I_{\text{agg}})\mu\beta r^{\eta}}{P_{\text{t}} A}\right)\right] \\
&= 1 - \exp\left(-\frac{\sigma^2 \mu\beta r^{\eta}}{P_{\text{t}} A}\right) \mathbb{E}_{\mathcal{I}}\left[\exp\left(-\frac{\mathcal{I}\mu\beta r^{\eta}}{P_{\text{t}} A}\right)\right] \\
&= 1 - \exp\left(-\frac{\sigma^2 \mu\beta r^{\eta}}{P_{\text{t}} A}\right) \mathcal{L}_{\mathcal{I}}(s)|_{s=\frac{\mu\beta r^{\eta}}{P_{\text{t}} A}} \\
&= 1 - \exp\left(-\sigma^2 c\beta\right) \mathcal{L}_{\mathcal{I}}(s)|_{s=c\beta}
\end{aligned} \tag{2.5}$$

where $F_{h_0}(.)$ is the *cdf* of h_0, $f_{\mathcal{I}}(.)$ is the *pdf* of the aggregate interference, the expectation in (i) is w.r.t. both the point process and the channel gains between the interference sources and the test receiver, and $c = \frac{\mu r^{\eta}}{P_{\text{t}} A}$ is a constant. Relaxing the constant distance r is straightforward [12]. As will be shown later, the LT for the aggregate

interference can be found in a systematic manner (cf. [6, 7, 9, 10]). For interference-limited networks (i.e., $\mathcal{I} \gg \sigma^2$), the effect of noise can be ignored and the *cdf* reduces to $F_{\text{SINR}}(\beta) = 1 - \mathcal{L}_{I_{\text{agg}}}(s)\big|_{s=c\beta}$, which is the LT of the aggregate interference is evaluated at some constant c multiplied by the parameter β of the *cdf* of SINR. With the exact *cdf* of the SINR, different performance metrics such as the outage probability, transmission capacity, and the achievable data rate (i.e., obtained using Shannon's formula) can be quantified. Some examples where technique #1 is used can be found in [11, 12, 25–27, 32–35, 37, 39, 54–59, 61–65, 67, 76, 77, 79, 80, 82, 84, 85, 88, 89].

The main drawback of this technique is that it is only valid with the Rayleigh fading assumption for the desired link, which may not always be the case of interest. We can relax the Rayleigh fading assumption at the expense of the tractability of the model. As a result, it is possible to get only approximate solutions or tight bound on the SINR distribution.

2.3.2 ***Technique*** *#2: Resort to Dominant Interferers by Region Bounds or Nearest n Interferers*

Technique #2 is also a very popular technique because of its simplicity and accuracy. Technique #2 is based on the idea of obtaining a lower bound on the outage probability by only considering the subset of dominant interferers. The set of dominant interferers can be determined by a region bound or by considering only the closest n interferers. In the literature, it has been shown that, under a high path-loss exponent (e.g., $\eta = 4$), both the approaches (i.e., approaches based on region bounds and nearest n interferers) give tight lower bounds on the outage probability. However, when the path-loss exponent decreases and approaches 2 (in the planar case), the contribution of distant interferers to the outage events increases and becomes over-

whelming, and hence, both the approaches lose their accuracy, and therefore, should not be applied.

Assuming deterministic channel gains, the region bound is determined by the vulnerability circle around the test receiver. The vulnerability circle is the region where the signal power of any active transmitter measured at the test receiver is greater than the desired signal power at the test receiver multiplied by a certain threshold β [4]. In other words, for a given SINR threshold β, the vulnerability circle contains all transmitters where the transmission of any of them can alone corrupt the signal received at the test receiver. The notion of the vulnerability circle can be extended to random channel gains as in [76].

In the vulnerability region analysis, it is not required to derive the Laplace transform of the aggregate interference. Instead, only the spatial statistics of the PP are studied over the vulnerability region corresponding to the desired signal strength and the SINR threshold. That is, the outage probability (i.e., the *cdf* of the SINR) can be lower bounded by the probability that the vulnerability region is non-empty.

The approach based on the nearest n interferers leads to the same results (i.e., lower bounds), however, since the distribution of the distances for the n nearest interference sources needs to be determined, the analysis here is significantly more involved than the vulnerability region analysis. The distribution of distances for the PPP and BPP was derived in [36, 38].

Since the moments of the aggregate interference can be generated from the LT, CF, or the MGF, an upper bound for the outage probability can be obtained using the Markov inequality, Chebyshev's inequality, or the Chernoff bound. The Markov inequality is the easiest to compute, however, it gives the loosest bound. On the other hand, the Chernoff bound is quite tight for the tail probability, but its computation is

more involved and requires the knowledge of the MGF to be optimized. Generally, the lower bounds provided by the region bounds or the n nearest interferers are tighter than these upper bounds [26]. The lower bound obtained based on the vulnerability analysis was used in [17, 18, 21–26, 39, 43–45, 66, 68]. The bound based on the nearest n interferers was used in [19, 20, 35, 38, 80]. The Markov upper bound was used in [22, 25, 26, 39]. The Chebyshev's upper bound was used in [20–22, 26, 43, 68], and the Chernoff upper bound was used in [26].

2.3.3 ***Technique*** #3*: Resort to the Approximation of the* pdf *of the Aggregate Interference*

In technique #3, the *pdf* of the aggregate interference power is approximated by one of the known *pdf*s. The parameters of the approximate *pdf* are obtained via the LT, CF, or MGF. For instance, if the *pdf* of the aggregate interference is approximated by the Gaussian distribution, then the mean and the standard deviation will be obtained from LT, CF, or the MGF of the aggregate interference. The main drawback of this method is that there is no known criterion to choose which *pdf* to use and the approximation error can be only quantified by simulations.

In the literature, different papers used different *pdf*s according to the problem in hand and the results were verified via simulations. For a PPP, it was discussed in [25, 27] that under the bounded path-loss or a guard zone around the receiver, the moments of aggregate interference exist and the distribution of the aggregate interference approaches the Gaussian distribution. In [37, 43, 46], the aggregate interference was approximated via a Gaussian distribution. However, in [81] it was shown that the *pdf* of interference from a PPP with an exclusion region around the test receiver is skewed and hence deviates from normality. The authors in [81] showed that the

shifted log-normal distribution gives a better approximation than the Gaussian approximation for the *pdf* of the secondary users' aggregate interference in a cognitive network. In [83], the *pdf* of aggregate interference power was approximated by a truncated stable distribution, and in [75] by log-normal and shifted log-normal distributions. In [6, Sec. 5.5], the gamma, inverse Gaussian, and the inverse gamma distributions were used to model interference powers under general PPs. In [70], the *pdf* of the amplitude of the aggregate interference was approximated with a circularly symmetric complex Gaussian distribution.

2.3.4 ***Technique*** *#4: Resort to the Plancherel-Parseval Theorem*

The Plancherel-Parseval theorem [90] states that if $f_1(t)$ and $f_2(t)$ are square integrable complex functions, then

$$\int_{\mathbb{R}} f_1(t) f_2^*(t) dt = \int_{\mathbb{R}} \mathcal{F}_1(\omega) \mathcal{F}_2^*(\omega) d\omega \tag{2.6}$$

where $\mathcal{F}_1(\omega)$ is the Fourier transform (FT) of $f_1(t)$, $\mathcal{F}_2(\omega)$ is the FT of $f_2(t)$, and $f^*(t)$ denotes the conjugate of $f(t)$. The Fourier transform of a *pdf* is equivalent to the CF of that *pdf*, which is a special case of the Laplace transform and is obtained as $\mathcal{F}(\omega) = \mathcal{L}(s)|_{s=-\mathrm{i}\omega}$, where $\mathrm{i} = \sqrt{-1}$. The Plancherel-Parseval theorem precludes the need of inverting the LT (i.e., obtaining the *pdf* of the interference) obtained from the stochastic geometry analysis to obtain the performance metrics. For instance, the outage probability can be written as:

$$
\begin{aligned}
F_{\mathrm{SINR}}(\beta) &= \mathbb{P}\left\{\mathrm{SINR} \leq \beta\right\} \\
&= \mathbb{P}\left\{\frac{P_{\mathrm{t}} A h_0 r^{-\eta}}{\sigma^2 + \mathcal{I}} \leq \beta\right\} \\
&= \mathbb{P}\left\{\mathcal{I} \geq \frac{P_{\mathrm{t}} A h_0 r^{-\eta} - \beta\sigma^2}{\beta}\right\} \\
&= \int_x \mathbb{1}\left\{\mathcal{I} \geq \frac{P_{\mathrm{t}} A h_0 r^{-\eta} - \beta\sigma^2}{\beta}\right\} f_{\mathcal{I}}(x) dx
\end{aligned} \tag{2.7}
$$

where $\mathbb{1}\{.\}$ is the indicator function. Using the Plancherel-Parseval theorem, the integral in (2.7) can be evaluated via the CF of the aggregate interference as in (2.6). Therefore, with the aid of the Plancherel-Parseval theorem, results for general fading environment can be obtained by stochastic geometry analysis. However, the main drawback here is that the integrals are quite involved due to the complex nature of the characteristic function of the aggregate interference. Hence, the stochastic geometry analysis loses its main merit which is the analytical tractability that leads to simple closed-form equations, and in turn, helps understanding the behavior of the tested system in response to variations in the design variables. Nevertheless, the Plancherel-Parseval theorem provides a mathematically elegant technique to extend all of the existing stochastic geometry results for general fading environments. It was used in [9, 10, 32, 42].

2.3.5 ***Technique*** #5*: Inversion*

In this technique, the LT, CF, or MGF is inverted to obtain the *pdf* of the interference [28–31, 40, 41, 69, 70]. Due to the complex nature of the expressions for the LT, CF, or MGF, generally the *pdf* of the aggregate interference cannot be obtained in closed form. This technique is only useful for very special cases of the PPP where

the expressions for LT, CF, or MGF are invertible or match the LT, CF, or MGF of a known distribution [28, 29, 31, 69, 70]; otherwise, inversion is done numerically [30, 40, 41]. For instance, the LT of the aggregate interference, measured at a receiver located at an arbitrary origin in $\mathbb{R}^d$, associated with an infinite PPP that starts from that arbitrary origin (i.e., there is no interference protection region around the receiver defined by the MAC layer) with unbounded path-loss function matches the LT of an alpha-stable distribution[4] [3, 4, 6, 7]. Although this result looks promising, it is not very useful because the unbounded path-loss results in a significant deviation from reality due to the singularity at the origin [30]. Hence, the interference does not have finite moments. Moreover, dealing with alpha-stable distributions is tricky since they do not provide a closed-form expression for the *pdf*. The only two exceptions where the *pdf* of interference has a closed-form expression can be found in [28] for deterministic channels, and in [29] for Rayleigh fading channels. Both the closed-form *pdf*s were obtained under the assumptions of an unbounded path-loss model, an infinite PPP, and path-loss exponent $\eta = 4$.

2.3.6 Summary and Taxonomy

Fig. 2.6 and Table 2.1 provide a taxonomy for the literature according to the target network model, the point process used, and the technique to utilize the LT, CF, or the MGF for performance evaluation. Note that if the same reference appears in different categories of the taxonomy, this means that this reference uses all of these techniques. The contributions of the thesis to each of the network types, analysis techniques, and point processes in Fig. 2.6 and Table 2.1 are highlighted, where the abbreviation "Ch" is used to denote the chapter which utilizes each technique and point process for the

[4] Alpha-stable distributions generalize Gaussian distributions and have heavier tails [8, Sec. 5.1], [4].

Table 2.1: Taxonomy of the literature based on the network type, point process used, and the technique used to obtain the performance metrics

Network Type	**Used PP**	**Performance Evaluation Techniques**				
		Technique #1	**Technique #2**	**Technique #3**	**Technique #4**	**Technique #5**
Ad hoc & IEEE 802.11	PPP	[25–27, 32–35]	[17–26, 35]	[70]	[32]	[28–31, 70]
	BPP	[37]	[38]	[37]	-	-
	HCPP	[46], Ch4	[43–45], Ch3	[43]	[42]	[40, 41]
	PCP	[39]	[39]	-	-	-
Single-tier & Multi-tier Cellular	PPP	[11, 12, 54–59], [61–65, 67, 76], [77] Ch5-Ch7	[66, 68]	[75]	-	[69]
	BPP	-	-	-	-	-
	HCPP	[76, 77], Ch5	-	-	-	-
	PCP	-	-	-	-	-
Cognitive	PPP	[76, 77, 79, 80, 82], Ch5, Ch6	[80]	[75, 81, 83]	-	-
	BPP	-	-	-	-	-
	HCPP	[76, 77, 82], [84, 85]Ch5	-	-	-	-
	PCP	[82]	-	-	-	-

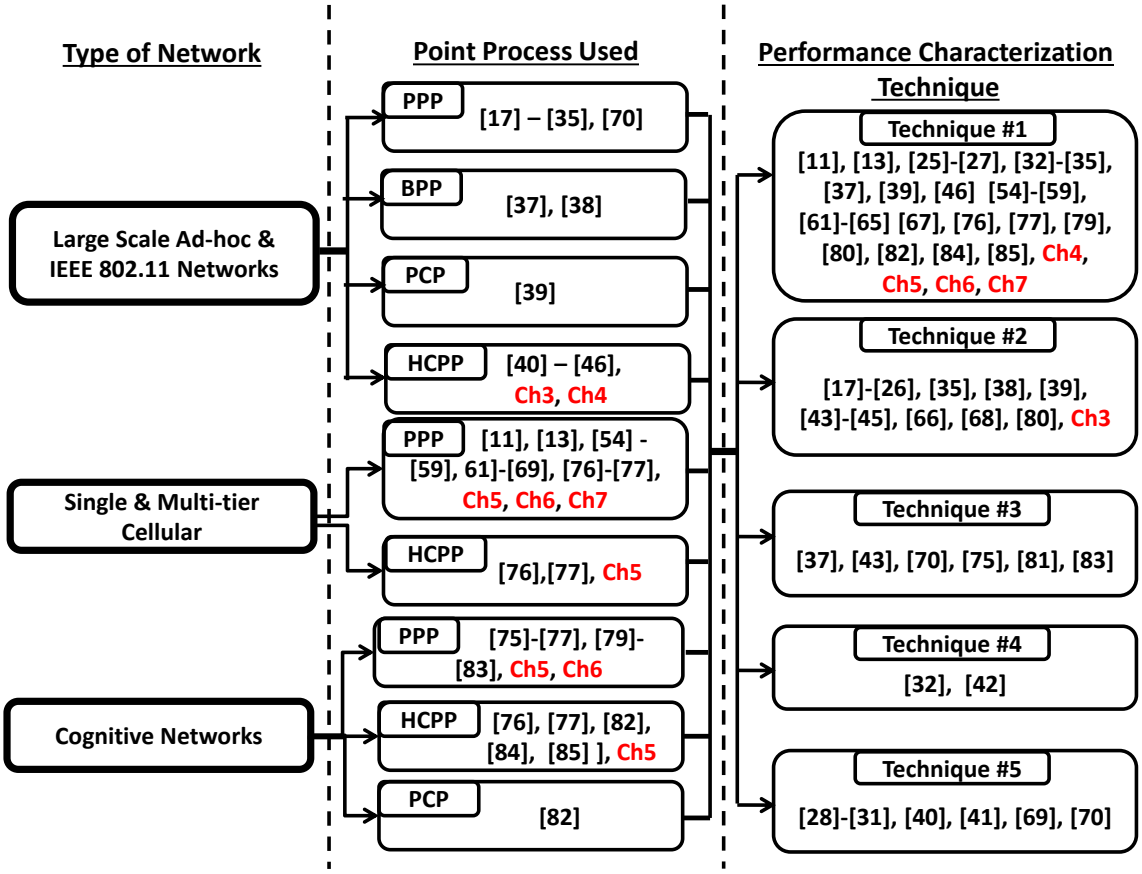

Figure 2.6: Taxonomy of the stochastic geometry-based models available in the literature for wireless networks.

given network type. The point processes and modeling techniques used for each of the networks addressed in this thesis are shown in Fig. 2.7.

The taxonomy in Fig. 2.6 and Table 2.1 clearly shows the popularity of each point process and each performance modeling technique. Fig. 2.6 and Table 2.1 show that the PPP is the most popular point process used in the literature because of its simplicity. Furthermore, the PPP provides accurate performance bounds and it is the parent point process for the HCPP and the PCP. The HCPP has also been extensively used to model wireless communication systems due to the hard core condition (i.e., the minimum distance r_{min}) which captures the contention-based spectrum access [40–51].

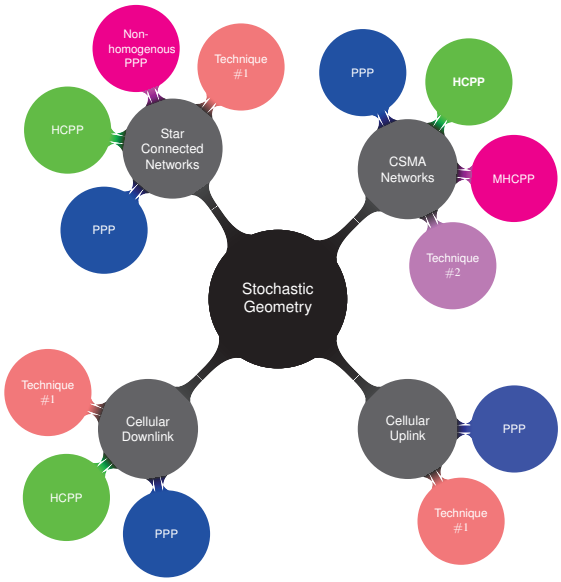

Figure 2.7: Point processes and techniques used in the thesis.

Furthermore, in [13], the authors showed that, compared to the PPP, the HCPP better captures the spatial distribution of the base stations in a real network deployment.

To summarize, in stochastic geometry modeling the locations of the network elements is modeled using point processes (PP). Then, the LT, CF, or the MGF of the aggregate interference is obtained. Up to this point, I have not shown how to obtain the LT, CF, or the MGF of the aggregate interference associated with the PP of interest because I have not yet introduced the required preliminaries to do the derivation. Finally, according to the accuracy, tractability, and practicability tradeoffs, one of the five techniques in the literature as discussed above is chosen to derive the performance metrics of interest from the LT, CF, or the MGF of the aggregate interference. Some examples that show when to use each of the five performance evaluation techniques are provided below.

- For a network with general fading in the interference links and Rayleigh fading

in the desired link, technique #1 is the right technique to use. As shown in Fig. 2.6 and Table 2.1, technique #1 has been extensively used in the literature because it is simple and gives the exact distribution for the SINR.

- If general fading is observed on the useful link, then a lower bound via technique #2 can be obtained. It is worth mentioning that the lower bound in technique #2 is generally tighter than the upper bounds [26]. Note that the accuracy of the lower bound increases for higher values of the path-loss exponent due to the faster signal power decay with distance which makes the effect of far interferers negligible.

- On the other hand, for lower values of the path-loss exponent, it is better to use technique #3 and have an approximate analysis. It has been shown that for the approximation of the *pdf* of interference, the shifted log-normal distribution is better than both the Gaussian and log-normal distributions [75, 81]. However, there is no known method to validate the approximation except by simulations.

- With general fading in the direct (i.e., useful) link, if an exact analysis is required, then technique #4 has to be used, but the analysis will be highly involved. From Fig. 2.6 and Table 2.1 it can be observed that technique #4 has not been frequently used in the literature due to its analytical complexity.

- Finally, technique #5 is only limited to some special cases as far as only the analytical evaluation is concerned.

To this end, I have introduced stochastic geometry modeling and classified the different modeling techniques used in the literature. The next chapter is the first chapter presenting the core contribution of the thesis. In the next chapter, I model

CSMA based ad hoc networks via the stochastic geometry and propose a paradigm to optimize the spectrum sensing threshold for the CSMA protocol.

Chapter 3

Characterizing Random CSMA Ad Hoc Networks

In this chapter, I characterize the random carrier sensing multiple access (CSMA) wireless networks by statistically quantifying the intensity of simultaneously active nodes and outage probability experienced by a generic node in the network. At first, I will show how the effect of the CSMA medium access control (MAC) protocol on the network topology is captured by the stochastic geometry analysis. In particular, I will show that the CSMA MAC protocol coordinates the spectrum access and brings correlations between the spatial locations of the set of simultaneously active transmitters. Consequently, the simple PPP (defined in Sec. 2.1.2) cannot be used for modeling, analysis, and design of CSMA protocol. Instead, the HCPP (defined in Sec. 2.1.5) is used because it captures the correlations imposed by the CSMA protocol. The Matérn HCPP type II (defined in Sec. 2.1.5) has been extensively used to model the spatial distribution of the simultaneously active nodes in CSMA networks. However, Matérn HCPP type II suffers from underestimating the intensity of simultaneously active transmitters [48, 51, 86, 87], and its intensity underestimation flaw

has not been really addressed in the literature. In this chapter, I propose a second order estimation method to determine the intensity of the hard core process, namely, the Modified HCPP (MHCPP). The MHCPP mitigates the well-known problem of underestimating the intensity of the simultaneously active nodes. Using the proposed MHCPP, I will show that the spectrum-sensing threshold is a very critical design parameter that should be chosen very carefully to maintain the balance between the spatial frequency reuse efficiency and the outage probability. To this end, I will provide insights for the spectrum-sensing (also denoted by carrier-sensing) threshold optimization.

3.1 Introduction

In distributed wireless networks with random node locations (e.g., ad-hoc/sensor networks, cognitive femtocell networks), a decentralized MAC protocol is required to control the access of the network nodes to the shared wireless spectrum in order to limit the mutual interference. CSMA protocols are very popular for this type of networks. In comparison to other popular multiple access techniques such as time-division multiple access (TDMA), frequency-division multiple access (FDMA), code-division multiple access (CDMA), and orthogonal frequency-division multiple access (OFDMA) [91], CSMA distinguishes itself with its distributed nature in coordinating the spectrum access. Moreover, with the introduction of cognitive radio, CSMA protocols will be used by secondary users on top of other multiple access protocols such as OFDMA to avoid interfering with primary users and coordinate spectrum access among the secondary users.

In CSMA networks, each transmitter having a packet to transmit generates a random backoff timer that decreases only when the channel is sensed idle and freezes

when the channel is sensed busy. The transmitter cannot access the channel to transmit its packet until the backoff timer expires. The channel busy/idle decision is based on the spectrum-sensing threshold defined by the CSMA protocol. From a geometric point of view, the spectrum-sensing threshold defines both the contention domain for each transmitter and the minimum distance between simultaneously active transmitters. The lower the spectrum-sensing threshold the higher the sensitivity of each transmitter to other transmissions occurring in the spatial domain, which increases the distances between simultaneously active transmitters and decreases the mutual interference at the expense of decreasing the spatial frequency reuse. Due to the randomness of the node locations as well as the channel fading conditions, the signal-to-interference-plus-noise ratio (SINR) experienced by a generic receiver in the network is random. Therefore, for a chosen spectrum-sensing threshold, there is a non-zero probability that the received SINR falls below the threshold for correct signal reception and the receiver goes into an outage. We define the frequency reuse efficiency as the ratio between the intensity of simultaneously active transmitters and the total intensity of the coexisting transmitters. In order to study the trade-off between the spatial frequency reuse efficiency and the outage probability, both of these performance metrics should be accurately estimated in terms of the spectrum-sensing threshold. As I will show later, the spectrum-sensing threshold is a very critical parameter that should be chosen very carefully to maintain the balance between the frequency reuse efficiency and the outage probability.

3.1.1 Stochastic Geometry Modeling for CSMA Networks

The CSMA protocol coordinates the spectrum access and thereby correlates the positions of the simultaneously active transmitters. Therefore, the HCPP (defined in

Sec. 2.1.5), is used to model the positions of the simultaneously transmitting nodes. There are two types of the HCPP, the Matérn HCPP type I and the Matérn HCPP type II (or simply type I and type II). Although the construction of these two types of HCPP are different, both result in a legitimate HCPP but with different intensities (i.e., no two points will coexist within a distance less than r_{min}). Starting from a *primary* PPP, type I is the *secondary* point process constructed by deleting all the primary points that coexist with a distance less than the hard core parameter r_{min}. Assuming that there is a time mark attached to each *primary* point, type II is the *secondary* point process constructed by deleting the *primary* points that coexist within a distance less than the hard core parameter r_{min} from another *primary* point having a lower time mark. It can be observed that type I only accounts for retaining the isolated primary points (i.e., points which are at least r_{min} away from every other point in the process). However, type II captures the contention among the *primary* points to be retained in the *secondary* HCPP. The contention is performed by means of the random time mark, where a *primary* point in the *primary* PPP is retained in the *secondary* type II point process if and only if (iff) it has the lowest time mark among the *primary* points coexisting within a distance of r_{min}, and deleted otherwise. Projecting to the CSMA networks, the *primary* PPP corresponds to the locations of the complete set of coexisting transmitters contending to access the spectrum, the time mark corresponds to the backoff timer randomly generated by the CSMA protocol for each transmitter, and the *secondary* type II point process can be used to model the locations of the subset of simultaneously active transmitters that win the contention and access the spectrum. The estimated intensity of the simultaneously active transmitters reflects the spatial frequency reuse efficiency and can be used to estimate the outage probability.

However, type II model suffers from underestimating the intensity of simultaneously active transmitters [48,51,86,87]. The main reason for this underestimation flaw is that type II accounts only for the points having the lowest mark in their contention domains. This means that the freezing property of the backoff counter in the CSMA protocol is not captured in the model to calculate the intensity of the simultaneously active transmitters. In a CSMA network, a transmitter can still access the channel if it does not have the lowest backoff timer in its contention domain given that all of the transmitters with lower backoff timers have frozen their timers due to transmissions in their own contention domains. The property of freezing the backoff counter can be captured by a third type of the repulsive HCPP, named, Matérn HCPP type III (or simply type III). Assuming that there is a time mark attached to each *primary* point, type III is constructed by deleting the *primary* points that coexist within a distance less than the hard core parameter r_{min} from another *secondary* point having a lower mark. The main difference between type III and type II is that type III involves a condition on the deleting probability (i.e., the complement of the retaining probability). That is, for constructing a type III process, a *primary* point (p_i) is deleted iff it lies within a distance r_{min} from another *primary* point (p_j) conditioning that the latter *primary* point (p_j) will not be deleted, and retained otherwise. Projecting to CSMA networks, a transmitter (t_1) will not access the spectrum (i.e., freeze its backoff counter) iff it lies within the sensing range of another transmitter (t_2) with a lower backoff timer conditioning on that the timer of the later transmitter (t_2) is not frozen (i.e., conditioning on that transmitter t_2 will succeed to access the spectrum). This condition will completely capture the freezing property of the CSMA backoff counter, however, it involves a chain of correlations among the *primary* points (transmitters) which terminates when it reaches a point (transmitter) which has the lowest mark

among all points (transmitters) with a separating distance less than r_{min}. This is why Matérn stopped discussing type III point process and stated that '*even an attempt to find its packing density tends to rather formidable mathematics*'. However, inspired by the definition of type III HCPP, I go one step in the correlation chain and propose my modified HCPP, as will be presented later.

3.1.2 Motivation and Contribution

In the context of wireless communications, type II has been extensively used to model the spatial distribution of the simultaneously active nodes in CSMA networks. However, the intensity underestimation flaw of type II has not been really addressed in the literature. This flaw was only mentioned in [48,51], but there was no effort to mitigate this flaw. In this chapter, my objective is to shed light on the underestimation flaw of type II point process, quantify it, and provide a one step towards mitigating it. We propose a second-order intensity estimation method that partially takes the backoff counter freezing property into consideration and reduces the *underestimated intensity* due to type II modeling (i.e., the gap between type II intensity and the actual intensity obtained by simulation) by at least 30%. The proposed method is generalized for a general fading environment. For brevity, hereafter I will use the classical HCPP (CHCPP) and the Modified HCPP (MHCPP) to denote, respectively, type II HCPP and the proposed 2^{nd} order estimation for the HCPP under general fading environment. Since I am using point processes to model the spatial distribution of nodes, I will use the terms 'a node in the network' and 'a point in the point process' interchangeably.

The main contributions of this work are as follows:

- The CHCPP model is generalized for fading channels.

- We demonstrate the node intensity underestimation flaw of the CHCPP model and propose a novel MHCPP which is generalized for general fading channels.
- Closed-form expressions are obtained for the intensity of the simultaneously active transmitters for both the point processes, namely, the CHCPP and the MHCPP.
- An expression for the approximate outage probability is obtained, and subsequently, the transmission capacity of the network is analyzed.

3.2 Related Work

In the literature, interference modeling for PPP has been sufficiently addressed, characterized and well understood (cf. Fig. 2.6). On the other hand, due to the added complexity, only a few works on HCPP exist. In the following, I review the work closely related to the work presented in this chapter.

In [40, 42], the authors extended the hard core point process model to Rayleigh fading environment. Then, an approximate expression for the Laplace functional of the aggregate interference experienced by the test node at the origin was obtained. In [41], the authors extended the model in [40] beyond the spatial averages of the performance metrics and obtained their distributions. They also relaxed the PPP assumption for the initial network setup. In [44], the authors incorporated Poisson distributed traffic into their model and optimized the spectrum-sensing threshold to maximize the spatial frequency reuse subject to an outage probability constraint. However, the intensity of the simultaneously active transmitters in CSMA networks was obtained via an iterative algorithm and only deterministic channel gains were assumed. In [92], the authors were able to extend the HCPP to capture the logical

carrier sensing for CSMA/CA protocol. A common approach in all of these works is that the contention-resolution process follows type II point process which suffers from the node intensity underestimation problem.

In [43], the authors derived the transmission capacity when applying a guard zone around the active receivers. However, the expression for Matérn hard core point process type I was used which highly underestimates the nodes intensity [48, 49]. In [88], the authors developed a model to characterize the asymptotic behavior of the outage probability in a large-scale ad-hoc network for a wide range of MAC protocols and general spatial distribution of nodes; however, it is valid only for high SINR regime (i.e., when intensity $\rightarrow 0$). Different from all of the above work in the literature, in this chapter, I propose a novel method to modify the classical HCPP in order to mitigate the well-known node intensity underestimation flaw.

3.3 System Model and Assumptions

We consider that the transmitter-receiver pairs in the network are distributed in an infinite 2-D plane according to a marked Poisson bipolar model [21, 32, 44]. In this model, $\mathbf{\Psi}_T = \{(x_i, m_i); i = 1, 2, 3, ...\}$ is a marked PPP, where the points $\mathbf{X} = \{x_i; i = 1, 2, 3, ...\}$ constitute a PPP with intensity λ_T in the $\mathbb{R}^2$ plane, and the time marks $\{m_i; i = 1, 2, 3, ...\}$ are independent from each other, independent from $\mathbf{X}$ and uniformly distributed in the range $[0, 1]$[1]. The point process $\mathbf{X}$ represents the spatial distribution of the potential transmitters in the network, where x_i denotes the position of the i^{th} transmitter in the $\mathbb{R}^2$ plane[2]. Throughout this chapter, I will say that the

[1] As proved in [87], assuming a uniform distribution for the time marks does not affect the generality of the model.

[2] We will use x_i to denote both the location of the i^{th} transmitter and the transmitter itself, and the notation r_{x_i} to denote both the location of the receiver attached to the transmitter x_i and the receiver itself.

transmitter x_i is older than the transmitter x_j (or equivalently x_j is younger than x_i) to denote that $m_i > m_j$. Each transmitter x_i has an associated receiver r_{x_i} located at a fixed distance R in a random direction (the receivers are not part of the PPP). R can be viewed as the average hop distance in a distributed multi-hop ad hoc network. Relaxing this assumption complicates the analysis without providing additional insights [21]. There is only one channel for the network operation, and each transmitter accesses this channel by means of a physical CSMA protocol to transmit infinitely-backlogged packets (i.e., saturation conditions are assumed) and all transmitters transmit with the same power P_t.

Let $P(x, y) = P_t\mathcal{D}(x, y)h(x, y))$ denote the power received at a location y from a transmitter located at x, where $\mathcal{D}(x, y)$ is the power gain due to bounded path-loss channel model between the two positions x and y and is given by [27]

$$\mathcal{D}(x,y) = \begin{cases} Ar_o^{-\eta}, & \|x-y\| < r_o \\ A\ \|x-y\|^{-\eta}, & \|x-y\| \geq r_o \end{cases} \tag{3.1}$$

where A is a propagation constant, $r_o > 0$ (e.g., $r_o = 1$), η is the path-loss exponent ($\eta > 2$), and $\|.\|$ is the Euclidean norm. In order to simplify the notations, I will denote $\max(r_o, \|x - y\|)$ by $dist(x, y)$. The random variable $h(x, y)$ represents the random channel (power) gain due to multi-path fading between the two locations x and y. The channel gains are assumed to be stationary, ergodic, symmetrical, independent from each other, independent from the locations (x and y), and identically distributed (i.i.d.) with probability density function (*pdf*) $f_h(h)$, cumulative distribution function (*cdf*) $F_h(h)$, and have finite first moment (i.e., $\int_{-\infty}^{\infty} hf_h(h) < \infty$). Block channel fading is assumed, where the channel gains are constant during the contention-resolution process and packet transmission. In other words, the channel coherence time is greater

than or equal to the contention resolution time plus the packet transmission time.

Each transmitter in the network contends with its neighbor nodes via the CSMA protocol to access the shared wireless channel[3]. For a generic transmitter $(x_i, m_i) \in \mathbf{\Psi}_T$, the neighborhood set $\mathbf{N}_{x_i} = \{(x_j, m_j) \in \mathbf{\Psi}_T | P(x_i, x_j) \geq \upsilon_s\}_{j \neq i}$ is defined as the set containing the nodes which receive x_i's signal power with a value greater than the spectrum-sensing threshold υ_s. Due to the symmetric channel gain, if a node is in the neighborhood set of x_i, then x_i is in the neighborhood set of that node. As will be discussed later, due to the system complexity, I will resort to the region bounds (i.e., technique #2 described in Sec. 2.3) to get the performance metrics. Therefore, I define the set of dominant interferers $\mathbf{I}_{x_i}^{(d)} = \left\{ x_j \in \mathbf{X} | \frac{h(x_i, r_{x_i}) \ dist(x_j, r_{x_i})^{\eta}}{h(x_j, r_{x_i}) \ R^{\eta}} < \beta \right\}_{j \neq i}$ as the set in which each of its members can alone corrupt the signal received at the receiver associated with x_i. In other words, a dominant interferer is a transmitter located within the vulnerability region of the receiver under observation.

3.4 Methodology of Analysis

In the considered network model, there are two sources of randomness. One is due to the random spatial distribution of the nodes and the other is due to the random channel gains. On the contrary, when assuming deterministic channel gains [43,44,51], there is only one source of randomness due to the spatial distribution of the nodes. Hence, it is possible to study certain events through studying the spatial statistics over a regular shaped area. For instance, if deterministic channel gains are assumed, the neighborhood set $\mathbf{N}_{x_i}$ of a generic node $(x_i, m_i) \in \mathbf{\Psi}_T$ consists of the nodes which coexist with x_i in $\mathbf{B}_{x_i}(r_s)$, where r_s is the spectrum-sensing range and is computed as $r_s = \left(\frac{P_t A}{\upsilon_s}\right)^{1/\eta}$. In the same manner, the crescent shaped area where the nodes

[3]For a generic transmitter x_i, I will use the term "neighborhood" to denote its contention domain and the term "neighbors" to denote the set of nodes belonging to that contention domain.

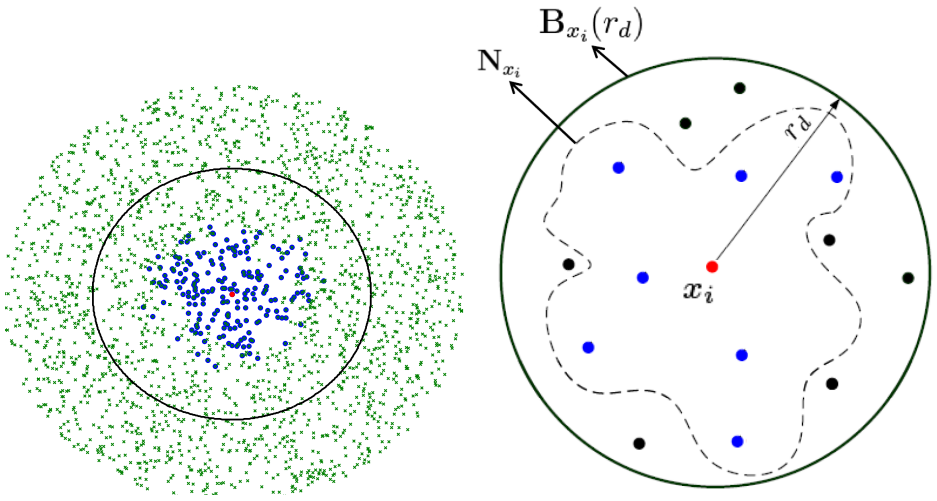

Figure 3.1: (a) Due to random channel gains there is no regular shaped separator between the neighbors (darker nodes) and non-neighbors (represented by lighter nodes) of the node at the centre of the circle, (b) a schematic representation for the random shape containing the neighbors of the center node.

in the set of dominant interferers $\mathbf{I}_{x_i}^{(d)}$ are located can be determined (sec. IV in [44]). Consequently, the average can be only taken over the spatial distribution in the area where the event of interest is located to obtain the probability that this event occurs. On the other hand, when considering fading channels, the previously mentioned methodology is not applicable, since the event of interest can not be related to a regular shaped area. Instead, each event is related to a dynamically changing random-shaped area (as shown in Fig. 3.1) which is determined by the instantaneous channel gains.

The main idea to overcome this difficulty is to bound my observation region (e.g., a circle with deterministic radius r_d) and search for the nodes that contribute to the event of interest. Hence, the spatial statistics within the deterministic observation region can be obtained. Then, the contribution of each node within the deterministic observation region to the event of interest will be Bernoulli distributed with a pa-

rameter that accounts for both the large-scale distance (location)-dependent fading and the small-scale fading. For instance, the neighborhood set of a generic transmitter x_i lies in a random shaped region which is unbounded in theory due to the infinite support domain of the *pdf* of channel power gain. However, the distribution of the number of transmitters in the neighborhood set can still be determined by bounding my observation region by $\mathbf{B}_{x_i}(r_d)$, where r_d is sufficiently large such that the probability for a transmitter located beyond r_d to become a neighbor of x_i is negligible (i.e., $\mathbb{P}\left\{\frac{P_t A h(x_i,x_j)}{dist(x_i,x_j)^\eta} \geq \upsilon_s | dist(x_i,x_j) > r_d\right\} \approx 0$). Then, due to small-scale fading, a transmitter $x_j \in \mathbf{\Psi}_T \cap \mathbf{B}_{x_i}(r_d)$ is in $\mathbf{N}_{x_i}$ iff $h(x_i,x_j) \geq \frac{\upsilon_s dist(x_i,x_j)^\eta}{P_t A}$ (i.e., x_j have a sufficiently high channel gain to keep the received signal power above υ_s when received at x_i). Mathematically, r_d can be calculated as follows: take a small value ϵ (e.g., $\epsilon = 10^{-6}$) such that $\mathbb{P}\left\{\frac{P_t A h(x_i,x_j)}{r_d^\eta} \geq \upsilon_s\right\} \leq \epsilon$ and calculate r_d as: $r_d = \left(\frac{P_t A}{\upsilon_s}\bar{F}_h^{-1}(\epsilon)\right)^{1/\eta}$, where $\bar{F}_h^{-1}(.)$ is the inverse of the complementary cumulative distribution function (*ccdf*) of the fading distribution. Now the neighborhood set can be redefined as $\mathbf{N}_{x_i} = \{(x_j,m_j) \in \mathbf{\Psi}_T \cap \mathbf{B}_{x_i}(r_d) | P(x_i,x_j) \geq \upsilon_s\}_{j\neq i}$ as shown in Fig. 3.1. Due to the infinite support domain of the *pdf* of channel power gain, no matter how big r_d is, the bounding approach will give a lower bound to the number of transmitters in the neighborhood set of x_i. However, due the finite first moment of the *pdf* of channel power gain, it can be proven (cf. **Appendix A.1**) that with the properly chosen r_d the probability $\mathbb{P}\{x_j \in \mathbf{N}_{x_i} | \, \|x_i - x_j\| > r_d\}$ becomes negligible and my approach is almost exact (as will be shown through numerical results presented later in this chapter).

Hereafter, the term *neighborhood success probability* is used to denote the probability that two transmitters in the *primary* PPP become neighbors. Note that different *neighborhood success probabilities* are defined based on the po-

sitions of the two transmitters with respect to (w.r.t.) each other (see Fig. 3.4). For instance, $\mathcal{P}_\upsilon = \mathbb{P}\{P(x_i, x_j) \geq \upsilon_s | x_j \in \mathbf{B}_{x_i}(r_d)\}$ is the *neighborhood success probability* between x_i and any other transmitter located inside $\mathbf{B}_{x_i}(r_d)$, $\mathcal{P}_\upsilon^* = \mathbb{P}\{P(x_j, x_k) \geq \upsilon_s | x_j, x_k \in \mathbf{B}_{x_i}(r_d)\}$ is the *neighborhood success probability* between any two transmitters located inside $\mathbf{B}_{x_i}(r_d)$, and $\mathcal{P}_\upsilon^{**} = \mathbb{P}\left\{P(x_j, x_k) \geq \upsilon_s | x_j \in \mathbf{B}_{x_i}(r_d), x_k \in \mathbf{B}_{x_j}(r_d) \setminus \mathbf{B}_{x_i}(r_d)\right\}$ is the *neighborhood success probability* between a transmitter x_j located in $\mathbf{B}_{x_i}(r_d)$ and any other transmitter located in the crescent shaped area defined by $\mathbf{B}_{x_j}(r_d) \setminus \mathbf{B}_{x_i}(r_d)$. The three probabilities ($\mathcal{P}_\upsilon$, $\mathcal{P}_\upsilon^*$, and $\mathcal{P}_\upsilon^{**}$) are calculated in Sec. 3.5.3.

Although the bounding approach is not the only method to deal with the random fading problem (see Sec. 3 in [40] and Sec. 4.1 in [7]), the bounding approach used in this chapter is exact (cf. **Appendix A.1**), independent of r_d when chosen properly, and facilitates analysis of the modified HCPP.

3.5 Modeling CSMA Networks by the Classical and Modified Hard Core Point Processes

The aim of this section is to derive the intensity of the simultaneously active transmitters through constructing the classical HCPP and the modified HCPP in a general fading environment. For the sake of better readability and ease of understanding, I divide the analysis of both the HCPPs into two main parts. In the first part, the problem is formulated and solved in terms of some parameters that are assumed to be available. In the second part, I calculate these parameters. These parameters are the three neighborhood success probabilities defined in the system model (i.e., $\mathcal{P}_\upsilon$, $\mathcal{P}_\upsilon^*$, and $\mathcal{P}_\upsilon^{**}$).

3.5.1 Generalizing the Classical Hard Core Point Process (CHCPP)

Let $\mathbf{\Psi}_{CSMA}^{C}$ be the *secondary* point process derived from the *primary* PPP $\mathbf{\Psi}_T$ using the CHCPP approach. To generalize the CHCPP to general fading environments, the notion of the minimum distance r_s, which is used in the construction of the CHCPP, should be replaced with the notion of the received signal power. However, the same construction methodology is used. A generic transmitter $(x_i, m_i) \in \mathbf{\Psi}_T$ is retained in $\mathbf{\Psi}_{CSMA}^{C}$ if and only if it has the lowest mark in its neighborhood set $\mathbf{N}_{x_i}$, where the neighborhood set $\mathbf{N}_{x_i}$ is bounded by a dynamically changing random-shaped region defined by the instantaneous channel gains. Applying the spatial and channel gain statistics to $\mathbf{\Psi}_T$, I obtain the following theorem:

Theorem 3.5.1. *In a random CSMA network under general fading environment, the retaining probability of a generic node $(x_i, m_i) \in \mathbf{\Psi}_T$ in $\mathbf{\Psi}_{CSMA}^{C}$ is given by $P_{CSMA}^{C} = \frac{1-e^{-\mathcal{N}\mathcal{P}_v}}{\mathcal{N}\mathcal{P}_v}$, where $\mathcal{N} = \lambda_T \pi r_d^2$ is the expected number of nodes in the disc $\mathbf{B}_{x_i}(r_d)$ and the deterministic radius r_d is defined in Sec. 3.3. The intensity of $\mathbf{\Psi}_{CSMA}^{C}$ (i.e., simultaneously active transmitters) is given by $\lambda_{CSMA}^{C} = \lambda_T P_{CSMA}^{C} = \frac{1-e^{-\mathcal{N}\mathcal{P}_v}}{\pi r_d^2 \mathcal{P}_v}$.*

Proof. A generic point $(x_i, m_i) \in \mathbf{\Psi}_T$ is retained in $\mathbf{\Psi}_{CSMA}^{C}$ if and only if it has the lowest mark in its neighborhood set $\mathbf{N}_{x_i}$. If x_i has n neighbors, due to the uniform distribution of the marks among x_i's neighbors, the probability that x_i has the lowest mark is $\frac{1}{n+1}$. Let P_k be the probability of having k points coexisting with x_i in $\mathbf{B}_{x_i}(r_d)$. From the PPP assumption, I have $P_k = \frac{e^{-\lambda_T \pi r_d^2} (\lambda_T \pi r_d^2)^k}{k!} = \frac{e^{-\mathcal{N}} \mathcal{N}^k}{k!}$. Averaging

over both spatial and channel gain statistics I obtain

$$\begin{aligned} P_{CSMA}^{C} &= \mathbb{P}\left\{x_i \text{ is retained in } \mathbf{\Psi}_{CSMA}^{C}\right\} \\ &= \sum_{n=0}^{\infty} \frac{1}{n+1} \sum_{k=n}^{\infty} P_k \binom{k}{n} \mathcal{P}_{\upsilon}^{n} (1-\mathcal{P}_{\upsilon})^{k-n} \\ &\overset{(*)}{=} \sum_{n=0}^{\infty} \frac{1}{(n+1)!} \mathcal{P}_{\upsilon}^{n} \sum_{m=0}^{\infty} \frac{e^{-\mathcal{N}} \mathcal{N}^{m+n}}{m!} (1-\mathcal{P}_{\upsilon})^{m} \\ &= \frac{e^{-\mathcal{N}}}{\mathcal{N}\mathcal{P}_{\upsilon}} \sum_{n=0}^{\infty} \frac{(\mathcal{N}\mathcal{P}_{\upsilon})^{n+1}}{(n+1)!} \sum_{m=0}^{\infty} \frac{(\mathcal{N}(1-\mathcal{P}_{\upsilon}))^{m}}{m!} \\ &= \frac{1-e^{-\mathcal{N}\mathcal{P}_{\upsilon}}}{\mathcal{N}\mathcal{P}_{\upsilon}} \end{aligned} \tag{3.2}$$

where $\binom{k}{n}\mathcal{P}_{\upsilon}^{n}(1-\mathcal{P}_{\upsilon})^{k-n}$ in the second line of (3.2) means that out of the k coexisting nodes in $\mathbf{B}_{x_i}(r_d)$, only n of them satisfy the neighborhood requirement (i.e., have sufficiently high channel gain to keep the received power at x_i from each of these n nodes greater than the spectrum-sensing threshold υ_s). In $(*)$ in (3.2), let $m = k-n$, and then substitute every k with $m+n$. □

It is worth mentioning that if a deterministic channel gain is assumed (i.e., $r_d = r_s$ and $\mathcal{P}_{\upsilon} = 1$), the model reduces to type II [1]. The main drawback of the CHCPP is that the contention-resolution process is resolved locally and the backoff timer freezing property is not captured. That is, a transmitter qualifies for transmission if and only if it has the lowest mark among its neighbors. Hence, the CHCPP underestimates the intensity of the simultaneously active transmitters [48, 86, 87].

As an example, in Fig. 3.2, according to the definition of the CHCPP, only the points with marks 0.1, 0.2, 0.9 are retained. The point with the mark 0.5 is deleted because it does not have the lowest mark in its contention domain (despite the fact that the point with the mark 0.3 will be deleted). It can be observed that the unse-

lected points (i.e., points which will be deleted) of the *primary* PPP still play a role in the selection process for the points to be retained in the *secondary* CHCPP. The role of the unselected points results in the underestimation problem of the CHCPP. Therefore, just looking into the contention domain of the point with the mark 0.5 does not convey the fact that the point with the mark 0.3 will be deleted. However, including the own contention domain of the point with the mark 0.3 conveys this fact. This means that there are spatial correlations among points lying in different contention domains, which is not captured by the CHCPP. Projecting this problem to the CSMA network, if the node with the backoff timer value of 0.2 qualifies for transmission[4], the node with the backoff timer value 0.3 should freeze its backoff counter which enables the node with the backoff timer value 0.5 to qualify for transmission as well.

Intuitively, the scenario described above may not appear for small intensities of the *primary* PPP, high values of the spectrum-sensing threshold, or for environments with severe channel fading conditions. However, when the intensity of the *primary* PPP increases, and/or the spectrum-sensing threshold decreases, and/or the channel condition becomes better, the number of nodes involved in the contention-resolution process increases, and it becomes more likely to have events similar to the one described in Fig. 3.2. Therefore, as the number of transmitters involved in the contention domain increases, the underestimation problem of the CHCPP aggravates and highly reduces the estimated density of the CHCPP (as will be evident from the numerical results). The inaccurate estimation of the number of interferers directly affects the estimation of the aggregate interference and the outage probability.

[4]This can be interpreted as a normalized version of the backoff timer value, which is an integer in practice.

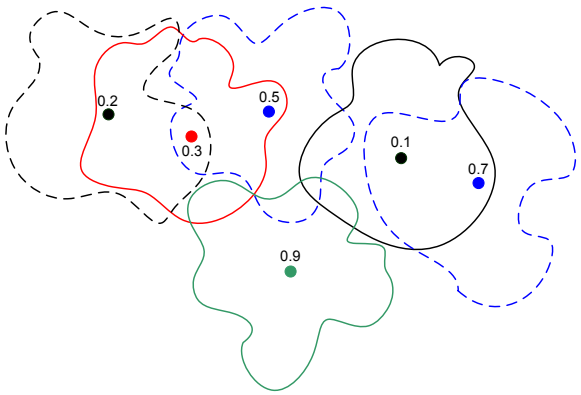

Figure 3.2: The underestimation flaw of the CHCPP.

3.5.2 The Generalized Modified Hard Core Point Process (MHCPP)

The main idea to mitigate the flaw of the CHCPP modeling approach is to reduce the role of the unselected points in the retaining probability by going one step further into the correlation chain defined by type III. Let $\mathbf{\Psi}_{CSMA}^{M}$ be the *secondary* point process derived from the *primary* PPP $\mathbf{\Psi}_T$ using the MHCPP. The role of unselected points can be reduced by adding following condition to the definition of the CHCPP. A generic point $(x_i, m_i) \in \mathbf{\Psi}_T$ is retained in $\mathbf{\Psi}_{CSMA}^{M}$ if it has the lowest mark among its neighbors $\mathbf{N}_{x_i}$, or if it has the second-lowest mark among its neighbors $\mathbf{N}_{x_i}$ given that the point with the lowest mark is freezing its backoff counter. (i.e., the point with the lowest mark will be deleted). More formally, a generic point $(x_i, m_i) \in \mathbf{\Psi}_T$ is retained in $\mathbf{\Psi}_{CSMA}^{M}$ if and only if: (i) $(m_i < m_j, \forall (x_j, m_j) \in \mathbf{N}_{x_i})$, or (ii) $(m_i > m_L | (x_L, m_L) \in \mathbf{N}_{x_i})$ and $(m_i < m_j, \forall (x_j, m_j) \in \mathbf{N}_{x_i} \setminus \{(x_L, m_L)\})$ given that $(m_L > m_m, \exists (x_m, m_m) \in \mathbf{N}_{x_L} \setminus \mathbf{N}_{x_i})$. The last condition $(m_L > m_m, \exists (x_m, m_m) \in \mathbf{N}_{x_L} \setminus \mathbf{N}_{x_i})$ means that there exist at least one younger point than x_L in $\mathbf{N}_{x_L} \setminus \mathbf{N}_{x_i}$. Note that I am only considering the points $\mathbf{N}_{x_L} \setminus \mathbf{N}_{x_i}$ to have lower marks than x_L as I have already conditioned that x_L has the lowest mark in $\mathbf{N}_{x_i}$. It is clear that the added condition

to the retaining probability in the MHCPP brings correlation between a node x_i and its second degree neighbors[5] w.r.t. x_L and takes the model one step towards type III. Hereafter, I will denote by x_L the node with the lowest mark in $\mathbf{N}_{x_i}$ when x_i has the second lowest mark. From the perspective of a CSMA network, this means that one of the 2^{nd} degree neighbors of x_i w.r.t. x_L is transmitting. Consequently, x_L freezes its backoff timer, and therefore, x_i is able to access the channel.

One of the main problem introduced by fading for the MHCPP is to estimate the number of the 2^{nd} degree neighbors of x_i w.r.t. x_L (i.e., the set $\mathbf{N}_{x_L} \setminus \mathbf{N}_{x_i}$). In this context, one of the main problems is that there is no closed-form expression (even for the simple Rayleigh fading channels) for the distribution of distance between two neighboring transmitters x_i and x_L considering the spatial correlation due to random fading (i.e., channel gain statistics). Therefore, I will ignore the effect of fading on the distribution of distance between the two neighboring transmitters x_i and x_L[6]. That is, I will assume that the distribution of the random distance (z) between the two neighbor transmitters x_i and x_L is given by$f_z(z) = \frac{2z}{r_d^2}$, $0 \leq z \leq r_d$ as given in [28] for deterministic channel gains. Then, I divide the set of x_i's 2^{nd} degree neighbors w.r.t. x_L (i.e., $\mathbf{N}_{x_L} \setminus \mathbf{N}_{x_i}$) into two subsets. The first subset is $\mathbf{N}_{x_L}^{in} = \mathbf{N}_{x_L} \cap (\mathbf{B}_{x_i}(r_d) \setminus (\mathbf{N}_{x_i} \cup \{x_i\}))$ that contains the neighbors of x_L inside the disc $\mathbf{B}_{x_i}(r_d)$ which are not in the neighborhood set of x_i (such as point x_1 in Fig. 3.3). The second subset is $\mathbf{N}_{x_L}^{out} = \mathbf{N}_{x_L} \setminus \mathbf{B}_{x_i}(r_d)$, which contains the neighbors of x_L outside $\mathbf{B}_{x_i}(r_d)$ but inside the shaded region $A_r(z)$ in Fig. 3.3 (such as point x_2). Applying the spatial and channel gain statistics to $\mathbf{\Psi}_T$, I have the following theorem:

Theorem 3.5.2. *In a random CSMA network under general fading environment,*

[5]A generic point x_j is denoted as a 2^{nd} degree neighbor to x_i w.r.t. x_L if $x_j \in \mathbf{N}_{x_L} \setminus \mathbf{N}_{x_i}$, given that $x_L \in \mathbf{N}_{x_i}$.

[6]The effect of this approximation will be discussed in Sec. 3.7.2.

the retaining probability of a generic node $(x_i, m_i) \in \mathbf{\Psi}_T$ *in* $\mathbf{\Psi}^M_{CSMA}$ *is given by:* $P^M_{CSMA} = P^C_{CSMA} + P_{in} + P_{out} - P_{in}P_{out}$*, where* P_{in} *and* P_{out} *denote the probabilities that a younger point than* x_L *exists in* $\mathbf{N}^{in}_{x_L}$ *and* $\mathbf{N}^{out}_{x_L}$*, respectively, when* x_i *has the second lowest mark in* $\mathbf{N}_{x_i}$*(i.e.,* x_L *freezes its backoff timer and postpones its transmission).* P_{in} *is given by*

$$P_{in} = \frac{\mathcal{N}^*_v \left(1 - e^{-(\mathcal{N}_v + \mathcal{N}^*_v)}\right)}{\mathcal{N}_v(\mathcal{N}_v + \mathcal{N}^*_v)} + e^{-\mathcal{N}_v}\left(\frac{(\mathcal{N}^*_v - \mathcal{N}_v)(e^{-\mathcal{N}^*_v} - 1)}{\mathcal{N}_v\mathcal{N}^*_v} - 1\right) \quad (3.3)$$

and P_{out} *is given by*

$$P_{out} = \frac{\mathcal{N}^{**}_v \left(1 - e^{-(\mathcal{N}_v + \mathcal{N}^{**}_v)}\right)}{\mathcal{N}_v(\mathcal{N}_v + \mathcal{N}^{**}_v)} + e^{-\mathcal{N}_v}\left(\frac{(\mathcal{N}^{**}_v - \mathcal{N}_v)(e^{-\mathcal{N}^{**}_v} - 1)}{\mathcal{N}_v\mathcal{N}^{**}_v} - 1\right) \quad (3.4)$$

where $\mathcal{N}_v = \mathcal{N}\mathcal{P}_v$*,* $\mathcal{N}^*_v = \mathcal{P}^*_v\mathcal{N}(1 - \mathcal{P}_v)$*,* $\mathcal{N}^{**}_v = \lambda_T\mathcal{P}^{**}_v E_z[A_r(z)]$*,* $A_r(z) = \pi r_d^2 - 2r_d^2\cos^{-1}(\frac{z}{2r_d}) + \frac{1}{2}z\sqrt{4r_d^2 - z^2}$ *and* $E_z[.]$ *is the expectation over the random distance* z *between* x_i *and* x_L*. The intensity of* $\mathbf{\Psi}^M_{CSMA}$ *is given by:* $\lambda^M_{CSMA} = \lambda_T \times P^M_{CSMA}$*.*

Proof. P^C_{CSMA} is the probability that x_i has the lowest mark among its neighborhood set $\mathbf{N}_{x_i}$ given in **Theorem 3.5.1**. P_{in}, which is the probability that a point younger

than x_L exists in $\mathbf{N}^{in}_{x_L}$, is given by

$$\begin{aligned}
P_{in} &= \sum_{n=1}^{\infty} \frac{1}{n+1} \sum_{k=n}^{\infty} P_k \binom{k}{n} \mathcal{P}_v^n (1-\mathcal{P}_v)^{k-n} \sum_{t=0}^{k-n} \\
&\quad \left(\frac{t}{n+t+1}\right) \binom{k-n}{t} (\mathcal{P}_v^*)^t (1-\mathcal{P}_v^*)^{k-n-t} \\
&= \frac{e^{-\mathcal{N}}}{\mathcal{N}\mathcal{P}_v} \sum_{n=1}^{\infty} \frac{(\mathcal{N}\mathcal{P}_v)^{n+1}}{(n+1)!} \sum_{t=0}^{\infty} \frac{t}{n+t+1} \left(\frac{\mathcal{P}_v^*}{1-\mathcal{P}_v^*}\right)^t \sum_{m=t}^{\infty} \\
&\quad \binom{m}{t} \frac{(\mathcal{N}(1-\mathcal{P}_v)(1-\mathcal{P}_v^*))^m}{m!} \\
&= \frac{e^{-\mathcal{N}}}{\mathcal{N}\mathcal{P}_v} \sum_{n=1}^{\infty} \frac{(\mathcal{N}\mathcal{P}_v)^{n+1}}{(n+1)!} \sum_{t=1}^{\infty} \frac{1}{(n+t+1)(t-1)!} \\
&\quad (\mathcal{P}_v^* \mathcal{N}(1-\mathcal{P}_v))^t \, e^{(\mathcal{N}(1-\mathcal{P}_v)(1-\mathcal{P}_v^*))} \\
&\overset{(a)}{=} \frac{\mathcal{N}_v^* \left(1 - e^{-(\mathcal{N}_v + \mathcal{N}_v^*)}\right)}{\mathcal{N}_v(\mathcal{N}_v + \mathcal{N}_v^*)} + \\
&\quad e^{-\mathcal{N}_v} \left(\frac{(\mathcal{N}_v^* - \mathcal{N}_v)(e^{-\mathcal{N}_v^*} - 1)}{\mathcal{N}_v \mathcal{N}_v^*} - 1 \right)
\end{aligned}$$

where $P_k \binom{k}{n} \mathcal{P}_v^n (1-\mathcal{P}_v)^{k-n}$ in the first line is the probability that x_i has n neighbors out of k coexisting points in $\mathbf{B}_{x_i}(r_d)$. Then, I divide it by $n+1$ to obtain the probability that x_i has the second lowest mark. In the same line, $\binom{k-n}{t}(\mathcal{P}_v^*)^t(1-\mathcal{P}_v^*)^{k-n-t}$ is the probability that t out of the $k-n$ non-neighbors of x_i are neighbors to x_L. Then, I multiply it by $\frac{t}{n+t+1}$ to obtain the conditional probability (i.e., conditioning that x_L has the lowest mark in $\mathbf{N}_{x_i}$) that any of these t points has a mark lower than x_L. The proof of (a) in the last line of (3.3) is given in (cf. **Appendix A.2**).

Following the definition of the PPP, the number of points existing in $A_r(z)$ is independent of the number of points existing in $\mathbf{B}_{x_i}(r_d)$, but is dependent on the area $A_r(z)$, which is a function of the random distance z between x_i and x_L. Let $\mathcal{N}_1 = \lambda_T E\left[A_r(z)\right]$ and $P_s = \frac{\mathcal{N}_1 e^{-\mathcal{N}_1}}{s!}$. Then averaging over both spatial and channel gain statistics, P_{out}, which is the probability that a point younger than x_L exists in

$\mathbf{N}_{x_L}^{out}$, can be written as

$$\begin{aligned}
P_{out} &= \sum_{n=1}^{\infty} \frac{1}{n+1} \sum_{k=n}^{\infty} P_k \binom{k}{n} \mathcal{P}_v^n (1-\mathcal{P}_v)^{k-n} \\
&\quad \sum_{t=1}^{\infty} \left(\frac{t}{n+t+1} \right) \sum_{s=t}^{\infty} P_s \binom{s}{t} (\mathcal{P}_v^{**})^t (1-\mathcal{P}_v^{**})^{s-t} \\
&= \frac{\mathcal{N}_1 \mathcal{P}_v^{**} e^{-(\mathcal{N}+\mathcal{N}_1)}}{\mathcal{N}\mathcal{P}_v} \sum_{n=1}^{\infty} \frac{(\mathcal{N}\mathcal{P}_v)^{n+1}}{(n+1)!} \sum_{m=0}^{\infty} \frac{(\mathcal{N}(1-\mathcal{P}_v))^m}{m!} \\
&\quad \sum_{t=1}^{\infty} \frac{(\mathcal{N}_1 \mathcal{P}_v^{**})^{t-1}}{(n+t+1)(t-1)!} \sum_{u=0}^{\infty} \frac{(\mathcal{N}_1(1-\mathcal{P}_v^{**}))^u}{u!} \\
&= \frac{\mathcal{N}_1 \mathcal{P}_v^{**} e^{-(\mathcal{N}\mathcal{P}_v + \mathcal{N}_1 \mathcal{P}_v^{**})}}{\mathcal{N}\mathcal{P}_v} \sum_{n=1}^{\infty} \frac{(\mathcal{N}\mathcal{P}_v)^{n+1}}{(n+1)!} \sum_{t=1}^{\infty} \\
&\quad \frac{(\mathcal{N}_1 \mathcal{P}_v^{**})^{t-1}}{(n+t+1)(t-1)!} \\
&\overset{(b)}{=} \frac{\mathcal{N}_v^{**} \left(1 - e^{-(\mathcal{N}_v + \mathcal{N}_v^{**})}\right)}{\mathcal{N}_v(\mathcal{N}_v + \mathcal{N}_v^{**})} + \\
&\quad e^{-\mathcal{N}_v} \left(\frac{(\mathcal{N}_v^{**} - \mathcal{N}_v)(e^{-\mathcal{N}_v^{**}} - 1)}{\mathcal{N}_v \mathcal{N}_v^{**}} - 1 \right).
\end{aligned}$$

The first line in the expression for P_{out} has the same interpretation as that of the first line in the expression for P_{in}. However, the only difference is that the number of nodes (s) existing in the area $A_r(z)$ is independent of the number of nodes existing in $\mathbf{B}_{x_i}(r_d)$. Therefore, I have the extra summation in P_{out} for the random variable s in order to average over all possible probabilities. For the proof of (b) in the last line, see (cf. **Appendix A.2**).

□

Following the terminology in [86], an m^{th}-generation point is a retained point in the *secondary* HCPP that has the m^{th} lowest mark in its neighborhood in the *primary* PPP. For instance, type II captures the 1^{st}-generation points only, while the MHCPP takes one step towards type III and captures the 1^{st} and 2^{nd}-generation points. We

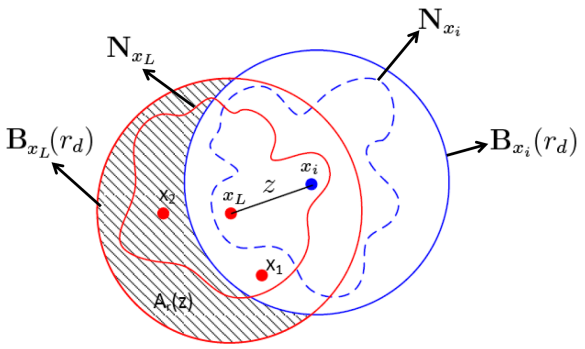

Figure 3.3: Determining the neighborhood set of the point with the lowest mark x_L.

can further refine the accuracy of the MHCPP by including more generations in the intensity calculation and thereby getting closer to type III point process. However, considering any generation beyond the 2^{nd} generation highly complicates the analysis. Therefore, for analytical tractability, I consider only the 1^{st} and 2^{nd} generations. In [86], it was shown by simulations that type II saturates at around 50% of the total intensity of type III, while considering the 2^{nd}-generation points mitigates at least 30% of the underestimated intensity by type II. It was also shown in [86] that no points beyond the 7^{th}-generation contribute to the intensity of type III point process.

3.5.3 Derivation of the Probabilities $\mathcal{P}_{\upsilon}$, $\mathcal{P}^{*}_{\upsilon}$, and $\mathcal{P}^{**}_{\upsilon}$

$\mathcal{P}_{\upsilon}$, $\mathcal{P}^{*}_{\upsilon}$, and $\mathcal{P}^{**}_{\upsilon}$ are the *neighborhood success probabilities* between two nodes in a PPP. The differences among them lie in the positions of the nodes w.r.t. each other. At first, I define three random variables z, w, and l. The random variable z denotes the random distance between a point x_i and any other point existing in $\mathbf{B}_{x_i}(r_d)$. The random variable w denotes the distance between any two points existing in $\mathbf{B}_{x_i}(r_d)$. The random variable l denotes the random distance between a point x_j existing in $\mathbf{B}_{x_i}(r_d)$ and any other point existing in $\mathbf{B}_{x_j}(r_d) \setminus \mathbf{B}_{x_i}(r_d)$. Fig. 3.4 shows the three

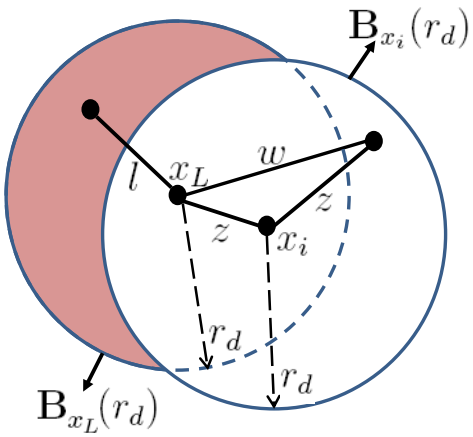

Figure 3.4: Distances between nodes.

random variables. Each of these three probabilities (i.e., $\mathcal{P}_v$, $\mathcal{P}_v^*$, and $\mathcal{P}_v^{**}$) is governed by a relation between two random variables, namely, the random channel gain and the random distance between the two points.

Following the definition of PPP, the locations of the points are independent and uniformly distributed across the area of interest. Using this fact, the distribution of the random distance w can be obtained as $f_w(w) = \frac{2w}{r_d^2} - \frac{w^2\sqrt{(2r_d)^2-w^2}}{\pi r_d^4} - \frac{4w}{\pi r_d^2}\sin^{-1}\left(\frac{w}{2r_d}\right)$, $0 \leq w \leq 2r_d$ (cf. **Appendix A.3**) and the distribution of the random distance l can be obtained as $f_l(l) = \frac{4l}{r_d^2}\ln\left(\frac{r_d+l}{r_d}\right)$, $0 \leq l \leq r_d$ (cf. **Appendix A.4**). Given that the random channel gain distribution is $f_h(h)$, $\mathcal{P}_v$, $\mathcal{P}_v^*$, and $\mathcal{P}_v^{**}$ can be derived as follows.

First, I condition on the distance between the two nodes under consideration (i.e., conditioning on that $dist(x_i, x_j) = r$) to obtain the expression for their *neighborhood success probability*, which is in fact the complementary *cdf* of the channel gain (i.e., $1 - F_h(\frac{\upsilon_s r^\eta}{P_t A})$). Then, removing the condition on the random distance, the unconditional *neighborhood success probability* is obtained.

Depending on the probability of interest, $dist(x_i, x_j)$ should be replaced with

distance z, w, or l. For $\mathcal{P}_\upsilon$, $dist(x_i, x_j)$ is replaced with z. Therefore, $\mathcal{P}_\upsilon$ is given by

$$\begin{aligned}\mathcal{P}_\upsilon &= \int_0^{r_o} \left(1 - F_h\left(\frac{\upsilon_s r_o^\eta}{P_t A}\right)\right) f_z(z)\, dz + \int_{r_o}^{r_d} \left(1 - F_h\left(\frac{\upsilon_s z^\eta}{P_t A}\right)\right) f_z(z)\, dz \\ &= \int_0^{r_o} \frac{2z}{r_d^2}\left(1 - F_h\left(\frac{\upsilon_s r_o^\eta}{P_t A}\right)\right)\, dz + \int_{r_o}^{r_d} \frac{2z}{r_d^2}\left(1 - F_h\left(\frac{\upsilon_s z^\eta}{P_t A}\right)\right)\, dz. \qquad (3.5)\end{aligned}$$

For $\mathcal{P}_\upsilon^*$, $dist(x_i, x_j)$ is replaced with w. Therefore, $\mathcal{P}_\upsilon^*$ is given by

$$\begin{aligned}\mathcal{P}_\upsilon^* = &\int_0^{r_o} \left(1 - F_h\left(\tfrac{\upsilon_s r_o^\eta}{P_t A}\right)\right) f_w(w)\, dw + \int_{r_o}^{2r_d} \left(1 - F_h\left(\tfrac{\upsilon_s w^\eta}{P_t A}\right)\right) f_w(w)\, dw \\ = &\int_0^{r_o} \left(\tfrac{2w}{r_d^2} - \tfrac{w^2\sqrt{(2r_d)^2 - w^2}}{\pi r_d^4} - \tfrac{4w}{\pi r_d^2}\sin^{-1}\left(\tfrac{w}{2r_d}\right)\right)\left(1 - F_h\left(\tfrac{\upsilon_s r_o^\eta}{P_t A}\right)\right)\, dw \\ &+ \int_{r_o}^{2r_d} \left(\tfrac{2w}{r_d^2} - \tfrac{w^2\sqrt{(2r_d)^2 - w^2}}{\pi r_d^4} - \tfrac{4w}{\pi r_d^2}\sin^{-1}\left(\tfrac{w}{2r_d}\right)\right)\left(1 - F_h\left(\tfrac{\upsilon_s w^\eta}{P_t A}\right)\right)\, dw. \qquad (3.6)\end{aligned}$$

For $\mathcal{P}_\upsilon^{**}$, $dist(x_i, x_j)$ is replaced with l. Therefore, $\mathcal{P}_\upsilon^{**}$ is given by

$$\begin{aligned}\mathcal{P}_\upsilon^{**} &= \int_0^{r_o} \left(1 - F_h\left(\frac{\upsilon_s r_o^\eta}{P_t A}\right)\right) f_l(l)\, dl + \int_{r_o}^{r_d} \left(1 - F_h\left(\frac{\upsilon_s l^\eta}{P_t A}\right)\right) f_l(l)\, dl \\ &= \int_0^{r_o} \frac{4l}{r_d^2}\ln\left(\frac{r+l}{r}\right)\left(1 - F_h\left(\frac{\upsilon_s r_o^\eta}{P_t A}\right)\right)\, dl + \\ &\quad \int_{r_o}^{r_d} \frac{4l}{r_d^2}\ln\left(\frac{r+l}{r}\right)\left(1 - F_h\left(\frac{\upsilon_s l^\eta}{P_t A}\right)\right)\, dl. \qquad (3.7)\end{aligned}$$

To summarize, given the intensity of the contending transmitters and the *pdf* of the channel power gain, r_d is computed as $r_d = \left(\frac{P_t A}{\upsilon_s}\bar{F}_h^{-1}(\epsilon)\right)^{1/\eta}$. Then, the three *neighborhood success probabilities* (i.e., P_υ, $\mathcal{P}_\upsilon^*$, and $\mathcal{P}_\upsilon^{**}$) are obtained, respectively, by numerically evaluating the integrals given in (3.5), (3.6), and (3.7). Then, the intensity of the MHCPP can be calculated by using **Theorem 3.5.2**.

3.6 Analysis of Outage Probability and Transmission Capacity

Up to this point I have estimated the intensity of the simultaneously active transmitters. In this section, I will estimate the outage probability for a generic receiver in the network given that its associated transmitter is transmitting. In order to study the outage probability, I assume that the test receiver r_{x_i} is located at an arbitrary origin "o" and its transmitter located at $x_i = (R, \theta)$ is retained in $\mathbf{\Psi}^{M}_{CSMA}$. This assumption is valid because an HCPP is invariant under translation (i.e., stationary) [3]. Ignoring the effect of noise, the outage probability for the test receiver r_{x_i} located at the origin is then defined as follows: $\mathcal{O} = \mathbb{P}\left\{\frac{P_t A h(x_i,o) R^{-\eta}}{\mathcal{I}} \leq \beta\right\}$, where β is the required signal-to-interference ratio (SIR) for correct reception, $\mathcal{I}$ is the aggregate interference from the simultaneously active transmitters. Note that the effect of noise could be prominent only when the spectrum-sensing threshold is equal to the receiver sensitivity. In such a case, the interference will be very low and comparable with the noise. However, the spatial reuse of the channel would be very low. On the other hand, if I am trying to optimize the spectrum-sensing threshold to maximize the spatial reuse efficiency subject to an outage probability constraint, then the interference becomes the major performance limiting factor and the background noise can be neglected [21], [26].

The main difficulty in computing the outage probability lies in obtaining the distribution of the aggregate interference $\mathcal{I}$. As discussed before in Sec. 2.2, there is no useful expression for the *pdf* of the aggregate interference in large scale wireless networks. The only known closed-form expression for the distribution of the aggregate interference $\mathcal{I}$ was derived for ALOHA networks with deterministic channel model and no interference protection for $\eta = 4$ [28]. For a random CSMA network, since there is no known expression for the probability generating functional for the HCPP, it is

extremely difficult (if not impossible) to find the exact distribution of the aggregate interference [40, 49]. However, I can find tight lower bound on the outage probability by only considering the set of dominant interferers (i.e., technique #2 in Sec. 2.3) retained in $\mathbf{\Psi}^{M}_{CSMA}$ after the contention resolution. Hence, the lower-bound on the outage probability can be expressed as $\mathcal{O}^{l} = \mathbb{P}\left\{\mathbf{I}^{d}_{x_i} \cap \mathbf{\Psi}^{M}_{CSMA} \neq \phi\right\}$. This expression is a direct consequence of the construction of the set of dominant interferers and the fact that the interference from only one dominant interferer will corrupt the signal received at the test receiver (i.e., the SIR will decrease below β).

Since the set of retained dominant interferers $\mathbf{I}^{d}_{x_i} \cap \mathbf{\Psi}^{M}_{CSMA}$ constitutes an HCPP in the vulnerability region of the test receiver r_{x_i}, it is still very difficult to find an exact expression for the probability of the event $\mathbf{I}^{d}_{x_i} \cap \mathbf{\Psi}^{M}_{CSMA} = \phi$ [44]. Therefore, following [40, 44, 49], the set of retained dominant interferers $\mathbf{I}^{d}_{x_i} \cap \mathbf{\Psi}^{M}_{CSMA}$ will be approximated by a PPP of intensity λ^{M}_{CSMA} in the vulnerability region of r_{x_i} but outside the contention domain of x_i. Note that the contention domain of x_i is excluded because, according to the CSMA protocol, if x_i is transmitting, none of its neighbors can simultaneously transmit. Physically, this approximation means that I am partially ignoring the contention among the dominant interferers. The contention among the coexisting transmitters has been already captured in the intensity λ^{M}_{CSMA}, and the condition on the minimum distance between the test transmitter and any of the interference sources is captured by excluding x_i's contention domain. However, the condition on having a minimum distance between interference sources is the only ignored parameter in the computed lower-bound. Since the PPP does not bound the number of points coexisting in a bounded region and the derived lower bound ($\mathcal{O}^{l}$) is very tight [26], the lower-bound on outage probability $\mathcal{O}^{l}$ increases and becomes an approximate solution for the outage probability as will be evident from the results.[7]

[7] Similar results were also shown in [44].

Due to random channel fading, the vulnerability region of the test receiver has a random shape. Therefore, I bound my observation region to search for dominant interferers by a deterministic radius r_{vul} such that $\mathbb{P}\left\{\frac{h(x_i,o)R^{-\eta}}{h(x_j,o)dist(x_j,o)^{-\eta}} \leq \beta | dist(x_j,o) > r_{\text{vul}}\right\} \approx 0$. Note that r_{vul} can be calculated in the same manner as r_d as follows: $r_{\text{vul}} = R\left(\beta \bar{F}^{-1}_{\frac{h(x_j,o)}{h(x_i,o)}}(\epsilon)\right)^{1/\eta}$, where $\bar{F}^{-1}_{\frac{h(x_j,o)}{h(x_i,o)}}(.)$ is the *ccdf* if the random variable $\frac{h(x_j,o)}{h(x_i,o)}$ [93]. Averaging over the spatial and channel gain distributions, I have the following theorem:

Theorem 3.6.1. *In a random CSMA network under general fading environment, the outage probability can be approximated as*

$$\mathcal{O} \approx 1 - e^{-\mathcal{N}_{csma} P_\beta \left(1 - \mathcal{P}_v^{(R)}\right)} \tag{3.8}$$

where $\mathcal{N}_{csma} = \lambda^M_{CSMA} \pi r^2_{\text{vul}}$ *is the expected number of transmitters in* $\mathbf{B}_{r_{x_i}}(r_{\text{vul}})$, $\mathbf{B}_{r_{x_i}}(r_{\text{vul}})$ *is the set that bounds the vulnerability region of the intended receiver* r_{x_i}, *and* P_β *is the probability that a transmitter in* $\mathbf{B}_{r_{x_i}}(r_{\text{vul}})$ *has sufficiently high channel gain with* r_{x_i} *to violate the* SIR *constraint at* r_{x_i}. P_β *is given by*

$$P_\beta = \int_0^{\frac{r^\eta_{\text{vul}}}{\beta R^\eta}} \frac{\left(\beta R^\eta h(x_i,o)\right)^{\frac{2}{\eta}}}{r^2_{\text{vul}}} f_{\frac{h(x_j,o)}{h(x_i,o)}}(h)\, dh + \int_{\frac{r^\eta_{\text{vul}}}{\beta R^\eta}}^{\infty} f_{\frac{h(x_j,o)}{h(x_i,o)}}(h)\, dh \tag{3.9}$$

where $f_{\frac{h(x_j,o)}{h(x_i,o)}}(h)$ *is the* pdf *of random variable* $\frac{h(x_j,o)}{h(x_i,o)}$.[8] $\mathcal{P}_v^{(R)} = \mathbb{P}\left\{x_j \in \mathbf{N}_{x_i} | x_j \in \mathbf{B}_{r_{x_i}}(r_{\text{vul}})\right\}$ *is the* neighborhood success probability *for the*

[8] Note that $f_{\frac{h(x_j,o)}{h(x_i,o)}}(h)$ was derived in [93] for Rayleigh, log-normal, and Nakagami fading.

transmitters existing in $\mathbf{B}_{r_{x_i}}(r_{\text{vul}})$ *with the test transmitter* x_i *and is given by*

$$\mathcal{P}_{\upsilon}^{(R)} = \int_0^{r_o} \frac{2\text{v}}{r_{\text{vul}}^2}\left(1 - F_h\left(\frac{\upsilon_s}{P_t A}\right)\right) d\text{v} + \int_{r_o}^{r_{\text{vul}}-R} \frac{2\text{v}}{r_{\text{vul}}^2}\left(1 - F_h\left(\frac{\upsilon_s \text{v}^\eta}{P_t A}\right)\right) d\text{v} + \int_{r_{\text{vul}}-R}^{r_{\text{vul}}+R} \left(\frac{\text{v}}{r_{\text{vul}}^2} - \frac{2\text{v}}{\pi r_{\text{vul}}^2}\sin^{-1}\left(\frac{\text{v}^2 + R^2 - r_{\text{vul}}^2}{2\text{v}R}\right)\right)\left(1 - F_h\left(\frac{\upsilon_s \text{v}^\eta}{P_t A}\right)\right) d\text{v}. \tag{3.10}$$

Proof. The outage probability can be approximated by the probability to find an active interferer hidden from the intended transmitter and located inside the vulnerability region of the intended receiver. Using the PPP approximation for the interferers [44] and averaging over the spatial and channel statistics, I have

$$\begin{aligned}
\mathcal{O} &\approx \sum_{n=1}^{\infty}\sum_{k=n}^{\infty} \frac{e^{-\mathcal{N}_{csma}}\mathcal{N}_{csma}^k}{k!}\binom{k}{n}\left(1-\mathcal{P}_{\upsilon}^{(R)}\right)^n\left(\mathcal{P}_{\upsilon}^{(R)}\right)^{k-n} \\
&\quad \sum_{t=1}^{n}\binom{n}{t}P_\beta^t(1-P_\beta)^{n-t} \\
&= e^{-\mathcal{N}_{csma}}\sum_{n=1}^{\infty}\sum_{t=1}^{n}\binom{n}{t}P_\beta^t(1-P_\beta)^{n-t}\sum_{k=n}^{\infty}\frac{\mathcal{N}_{csma}^k}{k!}\frac{k!}{n!(k-n)!} \\
&\quad \left(1-\mathcal{P}_{\upsilon}^{(R)}\right)^n\left(\mathcal{P}_{\upsilon}^{(R)}\right)^{k-n} \\
&= e^{-\mathcal{N}_{csma}} \times \left(e^{\mathcal{N}_{csma}\left(1-\mathcal{P}_{\upsilon}^{(R)}\right)} - 1\right) e^{\mathcal{N}_{csma}\mathcal{P}_{\upsilon}^{(R)}} - \\
&\quad e^{-\mathcal{N}_{csma}} \times \left(e^{\mathcal{N}_{csma}\left(1-\mathcal{P}_{\upsilon}^{(R)}\right)(1-P_\beta)} - 1\right) e^{\mathcal{N}_{csma}\mathcal{P}_{\upsilon}^{(R)}} \\
&= \left(1 - e^{-\mathcal{N}_{csma}\left(1-\mathcal{P}_{\upsilon}^{(R)}\right)}\right) - \\
&\quad \left(e^{-\mathcal{N}_{csma}P_\beta\left(1-\mathcal{P}_{\upsilon}^{(R)}\right)} - e^{-\mathcal{N}_{csma}\left(1-\mathcal{P}_{\upsilon}^{(R)}\right)}\right) \\
&= 1 - e^{-\mathcal{N}_{csma}P_\beta\left(1-\mathcal{P}_{\upsilon}^{(R)}\right)}
\end{aligned}$$

where P_β is the probability that a transmitter located in $\mathbf{B}_{r_{x_i}}(r_{\text{vul}})$ can alone corrupt the received signal at the receiver and $\mathcal{P}_{\upsilon}^{(R)}$ is the *neighborhood success probability*

between the test transmitter x_i and the transmitters located in the vulnerability region of the test receiver r_{x_i}. The first equation reflects that a transmitter is only considered in the outage probability calculation if it is not a neighbor of x_i (with probability $\left(1-\mathcal{P}_v^{(R)}\right)$) and can alone corrupt the signal of r_{x_i} (with probability P_β). Since the test receiver (r_{x_i}) is located at the origin 'o', P_β can be expressed as

$$\begin{aligned} P_\beta &= \mathbb{P}\left\{\frac{P_t h(x_i,o) R^{-\eta}}{P_t h(x_j,o)\left\|x_j\right\|^{-\eta}} < \beta\right\} \\ &= \mathbb{P}\left\{\frac{h(x_j,o)}{h(x_i,o)} > \frac{\|x_j\|^\eta}{\beta R^\eta}\right\}. \end{aligned} \tag{3.11}$$

From the PPP approximation for the dominant interferers, x_j is uniformly distributed in the vulnerability circle of the test receiver r_{x_i} located at the origin. Therefore, $\tilde{z} = \|x_j\|$ is a random variable with *pdf* $f_{\tilde{z}}(z) = \frac{2z}{r_{\text{vul}}^2}$, $z \le r_{\text{vul}}$. Let $z_\beta = \frac{\tilde{z}^\eta}{\beta R^\eta}$, then the *pdf* of z_β is $f_{z_\beta}(z) = \frac{2\beta R^\eta (\beta R^\eta z)^{\frac{2}{\eta}-1}}{\eta r_{\text{vul}}^2}$, and the *cdf* of z_β is $F_{z_\beta}(z) = \frac{(\beta R^\eta z)^{\frac{2}{\eta}}}{r_{\text{vul}}^2}$, where $0 \le z \le \frac{r_{\text{vul}}^\eta}{\beta R^\eta}$. Then P_β is given by

$$\begin{aligned} P_\beta &= \int_0^\infty f_{\frac{h(x_j,o)}{h(x_i,o)}}(h) F_{z_\beta}(h)\, dh \\ &= \int_0^{\frac{r_{\text{vul}}^\eta}{\beta R^\eta}} \frac{(\beta R^\eta h)^{\frac{2}{\eta}}}{r_{\text{vul}}^2} f_{\frac{h(x_j,o)}{h(x_i,o)}}(h)\, dh + \int_{\frac{r_{\text{vul}}^\eta}{\beta R^\eta}}^\infty f_{\frac{h(x_j,o)}{h(x_i,o)}}(h)\, dh \end{aligned} \tag{3.12}$$

where $f_{\frac{h(x_j,o)}{h(x_i,o)}}(h)$ is the *pdf* of the random variable $\frac{h(x_j,o)}{h(x_i,o)}$ [93].

Let v be the random distance between x_i and any other transmitter uniformly distributed in $\mathbf{B}_{r_{x_i}}(r_{\text{vul}})$. The *pdf* of v can be obtained as follows (see (cf. **Appendix A.5**):

$$f_{\mathrm{v}}(\mathrm{v}) = \begin{cases} \frac{2\mathrm{v}}{r_{\mathrm{vul}}^2}, & 0 \leq \mathrm{v} \leq (r_{\mathrm{vul}} - R) \\ \frac{\mathrm{v}}{r_{\mathrm{vul}}^2} - \frac{2\mathrm{v}}{\pi r_{\mathrm{vul}}^2} \sin^{-1}\left(\frac{\mathrm{v}}{2R} + \frac{R^2 - r_{\mathrm{vul}}^2}{2\mathrm{v}R}\right), & (r_{\mathrm{vul}} - R) < \mathrm{v} \leq (r_{\mathrm{vul}} + R). \end{cases} \tag{3.13}$$

Due to the piecewise nature of both the path-loss model in (3.1) and the *pdf* of the random distance v, the *neighborhood success probability* between a transmitter $x_j \in \mathbf{B}_{r_{x_i}(r_{\mathrm{vul}})}$ and the test transmitter x_i is given by

$$\begin{aligned} \mathcal{P}_{\upsilon}^{(R)} &= \mathbb{P}\left\{\frac{P_t A h(x_i, x_j)}{\mathrm{v}^{\eta}} > \upsilon_s\right\} \\ &= \mathbb{P}\left\{h(x_i, x_j) > \frac{\upsilon_s \mathrm{v}^{\eta}}{P_t A}\right\} \\ &= \int_0^{r_o} \frac{2\mathrm{v}}{r_{\mathrm{vul}}^2}\left(1 - F_h\left(\frac{\upsilon_s}{P_t A}\right)\right) d\mathrm{v} + \int_{r_o}^{r_{\mathrm{vul}}-R} \frac{2\mathrm{v}}{r_{\mathrm{vul}}^2}\left(1 - F_h\left(\frac{\upsilon_s \mathrm{v}^{\eta}}{P_t A}\right)\right) dv \\ &+ \int_{r_{\mathrm{vul}}-R}^{r_{\mathrm{vul}}+R} \left(\frac{\upsilon}{r_{\mathrm{vul}}^2} - \frac{2\mathrm{v}}{\pi r_{\mathrm{vul}}^2} \sin^{-1}\left(\frac{\mathrm{v}^2 + R^2 - r_{\mathrm{vul}}^2}{2\mathrm{v}R}\right)\right)\left(1 - F_h\left(\frac{\upsilon_s \mathrm{v}^{\eta}}{P_t A}\right)\right) d\mathrm{v} \end{aligned} \tag{3.14}$$

□

It is worth mentioning that the outage probability given by $\mathcal{O}$ in **Theorem 3.6.1** is the general case of the lower-bound on outage probability given by (23) in [26] for ALOHA networks. The expression of $\mathcal{O}$ can be interpreted as follows: $\lambda_{CSMA}^{M} \pi r_{\mathrm{vul}}^2$ gives the expected number of active transmitters within the area πr_{vul}^2, P_β gives the portion of the area πr_{vul}^2 where the dominant interferers are located, and $(1 - \mathcal{P}_{\upsilon}^{(R)})$ excludes the area where x_i's neighbors are located. Hence, $\mathcal{O}$ gives the probability that the region that bounds the dominant interferers is not empty. For an ALOHA network with deterministic path-loss, the area will be $\pi\left(R\beta^{\frac{1}{\eta}}\right)^2$ and every node is an active transmitter which gives (23) in [26].

The transmission capacity ($\mathcal{T}$) is defined as the number of successful transmissions

per unit area and is given by $\mathcal{T} = \lambda_{CSMA}^{M}(1 - \mathcal{O})$. In random CSMA networks, the spectrum-sensing threshold is a very critical parameter that highly affects the transmission capacity. The optimal value of the spectrum-sensing threshold can be obtained numerically from the following optimization problem:

$$\begin{aligned} \text{maximize} \quad & \mathcal{T} = \lambda_{CSMA}^{M}(1 - \mathcal{O}) \\ \text{subject to} \quad & \mathcal{O} \leq \rho \end{aligned} \tag{3.15}$$

where ρ is the outage probability threshold. We numerically solve this optimization problem and show the existence of an optimal value for the spectrum-sensing threshold (υ_s^*) which maximizes the transmission capacity.

3.7 Results and Discussions

3.7.1 Numerical and Simulation Results

We compare the classical hard core point process (CHCPP) and the modified hard core point process (MHCPP) in a Nakagami fading environment via Monte Carlo simulations using MATLAB to check the accuracy of both the modeling approaches. With Nakagami fading, the *pdf* and the *cdf* of channel power gain are defined, respectively, as $f_h(h) = \frac{h^{k-1}e^{-x/s}}{s^k \upsilon(k)}$ and $F_h(h) = 1 - \frac{\Gamma_u(k,h/s)}{\Gamma(k)}$, where $\Gamma(.)$ is the gamma function, $\Gamma(s,x) = \int_x^\infty t^{s-1}e^{-1}dt$ is the upper incomplete gamma function, k is the shape parameter, s is the scale parameter, and $\mu_{ch} = ks$ is the mean channel gain due to fading. Note that any other fading environment can be considered as long as the *pdf* and the *cdf* of the corresponding channel power gain exist and the first moment of the channel power gain is finite. With the carrier frequency $f_c = 2.4$ GHz, assuming isotropic antennas with unit gains for all transmitters, the propagation constant is

computed as $A = 9.9 \times 10^{-5}$. We choose r_d such that $\epsilon = 10^{-6}$.

In each simulation run, I realize the transmitters according to a PPP with intensity λ_T in a circle with radius equal to 20 m. Then, beginning with a random transmitter, I simulate the contention resolution process. A transmitter in the realized PPP is retained in the HCPP if the received power from all the previously retained transmitters is less than the spectrum-sensing threshold υ_s. The simulation is repeated 2000 times and the average number of nodes and the average aggregate interference are compared with those obtained from analysis of the CHCPP and the MHCPP. To simulate the outage probability, I divide the number of times the signal-to-interference ratio (SIR) at the test receiver falls below the SIR threshold β (= 2 dB as in the IEEE 802.15.4 MAC [94]) by the total number of simulation runs. The transmitted power is chosen as $P_t = 1$ mW, the reference distance is chosen as $r_o = 1$ m, the Tx-Rx distance is chosen as $R = 1$ m, and the path-loss exponent is chosen to be $\eta = 4$.

Fig. 3.5 shows the effect of the *primary* intensity of the transmitters on the intensity of the simultaneously active transmitters as well as its effect on the outage probability. Fig. 3.5(a) compares the CHCPP and the MHCPP modeling approaches with the HCPP realization via Monte Carlo simulation. The figure shows the effect of λ_T on the node intensity underestimation problem of the CHCPP. As the *primary* intensity λ_T increases, the role of unselected points increases and the underestimation problem aggravates. Fig. 3.5(b) shows that as the *primary* intensity λ_T increases, more active transmitters are retained, which adds to the aggregate interference and increases the outage probability. This figure also shows the accuracy of the analytically derived expression (via technique #2 Sec. 2.3) for outage probability.

Fig. 3.6 shows the effect of fading on the intensity of the simultaneously active

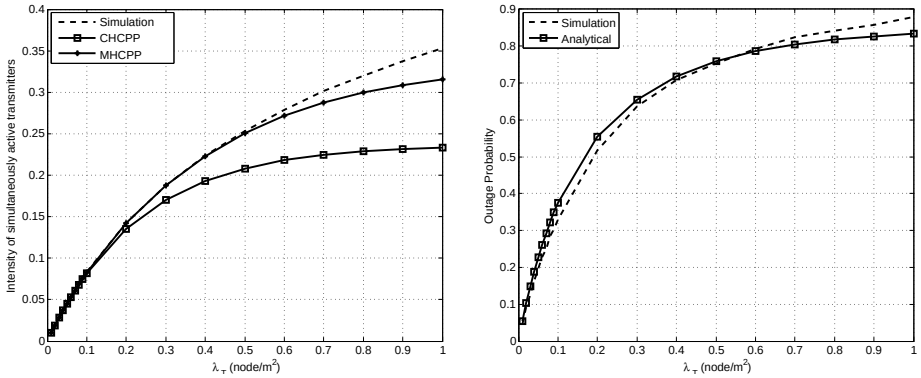

(a) (b)

Figure 3.5: (a) Number of nodes vs. λ_T (for $\mu_{ch} = 0.3$ and $\upsilon_s = 10^{-5}$), (b) outage probability vs. λ (for $\mu_{ch} = 0.3$ and $\upsilon_s = 10^{-5}$).

transmitters as well as its effect on the outage probability. Fig. 3.6(a) compares the CHCPP and the MHCPP modeling approaches with the HCPP realization via Monte Carlo simulation. The figure shows the effect of the mean channel gain μ_{ch} on the underestimation problem of the CHCPP. As fading conditions become better, more nodes are considered in the contention-resolution and the underestimation problem aggravates. Fig. 3.6(b) shows that as the mean channel gain becomes higher, fewer number of nodes are retained which decreases the aggregate interference and the hidden node problem. On the other hand, the average channel gain between a transmitter and its intended receiver becomes higher. These two events decrease the outage probability with the increase of the mean channel gain. The figure also validates the accuracy of the analytically derived expression (via technique #2 Sec. 2.3) for outage probability.

Fig. 3.7 shows the effect of the spectrum-sensing threshold υ_s on the intensity of the simultaneously active transmitters as well as its effect on the outage probability. Fig. 3.7(a) shows the effect of υ_s on the intensity of the simultaneously active transmitters. As υ_s decreases, the CSMA protocol becomes more conservative and

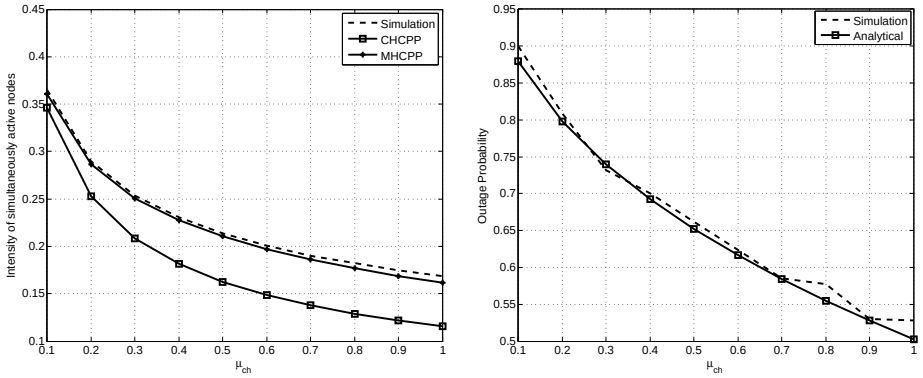

(a) (b)

Figure 3.6: (a) Number of nodes vs. μ_{ch} (for $\lambda = 0.5$ and $\upsilon_s = 10^{-5}$), (b) outage probability vs. μ_{ch} (for $\lambda = 0.5$ and $\upsilon_s = 10^{-5}$).

the intensity of the simultaneously active transmitters as well as the frequency reuse efficiency decrease, and vice versa. The figure also shows the effect of υ_s on the underestimation problem of the CHCPP. As υ_s decreases, more nodes are involved in the contention resolution process and the role of the unselected points dominates which aggravates the node intensity underestimation problem. Fig. 3.7(b) shows that decreasing υ_s decreases the intensity of the simultaneously active transmitters as well as the hidden node problem (i.e., the CSMA protocol becomes more conservative). On the other hand, increasing υ_s makes the CSMA protocol more aggressive, and consequently, the outage probability increases.

Fig. 3.8 shows the existence of an optimal υ_s which depends on the operating conditions of the network. Fig. 3.8(a) shows the effect of the mean channel gain on υ_s. From Fig. 3.6(b), as the channel condition deteriorates, the outage probability increases. This means that the CSMA protocol should be more conservative to attain the same outage probability. The maximum transmission capacity does not change dramatically since the conservativeness of the CSMA protocol is compensated by the low average channel gain which increases the coexistence capability of the network

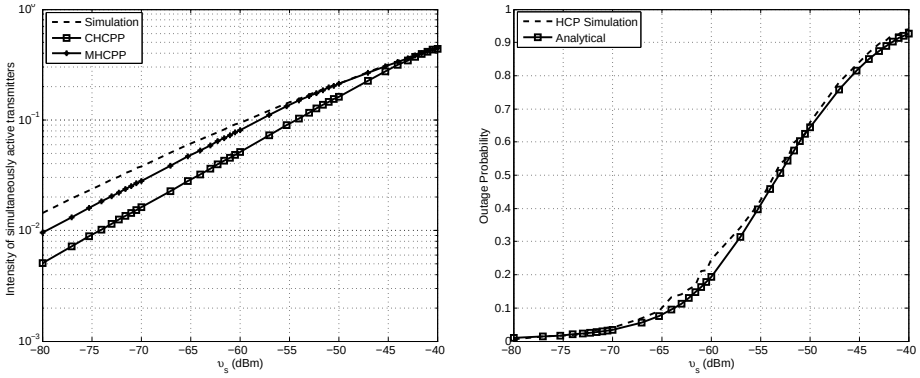

(a) (b)

Figure 3.7: (a) Number of nodes vs. υ_s (for $\lambda = 0.5$ and $\mu_{ch} = 0.5$), (b) outage probability vs. υ_s (for $\lambda = 0.5$ and $\mu_{ch} = 0.5$).

nodes (see Fig. 3.6(a)). Fig. 3.8(b) shows the effect of the *primary* intensity of the transmitters λ_T on the transmission capacity. As λ_T increases, the transmission capacity increases and the transmission capacity saturates with the increase of λ_T because the intensity of the simultaneously active transmitters saturates (Fig. 3.5).

Fig. 9 shows the effect of the bounding approach on my model. To see the rate of decay of ϵ with the distance r I plot Fig. 3.9(a). The figure shows that the value of r_d which gives $\epsilon = 10^{-6}$ will be different for different fading and path-loss conditions. However, the probability to have a neighbor transmitter beyond r_d decays very rapidly. To show the accuracy of the bounding approach used in the analysis, I compare the exact and the approximated probability mass functions (*pmf*s) of the number of transmitters in the neighborhood domain of a generic transmitter. Fig. 3.9(b) shows that the *pmf* obtained via the bounding approach matches exactly with the actual *pmf*.

As has been mentioned before, the underestimation flaw depends on the spectrum-sensing threshold, the fading parameters and the intensity of the transmitters contending for accessing the spectrum. Since the effects of all these three parameters are

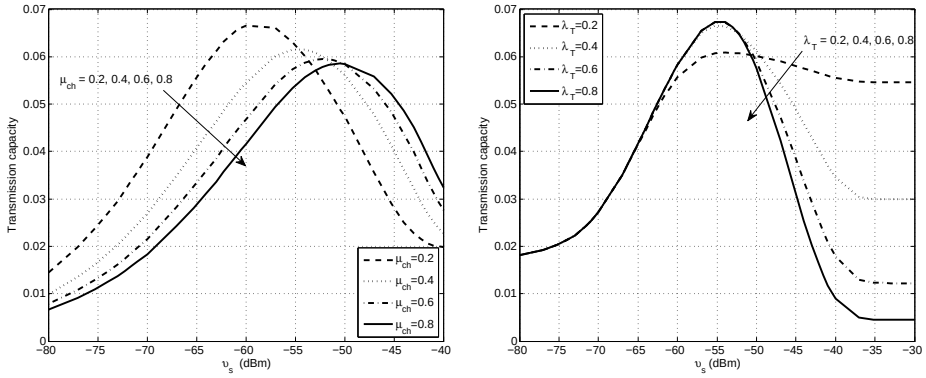

(a) (b)

Figure 3.8: (a) Transmission capacity vs. υ_s (for $\lambda = 0.5$), (b) transmission capacity vs. υ_s (for $\mu_{ch} = 0.5$).

reflected in the mean number of transmitters in the contention domain, I quantify the underestimation flaw against the mean number of transmitters in the contention domain as in [86]. As shown in Fig. 3.10(a), the mean number of transmitters in the contention domain reflects all of these variables, namely, the spectrum-sensing threshold, fading parameters, and intensity of transmitters. Fig. 3.10(b) shows the estimated intensity obtained by using each analytical model normalized w.r.t. the simulations (i.e., normalized with w.r.t. the actual retained transmitters). The figure shows that the CHCPP saturates at 50% of the total intensity of simulation. That is, the CHCPP underestimates up to 50% of the intensity of the simultaneously active transmitters. The figure also shows that the MHCPP reduces the underestimated intensity (i.e., the gap between type II intensity and the intensity obtained from simulation) by at least 30%. Given the system parameters, the mean number of transmitters in the contention domain ($\mathcal{N} = \lambda_T \pi r_d^2 \mathcal{P}_\upsilon$) can be easily calculated. Then, the underestimation error can be observed as shown in Fig. 3.10(b). For instance, with $\mathcal{N} = 5$ nodes, the MHCPP and the CHCPP estimate (underestimate), respectively, 95% and 75% (5% and 25%) of the intensity of the simultaneously ac-

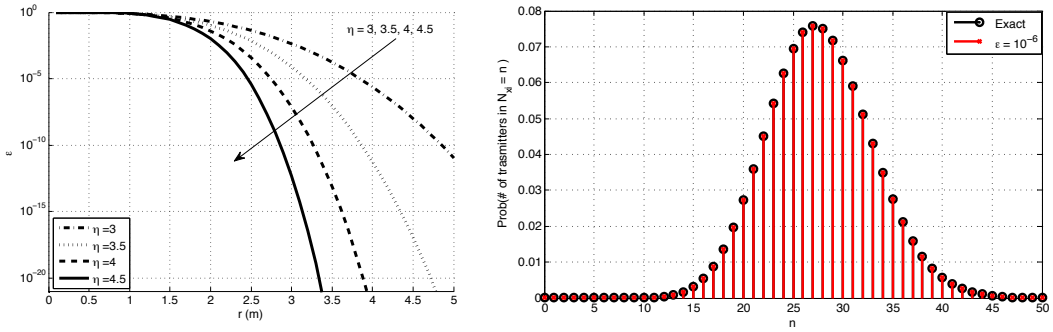

(a) (b)

Figure 3.9: a) The decay of ϵ with r for $\mu_{ch} = 1$, υ_s = - 60 dBm, and $\lambda_T = 1$, b) exact vs. approximated *pmf* of the number of transmitters in the neighborhood set of a generic transmitter $\mathbf{N}_{x_i}$ for $\mu_{ch} = 1$, $\eta = 4$, υ_s = - 60 dBm, and $\lambda_T = 1$.

tive transmitters. However, with $\mathcal{N} = 10$ nodes, the MHCPP and the CHCPP estimate (underestimate), respectively, 82% and 62% (18% and 38%) of the intensity of the simultaneously active transmitters. It is worth mentioning that the results in Fig. 3.10(b) match with the results in [86].

3.7.2 Summary and Discussions

As a result of ignoring the freezing property of the backoff timer in the CSMA protocol, there exists a node intensity underestimation flaw in the classical HCPP (CHCPP) which aggravates when the mean number of transmitters involved in the contention resolution process increases. The modified HCPP (MHCPP) presented in this work mitigates the intensity underestimation flaw of CHCPP by at least 30%. For instance, when the mean number of transmitters in a contention domain is 5 (i.e., $\mathcal{N} = 5$), the intensity underestimation flaw is reduced by about 80%. The intensity underestimation flaw still exists in the MHCPP since it only goes one step towards type III HCPP and partially captures the freezing property of the CSMA backoff timer.

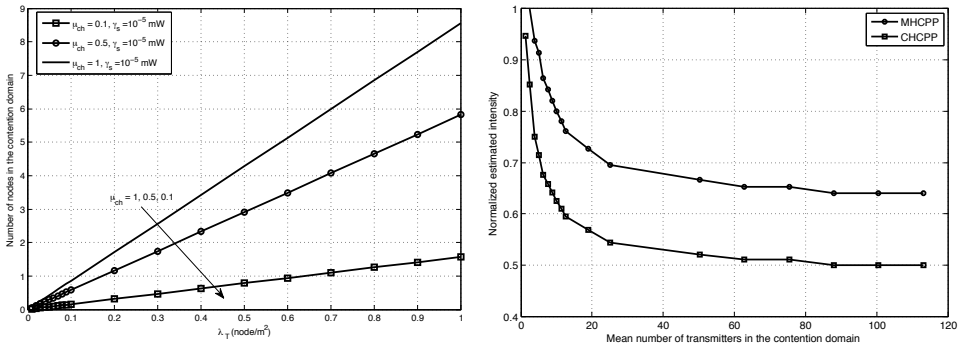

(a) (b)

Figure 3.10: (a) Normalized estimated intensity, (b) mean number of neighbors in the contention domain $\mathcal{N}$.

The presented model can be used to optimize the tradeoff between the spatial frequency reuse and the outage probability, hence, maximizing the transmission capacity. The obtained results reveal that significant amount of spectrum opportunities could be missed in a practical CSMA wireless network if the spectrum-sensing threshold is not optimized. For instance, with $\mu_{ch} = 0.2$ and $\lambda_T = 0.5$, a transmission capacity gain of at least 6.4 dB can be obtained if the optimal sensing threshold is used rather that adjusting the carrier sensing threshold to the receiver sensitivity (i.e., $\upsilon_s < -80$ dBm). On the other hand, with $\mu_{ch} = 0.5$ and $\lambda_T = 0.8$, a transmission capacity gain of 11 dB can be achieved if the optimal sensing threshold is used rather than an aggressive spectrum access threshold (i.e., $\upsilon_s > -30$ dBm).

Given a required link quality, as the fading conditions become worse, two neighboring nodes should be closer to each other. Therefore, ignoring the effect of fading between the two neighbors x_i and x_L results in an overestimation of the distance between them. This results in an underestimation of the number of common neighbors between x_i and x_L (i.e., $|\mathbf{N}_{x_L} \cap \mathbf{N}_{x_i}|$), and hence, an overestimation of the number of 2^{nd}-degree neighbors of x_i w.r.t. x_L (i.e., $|\mathbf{N}_{x_L} \setminus \mathbf{N}_{x_i}|$). As a result, the probability

that x_i will access the channel given that it has the 2^{nd} lowest mark in its neighborhood will be overestimated. This is due to the fact that the chance for having a transmitter in the $\mathbf{N}_{x_L} \setminus \mathbf{N}_{x_i}$ with a mark lower than x_L increases with the number of transmitters in $\mathbf{N}_{x_L} \setminus \mathbf{N}_{x_i}$. This leads to an increase in the probability that x_L will freeze its counter and x_i will access the channel given that x_i has the 2^{nd} lowest mark in its contention domain. Since the intensity underestimation flaw still exists in the MHCPP, overestimating the probability that a generic transmitter x_i will access the spectrum should have a positive impact on the MHCPP (i.e., decreases the underestimation flaw).

The results shown in Fig. 3.6(b) and Fig. 3.8(a) are particularly insightful. Intuitively, channel fading should add to the signal attenuation and hence decrease the aggregate interference and the outage probability. However, the results show that the outage probability increases when the channel condition becomes worse. This behavior can be explained as follows. As the channel condition deteriorates, although the aggregate interference reduces, the hidden node problem aggravates and dominates the outage probability. To avoid this problem, as the channel condition deteriorates (e.g., the average channel gain decreases), the CSMA protocol needs to be more conservative in order to achieve the optimal transmission capacity (as shown in Fig. 3.8(b)). That is, each transmitter needs to increase its transmission range to protect its receiver from interference caused due to the hidden node problem.

3.8 Chapter Summary

We have applied stochastic geometry tools for characterizing CSMA ad hoc networks. We have shown how the effect of the CSMA mac protocol on the network topology has been captured be the HCPP. To this end, I have presented a framework for modeling

the intensity of simultaneous active transmitters, the outage probability, and the transmission capacity of random CSMA wireless networks ad hoc under general fading environments. First, I have generalized the Matérn hard core point process type II and demonstrated the node intensity underestimation flaw of this model to capture the spatial distribution of the simultaneously active transmitters in random CSMA networks. To mitigate this flaw, I have then proposed a generalized modified hard core point process model. Based on this model, an approximate expression for the outage probability based on the region bounds (i.e., technique #2 Sec. 2.3) has been obtained and its accuracy has been validated by simulations. It has been also shown that, for a given set of network parameters, there exists an optimal spectrum-sensing threshold. The proposed framework will be useful for optimizing the performance of large-scale CSMA wireless networks.

In this chapter I developed a modeling paradigm for ad hoc networks using CSMA protocol in a single channel environment. In the next chapter I incorporate the stochastic geometry modeling into a complete design paradigm for star-connected sensor networks. We also extend the stochastic geometry analysis to multi-channel environment.

Chapter 4

Spectrum Efficient Design for Star-Connected Wireless Sensor Networks

In this chapter, I use stochastic geometry analysis to develop a novel spectrum-efficient design framework for random large scale star connected wireless sensor networks in a multi-channel environment. Although I use the IEEE 802.15.4 standard as my case study for the sensor network, the framework can be applied to different technologies. The proposed framework maximizes both spatial and time domain frequency utilization under channel gain uncertainties to minimize the number of frequency channels required to accommodate a certain population of coexisting IEEE 802.15.4 networks. The performance metrics are the outage probability and the self-admission failure probability. We relax the single channel assumption that has been used traditionally in the stochastic geometry analysis. We show that the intensity of the admitted networks does not increase linearly with the number of channels and the rate of increase of the intensity of the admitted networks decreases with the number of channels.

By using graph theory, I obtain the minimum required number of channels to accommodate a certain intensity of coexisting networks under a self-admission failure probability constraint. To this end, I design a superframe structure for the coexisting IEEE 802.15.4 networks and a method for time-domain interference alignment.

4.1 Introduction

The IEEE 802.15.4-based wireless personal area networks (WPANs) offer high power efficiency when operating in the beacon-enabled mode, and therefore, they are suitable for applications having critical power efficiency constraints [95]. However, due to their limited power capabilities, the IEEE 802.15.4-based WPANs are considered to be the most affected networks by mutual interference in the ISM (Industrial, Scientific, and Medical) band [96]- [98]. The significant impact of mutual interference on the IEEE 802.15.4 WPANs from other networks coexisting in the ISM band limits their coexistence capability and drastically degrades their performance. Furthermore, in the beacon enabled mode, the IEEE 802.15.4 WPANs follow long term periodic superframe structures that determine their sleep/active patterns (see Fig. 4.1). Therefore, an IEEE 802.15.4 WPAN operating in the beacon enabled mode cannot efficiently utilize the randomized short term spectrum opportunities as proposed in [99]. On the contrary, it requires a channel that does not have any strong interference (e.g., interference from Wi-Fi networks)[1]. Therefore, for the operation of the IEEE 802.15.4 WPANs in beacon enabled mode in the crowded ISM band, a vacant channel[2] (i.e., not utilized by other technologies such as the IEEE 802.11b) is considered to be a

[1]The IEEE 802.11 WLANs can have a maximum of 3 non-overlapping channels, which leaves at least four channels for the IEEE 802.15.4 WPANs without interference from the IEEE 802.11 WLANs [100].

[2]Hereafter, the term *vacant channel* is used to denote a channel with relatively low heterogeneous interference (i.e., interference from systems other than those using the IEEE 802.15.4 standard) in the ISM band. More discussions on heterogeneous interference are provided in Sec. 4.8.2.

very precious resource that has to be utilized carefully. This motivates me to develop a design framework for the IEEE 802.15.4 networks that maximizes both the spatial and time domain utilizations of each vacant channel available for the operation of these networks. In other words, my goal is to increase the number of IEEE 802.15.4 WPANs that can coexist in the same frequency channel, hence, increase their coexistence capability in the crowded ISM band.

We consider the IEEE 802.15.4-based ad-hoc and sensor networks that are spatially distributed in the form of star-connected networks (SCNs) and operating in the beacon-enabled mode. One example of such a network is a wireless body-area sensor network (WBASN) implemented using a two-hop communication system, where a body control unit (BCU) acts as a coordinator for light-weight low-power biomedical sensors attached to the human body. The BCU and the associated biomedical sensors form an SCN. Each coexisting SCN consists of a master coordinator node (CN) and some slave network nodes (SNs).

4.1.1 The IEEE 802.15.4 Operation

In the IEEE 802.15.4 network, the CN is responsible for coordinating the traffic within its SCN. Each CN and its attached SNs follow a periodic superframe structure (as shown in Fig. 4.1) for their communications. The members of the SCN become active for the intra-network communication during the active period in a superframe, and for power saving, they go to the sleep mode during the inactive period. The active period in a superframe is divided into three main parts: the beacon, the contention access period (CAP), and the contention free period (CFP). In a coexistence scenario where many independent SCNs coexist in the same vicinity, if the active periods of different SCNs overlap, the transmissions will interfere with each other and thus cause

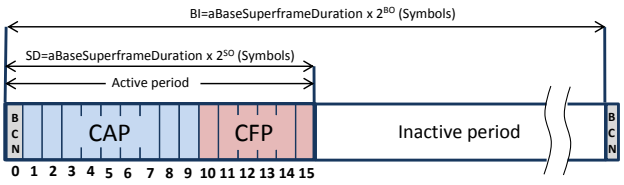

Figure 4.1: IEEE 802.15.4 superframe structure. The superframe's active period is divided into three main parts: the beacon, the contention-access period (CAP), and the contention-free period (CFP).

transmission errors.

In an IEEE 802.15.4 network, each coexisting CN listens to the spectrum, measures the power level, and compares it to a spectrum sensing threshold[3]. The access policy in the IEEE 802.15.4 standard requires that a CN does not access a frequency channel unless the power measured on that channel is less than the spectrum sensing threshold. The spectrum sensing threshold is a very crucial design parameter that should be adjusted very carefully. The lower the spectrum sensing threshold, the more conservative the system is and the same channel is reused after larger spatial intervals. Hence, the aggregate interference and the outage probability decrease. The outage probability refers to the probability that the signal-to-interference-plus-noise-ratio (SINR) at the intended receiver falls below the threshold level required for correct reception. On the other hand, the higher the spectrum sensing threshold, the more aggressive the system becomes and the same channel can be reused after smaller spatial intervals. Hence, the aggregate interference and outage probability increase. Therefore, the spectrum sensing threshold must be carefully tuned to achieve the required tradeoff between the spatial reuse efficiency and the outage probability. Note that the superframe scheduling decision taken by the CN is a long term decision and

[3]The power level is measured using the ED (energy detection) service specified by the physical layer of the standard.

has to account for the channel gain uncertainties. That is, the channel gains realization will change over the time from the channel gains at the time instant when the CN listened to the spectrum and obtained the beacons information and power levels of the coexisting SCNs to schedule its superfame. Therefore, for efficient and reliable operation of the IEEE 802.15.4 beacon enabled WPANs, it is of primary importance that the sensing threshold optimization accounts for the channel gain uncertainties.

According to the IEEE 802.15.4 standard, the spectrum sensing threshold is very low as its value is set within 10 dB of the receiver sensitivity (i.e., the spectrum sensing threshold will always be less than -75 dBm) which lead to a very conservative operation and degraded frequency reuse efficiency [94, 98]. Moreover, from the time-domain perspective, the access policy in the standard requires that each IEEE 802.15.4 SCN will be exclusively operating in a given frequency channel, and therefore, the entire inactive period of the superframe is wasted.

4.1.2 Motivation and Contribution

Motivated by the conservativeness of the IEEE 802.15.4 standard, its vulnerability to interference, and the requirement for a spectrum-efficient operation of a large-scale deployment of IEEE 802.15.4 networks, I use stochastic geometry analysis to design a framework for multi-channel coexistence of IEEE 802.15.4 WPANs operating in the beacon-enabled mode. The proposed framework optimizes the spectrum sensing threshold while accounting for the channel gain uncertainties to maximize the spatial frequency reuse, optimizes the superframe structure to maximize the time domain utilization, and calculates the minimum number of channels required for a certain population of the IEEE 802.15.4 WPANs to coexist and operate properly (i.e., subject to some performance constraints). Intuitively, if there are m channels available, the

total number of SCNs that can coexist in the same vicinity will be the m fold of the number of SCNs coexisting in one channel. In other words, if there are N networks to coexist in a certain area, then a total of m channels are needed to accommodate the N coexisting networks when one channel can accommodate N/m networks. While this is true for grid-based networks, I will show that it is not true for random networks. The major contributions of the work can be summarized as follows:

- development of a unified framework for the design of a multi-channel coexistence model for random IEEE 802.15.4-based networks,
- account for the channel gain uncertainties for the long term superframe scheduling decision,
- calculation of the optimal sensing threshold and the optimal number of channels required for the operation of the coexisting SCNs,
- derivation of a closed-form expression for the intensity of SCNs that can coexist in multiple channels and the coexistence gain offered by each extra channel,
- discovery of the fact that the relationship between the number of channels and the total number of coexisting networks is non-linear. More precisely, due to the randomness of the network topology, the added value of each extra channel to the coexistence gain decreases, and therefore, the traditional one channel analysis can be quite misleading for the design of multi-channel carrier sensing-based random wireless networks.

4.2 Related Work

Since carrier sensing-based protocols such as the carrier sense multiple access with collision avoidance (CSMA/CA) protocol is a fundamental multiple access protocol that is extensively used in modern wireless networks, CSMA has been the main point of interest of many research work in the literature. In the following I divide the related work into two sections. The first section reviews the related work on stochastic geometry and random ad hoc and sensor networks. The second section reviews the related work on the IEEE 802.15.4 and multi-channel analysis of ad hoc and sensor networks where the network topology is either abstracted or follows a grid model.

4.2.1 Random Network Topologies

Most of the available results for random network topologies are for ALOHA MAC protocol [21, 25–28, 32] because the tractable PPP directly fits to model the spatial distribution of the network nodes. On the other hand, due to correlation among the points of the HCPP, it is more complicated to model the CSMA networks. Hence, there are fewer results related to random CSMA network and I will highlight some of them in this section. In [44], the authors compared the performances of pure ALOHA, slotted ALOHA, and two versions of CSMA protocols to study the effect of the MAC protocol on the outage probability. An optimization problem was formulated and solved numerically to optimize the sensing threshold in order to minimize the outage probability in CSMA networks. However, the vulnerability circle model was used for the outage probability, and the intensity of simultaneously active users was obtained via an iterative solution. In [40], the authors used a modified HCPP to model the spatial distribution of the simultaneously active transmitters in a random CSMA network. Then approximate expressions for the Laplace functional of

the aggregate interference experienced by the test node at the origin as well as the coverage probability were obtained. In [42], the authors proposed and analyzed two channel-aware versions of the CSMA protocol based on a modified HCPP which was used in [40]. The modified version of the HCPP, namely, the modified Matérn CSMA process introduced in [40, 42] defines the retaining probability of HCPP in terms of channel gains rather than distances. In [41], the authors extended the model presented in [40] to obtain the distribution of the throughput achieved by the nodes rather than just its spatial average. In [89], the authors characterized the asymptotic behavior of the outage probability in random ad hoc networks by $P_{outage} \sim a\lambda^b$ when $\lambda \to 0$ (λ is the intensity of concurrent transmitters). The two constants a and b were obtained for general fading and general node distribution. In [51], a novel modified HCPP was proposed to model the spatial distribution of the simultaneously active nodes in a CSMA network in order to overcome the well-known underestimation flaw of the Matérn HCPP type II. In [50], the Matérn HCPP type II was generalized to a general fading environment. A common assumption in all of the above work is that only one channel in available for the coexisting nodes. Different from all the above work in the literature, in this work, I consider that m channels are available for the coexisting CSMA nodes. Then, I obtain the optimal number of channels subject to a self-admission failure probability constraint.

4.2.2 Abstracted and Grid Model for Network Topologies

Maximizing the spatial frequency reuse of IEEE 802.11 WLANs has been a hot research topic for more than two decades. In Sec. 4.2.1 I have cited most of the related work which use the stochastic geometry approach accounting for the random network topology explicitly. Another stream of work in the literature either considered the

worst-case packing (i.e., the hexagonal gird model) [14, 15, 102] or assumed arbitrary locations for the nodes [98, 105]. For instance, [102] examined the effect of controlling the transmit power control vs. adjusting the CSMA sensing threshold to maximize the network throughput. In [14], the authors obtained an upper bound for the spectrum sensing threshold for the safe network operation under cumulative interference in a grid-based network model. However, both [14, 102] considered a hexagonal grid-based model which corresponds to the most dense packed network topology to consider the worst-case scenario. In such a setup, very conservative operating parameters will be obtained (i.e., 0% outage regime) and the spatial frequency reused is not optimized (as shown in Fig. 4.4).

In [98], comprehensive experiments were performed to quantify the effect of IEEE 802.11g/n coexistence on the packet delivery ratio of an IEEE 802.15.4 pair. In the experimental setup, the transmitter was configured to transmit a certain amount of payload and the receiver calculated the number of correctly received packets. The packet delivery ratio at the receiver can be affected by either reporting a channel busy or due to SINR outage. It was concluded that the conservative spectrum sensing threshold (-77 dBm) significantly degrades the packet delivery ratio due to reporting the channel busy. It was also observed that increasing the spectrum sensing threshold from -77 dBm to -65 dBm gives higher performance gain than increasing it from -65 dBm to -55 dBm. This is because, at higher sensing threshold, although the channel is usually reported idle, the SINR outage degrades the packet delivery ratio which confirms my results. For the IEEE 802.15.4 MAC, the concept of utilizing the inactive period in a superframe was first proposed in [101]. However, in [101], the network topology was abstracted and the collision model was assumed. The proposed spectrum sharing method in [101] requires global information about the traffic

requirements of all of the coexisting WPANs and does not take the GTS transmissions into considerations. The work in [100] extended the idea in [101] for the SINR capture model, however, only simulations were presented to reveal the conservativeness of the IEEE 802.15.4 standard.

In [106, 107], multi-channel MAC protocols were analyzed for ad hoc and sensor networks. In this type of multi-channel access, the coexisting nodes communicate on all the available channels through coordination or hopping patterns. We emphasize that in my network model, each SCN tries to access any of the available frequency channels, and once it succeeds to access the channel it remains on it using the superframe structure shown in Fig. 4.1 and Fig. 4.3. That is, to comply with the IEEE 802.15.4 standard, the multiple available channels are used for accommodating multiple SCNs and they are not used for interference avoidance through frequency hopping.

4.3 System Model and Assumptions

4.3.1 Network Model

The network model considered in this chapter consists of multiple stationary SCNs (each with a CN and one or multiple SNs) coexisting in the $\mathbb{R}^2$ Euclidean space as shown in Fig. 4.2. All of the coexisting SCNs have identical traffic load requirement and use the IEEE 802.15.4-based medium access control (MAC) in the beacon-enabled mode. Let $\mathbf{\Psi} = \{x_i; i = 1, 2, 3, ...\}$ be the point process modeling the spatial locations of the CNs, where x_i is the location of the i^{th} CN in the $\mathbb{R}^2$ Euclidean space[4]. Each CN located at x_i has a set of associated SNs randomly located within a fixed distance R_{max}, where R_{max} is the maximum radius of the star network. It is assumed that

[4]We will use x_i to denote both the location of the i^{th} CN as well as the CN itself.

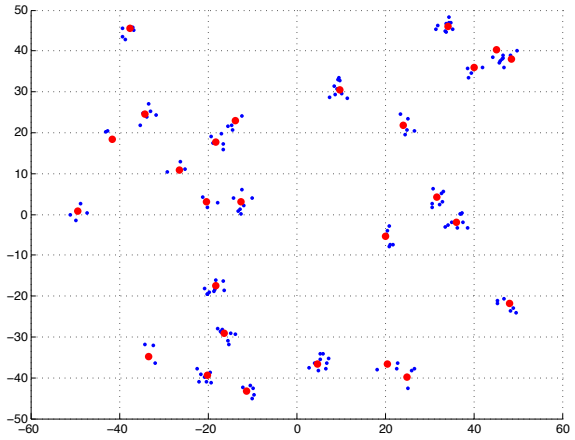

Figure 4.2: The red dots (dots with larger radius) represents the CNs while the blue dots (dots with smaller radius) represents the SNs.

the locations of all CNs are independent, hence, the network can be modeled via a Poisson cluster process [8].

To simplify the analysis, I exploit the fact that, according to the IEEE 802.15.4 standard, in the beacon enabled mode, each CN coordinates the spectrum access within its SCN. Hence, at any generic time instant there is only one active link within any SCN. Therefore, a Poisson bipolar model with a transmitter receiver separation of R_{max} is used to model the spatial distribution of the coexisting SCNs [32]. The maximum link distance R_{max} is used in the Poisson bipolar model [32] to ensure that the optimized spectrum sensing threshold maintains the outage probability for all links within the coexisting SCNs. Therefore, $\mathbf{\Psi}$ is a Poisson point process (PPP) with intensity λ and the SNs are not a part of that PPP. Since I am using point processes to model the CNs, hereafter, I will use the notations "a point in the point process" and "a CN in the network" interchangeably. We will also denote an SCN by its CN.

4.3.2 Channel Model

We consider a general power-law path loss model in which the signal power decays at the rate $Ar^{-\eta}$ with the distance r, where A is a frequency dependent propagation constant, and η is the path-loss exponent. For analysis, only Rayleigh fading environment is assumed[5]. The channel (power) gains from a generic location $x \in \mathbb{R}^2$ to another generic location $y \in \mathbb{R}^2$ is denoted by $h(x, y)$, where $h(x, y) \sim \text{Exp}\ (\mu)$ with mean $\frac{1}{\mu}$. All the channel gains are assumed to be independent from each other, independent from the locations, symmetric, and identically distributed. Hence, for the brevity of exposition, hereafter, the spatial index (x, y) is dropped. A receiver can successfully decode a signal if the received signal power exceeds the received aggregate interference power plus the noise power by a certain threshold β. In other words, the signal-to-interference-plus-noise-ratio (SINR) of a signal should be greater that a certain threshold β for the signal to be successfully decoded by its intended receiver. Otherwise, the intended receiver will experience an outage. All the nodes transmit with the same transmit power P_t and every active SCN always have an active link (i.e., saturation conditions are assumed).

4.3.3 Spatial and Time-Domain Co-existence

According to the IEEE 802.15.4, the CN is responsible to find the channel to schedule the superframe for its SCN's operation. When an SCN is activated, the CN scans the available frequency channels in a sequential order until it finds a channel to schedule its superframe [94]. At each frequency, the CN listens and stores all broadcasted beacons and uses an algorithm similar to the one provided in [100, 101] (which is discussed in Sec. 4.7.2) to choose a time offset such that its active period does not

[5]Rayleigh fading provides tractable ans exact results for the system behavior, techniques to relax the Rayleigh fading assumption is discussed in Sec. 2.3

overlap with the active period of any other SCN within its contention domain. The contention domain is defined by the spectrum sensing threshold υ_s. As discussed in Sec. 3.4, due to channel fading, there is no regular shaped region to determine the contention domain of a CN. Instead, the contention domain of each CN is a random shaped region that depends on the realization of the channel gains. Therefore, I define the set containing the CNs in the contention domain of a test CN located at a generic position $x \in \mathbb{R}^2$ as $\mathbf{N}_x = \left\{y : P_t A h \left\|x - y\right\|^{-\eta} \geq \upsilon_s\right\}$, where $\|.\|$ denotes the Euclidean norm. Fig. 4.3 shows the spatial and time-domain coexistence strategy per frequency channel for the coexisting SCNs. As shown in this figure, if deterministic channel gains are assumed, r_e is the minimum distance where the same logical channel can be reused. On the contrary, if channel fading is considered, r_e will be a random variable which depends on the channel gain realizations. A logical channel is determined by a frequency channel and a time offset [100, 101].

Ideally, in the time domain, the coexisting SCNs should align their superframes such that no two SCNs operate in the same frequency channel at the same time if they are in the same contention domain (as shown in Fig. 4.3)[6]. However, since the superframe scheduling is a long term decision and the channel gains are time-varying stochastic processes, an overlap-free operation between SCNs in the same contention domain is impossible. That is, at the time instant a generic test CN is sensing the channel to schedule its superframe, a nearby CN could have a poor channel gain that excludes it from being in the contention domain of the test CN. On the long run, due to the time variations of the channel gains, the test CN will experience high interference from that nearby CN. Interference from nearby CNs can be limited by tuning the sensing threshold to be more conservative, hence, it is less likely that a nearby CN is excluded from being in the contention domain of the test

[6]The idea of time domain superframe alignment is inspired by the idea presented in [101].

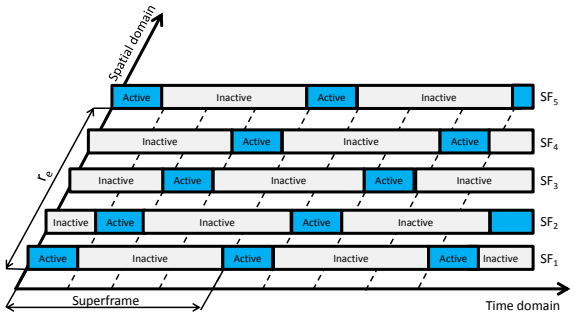

Figure 4.3: Spatial and time-domain coexistence model.

CN. However, a conservative spectrum sensing threshold will decrease the spatial frequency reuse efficiency and increase the self-admission failures of the coexisting SCNs. A self-admission failure is declared if there is insufficient space in the time domain over all available frequency channels for a certain CN to align its superframe without overlapping its active period with the CNs in its contention domain. The self-admission failure reflects the spatial frequency reuse efficiency. That is, the higher the spatial frequency reuse efficiency the lesser the self-admission failures, and vice versa. In a distributed network, the self-admission failure probability is analogous to the blocking probability in a centralized network. When an SCN is activated the CN searches for a logical channel to schedule its superframe. If there exists a time offset that ensures an overlap-free operation of active periods, the CN transmits its beacon and starts its SCN operation. Otherwise, the CN scans the next channel. If the CN cannot align its superframe in the time domain over all available channels, it declares a self-admission failure.

Perfect coordination is assumed within each of the coexisting SCNs. That is, an outage occurs due to the interference from the coexisting SCNs only, not from collisions within the SCN. In my model, the contention resolution process takes place among the coordinator nodes, and the slave nodes are not involved in the contention

resolution process. For optimizing the spectrum sensing threshold, I consider the uplink transmission scenario. However, I would like to emphasize that although I am modeling the interference in the uplink at the CN, the spectrum access coordination among the SCNs (i.e., superframe scheduling) is also performed by the CNs as defined by the IEEE 802.15.4 standard [94].

4.4 Design Methodology

The proposed multi-channel network design is performed in the following steps. First, given an outage probability constraint at a CN, analysis for a single channel network is performed to obtain the optimal spectrum sensing threshold for the CNs that maximizes the spatial frequency reuse for each channel. Then, using the optimal spectrum sensing threshold, I obtain the minimum number of channels required to accommodate the coexisting IEEE 802.15.4-based SCNs subject to a self-admission failure probability constraint. To this end, the superframe structure of the IEEE 802.15.4 is designed for an SCN to maximize spectrum utilization through time-domain interference alignment taking the traffic load requirements in that SCN into account, where the traffic load is defined in terms of the minimum data rate required to be supported by the SCN. Note that for the IEEE 802.15.4 operating in the beacon-enabled mode, the ratio of the active and inactive periods in the superframe is a design parameter that can be manipulated by setting the beacon order (BO) and the superframe order (SO) [94]- [101]. This ratio determines the data rate delivered within the network as well as the number of IEEE 802.15.4 networks that can coexist in the same frequency channel in the same contention domain [100, 101]. Having the number of required channels and the number of logical channels available per frequency, the number of frequency channels required for the network operation can

be easily calculated.

4.5 Optimization of the spectrum sensing threshold

4.5.1 Problem Formulation

The efficiency of a carrier sensing protocol depends on the accurate choice of the spectrum sensing threshold υ_s. Increasing the spectrum sensing threshold decreases the contention domain of each CN, hence, increases the number of CNs that can use the same logical channel which increases the spatial frequency reuse. However, it increases the interference level and the outage probability. Taking this trade-off into account, I optimize the spectrum sensing threshold to maximize the spatial frequency reuse for a single channel subject to an outage probability constraint. Note that the spatial frequency reuse is maximized through maximizing the intensity of SCNs that can operate in the same logical channel. The spectrum sensing threshold is optimized through the following optimization problem:

$$\begin{aligned} \underset{\upsilon_s}{\text{maximize}} \quad & \lambda_C(\upsilon_s, 1) \\ \text{subject to} \quad & \mathcal{O}(\upsilon_s) \leq q \end{aligned} \tag{4.1}$$

where $\lambda_C(\upsilon_s, 1)$ is the intensity of simultaneously active CNs in one channel, $\mathcal{O}(\upsilon_s)$ is the outage probability, and q is the maximum tolerable outage probability. In order to solve this optimization problem, I should first estimate the intensity of simultaneously active CNs and the outage probability in terms of the sensing threshold.

4.5.2 Estimating the Intensity of the Simultaneously Active SCNs Per Channel

A carrier sensing protocol bounds the mutual interference and guarantees a maximum outage probability by conditioning that no two nodes, belonging to the same contention domain, simultaneously use the same logical channel. This condition on the simultaneously active CNs brings correlations among them, and hence, a PPP cannot be directly used to model their spatial distribution. Instead, the Matérn hard core point process (HCPP) can be used since it can capture the condition of having a minimum separation among the points of the process [8].

Matérn HCPP type II is an analytical method used to construct an HCPP ($\mathbf{\Psi}_C$) from a parent PPP ($\mathbf{\Psi}$). In my case, the PPP is the complete set of CNs contending for one channel and the HCPP is the subset of simultaneously active CNs on that channel (i.e., the CNs which have won the contention process). Matérn HCPP type II defines two steps to derive $\mathbf{\Psi}_C$ from the parent PPP $\mathbf{\Psi}$. At first, the marked point process $\tilde{\mathbf{\Psi}}$ is constructed by applying an independent mark uniformly distributed from $[0, 1]$ to $\mathbf{\Psi}$. Then, a marked point (x_i, M_{x_i}) is selected to be in $\mathbf{\Psi}_C$ (i.e., retained in $\mathbf{\Psi}_C$) if and only if it has the lowest mark in its contention domain (i.e., $M_{x_i} < M_{x_j}, \forall j : x_j \in \mathbf{N}_{x_i}$). In my model, since I am including the Rayleigh channel fading, the contention domain of each CN is a random shaped region which is unbounded in theory due to the infinite support domain of the exponential distribution. Following the definition of the Matérn HCPP type II, the intensity of the simultaneously active nodes is given by the following lemma

Lemma 4.5.1. *In a Rayleigh fading environment, for a spectrum sensing threshold*

υ_s, the intensity of CNs that can access the same logical channel is given by

$$\lambda_C(\upsilon_s, 1) = \frac{\lambda\left(1 - e^{-\mathcal{N}(\upsilon_s)}\right)}{\mathcal{N}(\upsilon_s)} \tag{4.2}$$

where $\mathcal{N}(\upsilon_s) = \pi\lambda\left(\frac{P_t A}{\mu\upsilon_s}\right)^{\frac{2}{\eta}}\Gamma(1+\frac{2}{\eta})$ is the mean number of CNs in the contention domain of a generic CN for a given spectrum sensing threshold υ_s.

Proof. In order to obtain an expression for the intensity of CNs that can simultaneously access the same logical channel, I have to drive the distribution of the number of CNs existing in the contention domain of a generic CN. Without loss in generality, I will derive the distribution of the number of CNs in the contention domain of a test CN conditioned on having that test CN at the origin. By Slivnyak's theorem, the results will hold for a generic CN [8]. A generic CN located at $x_i \in \mathbb{R}^2$ is in the contention domain of the test CN located at the origin ($o = (0,0)$) if and only if $P_t A h_i \left\|x_i\right\|^{-\eta} > \upsilon_s$. Hence, the random variable $|\mathbf{N}_o|$, where $|.|$ denotes the set cardinality, can be expressed as a sum of indicator functions as follows:

$$|\mathbf{N}_o| = \sum_{x_i \in \mathbf{\Psi}} \mathbb{1}\{P_t A h_i \left\|x_i\right\|^{-\eta} > \upsilon_s\}. \tag{4.3}$$

Since the distribution of a random variable is uniquely characterized by its moment generating function (*mgf*), I will derive the *mgf* of $|\mathbf{N}_o|$ to infer its distribution. The

mgf of $|\mathbf{N}_o|$ can be expressed as

$$\begin{aligned}
\mathbb{E}\left[e^{t|\mathbf{N}_o|}\right] &= \mathbb{E}\left[e^{t\sum\limits_{x_i\in\mathbf{\Psi}}\mathbb{1}\{P_tAh_i\|x_i\|^{-\eta}>\upsilon_s\}}\right] \\
&= \mathbb{E}_{\mathbf{\Psi}}\left[\prod_{x_i\in\mathbf{\Psi}}\mathbb{E}_{h_i}\left[e^{t\mathbb{1}\{P_tAh_i\|x_i\|^{-\eta}>\upsilon_s\}}\right]\right] \\
&\overset{\text{(i)}}{=} \exp\left\{-\mathbb{E}_h\left[\int_0^{2\pi}\int_0^{\left(\frac{P_tAh}{\upsilon_s}\right)^{\frac{1}{\eta}}}(1-e^t)\lambda r dr d\theta\right]\right\} \\
&= \exp\left\{-\lambda\pi\mathbb{E}_g\left[h^{\frac{2}{\eta}}\right]\left(\frac{P_t}{\upsilon_s}\right)^{\frac{2}{\eta}}(1-e^t)\right\} \\
&= \exp\left\{-(1-e^t)\pi\lambda\left(\frac{P_tA}{\mu\upsilon_s}\right)^{\frac{2}{\eta}}\Gamma\left(1+\frac{2}{\eta}\right)\right\} \qquad (4.4)
\end{aligned}$$

where $\mathbb{E}_{\mathbf{\Psi}}[.]$ is the expectation w.r.t. the point process $\mathbf{\Psi}$ and $\mathbb{E}_h[.]$ is the expectation w.r.t. the channel gain h. The equality (i) is obtained by the probability generating functional of the PPP and switching the order of the integration and the expectation. Differentiating (4.4) and equating with zero, the first moment of $|\mathbf{N}_x|$ is obtained as $\mathbb{E}[|\mathbf{N}_o|] = \pi\lambda\left(\frac{P_tA}{\mu\upsilon_s}\right)^{\frac{2}{\eta}}\Gamma(1+\frac{2}{\eta})$. Hence, the moment generating function of $|\mathbf{N}_o|$ is in the form $\mathbb{E}\left[e^{t|\mathbf{N}_o|}\right] = \exp\left\{(e^t-1)\mathbb{E}[|\mathbf{N}_o|]\right\}$ which is the moment generating function of the Poisson distribution. By Slivnyak's theorem, $|\mathbf{N}_x| \overset{d}{=} |\mathbf{N}_o|$, where $\overset{d}{=}$ denotes the equality in distribution.

Having the distribution of the number of CNs in the contention domain of a generic CN, it is easy to derive its channel access probability. According to the HCPP, a CN can access the channel if and only if it has the lowest mark in its contention domain. Therefore, according to the law of total probability, the channel access probability for a generic CN given that there is only one channel available can be expressed as:

$$\mathcal{P}_{ac}(\upsilon_s,1) = \sum_{n=0}^{\infty} \frac{1}{n+1} \frac{\left(\pi\lambda\left(\frac{P_tA}{\mu\upsilon_s}\right)^{\frac{2}{\eta}}\Gamma(1+\frac{2}{\eta})\right)^n e^{-\pi\lambda\left(\frac{P_tA}{\mu\upsilon_s}\right)^{\frac{2}{\eta}}\Gamma(1+\frac{2}{\eta})}}{n!}$$
$$= \left(\frac{\mu\upsilon_s}{P_tA}\right)^{\frac{2}{\eta}} \frac{1-e^{-\pi\lambda\left(\frac{P_tA}{\mu\upsilon_s}\right)^{\frac{2}{\eta}}\Gamma(1+\frac{2}{\eta})}}{\pi\lambda\Gamma(1+\frac{2}{\eta})}. \quad (4.5)$$

Having the channel access probability, the intensity of the CNs that can use the same logical channel can be expressed as $\lambda\mathcal{P}(\upsilon_s,1)$ and **Lemma 4.5.1** is proved. □

Note that, as discussed in Chapter 3, the HCPP suffers from the intensity underestimation problem for relatively high intensity of CNs (e.g., $\mathbb{E}[|\mathbf{N}_x|] \geq 5$). This underestimation problem can be corrected by an intensity dependent correction factor using Fig. 3.10.

4.5.3 Modeling the Aggregate Interference and Outage Probability

Carrier sensing and the contention based access are meant to limit the aggregate interference and outage probability. According to system model, the CN senses the spectrum and schedules its superframe to guarantee an overlap free operation with the set of CNs in its contention domain. The main problem is that the superframe scheduling is a long term decision, while, for a given sensing threshold, the contention domain is random and dynamically changing with the channel gain variations for each CN. Therefore, the CN decision for scheduling its superframe cannot guarantee a 100% overlap-free operation with all other CNs coexisting in the different realization of its contention domain. Instead, it only guarantees an overlap-free operation with the CNs belonging to the contention domain realized at the point of time when the CN listens to the spectrum and acquires the beacons information to schedule

its superframe. Therefore, in the long run, an SCN may suffer unexpectedly high interference due to the time variation of the channel gains. In this section, I will account for the time-varying channel gains and derive the outage probability as a function of the spectrum sensing threshold.

At the time instant when the test CN located at an arbitrary origin is sensing the channel and scheduling its superframe, the interference from the set of CNs defined as $\mathbf{N}_x = \left\{x_i : P_t A h_i \left\|x_i\right\|^{-\eta} > \upsilon_s\right\}$ is avoided. Hence, interference is only experienced from the set of CNs defined as $\mathbf{\Psi} \setminus \mathbf{N}_x = \left\{x_i : P_t A h_i \left\|x_i\right\|^{-\eta} < \upsilon_s\right\}$. Therefore, based on the location of the CN and the corresponding instantaneous channel gain, it can be determined whether it is in the contention domain of the test CN or not. That is, a generic CN located at a distance r away from the test CN is not in the contention domain of the test CN with probability $F_h\left(\frac{\upsilon_s r^\eta}{P_{tA}}\right)$, where $F_h(.)$ denotes the cumulative distribution function (*cdf*) of the channel (power) gains. Since all channel gains are i.i.d. and the CNs access the same logical channel by contention, the interference sources will constitute a non-homogenous PPP $\mathbf{\Psi}_{\mathcal{I}}$ with intensity $\lambda_I = \lambda_C(\upsilon_s, 1) F_h\left(\frac{\upsilon_s r^\eta}{P_{tA}}\right)$. Note that the interference sources constitute a PPP (not an HCPP) due to the channel gain variations with time. That is, due to the channel gain variations, the condition that no two CNs in the same contention domain operate on the same logical channel does not hold throughout the operation of the CNs. With this interpretation of the aggregate interference, the outage probability for a generic CN at a generic time instant can be given by the following lemma:

Lemma 4.5.2. *In a Rayleigh fading environment, for a spectrum sensing threshold*

υ_s, the outage probability of a generic CN is given by:

$$\mathcal{O}(\upsilon_s) = 1 - \exp\left\{ -\frac{\sigma^2 \mu \beta R_{max}^{\eta}}{P_t A} - \frac{2\pi\lambda_C(\upsilon_s, 1)}{\eta} \left(\frac{P_t A}{\upsilon_s \mu}\right)^{\frac{2}{\eta}} \int_0^{\infty} \frac{x^{\frac{2}{\eta}-1}}{\left(1 + \frac{P_t A x}{\mu \beta \upsilon_s R_{max}^{\eta}}\right)} \left(1 - e^{-x}\right) dx \right\}. \tag{4.6}$$

where σ^2 is the thermal noise variance.

Proof. The outage probability of a generic CN can be written as

$$\begin{aligned}
\mathcal{O}(\upsilon_s) &= \mathbb{P}\left\{\text{SINR} \leq \beta\right\} \\
&= \mathbb{P}\left\{\frac{P_t A h R_{max}^{-\eta}}{\sigma^2 + \mathcal{I}} \leq \beta\right\} \\
&= 1 - \mathbb{P}\left\{h > \frac{(\sigma^2 + \mathcal{I})\beta R_{max}^{\eta}}{P_t A}\right\} \\
&= 1 - \mathbb{E}_{\mathcal{I}}\left[\exp\left(-\frac{(\sigma^2 + \mathcal{I})\mu\beta R_{max}^{\eta}}{P_t A}\right)\right] \\
&= 1 - \exp\left(-\frac{\sigma^2 \mu \beta R_{max}^{\eta}}{P_t A}\right) \mathbb{E}_{\mathcal{I}}\left[\exp\left(-\frac{\mathcal{I}\mu\beta R_{max}^{\eta}}{P_t A}\right)\right] \\
&= 1 - \exp\left(-\frac{\sigma^2 \mu \beta R_{max}^{\eta}}{P_t A}\right) \mathcal{L}_{\mathcal{I}}(s)\big|_{s=\frac{\mu\beta R_{max}^{\eta}}{P_t A}}
\end{aligned} \tag{4.7}$$

where $\mathcal{I}$ is the aggregate interference experienced by the test CN, and $\mathcal{L}_{\mathcal{I}}(.)$ is the Laplace transform of the probability density function (*pdf*) of the aggregate interference. The aggregate interference experienced by the test CN from the interference sources can be written as

$$\mathcal{I} = \sum_{x_i \in \mathbf{\Psi}_{\mathcal{I}}} P_t A h_i \left\|x_i\right\|^{-\eta}. \tag{4.8}$$

The Laplace transform of the *pdf* of aggregate interference can be written as

$$\begin{aligned}
\mathcal{L}_{\mathcal{I}}(s) = \mathbb{E}\left[e^{-s\mathcal{I}}\right] &= \mathbb{E}\left[e^{-s\sum\limits_{x_i\in\mathbf{\Psi}_{\mathcal{I}}} P_t A h_i \|x_i\|^{-\eta}}\right] = \mathbb{E}_{\mathbf{\Psi}}\left[\prod_{x_i\in\mathbf{\Psi}_{\mathcal{I}}} \mathbb{E}_{h_{x_i}}\left[e^{-sP_tAh_i\|x_i\|^{-\eta}}\right]\right] \\
&\overset{\text{(ii)}}{=} \exp\left\{-\mathbb{E}_h\left[\int_0^{2\pi}\int_0^{\infty}(1-e^{-sP_tAhr^{-\eta}})\lambda_C(\upsilon_s,1)F_h\left(\frac{\upsilon_s r^{\eta}}{P_tA}\right)rdrd\theta\right]\right\} \\
&= \exp\left\{-2\pi\lambda_C(\upsilon_s,1)\mathbb{E}_h\left[\int_0^{\infty}(1-e^{-sP_tAhr^{-\eta}})F_h\left(\frac{\upsilon_s r^{\eta}}{P_tA}\right)rdr\right]\right\} \\
&= \exp\left\{-2\pi\lambda_C(\upsilon_s,1)\left[\int_0^{\infty}(1-\mathcal{L}_h\left(sP_tAr^{-\eta}\right))F_h\left(\frac{\upsilon_s r^{\eta}}{P_tA}\right)rdr\right]\right\} \\
&\overset{\text{(iii)}}{=} \exp\left\{-\frac{2\pi\lambda_C(\upsilon_s,1)}{\eta}\left(\frac{P_tA}{\upsilon_s\mu}\right)^{\frac{2}{\eta}}\int_0^{\infty}\frac{s\upsilon_s x^{\frac{2}{\eta}-1}}{s\upsilon_s+x}\left(1-e^{-x}\right)dx\right\}.
\end{aligned} \tag{4.9}$$

where (ii) is obtained similar to (i) in (4.4), and (iii) is obtained by writing the expressions for the Laplace transform of the *pdf* of the channel gains $\mathcal{L}_h(s) = \left(1+\frac{s}{\mu}\right)^{-1}$, the *cdf* of the channel gains $F_h(g) = 1-e^{-\mu g}$, and changing variables $x = \frac{\upsilon_s r^{\eta}}{P_tA}$. By substituting the expression for the Laplace transform in (4.9) into (4.7), the outage probability is obtained. □

It is very hard to find an explicit form for the optimal exclusion region due to the complicated nature of the intensity and the outage probability expressions. However, since both the objective function and the constraint in (4.1) are non-decreasing in υ_s, a unique optimal value exists at the extreme boundary of the constraint (i.e., when the constraint is satisfied with equality). Hence, the optimal spectrum sensing threshold ($\upsilon_s{}^*$) which maximizes the spatial frequency reuse can be obtained numerically.

4.6 Coexistence Analysis for the Multi-channel Scenario

In a multi-channel environment, let $\mathbf{\Psi}_C^m$ denote the point process which models the spatial distribution of the admitted CNs in all of the m channels. It is straightforward to extend the HCPP definition from one channel to the m-channel case. Due to the availability of m channels, there is no contention in the contention domain as long as the number of channels is greater than or equal to the number of contending nodes. Therefore, the only modification (of the one channel case) is that a marked point (x_i, M_{x_i}) will be selected to be in $\mathbf{\Psi}_C^m$ if and only if it has any of the lowest m marks in its contention domain ($\mathbf{N}_{x_i}$). According to this definition, I can specify the probability of retaining a point as follows: a random point $x_i \in \mathbf{\Psi}$ is retained in $\mathbf{\Psi}_C^m$ if it coexists with $(m-1)$ or fewer number of points in $\mathbf{N}_{x_i}$, or if it coexists with n points $(n \geq m)$ in $\mathbf{N}_{x_i}$ given that it has one of the m^{th} lowest marks among all of the coexisting n points. Due to the uniform distribution of the marks among the n points coexisting with x_i in $\mathbf{N}_{x_i}$, the probability that x_i has one of the lowest m marks is given by $m/(n+1)$. Hence, by the law of total probability, I have the following result.

Theorem 4.6.1. *In an m channel carrier sensing-based random network in a Rayleigh fading environment, the retaining probability of a generic CN $x_i \in \mathbf{\Psi}$ in $\mathbf{\Psi}_C^m$ is given by*

$$\mathcal{P}_{ac}(\upsilon_s, m) = \frac{e^{-\mathcal{N}(\upsilon_s)}}{\mathcal{N}(\upsilon_s)} \left[m\left(e^{\mathcal{N}(\upsilon_s)} - 1\right) - \sum_{n=1}^{m} \frac{(m-n)\left(\mathcal{N}(\upsilon_s)\right)^n}{n!} \right] \tag{4.10}$$

where $\mathcal{N}(\upsilon_s)$ is as defined in (4.2). Since the intensity of the m-channel point process is given by $\lambda_C(\upsilon_s, m) = \mathcal{P}(\upsilon_s, m)\lambda$, I have

$$\lambda_C(\upsilon_s, m) = \frac{\lambda e^{-\mathcal{N}(\upsilon_s)}}{\mathcal{N}(\upsilon_s)} \left[m\left(e^{\mathcal{N}(\upsilon_s)} - 1\right) - \sum_{n=1}^{m} \frac{(m-n)\left(\mathcal{N}(\upsilon_s)\right)^n}{n!} \right]. \tag{4.11}$$

Proof. Since the contention resolution process takes place only when the number of channels is less than the number of nodes, the retaining probability of a generic node $x_i \in \mathbf{\Psi}$ in $\mathbf{\Psi}_C^m$ can be written as

$$\begin{aligned}\mathcal{P}_{ac}(\upsilon_s, m) &= \sum_{n=0}^{m-1} \frac{(\mathcal{N}(\upsilon_s))^n \, e^{-\mathcal{N}(\upsilon_s)}}{n!} + \sum_{n=m}^{\infty} \frac{m}{n+1} \frac{(\mathcal{N}(\upsilon_s))^n \, e^{-\mathcal{N}(\upsilon_s)}}{n!} \\ &= e^{-\mathcal{N}(\upsilon_s)} \left[\frac{m\left(e^{\mathcal{N}(\upsilon_s)} - 1\right)}{\mathcal{N}(\upsilon_s)} - \sum_{n=0}^{m-1} \frac{(m-(n+1))\,(\mathcal{N}(\upsilon_s))^n}{(n+1)!} \right] \\ &= \frac{e^{-\mathcal{N}(\upsilon_s)}}{\mathcal{N}(\upsilon_s)} \left[m\left(e^{\mathcal{N}(\upsilon_s)} - 1\right) - \sum_{n=1}^{m} \frac{(m-n)\,(\mathcal{N}(\upsilon_s))^n}{n!} \right].\end{aligned}$$

□

It can be observed that the intensity of an m-channel point process is less than or equal to the m-fold intensity of the one channel HCPP (i.e., $\lambda_C(\upsilon_s, m) \leq m \times \lambda_C(\upsilon_s, 1)$). The equality is only obtained when $\lambda \to \infty$. That is, $\lim\limits_{\lambda\to\infty} \lambda_C(\upsilon_s, m) = m \lim\limits_{\lambda\to\infty} \lambda_C(\upsilon_s, 1) = \frac{m}{\pi\left(\frac{P_t A}{\mu \upsilon_s}\right)^{\frac{2}{\eta}} \Gamma(1+\frac{2}{\eta})}$. This is quite intuitive because as $\lambda \to \infty$ each contention domain within the network will always have some unadmitted nodes. Therefore, each extra channel accommodates as many SCNs as any of the previously added channels did. It is worth mentioning that, for $m = 1$, the model reduces to the Matérn HCPP type II (see equation (4.2)).

The m-th channel coexistence gain $\mathcal{G}(m)$ is defined as the additional intensity that can be accommodated by the system if the number of channels is increased from $(m-1)$ to m. $\mathcal{G}(m)$ is given by

$$\begin{aligned}\mathcal{G}(m) &= \lambda_C(\upsilon_s, m) - \lambda_C(\upsilon_s, m-1) \\ &= \frac{\lambda\left(1 - e^{-\mathcal{N}(\upsilon_s)}\right)}{\mathcal{N}(\upsilon_s)} - \sum_{n=1}^{m} \frac{\lambda\,(\mathcal{N}(\upsilon_s))^{n-1}\, e^{-\mathcal{N}(\upsilon_s)}}{\mathcal{N}(\upsilon_s) n!}. \qquad (4.12)\end{aligned}$$

In order to obtain the minimum number of channels that can accommodate the

coexisting SCNs subject to the self-admission failure probability constraint ψ, I formulate an optimization problem as follows:

$$\begin{aligned} &\text{minimize} \quad && m \\ &\text{subject to} \quad && \sum_{k=1}^{m} \mathcal{G}(k) \geq (1-\psi)\lambda \\ & && m \in \mathbb{Z}^+ \end{aligned} \tag{4.13}$$

where $\mathbb{Z}^+$ is the set of all positive integers. Due to the nature of $\mathcal{G}(m)$, it is hard to find an explicit expression for the optimal number of channels required to accommodate $(1-\psi)$ percent of the total number of coexisting SCNs. Therefore, the optimal number of channels can be obtained by solving (4.13) numerically. However, I can find bounds on m as well as a good initial value of m for the numerical solution of (4.13).

Using graph theory, the optimization problem in (4.13) can be reduced to a vertex coloring problem. The Graph $G = \{V, E\}$ is said to be m-colorable if each vertex $v \in V$ can be colored with one of the m colors and no two adjacent vertices share the same color. For any realization of the PPP, a graph $G = \{V, E\}$ can be constructed. Each SCN is considered as a vertex and there are edges connecting the star networks (vertices) in the same contention domain. The chromatic number (minimum number of colors required to color G) for the graph G corresponds to the minimum number of channels required to accommodate the coexisting SCNs. According to the graph theory, the chromatic number for any graph G is upper bounded by $\Delta_{max} + 1$, where Δ_{max} is the maximum degree of a vertex in the graph G [104]. According to the original PPP problem, the degree Δ of any vertex $v \in V$ is a Poisson random variable. The maximum degree Δ_{max} is chosen such that Prob $\{\Delta > \Delta_{max}\} \leq \psi$ is satisfied.

Then, the optimization problem in (4.13) can be rewritten as follows:

$$\begin{aligned} &\text{minimize} \quad m \\ &\text{subject to} \quad \sum_{k=1}^{m} \mathcal{G}(k) \geq (1-\psi)\lambda \\ &\qquad\qquad 1 \leq m \leq \Delta_{max} + 1. \end{aligned} \tag{4.14}$$

Two good initial values can be used for (4.14). First, Δ_{max} can be used as the initial value, however, due to the nature of the cumulative distribution function (CDF) of the Poisson distribution, Δ_{max} does not have a closed-form expression. Second, the average degree value ($\mathbb{E}[\Delta] = \mathcal{N}(\upsilon_s)$) can be used as the initial value since it has an explicit expression. Since the achievable intensity $\lambda_C(\upsilon_s, m)$ is a non-decreasing function of the number of channels (m), there is a global optimal value for m which just satisfies the self-admission failure constraint in (4.14). Note that the optimal value m^* here is the optimal number of channels if each of the coexisting SCNs chooses a random channel upon availability.

4.7 Superframe Design and Time-Domain Interference Alignment

Up to this point, I have optimized the sensing threshold υ_s and calculated the total number of channels (m^*) required for the operation of the coexisting SCNs. In this section, I complete my framework and design the superframe structure by choosing the values of BO and SO. Then, I calculate m_t, which is the number of SCNs that can align their superframes per frequency channel. Finally, the number of required frequency channels is given by $m_f = m^*/m_t$.

4.7.1 Superframe Design

According to the application supported by the SCN, a minimum data rate of δ is required to be supported. Given the required data rate of δ Mb/s for each SCN, the superframe of the IEEE 802.15.4 can be designed. According to the standard, the superframe duration is defined in terms of the standard value $aBaseSuperframeDuration = aBaseSlotDuration \times aNumSuperframeSlots$ as shown in Fig. 4.1. Regardless of the active period duration, $aNumSuperframeSlots$ is always equal to 16 time slots. The time slot duration is given by $aBaseSlotDuration \times 2^{SO}$, where $aBaseSlotDuration = 60$ symbols. Each symbol consists of 4 bits. Therefore, the total number of bits transmitted per superframe $B_s = 4 \times 60 \times 16 \times 2^{SO}$. The beacon interval BI is given by $BI = aBaseSuperframeDuration \times 2^{BO}$ symbols $= 4 \times 60 \times 16 \times 2^{BO}$. According to the standard, the bit duration is equal to 4 μs. Then, $BI = 16 \times 60 \times 16 \times 2^{BO} \mu s$. Hence, the total data rate served within each SCN is $D_t = \frac{B_s}{BI} = 2^{SO-BO-2}$ Mb/s. Since $(0 \leq SO \leq BO \leq 14)$, if I let $BO = SO$ (i.e., the SCN is always active), then the maximum achievable data rate $D_{max} = 2^{-2}$ Mb/s = 250 kb/s which is the maximum achievable bit rate defined by the IEEE 802.15.4 standard.

From the previous analysis, the values of BO and SO should be chosen to satisfy the following:

$$BO - SO \leq \log_2 \left(\frac{1}{\delta}\right) - 2 \tag{4.15}$$

where δ is in Mb/s. According to the standard, I have $0 \leq SO \leq BO \leq 14$, hence, there are feasible solutions for (4.15) unless $\delta \geq 0.25$ Mb/s, which is the maximum achievable data rate for the IEEE 802.15.4 technology. It is worth mentioning that the supported data rate is independent of the actual values of BO and SO. Instead, it depends on their difference as shown in (4.15) which is consistent with the experiment

done in [101].

4.7.2 Time-Domain Interference Alignment

According to the IEEE 802.15.4 standard, two SCNs coexisting in the same contention domain can operate simultaneously in the same frequency channel without any mutual interference if they avoid overlapping the active periods of their superframes. This overlap-free operation can be achieved through time-domain superframe alignment. Let me consider a general scenario where there are n SCNs coexisting and operating in the same contention domain of the incoming SCN. The incoming SCN can coexist with an overlap-free operation if and only if $\left(2^{BO} - 2^{SO}\right) \geq \sum_{i=1}^{n} 2^{SO_i}$. In other words, at most 2^{BO-SO} SCNs can coexist and operate simultaneously in one frequency channel without overlapping their superframes if perfect superframe alignment is ensured (as shown in Fig. 4.3 for $BO - SO = 2$). Due to the exponential nature of the superframe duration (SD) and the beacon interval (BI), perfect superframe alignment can be easily achieved if the time offset to align the superframes of the coexisting SCNs is chosen to be a multiple of the superframe duration, that is: $T_{\text{offset}} = k \times aBaseSuperframeDuration \times 2^{SO}$, for $0 \leq k \leq 2^{BO-SO} - 1$.

The main idea of the coexistence strategy proposed in this work is that each SCN should avoid interfering with SCNs within its contention domain (i.e., major interferers). But it can interfere with SCNs outside its contention domain. Interference with major interferers can be avoided using the time-domain superframe alignment discussed above. Consequently, an incoming SCN located at $x \in \mathbf{\Psi}$ divides the coexisting SCNs (according to the received beacon power from each CN) into two sets $\mathbf{N}_x$ and $\mathbf{\Psi} \setminus \mathbf{N}_x$ for neighbors and non-neighbors SCNs, respectively. Each coexisting SCN is considered to be a neighbor SCN if the received power of its beacon is

greater than $\upsilon_s{}^*$ (i.e., the major interference source that should be avoided), and is considered to be a non-neighbor SCN if the received power of its beacon is less than the spectrum sensing threshold $\upsilon_s{}^*$ (i.e., the minor interference source that can be tolerated). An incoming SCN listens to the beacons and obtains their time offsets. Then, the incoming SCN will try to align its superframe with the SCNs in $\mathbf{N}_x$, and will access the channel if an overlap free operation is ensured. If not, the SCN will try a different channel. If it fails to coexist in any of the available channels, it declares a self-admission failure.

The channel listening period is controlled through the scan duration ($ScanDuration$) field in ($MLME-SCAN.request$) generated by the network layer of the standard [94]. According to the IEEE 802.15.4 standard, the scan duration is defined by $aBaseSuperframeDuration \times (2^y + 1)$, where $0 \leq y \leq 14$. It can be observed that y has the same range of values as BO. Therefore, by simply replacing y with BO used for the coexisting SCN superframes, the incoming WPAN will listen to the channel for a time equal to the beacon interval, and register the time offset for each beacon. Then, it calculates the set of time offsets to schedule its superframe. It is worth mentioning that it is sufficient to characterize the channel occupancy by a single BI duration, as what will follow is just a repeated version of this duration [100, 101].

According to the proposed time-domain superframe alignment, the number of channels available per frequency is equal to the total number of superframes that can be aligned per frequency channel. Therefore, the number of channels available per

frequency (m_t) can be maximized through the following simple optimization problem:

$$\begin{aligned} \underset{BO,SO}{\text{maximize}} \quad & m_t = 2^{BO-SO} \\ \text{subject to} \quad & BO - SO \leq \log_2\left(\frac{1}{\delta}\right) - 2 \\ & (BO - SO) \in \{0, 1, 2, ..., 14\}. \end{aligned} \tag{4.16}$$

The solution for this optimization problem is given by any values of BO and SO that satisfies $BO - SO = \left\lfloor \log_2\left(\frac{1}{\delta}\right) - 2 \right\rfloor$. Then, the number of frequency channels required for the coexisting SCNs operation is given by $m_f = \lceil m/m_t \rceil$.

4.8 Performance Evaluation

4.8.1 Numerical Results

For the numerical evaluation (using Matlab), a unit transmit power is chosen for every transmitter, $\eta = 4$ for the path-loss exponent, and $\beta = 2$ for the SIR threshold to insure bit error rate less than 10^{-6} [94]. The noise power is ignored due to the interference power dominance [26].

Fig. 4.4 shows the behavior of the objective function and the constraint of the sensing threshold optimization problem in (4.1) for different mean channel gains as the sensing threshold varies. Note that the success probability is just $(1 - \mathcal{O}(\upsilon_s))$. The figure shows that there is a unique optimal solution which is at the boundary of the constraint. That is, if the outage probability threshold is $q \leq 0.1$ (i.e., success probability ≥ 0.9), then the optimal sensing threshold is $\upsilon_s{}^* =$ - 65 dBm, -56 dBm, and -54 dBm, respectively, for $\frac{1}{\mu} = 0.1$, 0.5, and 1 (which are the spectrum sensing thresholds corresponding to success probability of 0.9). The figure also confirms the conservativeness of the IEEE 802.15.4 standard (where the sensing threshold is less

than -75 dBm) and shows the importance of spatial frequency reuse. For instance, the figure shows that, with $\frac{1}{\mu} = 0.5$, the intensity of the coexisting SCNs can be tripled (from its original value at $\upsilon_s = -75$ dBm) by sacrificing 1% outage probability and can by increased 10 times by sacrificing 5% outage probability. Note that the proposed design paradigm will enable SCNs with intensity of $2^{BO-SO}\lambda_C({\upsilon_s}^*, 1)$ to coexist per channel instead of intensity $\lambda_C(-75, 1)$.

An insightful observation from fig. 4.4 is that as the mean channel gain decreases, the CNs are required to be more conservative to attain the same success probability. To explain this behavior, in Fig. 4.5, I plot the intensity of interference sources vs the distance from the test CN[7] for different mean channel gains and spectrum sensing thresholds. In Fig. 4.5, as the mean channel gain decreases, it is more likely to have nearby CNs excluded from the contention domain, hence, during the operation of the intended CN, the interference sources may start from a relatively near distance. Therefore, the CNs are required to be more conservative to avoid interference from nearby SCNs. Note that the intensity of the non-homogenous PPP of the interference sources saturates at $\lambda_C(\upsilon_s, 1)$.

It is worth mentioning that my results on optimal spectrum sensing threshold are consistent with the experimental results in [98] for coexistence between the IEEE 802.15.4 and IEEE 802.11 networks. In [98], the authors reported that the spectrum sensing threshold defined in the standard is very conservative for coexistence between the IEEE 802.15.4 and IEEE 802.11 networks. The optimal sensing threshold in [98] falls within the same range of the optimal sensing thresholds reported in this work. Although, the authors in [98] did not provide any analytical technique to obtain the optimal sensing threshold, their results confirm the conservativeness of the IEEE 802.15.4 standard for choosing a very low spectrum sensing threshold which

[7]By Slivnyak's theorem [8], the results hold for any CN.

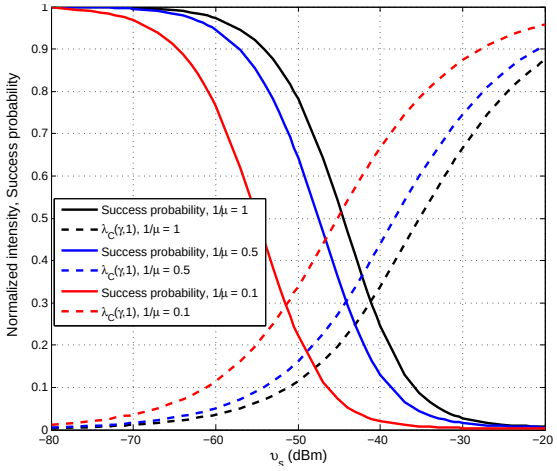

Figure 4.4: Behavior of the normalized intensity λ_c and the success probability with the spectrum sensing threshold υ_s.

significantly degrades the spatial reuse intensity.

Fig. 4.6 shows that for relatively high intensity of the parent PPP (e.g., $\lambda \geq 0.5$), the main factor controlling the outage probability as well as the intensity of simultaneously active nodes $\lambda_C(\upsilon_s, 1)$ is the spectrum sensing threshold υ_s. This means that with the proper choice of υ_s, the SIR experienced by any node in the network becomes independent of the intensity of the nodes contending for the spectrum. Hence, the spectrum sensing threshold υ_s is the only design parameter for the single channel design of carrier sensing-based distributed random networks.

Fig. 4.7 compares $\lambda_C(\upsilon_s, m)$ and $m \times \lambda_C(\upsilon_s, 1)$ to the m-channel point process realization for $m = 2$. The results show that the $m \times \lambda_C(\upsilon_s, 1)$ is quite inaccurate as it highly overestimates the number of nodes that can coexist in 2 channels. Note that the λ curve shows the maximum intensity of SCNs that can coexist; hence, $m \times \lambda_C(\upsilon_s, 1)$ gives an infeasible solution. On the other hand, the proposed model (i.e., $\lambda_C(\upsilon_s, 2)$) can estimate the intensity of the simultaneously active SCNs in 2 channels.

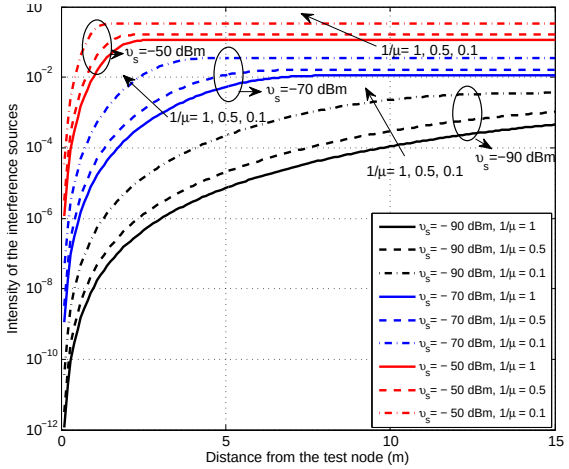

Figure 4.5: Intensity of interfering SCNs vs. the distance from the test CN.

Fig. 4.8 shows that nonlinear relationship between number of channels and the intensity of coexisting SCNs. Fig. 4.8(a) shows the normalized achievable intensity $\frac{\lambda_C(\upsilon_s,m)}{\lambda}$ with the number of channels for different intensities of SCNs. The results show that the achievable coexistence intensity ($\lambda_C(\upsilon_s, m)$) does not linearly increase with the number of channels. The rate of increase in the achievable intensity decreases with the number of channels and then it saturates when all of the SCNs can be admitted. Fig. 4.8(b) shows the normalized added value of each extra channel $\frac{\mathcal{G}(m)}{\lambda}$ for different intensities of SCNs. The results show that for low intensities, the value of each extra channel decreases in terms of the coexistence gain. On the other hand, for high intensities, the value of each extra channel remains constant until a certain value, and then it begins to decrease. This is due to the fact that, for high intensities (see Fig. 4.8(b) for the $\lambda = 2$ node/m^2 case), when adding the first 4 channels, each contention domain still contains the unadmitted SCNs. Therefore, the value of each extra channel remains almost constant. Then, for each extra channel after the fourth, some contention domains have been already saturated since all of the coexisting SCNs within it are admitted. Therefore, this extra channel is wasted in some contention

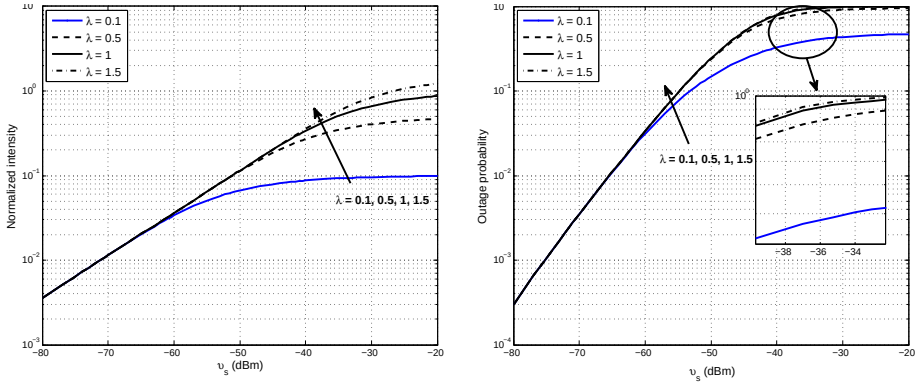

(a) (b)

Figure 4.6: Effect of spectrum sensing threshold υ_s under different node intensities (for $m = 1$ channel).

Table 4.1: The optimal number of channels (m^*)

λ	$\lceil \mathbb{E}[\Delta] \rceil$	$\psi = 0.1$		$\psi = 0.01$	
		m^*	$\Delta_{max}+1$	m^*	$\Delta_{max}+1$
0.1	1	2	2	3	3
0.5	2	3	4	6	6
1	4	4	6	7	9
1.5	5	6	9	9	11
2	7	8	11	10	14

domains.

Finally, Table 4.1 shows that the optimal number of channels m^* is always upper-bounded by $\Delta_{max}+1$ and that the average degree $\lceil \mathbb{E}[\Delta] \rceil$ gives a good initial point for solving (4.14) numerically.

4.8.2 Discussions

The main focus of this work is to develop a distributed approach to orchestrate the superfames (i.e., the active periods) and to adjust the sensing thresholds of the coexisting IEEE 802.15.4 SCNs in order to maximize the time and spatial domain utilization of radio spectrum, and hence, maximize the number of IEEE 802.15.4 SCNs that

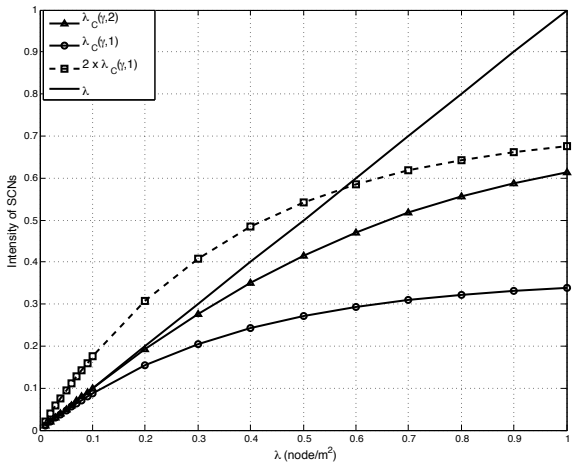

Figure 4.7: Comparing the results for $\lambda_C(\upsilon_s, m)$ and $m \times \lambda_C(\upsilon_s, 1)$ for $m = 2$ channels at $\lambda = 1$ node/m^2, $\upsilon_s = 10^{-5}$ dBm and $\frac{1}{\mu} = 0.1$.

can operate in each vacant channel in the crowded ISM band. However, it is worth mentioning that in the ISM band, in certain scenarios, it could be very hard to find a completely vacant channel for the operation of IEEE 802.15.4 SCNs. An in-depth study on heterogeneous interference (i.e., interference from radios having different parameters such as transmission bandwidth and power) in the ISM band was conducted in [108] using stochastic geometry. Given the independence between the technologies coexisting in the ISM band, the total outage probability for an SCN will be the union of the two outage events, namely, the outage due to homogenous interference (i.e., the interference resulting from other IEEE 802.15.4 SCNs) calculated in this chapter and the outage due to heterogeneous interference sources (e.g., IEEE 802.11 nodes or microwave ovens) as calculated in [108].

Another important contribution of the developed paradigm is the calculation of the minimum number of channels required to accommodate a certain intensity of IEEE 802.15.4 SCNs subject to a certain self-admission failure probability. In some scenarios, the number of channels is not a design parameter and the network designer

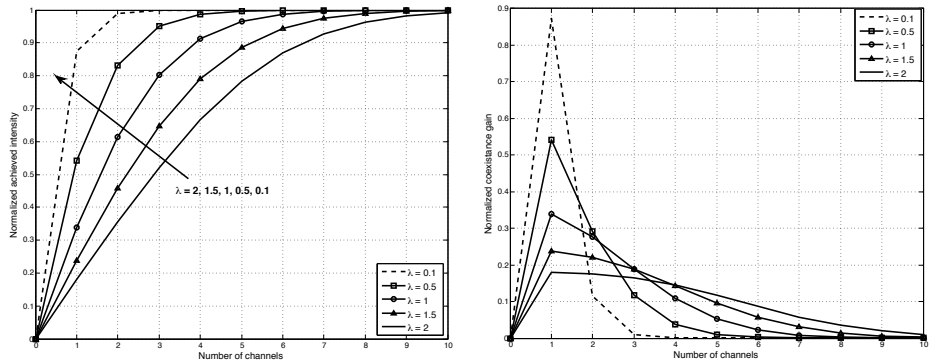

(a) (b)

Figure 4.8: a) Normalized achievable intensity per channel at $\upsilon_s = 10^{-5}$ dBm and $\frac{1}{\mu} = 0.1$, b) Normalized coexistence gain per channel at $\upsilon_s = 10^{-5}$ dBm and $\frac{1}{\mu} = 0.1$.

is limited by a certain number channels. For those scenarios, my model can be used to quantify the performance degradation due to the unavailability of sufficient number of channels and to choose where to sacrifice the performance (i.e., sacrifice the outage probability, the supported data rate per SCN, or the self-admission failure probability).

The results shown in Figures/figs-ch3. 4.4-4.6 highlight the criticality of the choice of the spectrum sensing threshold. For instance, with $\frac{1}{\mu} = 0.5$, from Fig. 4.4, it can be observed that for spectrum sensing threshold in the range of -80 to -60 dBm, the achievable intensity of SCNs per channel (spatial-domain efficiency) is increased 10 times from its original value at -80 dBm with a small increase (i.e., 5%) in outage probability. On the other hand, due to the sharp increase in the outage probability when $\upsilon_s > -60$ dBm, a 1 dBm difference in the sensing threshold can cause up to 10% more outage for a negligible increase in the achievable intensity of SCNs per channel. Note that according to the IEEE 802.15.4 standard, the sensing threshold is equal to the receiver sensitivity which is less than or equal to -75 dBm, and this is very far from optimal. Note that the coexistence experiments between the IEEE

802.15.4 and the IEEE 802.11 WLAN done in [98] confirmed the conservativeness of the IEEE 802.15.4 standard in choosing the spectrum sensing threshold.

The sensing threshold is optimized through a one channel analysis for two reasons. The first reason is to bound the worst-case scenario where all of the coexisting SCNs choose the same channel for their operation. Second, for relatively high intensity of the coexisting SCNs, the sensing threshold is the only limiting parameter for the interference as well as the achievable intensity as shown in Fig. 4.6. Therefore, for relatively high intensities of SCNs, the optimality of the sensing threshold in one channel holds for multiple channels.

Another very insightful observation is that the results reveal how misleading the one channel results can be for the multi-channel planning of random wireless networks. That this, if the one channel analysis results in the admission of 50% of the total coexisting SCNs, then, the network designer may think that 2 channels should be enough to accommodate the total coexisting SCNs. However, looking into the results (see Fig. 4.8(a) for $\lambda = 0.5$ node/m^2 case), while the first channel can accommodate 53% of the total coexisting SCNs, the second channel will only accommodate an additional 29% of the total coexisting SCNs, resulting in a total admission of 82% of the coexisting SCNs. That is, 18% of the coexisting SCN will encounter self-admission failure. The same observation applies to all other intensities of SCNs. This insightful observation illustrates the importance of the developed framework in the design and analysis of multi-channel random networks.

4.9 Chapter Summary

We have addressed the problem of multi-channel analysis and spectrum-efficient design of IEEE 802.15.4-based random wireless networks operating in the beacon-

enabled mode. A novel framework has been developed to optimize the spectrum sensing threshold under channel gains uncertainties to maximize the spatial-domain utilization, obtain the minimum number of channels required for the coexistence of 802.15.4 networks, and design the optimal superframe structure that maximizes the time-domain utilization. The results have showed that as the channel conditions deteriorate, the SCNs should be more conservative to decrease the probability of having nearby interference sources during its operation. For the single channel case, the spectrum sensing threshold is the performance limiting design parameter that has to be chosen very carefully. For the multi-channel case, the intensity of the accommodated network nodes does not linearly increase with the number of channels - a concept that is counter intuitive and different from that for the grid-based networks. The results have also showed how the one channel analysis can be misleading for the network designers and can result in a high probability of self-admission failure for the coexisting networks.

To this end, I have applied stochastic geometry analysis to ad hoc and sensor networks. Starting from the next chapter, I apply stochastic geometry analysis to multi-tier cellular networks.

Chapter 5

Downlink Two-tier Cellular Networks with Cognitive Femtocells

Modern cellular networks are foreseen as network with random topologies rather than a grid infrastructure. That is, the variations of the capacity demand across the service areas and the infeasibility to exactly follow a grid based deployment for cellular networks have brought uncertainties to the base stations' (BSs) locations [12, 54]. Therefore, modeling and analysis of cellular networks via stochastic geometry has recently received much attention due to its tractability and accuracy [5]. Stochastic geometry not only captures the uncertainties in the BSs' locations, but also results in simple expressions which help to characterize and understand the network behavior. In this chapter, I use stochastic geometry to model and analyze performance of two-tier cellular networks composed of macro BSs and cognitive FAPs in a multichannel environment. The proposed model explicitly accounts for the spatial distribution of the macro BSs, FAPs, and users in a Rayleigh fading environment. We quantify the

performance gain in outage probability obtained by introducing cognition into the femto-tier, provide design guidelines, and show the existence of an optimal spectrum sensing threshold for the cognitive FAPs which depends on the cellular network parameters. We also show that looking into the overall performance of the network is quite misleading in the scenarios where the majority of users are served by the macro BSs. Therefore, the performance of femto-tier needs to be explicitly accounted for and optimized.

5.1 Introduction

In a multi-tier cellular network, different network tiers, which may differ in terms of supported data rate, channel access protocol, transmission power, coverage range and mobility support, coexist in the same vicinity and operate simultaneously. In a typical two-tier cellular network scenario consisting of macro base stations (BSs) and femto access points (FAPs), the transmission power of a macro BS can be up to 1000 times higher than that of a FAP. Therefore, the inter-tier (or cross-tier) interference from the macro BSs to the femtocell users can be very significant. Introducing cognition into the FAPs helps them avoiding major interference sources and improving their performance [109–111]. A cognitive FAP will sense the spectrum and avoid using the same frequency channels which are used simultaneously by major interference sources. Based on a spectrum sensing threshold, an interference source (which can be either a macro BS or a FAP) is considered either a major interference source that should be avoided or a minor interference source that can be tolerated. From a geometric perspective, the spectrum sensing threshold of a cognitive FAP defines the spectrum sensing range (SSR) around the FAP where no interference sources exist (i.e., the *interference exclusion region*). The spectrum sensing threshold is a very critical design

parameter that should be carefully tuned to achieve the desired tradeoff between the aggregate interference (and hence outage probability) and the spatial frequency reuse efficiency. The lower the spectrum sensing threshold, the larger is the SSR and the lower is the aggregate interference, however, the same frequency channel is reused after larger spatial intervals which results in a poor spatial frequency reuse efficiency. Modeling and analysis of this tradeoff in a two-tier cellular network with cognitive femtocells is the focus of this work.

5.1.1 Topology Abstraction

As discussed before, the Poisson point process (PPP) is the most popular and well-understood point process in the literature due to its simplicity and tractability. Because the PPP assumes that the positions of the points are uncorrelated, the PPP might be valid to abstract the spatial locations for the FAPs which are deployed according to the customer needs without any network planning. On the other hand, although there is randomness in the locations of the BSs due to the variable capacity demand across the coverage area, it might seem unrealistic to assume that the positions of the BSs are completely uncorrelated and follow a PPP. This is because the BSs are deployed through a sophisticated network planning procedure and there are correlations among their locations. However, in [12], it was shown that the PPP assumption for the spatial locations of the BSs provides a lower bound on coverage probability (i.e., the complement of the outage probability) and the average achievable rate, which is as much tight as the upper bound provided by the idealized grid-based model. The PPP modeling approach is more favorable than the grid-based model due to its simplicity and analytical tractability. To model and analyze the performance of cellular networks with cognitive femtocells, I will assume that both network

tiers follow the PPP. In [54], it was shown that the PPP assumption is accurate to within 1-2 dB of the performance of an actual LTE network overlaid by heterogeneous tiers modeled as PPP. Further validations of stochastic geometry-based modeling of cellular networks via PPP can be found in [11, 13, 119]

5.1.2 Motivation and Contribution

Although different techniques for uplink and downlink communications in cognitive femtocells have been proposed in the literature [113–115], the problem of optimizing the carrier sensing threshold for cognitive femtocells has not been addressed considering multiple macro BSs, multiple FAPs, multiple users, and multiple channels in a two-tier cellular network environment. In this chapter, I propose a framework for optimizing the carrier (i.e., spectrum) sensing threshold and show that the optimal spectrum sensing threshold depends on the network parameters such as the number of channels, the relative transmit powers of macro BSs and FAPs, and the intensities of FAPs and macro BSs. The proposed optimization framework may be used at the network service provider side (e.g., upon a change in the intensities of macro BSs/FAPs and/or other system parameters) and the optimal spectrum sensing threshold can be broadcast to the FAPs. The contributions of this work can be summarized as follows:

- Using stochastic geometry analysis, I model the outage probability for macrocell users as well as femtocell users for downlink transmission in a multi-channel environment when cognition is introduced into the FAPs.

- We quantify the performance gain due to cognition and show the existence of an optimal spectrum sensing threshold (which can be obtained numerically via the presented model) for the cognitive FAPs to minimize the outage probability.

- We comprehensively analyze the outage performance of the two-tier cellular network with cognitive femtocells under different intensities of the macro BSs and FAPs, their relative transmission powers, different number of channels and spectrum sensing thresholds for cognitive FAPs, and different signal-to-interference (SIR) threshold requirements.

- We show that it is quite misleading to account only for the overall outage probability (i.e., the outage probability for a generic user) and not explicitly consider the outage of the femtocell users.

We would like to emphasize that my model is completely different from the legacy cognitive radio analysis models (e.g., the work presented in [83, 116]). In a two-tier cellular network with open-access femtocells, both femto users and macro users are licensed users and there is no notion of priority. Therefore, in my model, there is no priority for the transmissions of macro BSs. However, the FAPs are burdened with the cognitive radio processing due to the self-organizing network (SON) feature recommended by the standards [109, 110] to avoid infeasible (in terms of complexity) centralized interference management, and to insure backward compatibility with the legacy cellular BSs and handsets. The absence of the priorities changes the optimization objective, and hence, changes the analysis. For instance, in the legacy cognitive radio systems, it is desirable to maximize the secondary users' performance subject to a tolerable degradation in the primary users' performance. On the contrary, in my model, performances of both femtocell and macrocell users are considered to maximize the overall network performance (e.g., in terms of outage probability).

5.2 Related Work

Although the idea of modeling infrastructure-based cellular networks via stochastic geometry dates back to the late 90's [52], much attention has been brought to this modeling technique after more than a decade because of the pioneering work in [12]. In [12], the authors were able to use the PPP to derive a tractable yet accurate model for important performance metrics for cellular networks such as the coverage probability and the average achievable rate. Following [12], many work have been done in the literature using the same methodology to adapt and extend the stochastic geometric approach to different network scenarios. For instance, [54] extended the model to HetNets with k-tiers and [58] extended the model to capture the effect of offloading the users from the macro-tier to femto-tier via biasing. [61] and [62] extended the model to capture the performance of the cellular networks deploying fractional frequency reuse, respectively. Parallel to these works, [65] derived the distribution for the SINR of a generic user in a multi-tier cellular network environment assuming that the user can instantly handover its connection between the candidate BSs from each network tier. In [63], the authors developed a capacity extension policy for a two-tier heterogeneous network and determined which type of base stations should be added or switched off to achieve the optimal base station density. In [71], the authors used the method in [118] to relax the Rayleigh channel assumption for the link to the serving BS, which was assumed in [12], to obtain the average achievable rate when the channel gain to the serving BS has a Nakagami distribution.

A common assumption in all of these works is that there is only one channel in the entire network and none of the network tiers is cognitive. Different from all of these works, I introduce cognition into the network model and use stochastic geometry for performance analysis and also relax the commonly used single channel assumption

in the network. In [67], the authors studied two subchannel allocation schemes in a two-tier cellular network under open and closed-access femtocell operations. In [67], the available subchannels are either aggressively used by both the network tiers or each network tier has its own subset of the available subchannels. Different from [67], in my work, the FAPs are cognitive and I consider the spatial reuse of channels, which is optimized through optimizing the spectrum sensing threshold.

5.3 System model, assumptions, and methodology

5.3.1 Network Model

We consider a two-tier cellular network consisting of macro BSs and FAPs. We assume that the two network tiers are independent and each is represented by an independent homogeneous PPP in the $\mathbb{R}^2$ plane. That is, the macro BSs are spatially distributed according to the homogeneous PPP $\mathbf{\Psi}_b = \{b_i; i = 1, 2, 3, ...\}$ with intensity $\mathcal{B}$ where b_i is the location of the i^{th} BS[1]. The FAPs are spatially distributed according to an independent homogeneous PPP $\mathbf{\Psi}_a = \{a_i; i = 1, 2, 3, ...\}$ with intensity $\mathcal{A}$, where a_i denotes the location of the i^{th} FAP[2]. The user equipments (UEs) are spatially distributed according to an independent homogeneous PPP $\mathbf{\Psi}_u = \{u_i; i = 1, 2, 3, ...\}$ with intensity $\mathcal{U}$. Both the network tiers share the same set of channels[3] $\mathbf{S}$. The channels have a specific order known to all macro BSs. All macro BSs transmit with the same power P_b, all FAPs transmit with the same power P_a, and the macro BSs and FAPs always have packets to transmit in the downlink (i.e., saturation conditions are assumed). All FAPs operate in the open access mode and each user will be associated

[1]The intensity of a homogeneous PPP is a positive constant measured as the number of points per unit area.

[2]With a slight abuse of notation I will use b_i to denote both the location of the i^{th} macro BS and the i^{th} BS itself, and the same for a_i.

[3]A channel can be, for example, one or multiple resource blocks (RB) in LTE-Advanced systems.

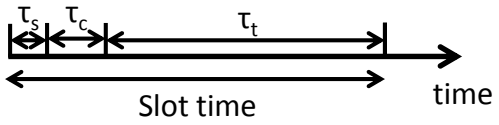

Figure 5.1: Time slot structure.

to the macro BS or the FAP providing the highest received signal strength (RSS) measured on the pilot signals from that macro BS or FAP. All other macro BSs and FAPs using the same channel are considered as interference sources.

Note that an associated user does not necessarily have an assigned channel since the macro BSs or FAPs will assign channels to their associated users only upon availability, however, association means that the user is registered in the user list of the serving network entity (i.e., a macro BS or a FAP), synchronized to it, and receives its control information. The users associated to a macro BS are assigned orthogonal channels, and therefore, there is no intra-cell interference experienced by the macro cell users.

5.3.2 Cognitive FAP

The FAPs are cognitive. Each FAP uses spectrum sensing to choose the channel which it will use for downlink transmission to its associated users to avoid interference with nearby BSs as well as nearby FAPs. A FAP uses a channel $s_i \in \mathbf{S}$, $i = 1, 2, ..., |\mathbf{S}|$ if and only if the received power from any neighboring macro BS/FAP on this channel[4] is less than the spectrum sensing threshold υ_s, where υ_s is a design parameter that should be carefully determined. The spectrum sensing threshold υ_s defines the *spectrum sensing region (SSR)* around each FAP and balances between the spatial frequency

[4]Note that this assumption, which does not consider the total aggregate power sensed on a channel, will lead to a tight lower bound on the probability that the channel is busy [21].

reuse efficiency and the experienced aggregate interference. The higher the value of the spectrum sensing threshold, the lower is the SSR and the more aggressive will be the FAPs in accessing the channels, and vice versa.

All channels are reused in all macro BSs (i.e., universal frequency reuse) where a macro BS assigns the channels to the users associated to it in a sequential manner (i.e., channel $s_i \in \mathbf{S}$ will be assigned before channel $s_{i+1} \in \mathbf{S}$ and so on until $s_{|\mathbf{S}|}$ is reached) and no channel is reused within the cell (i.e., no intra-cell interference). The assumption of the sequential channel assignment within the macro BSs balance the tradeoff between the macro users' performance and the opprtunistic channel access of the FAPs as will be discussed in Chapter 6.

Time is assumed to be divided into time slots. The time slot structure is shown is Fig. 5.1. A macro BS assigns channels to its associated users at the beginning of each time slot. The user who arrives to the macro BS or requests a session in the middle of a time slot will be assigned a channel in the next time slot. The FAPs are cognitive and access the available channels opportunistically. At the beginning of each time slot, a FAP senses the spectrum during the sensing time τ_s and determines the available channels (i.e., channels not used by the macro BSs within the SSR of this FAP). Then, the FAP will randomly choose one of the available channels and persistently sense it for a random duration uniformly distributed in the range $[0, \tau_c]$ (Fig. 5.1)[5]. If the channel is still available after the random sensing duration elapses (i.e., not used by another FAP), it will access the channel for downlink transmission[6] during the transmission interval τ_t. The random sensing duration before acquiring a channel minimizes the probability of interference with nearby FAPs (i.e., the probability that

[5]The random sensing duration is similar to the random backoff timer generated in a traditional carrier-sense multiple access (CSMA) protocol discussed in Chapter 3.

[6]Since my focus is on the analysis of outage, the actual method of sharing the accessed channel among the femto users for downlink transmission is not considered here.

two FAPs within the sensing range of each other use the same channel). In this work, I assume perfect spectrum sensing. All time slots have the same structure and the same spectrum access procedure is repeated in each time slot.

5.3.3 Radio Channel Model

We consider a general power-law path loss model in which the signal power decays at the rate $r^{-\eta}$ with the distance r, where η is the path-loss exponent. Although, in practice, different network tiers may have different path-loss exponents, I assume the same path-loss exponent for both the macro and femto tiers for analytical tractability. However, the favorable channel conditions towards the FAPs due to their indoor deployment can still be captured via assuming higher mean channel gain for the femto links. All the channel gains are assumed to be independent and the channels have a coherence time greater than or equal to a time slot. For analysis, only Rayleigh fading environment is assumed (i.e., technique #1 in Sec. 2.3). The channel (power) gains from a generic location $x \in \mathbb{R}^2$ to the macro BS b_i and the FAP a_i are denoted by $h_{b_i}(x) \sim \text{Exp}\,(\mu_b)$ and $h_{a_i}(x) \sim \text{Exp}\,(\mu_a)$ with mean $\frac{1}{\mu_b}$ and $\frac{1}{\mu_a}$, respectively. Note that for the brevity of exposition, hereafter, the spatial index x is dropped. A receiver can successfully decode a signal if the received signal power exceeds the received aggregate interference power plus the noise power by a certain threshold β. In other words, the signal-to-interference-plus-noise-ratio (SINR) of a signal should be greater that a certain threshold β for the signal to be successfully decoded by its intended receiver. We will use the notation χ to denote the serving network entity for a generic user. That is, $\chi = a$ if the user is associated to a FAP, and $\chi = b$ if the user is associated to a macro BS.

Without any loss in generality, the performance analysis is conducted for a typ-

ical user located at the origin. According to Slivnyak's theorem, conditioning on having a user at the origin does not change the statistical properties of the coexisting PPPs. Hence, the analysis holds for any generic user located at a generic location [1]. Therefore, the SINR at the typical user located at the origin (which also holds for any generic user) served by a macro BS or a FAP is given by

$$\text{SINR} = \frac{P_\chi h_\chi R_\chi^{-\eta}}{\sum\limits_{b_i \in \tilde{\mathbf{\Psi}}_{b\chi}} P_b h_{b_i} \left\|b_i\right\|^{-\eta} + \sum\limits_{a_i \in \tilde{\mathbf{\Psi}}_{a\chi}} P_a h_{a_i} \left\|a_i\right\|^{-\eta} + \sigma^2} \tag{5.1}$$

where R_χ is the distance from the user to the serving network entity (i.e., a macro BS or a FAP), $\tilde{\mathbf{\Psi}}_{b\chi}$ denotes the set of BSs interfering with the serving network entity, $\tilde{\mathbf{\Psi}}_{a\chi}$ denotes the set of FAPs interfering with the serving network entity, $\|.\|$ denotes the Euclidean norm, and σ^2 is the noise power.

5.3.4 Methodology of Analysis

For the system model described above, I intend to analyze the outage probability of the macro users and the femto users. The methodology of my analysis is as follows. At first, I need to calculate the tier association probability, the probability mass function (*pmf*) of the number of free channels, as well as the opportunistic spectrum access probability for cognitive FAPs. Then, I will calculate the outage probability of a generic user. The tier association probability is defined as the probability that a generic user is connected to either a macro BS or a FAP. The *pmf* of the number of free channels gives the probability to have $K_f \in \{0, 1, 2, ..., |\mathbf{S}|\}$ free channels (i.e., not used by macro BSs) in a specific region (e.g., within the SSR of a FAP) for opportunistic access by FAPs. Since the FAPs are cognitive, they access the available channels opportunistically, and therefore, finding an available channel is not guaranteed. The

opportunistic spectrum access probability for cognitive FAPs is the probability that a generic FAP finds an available channel and succeeds to use it during a time slot. Finally, the overall outage probability (i.e., the outage probability of a generic user) is obtained by considering the outage probabilities of both a femto user and a macro user each weighted by the corresponding tier association probability. Note that the femto users experience two types of outage. The first type is due to the opportunistic spectrum access of the cognitive FAPs. The second type is due to the inter-tier and intra-tier interference.

5.4 Calculation of Tier Association Probability

In this section, I derive the tier association probability for a generic user. Each network tier consists of either macro BSs or FAPs spatially distributed according to a PPP. Therefore, the coverage of each tier forms a Voronoi tessellation[7] and the network can be modeled via a weighted Voronoi tessellation as shown in Fig. 5.2(a). For simplicity, the network model can be approximated as a superposition of two independent Voronoi tessellations, one for the macro BSs and the other for the FAPs as shown in Fig. 5.2(b). By construction, the Voronoi cells belonging to the same tier do not intersect, hence, each user will fall in an intersection between two Voronoi cells belonging to different tiers (i.e., one of a macro BS and the other of a FAP). Based on the RSS level, each user will be associated to either the macro BS or the FAP of the Voronoi cells covering her (i.e., the user will always be connected to the nearest macro BS/FAP). The tier association probability can be obtained from the following lemma.

[7]A Voronoi tessellation is the planar graph constructed by perpendicular lines bisecting the distances between the points of a point process. The Voronoi cell corresponds to the BS coverage.

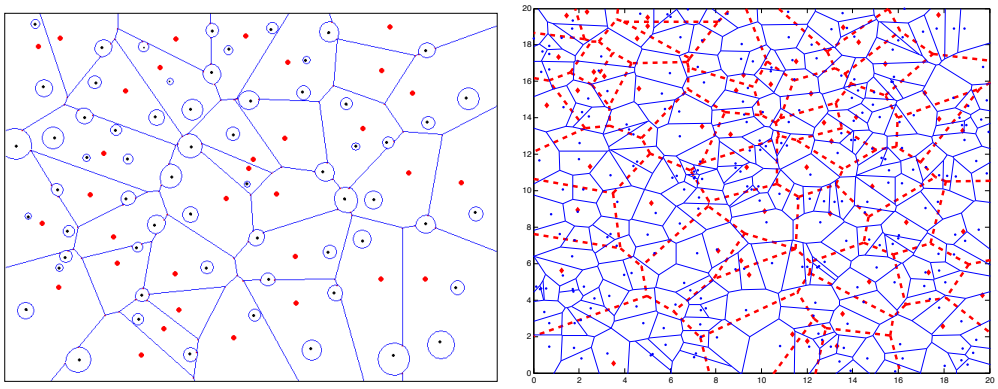

(a) (b)

Figure 5.2: (a) The network modeled as a weighted Voronoi tessellation, (b) the network modeled as a superposition of two independent Voronoi tessellations (the diamond dots with the dashed Voronoi represent the macro network tier).

Lemma 5.4.1. *In a Rayleigh fading environment, the probability that a generic user is associated to the femto network is given by*

$$\xi_a = 1 - \int_0^{\infty} \frac{\mu_a \mu_b \mathcal{B}}{(\mu_b + \mu_a h)^2 \left(\left(\frac{P_a}{P_b} h \right)^{\frac{2}{\eta}} \mathcal{A} + \mathcal{B} \right)} dh \tag{5.2}$$

and the probability that a generic user is associated to the macro network is given by

$$\xi_b = 1 - \xi_a = \int_0^{\infty} \frac{\mu_a \mu_b \mathcal{B}}{(\mu_b + \mu_a h)^2 \left(\left(\frac{P_a}{P_b} h \right)^{\frac{2}{\eta}} \mathcal{A} + \mathcal{B} \right)} dh. \tag{5.3}$$

Proof. Exploiting the result of Slivnyak's theorem for PPP, I can perform all of the analysis on a typical user located at the origin (i.e., conditioning on having that user at the origin) while maintaining the same properties of all coexisting PPPs. Let $R_a = \min_i(\|a_i\|)$, $\forall a_i \in \mathbf{\Psi}_a$ and $R_b = \min_i(\|b_i\|)$, $\forall b_i \in \mathbf{\Psi}_b$ denote, respectively, the distance between the tagged user located at the origin and the nearest FAP and the

nearest macro BS. Then, the probability that a typical user (u) is covered by the femto network can be written as

$$\begin{aligned}\xi_a &= \mathbb{P}\left\{P_a h_{a_i} R_a^{-\eta} > P_b h_{b_i} R_b^{-\eta}\right\} \\ &\overset{(*)}{=} \int_{h\geq 0} F_{R_{a/b}}\left(\frac{P_a}{P_b}h\right) f_{h_{a/b}}(h)dh \\ &= 1 - \int_0^{\infty} \left(\frac{\mu_a}{\mu_b}\right) \frac{\mathcal{B}}{(1+\frac{\mu_a}{\mu_b}h)^2 \left(\left(\frac{P_a}{P_b}h\right)^{\frac{2}{\eta}} \mathcal{A} + \mathcal{B}\right)} dh.\end{aligned}$$

In $(*)$, $R_{a/b} = \left(\frac{R_a}{R_b}\right)^{\eta}$, $h_{a/b} = \frac{h_{a_i}}{h_{b_i}}$, $F_{R_{a/b}}(r)$ is the cumulative distribution function (*cdf*) of $R_{a/b}$, and $f_{h_{a/b}}(h)$ is the probability density function (*pdf*) of $h_{a/b}$. Both the *pdf*s $f_{R_{a/b}}(r)$ and $f_{h_{a/b}}(h)$ are derived in **Appendix B.1**. □

Note that **Lemma 5.4.1** can be easily generalized to any fading environment (see [60]). Accounting for the random channel fading in the tier association probability has two merits. Firstly, the tier association probability is more generalized and captures the long term average association probability (i.e., based on the average channel gains) as in [58]. Secondly, I can explicitly account for the effect of the favorable channel conditions from the users towards the FAPs. The association probability can be directly interpreted as the probability that a generic user will be associated to one of the two network tiers. Also, the association probability can be viewed as the share that each network tier serves from the complete set of users, or can be viewed as the portion of the plane which each tier is serving. From these interpretations of the association probability and the fact that independently thinning a PPP produces another PPP [1], the PPP representing the complete set of users $\mathbf{\Psi}_u$ can be divided into two independent PPPs: $\mathbf{\Psi}_{ua}$ with intensity $\mathcal{U}_a = \mathcal{U}\xi_a$ and $\mathbf{\Psi}_{ub}$ with intensity $\mathcal{U}_b = \mathcal{U}\xi_b$, which denote, respectively, the PPP for the users associated to the FAPs

and the users associated to the macro BSs.

5.5 Calculation of the Opportunistic Spectrum Access Probability for Cognitive FAPs

5.5.1 Assumptions and Procedure

In each time slot, a cognitive FAP opportunistically uses a channel which is not used within its SSR. Due to the low transmission power of the FAPs, the high transmission power of macro BSs, and the unified sensing threshold υ_s, there are two different SSRs for each FAP, namely, the *femto SSR* (i.e., the SSR of a FAP with respect to [w.r.t.] other FAPs) and the *macro SSR* (i.e., the SSR of a FAP w.r.t. the macro BSs), as shown in Fig. 5.3. The spectrum sensing threshold along with the transmission power defines the region around the FAP where none of the used channels can be reused. That is, a FAP should not reuse any channel used by a macro BS within the *macro SSR*, or any channel used by a FAP within the *femto SSR*. Due to the higher transmission power of the macro BSs w.r.t. the FAPs, a FAP should keep a larger spatial channel reuse distance from macro BSs than that from FAPs as shown in Fig. 5.3. Therefore, the *macro SSR* is larger than the *femto SSR*. The macro BSs perform the channel assignment at the beginning of each time slot. Therefore, by sensing the spectrum at the beginning of each time slot for the spectrum sensing duration τ_s, the FAPs can identify the available spectrum opportunities (i.e., the channels that are not used by the macro BSs).

On the other hand, interference among the FAPs within the same *femto SSR* is avoided via a contention resolution procedure. As has been mentioned before, each FAP will randomly choose one of the available channels and persistently sense it for

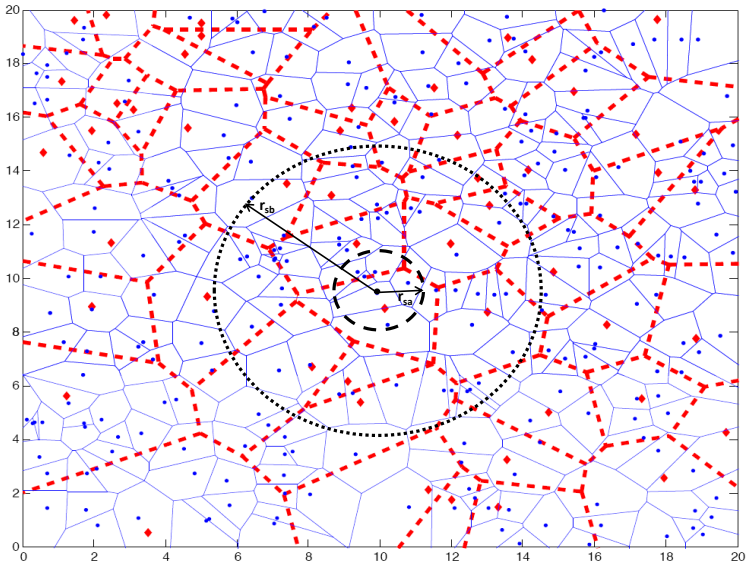

Figure 5.3: The two SSRs for a generic FAP (the black dot at the centre): the outer dotted circle and the inner dashed circle represent, respectively, the *macro SSR* and the *femto SSR*.

a random duration uniformly distributed in the range $[0, \tau_c]$. If the chosen channel is still available (i.e., not used by another FAP within the *femto SSR* during the random sensing duration) the FAP will use it for the rest of the current time slot, otherwise, the FAP experiences an outage due to the channel unavailability in the current slot.

Computing the opportunistic spectrum access probability for cognitive FAPs is a twofold problem. Given that there are K_f free channels (i.e., not utilized by the macro BSs) in the *macro SSR* of the test FAP, I have to model the contention between the test FAP and the other FAPs present in the test FAP's *femto SSR* for these channels in order to compute the conditional opportunistic access probability. Also, I have to compute the *pmf* of the number of free channels K_f in order to obtain the unconditional opportunistic spectrum access probability for cognitive FAPs. Exploiting Slivnyak's theorem it is possible to conduct the analysis for a FAP a_i existing at the origin (i.e., $a_i = (0, 0)$) and the results will hold for the entire set of FAPs [1].

5.5.2 Availability of Channels for Opportunistic Spectrum Access

In this section, for a test FAP located at the origin, I derive the *pmf* of the number of free channels within its *macro SSR*. The *pmf* of the number of free channels is calculated in three steps. First, the *pmf* of the number of channels used by a generic macro BS is obtained. Then, the *pmf* of the channels used by all macro BSs within the *macro SSR* of the test FAP is calculated. Finally, the *pmf* of the number of free channels within the *macro SSR* of the test FAP is calculated. As defined in the system model, users associated to the same macro BS will be assigned orthogonal channels, and therefore, the number of channels used in a generic macro cell is equal to the number of users associated to it. The distribution of the number of users associated to a generic macro BS is obtained from the following lemma:

Lemma 5.5.1. *Let N_{v} be the number of macro users associated to a generic BS. Then N_{v} has the following cumulative mass function (*cmf*):*

$$F_{N_{\mathrm{v}}}(k) \approx \sum_{n=0}^{k} \frac{\Gamma(n+c)}{\Gamma(n+1)\Gamma(c)} \frac{(\mathcal{U}_b)^n (\mathcal{B}c)^c}{(c\mathcal{B}+\mathcal{U}_b)^{n+c}}, \quad 0 \leq k < \infty \tag{5.4}$$

where $\Gamma(z) = \int_0^\infty t^{z-1}e^{-t}dt$ is the gamma function and $c = 3.575$ is a constant for Voronoi tessellation in $\mathbb{R}^2$.

Proof. See **Appendix B.2**. □

Note that the expression in (5.4) is an approximation because the exact distribution of the Voronoi cell area is not known (its derivation is an open problem [117, Chapter 5]), and the network model is approximated by the superposition of two independent Voronoi tessellations. Fig. 5.4 shows the accuracy of the *cmf* of the number of macro users N_{v} associated to a generic BS.

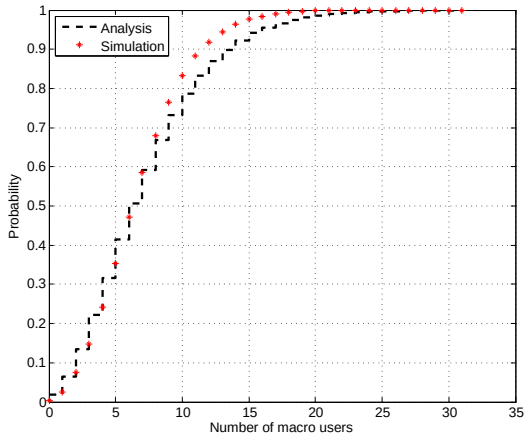

Figure 5.4: The accuracy of the proposed $F_{N_{\rm v}}(k)$ at $\mathcal{B} = 1$ BS/km^2, $\mathcal{A} = 10$ FAP/km^2, $\mathcal{U} = 30$ user/km^2.

Now I calculate the *pmf* of the number of channels used by all macro BSs within the *macro SSR* of the test FAP. Shown in Fig. 5.3, $r_{sb} = \left(\frac{P_b \mu_b}{\upsilon_s}\right)^{1/\eta}$ and $r_{sa} = \left(\frac{P_a \mu_a}{\upsilon_s}\right)^{1/\eta}$ are the average radii for the *macro SSR* and the *femto SSR*, respectively (here υ_s is the spectrum sensing threshold). Due to the Rayleigh fading assumption, the *macro SSR* and the *femto SSR* are random shaped regions (i.e., not circles) which depend on the instantaneous channel gains between the test FAP and the coexisting BSs/FAPs. That is, there could be a macro BS which is very far from the test FAP but still within its *macro SSR* due to good channel gain. On the other hand, there could be a macro BS near the test FAP but not included within its *macro SSR* due to poor channel gain. Since the Lebesgue measure of a random shaped region is hard to determine, I cannot directly study the spatial statistics of the macro BSs within the *macro SSR*. Moreover, in theory, the *macro SSR* may not be bounded due the infinite support domain of the exponential distribution. Let $\mathcal{N}_b$ be the number of macro BSs within the *macro SSR* of the test FAP. Then the distribution of $\mathcal{N}_b$ can be obtained from the following lemma:

Lemma 5.5.2. *Let $\mathcal{N}_b$ be the number of macro BSs in a generic FAP's* macro SSR *determined by the sensing threshold υ_s in a Rayleigh fading environment. Then, $\mathcal{N}_b$ has a Poisson distribution with the parameter $\varphi_b = \pi\mathcal{B}\left(\frac{P_b}{\mu_b \upsilon_s}\right)^{\frac{2}{\eta}} \Gamma(1+\frac{2}{\eta})$.*

Proof. See **Appendix B.3**. □

Having the distribution of $\mathcal{N}_b$, the distribution of the number of busy channels used by all macro BSs within the *macro SSR* of a generic FAP is obtained from the following lemma.

Lemma 5.5.3. *Let K_u be the number of channels used by all macro BSs within the* macro SSR *of a generic FAP located at a_i, $a_i \in \mathbb{R}^2$. The distribution function of K_u is given by*

$$F_{K_u}(k) = e^{-\varphi_b(1-F_{N_{\mathrm{v}}}(k))}, \quad 0 \leq k < \infty. \tag{5.5}$$

The pmf *of K_u is given by*

$$f_{K_u}(k) = \begin{cases} e^{-\varphi_b\left(1-\left(\frac{c\mathcal{B}}{c\mathcal{B}+\mathcal{U}_b}\right)^c\right)}, & k = 0 \\ e^{-\varphi_b(1-F_{N_{\mathrm{v}}}(k))} - e^{-\varphi_b(1-F_{N_{\mathrm{v}}}(k-1))}, & \textit{otherwise.} \end{cases} \tag{5.6}$$

Proof. See **Appendix B.4**. □

Now the distribution of the number of free channels within the *macro SSR* of a generic FAP can be obtained from the following Corollary.

Corollary 5.5.1. *Let $|\mathbf{S}|$ be the total number of channels, K_f be the number of free channels out of $|\mathbf{S}|$ within the* macro SSR *of a generic FAP located at a_i, $a_i \in \mathbb{R}^2$. Then, the distribution of K_f can be obtained from*

$$F_{K_f}(k) = \mathbb{P}\{K_f \leq k\}$$
$$= 1 - \mathbb{1}\{k < |\mathbf{S}|\} e^{-\varphi_b(1-F_{N_\mathrm{v}}(|\mathbf{S}|-k-1))}, \quad 0 \leq k \leq |\mathbf{S}| \tag{5.7}$$

where $\mathbb{1}\{.\}$ *is an indicator function which takes the value* 1 *when the statement* $\{.\}$ *is true and takes the value* 0 *otherwise. The* pmf *of* K_f *is given by*

$$f_{K_f}(k) = e^{-\varphi_b(1-F_{N_\mathrm{v}}(|\mathbf{S}|-k))\mathbb{1}\{k>0\}} - \mathbb{1}\{k < |\mathbf{S}|\} e^{-\varphi_b(1-F_{N_\mathrm{v}}(|\mathbf{S}|-k-1))}, \quad 0 \leq k \leq |\mathbf{S}|\,. \tag{5.8}$$

Proof. Exploiting the fact that the probability for k or fewer channels being free is equal to the probability that $|\mathbf{S}| - k$ or more channels are used, I can write $\mathbb{P}\{K_f \leq k\} = 1 - F_{K_u}(|\mathbf{S}| - k - 1)$, and hence, **Corollary 5.5.1** is proved. Note that, since K_u is a discrete random variable, $1 - F_{K_u}(|\mathbf{S}| - k - 1)$ is the probability that $|\mathbf{S}| - k$ or more channels are used. □

5.5.3 Opportunistic Spectrum Access Probability for FAPs

In this section, I model the contention among different FAPs to access the available channels in order to obtain the conditional opportunistic spectrum access probability for FAPs (i.e., conditioning on the number of free channels). As shown in Fig. 5.3, the test FAP will contend to access the spectrum with all other FAPs within its *femto SSR*. For analytical tractability, I assume that all the FAPs coexisting within the *femto SSR* of the test FAP have the same set of free channels. This assumption can be justified by the smaller *femto SSR* w.r.t. the *macro SSR*. Each FAP will generate a

random backoff timer and persistently sense a randomly chosen channel out of the K_f free channels. If the chosen channel is still available after the backoff timer elapses, the FAP acquires it and uses it for downlink transmission. Otherwise, it encounters an outage in the current time slot. Only FAPs with associated users will contend for channel access.

Similar to **Lemma 5.5.1**, it can be shown that the intensity of FAPs with at least one associated user is given by $\mathcal{A}_a = \mathcal{A}\left(1 - \left(\frac{c\mathcal{A}}{c\mathcal{A}+\mathcal{U}_a}\right)^c\right)$. Since each FAP randomly chooses one of the available channels to contend for, given that there are K_f channels available for contention in the test FAP's *macro SSR*, the intensity of FAPs with at least one associated user that are contending with the test FAP for accessing the same channel is given by

$$\mathcal{A}_c(K_f) = \frac{\mathcal{A}_a}{K_f} = \frac{\mathcal{A}}{K_f}\left(1 - \left(\frac{c\mathcal{A}}{c\mathcal{A}+\mathcal{U}_a}\right)^c\right). \tag{5.9}$$

Due to the carrier sensing-based channel access, the cognitive FAPs which simultaneously access the same channel constitute a Matérn hard core point process (HCPP) [1, 40, 50, 51]. As discussed in Sec. 2.1.5, a Matérn HCPP is a repulsive point process where no two points can coexist if their distance is less than the hard core radius r_{min}. The Matérn HCPP is derived from a PPP via dependent thinning. The dependent thinning is applied in two steps. First, an independent and uniformly distributed time mark is applied to the PPP. Then, a point is chosen to be in the Matérn HCPP if and only if it has the lowest mark in its contention domain. The contention domain of a point is defined by a circle of radius $r_{\min}$ around that point. Projecting to my network model, the PPP is the complete set of FAPs contending to access the same channel, the time mark corresponds to the backoff timer generated by each FAP for contention, and the HCPP corresponds to the FAPs that succeed

to access the spectrum. Similar to **Lemma 5.5.2**, it can be shown that the number of active FAPs (i.e., FAPs with at least one associated user) contending for the same channel within the *femto SSR* of a generic FAP has a Poisson distribution with parameter $\varphi_a(K_f) = \pi \mathcal{A}_c(K_f) \left(\frac{P_a}{\mu_b \upsilon_s}\right)^{\frac{2}{\eta}} \Gamma(1+\frac{2}{\eta})$. It can be shown that the opportunistic spectrum access probability for a generic FAP is given by (see [1, 40, 50, 51]):

$$\begin{aligned}\mathcal{P}_{ac}(K_f) &= \frac{1-e^{-\varphi_a(K_f)}}{\varphi_a(K_f)} \\ &= \frac{K_f \left(1 - e^{-\pi \frac{\mathcal{A}}{K_f}\left(1-\left(\frac{c\mathcal{A}}{c\mathcal{A}+\mathcal{U}_a}\right)^c\right)\left(\frac{P_a}{\mu_b \upsilon_s}\right)^{\frac{2}{\eta}}\Gamma(1+\frac{2}{\eta})}\right)}{\pi \mathcal{A}\left(1-\left(\frac{c\mathcal{A}}{c\mathcal{A}+\mathcal{U}_a}\right)^c\right)\left(\frac{P_a}{\mu_b \upsilon_s}\right)^{\frac{2}{\eta}}\Gamma(1+\frac{2}{\eta})}.\end{aligned} \tag{5.10}$$

The intensity of the FAPs which succeed to access the same channel $s_i \in \mathbf{S}$ can be calculated from the probability that the test FAP will access the given channel s_i. The channel s_i is available for the test FAP to contend for if it is not used by the macro BSs within its *macro SSR*. Due to the sequential channel assignment of the macro BSs, the channel s_i is available for contention for the test FAP if $(K_f \geq |\mathbf{S}| - (i-1))$, $i = 1, 2, 3, ..., |\mathbf{S}|$. Given that there are K_f free channels within the *macro SSR* of the test FAP, the test FAP will choose one of the available channels to contend for with probability $\frac{1}{K_f}$ and will succeed to access it with probability $\mathcal{P}_{ac}(K_f)$. Therefore, the probability that the test FAP succeeds to access the channel s_i is given by

$$\mathcal{P}_{s_i} = \sum_{k=|\mathbf{S}|-(i-1)}^{|\mathbf{S}|} \mathbb{P}\left\{K_f = k\right\} \frac{\mathcal{P}_{ac}(k)}{k}.$$

Note that, different from $\mathcal{P}_{s_i}$, $\mathcal{P}_{ac}(K_f)$ gives the probability that a FAP succeeds to access the spectrum on any of the free channels and not on a specific channel s_i. The

intensity of the FAPs succeeded to access the same channel s_i is given by

$$\mathcal{A}_{s_i} = \mathcal{A}_a \mathcal{P}_{s_i} = \mathcal{A}_a \sum_{k=|\mathbf{S}|-(i-1)}^{|\mathbf{S}|} \mathbb{P}\left\{K_f = k\right\} \frac{\mathcal{P}_{ac}(k)}{k}. \tag{5.11}$$

5.6 Analysis of Outage Probability

5.6.1 Assumptions and Methodology

Due to the sequential assignment of channels in the macro BSs, each channel s_i has its own interference statistics. That is, channel s_1 will have all macro BSs with one or more associated users causing interference to it. On the other hand, channel s_i will only have macro BSs with i or more associated users causing interference to it. In this section, I consider the worst-case scenario from interference point of view and model the outage on the channels experiencing the highest amount of interference from the macro-tier. For the macro-tier, I model outage on channel s_1, and for the femto-tier, given that there are K_f available channels, I model outage on channel $s_{|\mathbf{S}|-(K_f-1)}$.

Before going into the details of the outage probability, I give the following lemma which I will use as a building block in my analysis.

Lemma 5.6.1. *Following (sec. 3.7.1, [6]), in a Rayleigh fading environment, the Laplace transform of the* pdf *of the aggregate interference measured at the origin from a PPP with intensity λ and existing outside $\mathbf{B}_x(r_e)$ is given by*

$$\mathcal{L}_{\mathcal{I}}(s) = \exp\left\{-\lambda\pi\left((Ps)^{\frac{2}{\eta}}\mathbb{E}_h\left[h^{\frac{2}{\eta}}\gamma\left(1-\frac{2}{\eta}, sPhr_e^{-\eta}\right)\right] - \frac{Psr_e^2}{Ps+\mu r_e^{\eta}}\right)\right\}. \tag{5.12}$$

where $\gamma(z,y) = \int_0^y t^{z-1}e^{-t}dt$ is the lower incomplete gamma function, P is the transmission power of each interferer, η is the path-loss exponent, h is instantaneous chan-

nel power gain, and μ is the mean channel power gain.

Based on the RSS, a generic user first associates to either a macro BS or a FAP. The user can be associated to a FAP with probability ξ_a and to a macro BS with probability ξ_b. The outage probability $\mathcal{O}_b$ of a macro user is due to the SINR falling below the reception threshold β. On the other hand, given that the serving FAP has K_f free channels within its *macro SSR* (i.e., the channels not used by other macro BSs within the *macro SSR* of the FAP), the outage probability $\mathcal{O}_a(K_f)$ of the associated femto user is due to the SINR falling below the reception threshold β, or due to the unavailability of any spectrum access opportunity for the serving FAP. The outage probability of a femto user is a function of K_f. As K_f increases, the intensity of the FAPs contending for and accessing the same channel decreases, and hence, both the outage probabilities (i.e., due to the unavailability of channels and due to the insufficient SINR) decrease. Therefore, the outage probability of a generic user (i.e., the overall outage probability) is given by

$$\mathcal{O}_t = \sum_{k=0}^{|\mathbf{S}|} \mathbb{P}\left\{K_f = k\right\} \mathcal{O}(k), \quad \text{where} \tag{5.13}$$

$$\begin{aligned} \mathcal{O}(K_f) &= \xi_a \mathcal{O}_a(K_f) + \xi_b \mathcal{O}_b \\ &= \xi_a \left[\left(1 - \mathcal{O}_a^{access}(K_f)\right) \mathcal{O}_a^{\text{SINR}}(K_f) + \mathcal{O}_a^{access}(K_f) \right] + \xi_b \mathcal{O}_b \end{aligned} \tag{5.14}$$

in which $\mathcal{O}_a^{access}(K_f)$ is the outage probability of a femto user due to channel unavailability and $\mathcal{O}_a^{\text{SINR}}(K_f)$ is the outage probability of a femto user due to the SINR falling below the reception threshold β. Exploiting Slivnyak's theorem for PPP, I can perform the analysis for a typical user located at the origin and the results hold for

any generic user located at a generic location.

5.6.2 Outage Probability of a Macro User

For a user associated to a macro BS, according to the system model, the serving macro BS is the nearest BS to that user in the macro network tier. Also, the serving macro BS is outside the *macro SSR* of all interfering FAPs. Following [12], the outage probability of this user is given by

$$\begin{aligned}\mathcal{O}_b &= \mathbb{P}\left\{\text{SINR} < \beta\right\} \\ &= \mathbb{P}\left\{\frac{P_b h_b R_b^{-\eta}}{\mathcal{I}+\sigma^2} < \beta\right\} \\ &= \int_0^\infty 2\pi\mathcal{B}re^{-\mathcal{B}\pi r^2}\mathbb{P}\left\{h_b < \frac{\beta r^\eta\left(\mathcal{I}+\sigma^2\right)}{P_b}\right\}dr \\ &= 1-\int_0^\infty 2\pi\mathcal{B}re^{-\mathcal{B}\pi r^2}\mathcal{L}_{\mathcal{I}_{ab}}\left(\frac{\mu_b\beta r^\eta}{P_b}\right)\mathcal{L}_{\mathcal{I}_{bb}}\left(\frac{\mu_b\beta r^\eta}{P_b}\right)\exp\left\{-\frac{\mu_b\beta r^\eta\left(\sigma^2\right)}{P_b}\right\}dr\end{aligned} \tag{5.15}$$

where $\mathcal{L}_{\mathcal{I}_{ab}}\left(\frac{\mu_b\beta r^\eta}{P_b}\right)$ and $\mathcal{L}_{\mathcal{I}_{bb}}\left(\frac{\mu_b\beta r^\eta}{P_b}\right)$ are the Laplace transforms of the *pdf* of the interference, respectively, from the femto network tier and the macro network tier to the macro user evaluated at $\left(\frac{\mu_b\beta r^\eta}{P_b}\right)$. Then, following [12], the Laplace transform of the *pdf* of interference from other macro BSs can be obtained as

$$\mathcal{L}_{\mathcal{I}_{bb}}(s) = \exp\left\{-2\pi\mathcal{B}_{ac}\int_r^\infty\left(\frac{1}{\frac{\mu_b x^\eta}{sP_b}+1}\right)xdx\right\} \tag{5.16}$$

where $\mathcal{B}_{ac} = \left(1-\left(\frac{\mathcal{B}c}{\mathcal{B}c+\mathcal{U}_b}\right)^c\right)\mathcal{B}$ is the intensity of macro BSs interfering on channel s_1 (i.e., the macro BSs with at least one associated user). Now, plugging in $s = \frac{\mu_b\beta r^\eta}{P_b}$, I have

$$\mathcal{L}_{\mathcal{I}_{bb}}\left(\frac{\mu_b \beta r^{\eta}}{P_b}\right) = \exp\left\{-2\pi\mathcal{B}_{ac}\int_r^{\infty}\left(\frac{1}{\left(\frac{\beta^{-1/\eta}x}{r}\right)^{\eta}+1}\right)xdx\right\}$$
$$\stackrel{(**)}{=} \exp\left\{-\pi\mathcal{B}_{ac}r^2\beta^{2/\eta}\int_{\beta^{-2/\eta}}^{\infty}\left(\frac{1}{y^{\frac{\eta}{2}}+1}\right)dy\right\} \tag{5.17}$$

where $(**)$ is obtained by changing variables $y = \left(\frac{\beta^{-1/\eta}x}{r}\right)^2$. For $\eta = 4$, I have

$$\mathcal{L}_{\mathcal{I}_{bb}}\left(\frac{\mu_a \beta r^{\eta}}{P_a}\right) = \exp\left\{-\pi\mathcal{B}_{ac}r^2\sqrt{\beta}\left[\frac{\pi}{2} - \arctan\left(\sqrt{\frac{1}{\beta}}\right)\right]\right\}$$
$$= \exp\left\{-\pi\mathcal{B}_{ac}r^2\sqrt{\beta}\arctan\left(\sqrt{\beta}\right)\right\}. \tag{5.18}$$

Now I calculate the interference caused to a macro user from the femto network tier. Since all FAPs are cognitive, the set of interfering FAPs constitute an HCPP, and on average, the nearest interfering FAP to the serving BS will be r_{sb} away, hence, it will be $(r_{sb} - R_b)$ away from the test macro receiver. However, the exact Laplace transform of the *pdf* of the aggregate interference from FAPs cannot be calculated because the probability generating functional of the HCPP does not exist. Conventionally, the Laplace transform of the *pdf* of the aggregate interference due to an HCPP has been always approximated by the Laplace transform of the *pdf* of the aggregate interference due to a PPP with the same intensity but existing outside the contention domain of the test transmitter [40, 44, 49, 51]. The rationale behind this approximation is that the main factors affecting the aggregate interference are the number of interferers and their locations w.r.t. the test node. However, the locations of the interferers w.r.t. each other have minimal effect on the interference at the test node. The number of interferers has been captured in the calculation of the intensity of the HCPP

and the locations of the interferers w.r.t. the test receiver have been captured by conditioning on having the PPP outside the contention domain of the test transmitter. In [49], it was proved that the mean interference from an HCPP can be accurately approximated with the mean interference from a PPP with the same intensity and existing outside the exclusion region of the test transmitter and the approximation error never exceeds 1 dB. Therefore, using **Lemma 5.6.1**, the Laplace transform of the *pdf* of the aggregate interference resulting from the FAPs can be approximated by

$$\mathcal{L}_{\mathcal{I}_{ab}}(s) \approx \exp\left\{-\mathcal{A}_{s_1}\pi\left((P_a s)^{\frac{2}{\eta}}\mathbb{E}_{h_{a_i}}\left[h_{a_i}^{\frac{2}{\eta}}\gamma\left(1-\frac{2}{\eta}, sP_a h_{a_i}(r_{sb}-r)^{-\eta}\right)\right] - \frac{P_a s(r_{sb}-r)^2}{P_a s+\mu_a(r_{sb}-r)^{\eta}}\right)\right\} \tag{5.19}$$

where $\mathcal{A}_{s_1}$ is the intensity of FAPs interfering on channel s_1 and is calculated in (5.11). For $\eta = 4$, in **Appendix B.5**, I show that

$$\mathcal{L}_{\mathcal{I}_{ab}}(s) \approx \exp\left\{-\mathcal{A}_{s_1}\pi\sqrt{\frac{P_a s}{\mu_a}}\arctan\left(\frac{\sqrt{P_a s}}{r_{sb}^2\sqrt{\mu_a}}\right)\right\}. \tag{5.20}$$

Now plugging in $s = \frac{\mu_b \beta r^{\eta}}{P_b}$, I have

$$\mathcal{L}_{\mathcal{I}_{ab}}\left(\frac{\mu_b\beta r^4}{P_b}\right) \approx \exp\left\{-\mathcal{A}_{s_1}\pi r^2\sqrt{p\beta}\arctan\left(\frac{r^2\sqrt{p\beta}}{(r_{sb}-r)^2}\right)\right\} \tag{5.21}$$

where $p = \frac{P_a\mu_b}{P_b\mu_a}$. Substituting back in (5.15) for $\eta = 4$, I have

$$\mathcal{O}_b = 1 - \int_0^{\infty} 2\pi\mathcal{B}re^{-\mathcal{B}\pi r^2}\exp\left\{-\mathcal{A}_{s_1}\pi r^2\sqrt{p\beta}\arctan\left(\frac{r^2\sqrt{p\beta}}{(r_{sb}-r)^2}\right) - \pi\mathcal{B}_{ac}r^2\sqrt{\beta}\arctan\left(\sqrt{\beta}\right) - \frac{\mu_b\beta r^{\eta}\left(\sigma^2\right)}{P_b}\right\}dr.$$

Due to the relatively large value of r_{sb}, small value of P_a, and low intensity A_{s_1}, the interference from FAPs can be ignored. In interference-limited networks (i.e., ignoring noise), the outage probability of a macro user is given by

$$\begin{aligned}\mathcal{O}_b &= 1 - \int_0^\infty 2\pi\mathcal{B}re^{-\mathcal{B}\pi r^2} e^{-\pi\mathcal{B}_{ac}r^2\sqrt{\beta}\arctan\left(\sqrt{\beta}\right)} dr \\ &= 1 - \frac{\mathcal{B}}{\mathcal{B} + \mathcal{B}_{ac}\sqrt{\beta}\arctan\left(\sqrt{\beta}\right)} = \frac{\mathcal{B}_{ac}\sqrt{\beta}\arctan\left(\sqrt{\beta}\right)}{\mathcal{B} + \mathcal{B}_{ac}\sqrt{\beta}\arctan\left(\sqrt{\beta}\right)}. \end{aligned} \tag{5.22}$$

5.6.3 Outage Probability of a Femto User

Now I calculate the outage probability of a femto user. Similar to (5.15), the outage probability of a femto user due to the SINR falling below the reception threshold β is given by

$$\begin{aligned}\mathcal{O}_a^{(\mathrm{SINR})}(K_f) &= \mathbb{P}\left\{\mathrm{SINR} < \beta\right\} \\ &= \mathbb{P}\left\{\frac{P_a h_{a_i} R_a^{-\eta}}{\mathcal{I}(k) + \sigma^2} < \beta\right\} \\ &= 1 - \int_0^\infty 2\pi\mathcal{A}re^{-\mathcal{A}\pi r^2} \mathcal{L}_{\mathcal{I}_{aa}}\left(\frac{\mu_a\beta r^\eta}{P_a}, K_f\right) \mathcal{L}_{\mathcal{I}_{ba}}\left(\frac{\mu_a\beta r^\eta}{P_a}, K_f\right) \\ &\qquad \exp\left\{-\frac{\mu_a\beta r^\eta\left(\sigma^2\right)}{P_a}\right\} dr \end{aligned} \tag{5.23}$$

where $\mathcal{L}_{\mathcal{I}_{aa}}\left(\frac{\mu_a\beta r^\eta}{P_a}, K_f\right)$ and $\mathcal{L}_{\mathcal{I}_{ba}}\left(\frac{\mu_a\beta r^\eta}{P_a}, K_f\right)$ represent the Laplace transforms of the *pdf* of the interference, respectively, from the femto network tier and the macro network tier to the femto user, evaluated at $\frac{\mu_a\beta r^\eta}{P_a}$ given that there are K_f channels available to the serving FAP. Given that the user is associated to a FAP, from the system model, the serving FAP is the nearest FAP to that user in the femto network tier. Also, the interfering BSs and FAPs are outside the *macro SSR* and *femto SSR* of the serving FAP, respectively. Therefore, on average, the nearest interfering BSs

and FAPs to the test user are, respectively, $r_{sb} - R_a$ and $r_{sa} - R_a$ away from the test femto receiver. Similar to (5.20), for $\eta = 4$, the Laplace transform of the aggregate interference from FAPs is given by

$$\mathcal{L}_{\mathcal{I}_{aa}}\left(\frac{\mu_a \beta r^4}{P_a}, K_f\right) \approx \exp\left\{-\mathcal{A}_{s_{|\mathbf{S}|-(K_f-1)}} \pi r^2 \sqrt{\beta} \arctan\left(\frac{r^2\sqrt{\beta}}{(r_{sa}-r)^2}\right)\right\} \tag{5.24}$$

where $\mathcal{A}_{s_{|\mathbf{S}|-(K_f-1)}}$ is the intensity of simultaneously active FAPs on the channel $s_{|\mathbf{S}|-(K_f-1)}$ and is given in (5.11), and the Laplace transform of the *pdf* of the aggregate interference from macro BSs is given by

$$\mathcal{L}_{\mathcal{I}_{ba}}\left(\frac{\mu_a \beta r^4}{P_a}, K_f\right) = \exp\left\{-\mathcal{B}_{in}(K_f) \pi r^2 \sqrt{\frac{\beta}{p}} \arctan\left(\frac{r^2\sqrt{\frac{\beta}{p}}}{(r_{sb}-r)^2}\right)\right\} \tag{5.25}$$

where p is defined in (5.21) and $\mathcal{B}_{in}(K_f)$ in the intensity of the interfering macro BSs on channel $s_{|\mathbf{S}|-(K_f-1)}$ (i.e., BSs with at least $|\mathbf{S}| - (K_f - 1)$ associated users). The Laplace transform of the *pdf* of the aggregate interference from macro BSs is exact because the interfering BSs constitute a PPP with intensity $\mathcal{B}_{in}(K_f) = (1 - v(|\mathbf{S}| - K_f - 1))\,\mathcal{B}$ outside the *macro SSR* r_{sb} of the test FAP. Substituting back in (5.23), I have

$$\begin{aligned}\mathcal{O}_a^{(\mathrm{SINR})}(K_f) =& 1 - \int_0^\infty 2\pi \mathcal{A} r \exp\left\{-\mathcal{A}\pi r^2 - \mathcal{B}_{in}(K_f)\pi r^2 \sqrt{\frac{\beta}{p}} \arctan\left(\frac{r^2\sqrt{\frac{\beta}{p}}}{(r_{sb}-r)^2}\right)\right. \\ & \left. - \mathcal{A}_{s_{|\mathbf{S}|-(K_f-1)}} \pi r^2 \sqrt{\beta} \arctan\left(\frac{r^2\sqrt{\beta}}{(r_{sa}-r)^2}\right) - \frac{\beta r^\eta \left(\sigma^2\right)}{P_a}\right\} dr. \end{aligned} \tag{5.26}$$

Conditioning on having K_f available channels for the serving FAP, the outage probability of a femto user due to the unavailability of channels is given by

$$\mathcal{O}_a^{(access)}(K_f) = 1 - \mathcal{P}_{ac}(K_f) = 1 - \frac{K_f \left(1 - e^{-\pi \frac{\mathcal{A}}{K_f}\left(1-\left(\frac{c\mathcal{A}}{c\mathcal{A}+\mathcal{U}_a}\right)^c\right)\left(\frac{P_a}{\mu_b \upsilon_s}\right)^{\frac{2}{\eta}}\Gamma(1+\frac{2}{\eta})}\right)}{\pi\mathcal{A}\left(1-\left(\frac{c\mathcal{A}}{c\mathcal{A}+\mathcal{U}_a}\right)^c\right)\left(\frac{P_a}{\mu_b \upsilon_s}\right)^{\frac{2}{\eta}}\Gamma(1+\frac{2}{\eta})}. \tag{5.27}$$

The unconditional outage probability of the femtocell user can be calculated as

$$\mathcal{O}_a = \sum_{k=0}^{|\mathbf{S}|} \mathbb{P}\left\{K_f = k\right\}\left[\left(1 - \mathcal{O}_a^{access}(K_f)\right)\mathcal{O}_a^{\text{SINR}}(K_f) + \mathcal{O}_a^{access}(K_f)\right] \tag{5.28}$$

After calculating the outage probability of a generic user in each network tier, the overall outage can be calculated by using (5.13).

5.7 Performance Evaluation Results

5.7.1 Parameters and Assumptions

In this section I present the numerical results obtained from the previous analysis. In the numerical evaluations, unless otherwise stated, I choose $P_a = 20$ dBm, $\mathcal{B} = 1$ BS/km^2, $|\mathbf{S}| = 25$ channels, all the channel gains to have unit mean (i.e., $\frac{1}{\mu_a} = \frac{1}{\mu_b} = 1$), and $\eta = 4$. We usually vary the intensity of the FAPs $\mathcal{A}$ and the transmission power of the macro BSs P_b. The effect of noise is ignored (i.e., the network is interference-limited) [12,54]. Based on the analysis presented earlier in this chapter, the numerical results are obtained using MATLAB.

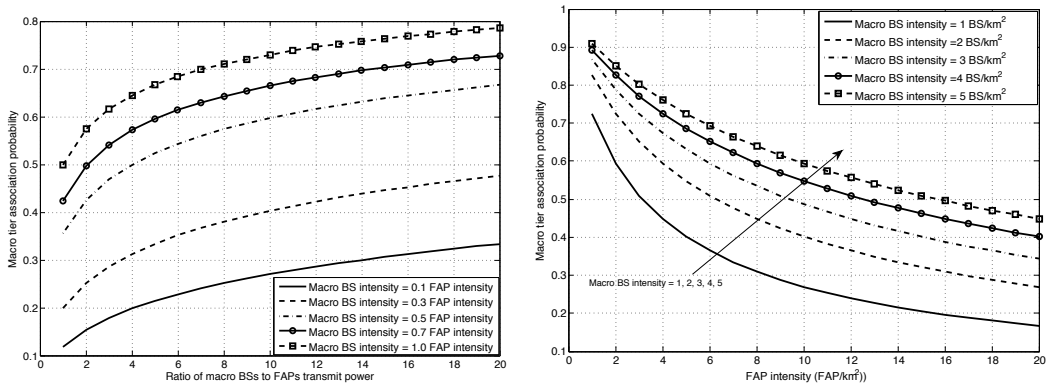

(a) (b)

Figure 5.5: (a) The macro-tier association probability vs. the normalized macro-tier transmission power $\frac{P_b}{P_a}$ for different normalized macro-tier intensities $\frac{\mathcal{B}}{\mathcal{A}}$, (b) the macro-tier association probability vs. intensity of each tier at $P_b = 10P_a$.

5.7.2 Numerical Results

Tier Association and Opportunistic Channel Access

Fig. 5.5 shows the variations in the macro BS association probability ξ_b (note that $1-\xi_b$ gives the femto tier association probability) with the intensities and transmission powers of the FAPs and macro BSs. It can be seen that the association probability with a given network tier is directly proportional to the intensity of corresponding macro BSs/FAPs and the transmission power. As shown in Fig. 5.5(a), if the two network tiers have the same parameters, then they will have equal association probability (i.e., $\xi_a = \xi_b = 0.5$). It can be also observed in Fig. 5.5(b) that the intensity of macro BSs/FAPs has a greater impact on the tier association probability than the relative transmission power. For instance, as shown in Fig. 5.5(b), a 10 dB power gain of the macro BSs over the FAPs can be equalized with only 5 dB intensity gain for the FAPs. That is, if $P_b = 10P_a$ and $\mathcal{A} = 3.1\mathcal{B}$, then $\xi_a = \xi_b = 0.5$.

Fig. 5.6(a) shows $(1 - F_{N_v}(k))$ at $k = 10$ (i.e., the probability of having more than

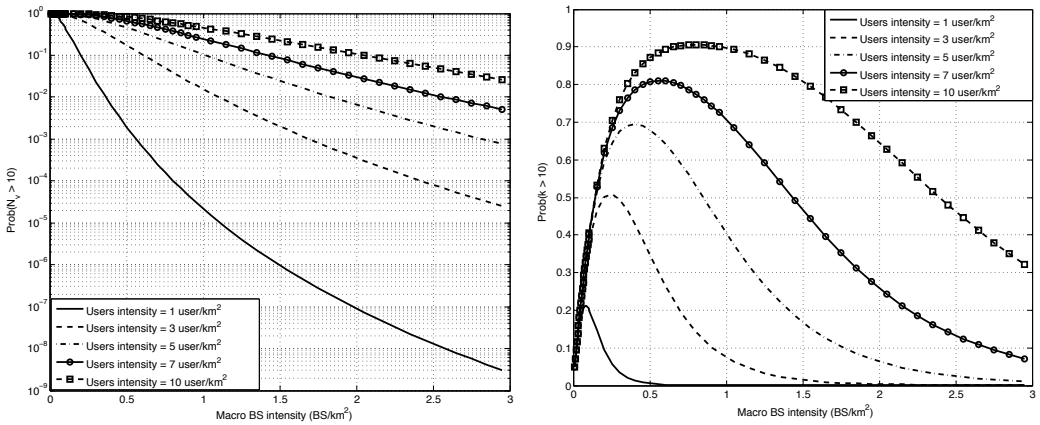

(a) (b)

Figure 5.6: (a) The probability of having more than 10 users in a BS's Voronoi cell, (b) the probability of having more than 10 channels used in the *macro SSR* of a generic FAP (for $\mu_{ch} = 1$, $P_b = 5$ W, and $\upsilon_s = -45$ dBm).

10 users associated to a generic BS) for different BS and user intensities. The figure shows that as the intensity of macro BSs ($\mathcal{B}$) increases, $(1-F_{N_v}(k))$ decreases because the areas of the Voronoi cells decrease with increasing $\mathcal{B}$, hence, each BS will cover a fewer number of users. Fig. 5.6(b) shows $(1 - F_K(k))$ at $k = 10$ (i.e., the probability of having more than 10 channels used within the *macro SSR* of a generic FAP) for different BS and user intensities. This figure is insightful because it shows that as $\mathcal{B}$ increases, $(1 - F_K(k))$ increases up to a certain point and then it starts decreasing. This behavior can be interpreted as follows. For very low values of $\mathcal{B}$, despite the fact that the area of the Voronoi cell of a macro BS is very large, it is a very rare event to find any macro BS within the *macro SSR* of the FAP. However, as $\mathcal{B}$ increases, it becomes more likely to find macro BSs within the *macro SSR* of the FAP, and hence $(1 - F_K(k))$ increases. Finally, when $\mathcal{B}$ becomes high enough, it becomes a very rare event not to find a macro BS within the *macro SSR* of the FAP. Therefore, the areas of the Vononoi cells of the macro BSs, which decrease with increasing $\mathcal{B}$, become the

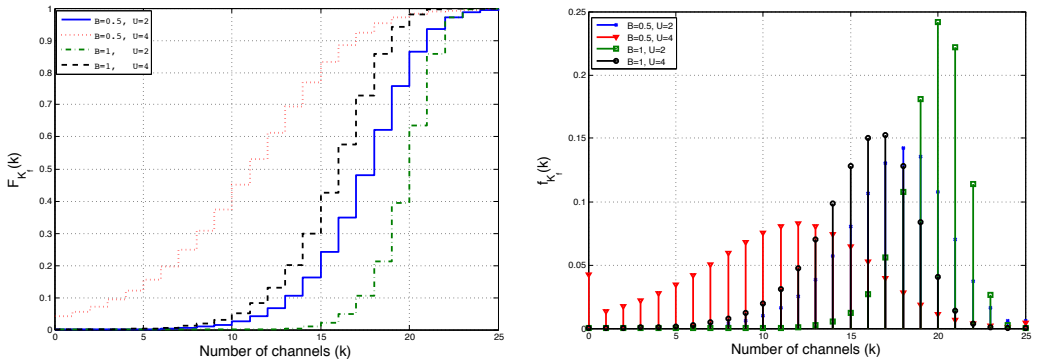

(a) (b)

Figure 5.7: (a) The *cmf* $F_{k_f}(k)$ of the number of free channels within the *macro SSR* of a generic FAP (for $\mu_b = 1$, $P_b = 5$ W, and $\upsilon_s = -45$ dBm), (b) the *pmf* $f_{k_f}(k)$ of the number of free channels within the *macro SSR* of a generic FAP (for the same parameters).

dominating factor for $(1 - F_K(k))$. On the other hand, Fig. 5.6 shows that both $(1 - F_{N_v}(k))$ and $(1 - F_K(k))$ always increase with $\mathcal{U}$.

Fig. 5.7 shows the *cmf* and the *pmf* of the number of free channels within the *macro SSR* of a generic FAP. As shown in the figure, at lower $\mathcal{B}$, it is more likely to find a lower number of free channels, however, there is a non-zero probability to find all the channels free. This is because the lower the value of $\mathcal{B}$, the larger are the Voronoi cells of macro BSs and the higher are the number of users associated to a macro BS. Since there is no intra-cell interference within a macrocell, a larger number of users associated to a macro BS implies that a larger number of channels are being used by that BS. However, at lower intensity of macro BSs, it is more likely that there will be no macro BS within the *macro SSR* of the FAP, and hence, all the channels are available for FAP usage. On the other hand, for higher intensity of macro BSs, it is very unlikely that there will be no macro BS within the *macro SSR* of a FAP, and therefore, the probability that all of the channels will be free for FAP usage will

be very low. At higher $\mathcal{B}$, the Voronoi cells of the macro BSs are smaller and a fewer number of users are associated to a BS, and hence, a lesser number of channels are used in each BS. Therefore, increasing the intensity of the macro BSs increases the spectrum opportunities for the cognitive FAPs.

Performance Gain Due to Cognition and Optimal Spectrum Sensing Threshold

Fig. 5.8 shows the performance gain in outage probability obtained by introducing cognition into the femto-tier for different values of SIR (signal-to-interference-ratio) threshold. Fig. 5.8(a) shows that for lower values of the spectrum sensing threshold, despite that the aggregate interference will be very low, the effect of channel unavailability dominates the outage probability and it results in a degraded outage performance. On the other hand, for higher values of spectrum sensing threshold, the spectrum opportunities for FAPs increase, however, the aggregate interference increases and dominates the outage probability and it also results in a degraded outage performance. For very high values of spectrum sensing threshold, the performance of cognitive FAPs saturates and matches that of the non-cognitive FAPs.

Fig. 5.8(b) shows that introducing cognition decreases the overall outage probability, however, its impact on the overall outage probability is not as much as its impact to the femto-tier. This is because the majority of users are served by the macro network tier due to the higher transmission power of the macro BSs and the comparable intensity of FAPs to the macro BSs. This figure shows the existence of an optimal spectrum sensing threshold which gives around 60% performance gain in outage probability for femto-tier and around 15% for the overall network performance.

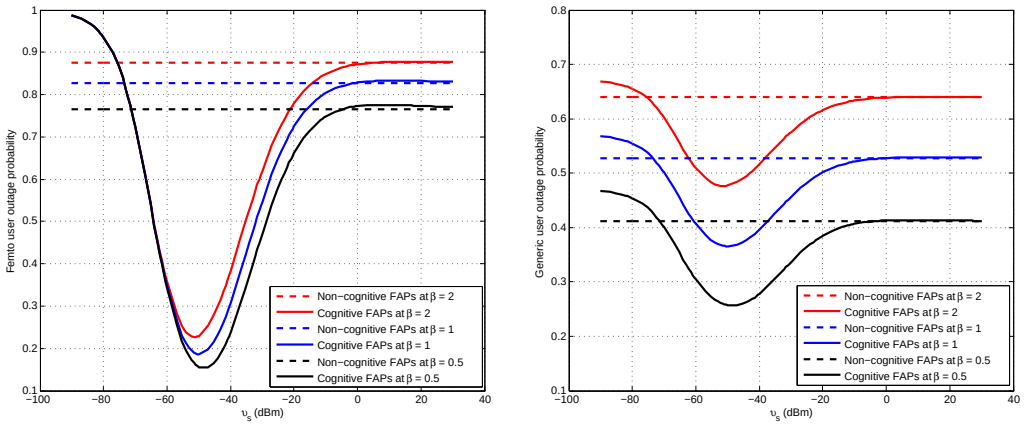

(a) (b)

Figure 5.8: The effects of cognition on the outage probability for different spectrum sensing thresholds for $P_b/P_a = 50$, $\mathcal{A}/\mathcal{B} = 2$, $|\mathbf{S}| = 25$, and $\mathcal{U} = 2(\mathcal{A} + \mathcal{B})$.

Macro BS/FAP Intensity and Outage Probability

Fig. 5.9 shows the effects of both the macro BS/FAP intensity and the spectrum sensing threshold on the outage probability. Fig. 5.9(a) shows that when the intensity of FAPs is smaller w.r.t. that of macro BSs, the FAPs should be conservative to avoid massive interference from macro BSs and maintain an acceptable outage probability. On the other hand, when the FAP intensity is higher w.r.t. the deployed macro BSs (i.e., in a heavily deployed FAP scenario), the FAPs are required to be more aggressive to maintain an acceptable outage probability. This behavior can be interpreted by the tradeoff between the outage probability due to the aggregate interference and the outage probability due to contention among the FAPs to access the channels.

In a sparsely deployed FAP scenario, the distance between a femto user and its serving FAP is relatively large (i.e., when compared to the highly deployed scenario). Hence, the useful signal received at the user equipment is weak and the FAPs should be more conservative to provide protection (i.e., interference exclusion region) around

the user equipment to avoid massive interference from macro BSs. Moreover, because of the relatively low intensity of the FAPs, the outage due to the aggregate interference dominates the outage due to the unavailability of channels resulting from the contention among the FAPs coexisting within the same *femto SSR*. On the other hand, in a heavily deployed FAP scenario, the distance between the FAP and its user is relatively small and hence the useful signal is strong enough to stabilize the SINR. Moreover, due to the relatively high intensity of the FAPs in a heavily deployed FAP scenario, the outage due to the unavailability of channels resulting from the contention among FAPs dominates the outage due to the aggregate interference.

Fig. 5.9(b) shows that the overall outage probability (i.e., the outage probability of a generic user) can be quite misleading and does not convey the poor performance of the femto users. For instance, at $\mathcal{A} = \mathcal{B}$, for a varying spectrum sensing threshold (υ_s), the outage probability of a FAP ranges from 30% to 95% while the overall outage probability is almost constant (i.e., the outage probability of a FAP is not reflected in the overall outage probability). This behavior can be understood by looking into the tier association probability. Due to the higher transmission powers of the macro BSs, for equal intensities of FAPs and macro BSs, the majority of the users are served by the macro BSs. Therefore, despite the fact that the femto users experience a higher outage probability, due to their small numbers compared to the macro users, their performance does not affect the overall outage probability. However, as shown in Fig. 5.9, by explicitly accounting for the performance of the femto users, the femto-tier network can be optimized without affecting the performance of the macro-tier network. On the other hand, in a heavily deployed FAP scenario, due to the high intensity of FAPs, the majority of the users are served by the femto-tier and the performance of the femto-tier highly affects the overall network performance.

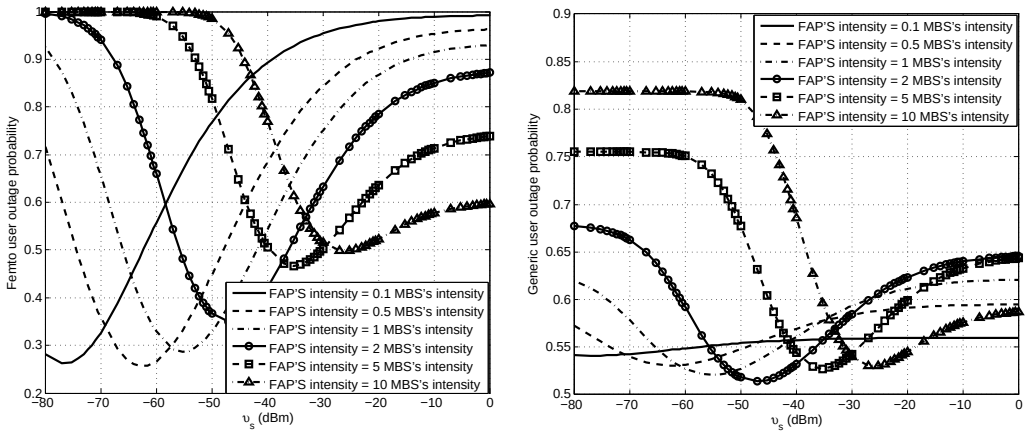

(a) (b)

Figure 5.9: The effects of the intensities of the macro BSs/FAPs and the spectrum sensing threshold on the outage probability for $P_b/P_a = 50$, $\beta = 2$, $|\mathbf{S}| = 25$, and $\mathcal{U} = 2(\mathcal{A} + \mathcal{B})$.

Although I have introduced cognition and relaxed the single channel assumption used in [12, 54], I am still able to compare my results with those in [12, 54]. This is because the overall outage probability is not much affected by the outage probability of femto users (i.e., when the FAP intensity is relatively low). It is worth mentioning that the results on the outage probabilities presented here match with those presented in [12,54] and the high values of outage probabilities are due to the high value of target SINR ($\beta = 2$).

Variation in Outage Probability with Spectrum Sensing Threshold and Required SIR

Fig. 5.10(a) shows that for high SIR requirements, the outage due to aggregate interference dominates the outage due to unavailability of channels and the FAPs are required to be more conservative to maintain a lower outage probability. When the SINR requirement is relaxed, the FAPs can be more aggressive to decrease outage

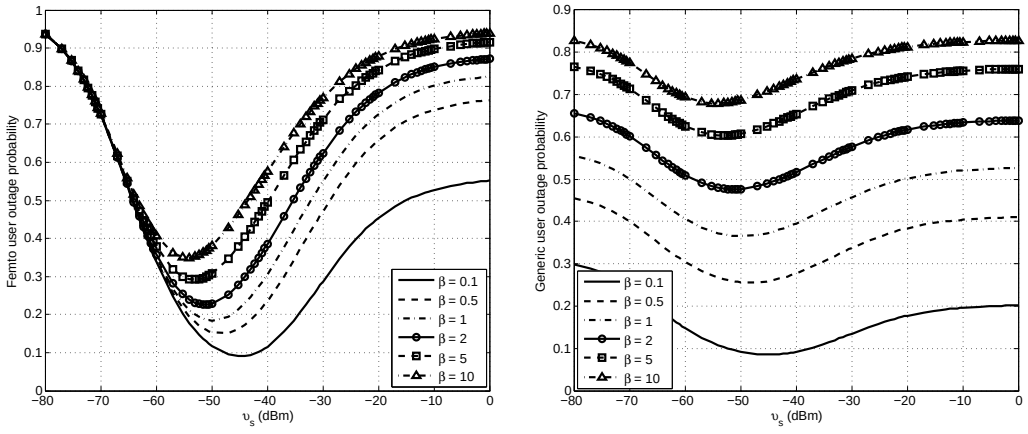

(a) (b)

Figure 5.10: The effects of the required SIR and the spectrum sensing threshold on the outage probability for $P_b/P_a = 50$, $|\mathbf{S}| = 25$, $\mathcal{A}/\mathcal{B} = 2$, and $\mathcal{U} = 2(\mathcal{A} + \mathcal{B})$.

due to the unavailability of channels. Fig. 5.10(b) shows that due to the higher transmission powers of the macro BSs, the overall outage probability does not clearly convey the performance of the FAPs. Fig. 5.10(b) also shows that as the SINR constrains become more stringent, the outage probability increases.

Effects of Number of Channels and Spectrum Sensing Threshold on Outage Probability

Fig. 5.11 shows that the optimal spectrum sensing threshold for the FAPs depends on the number of available channels. Fig. 5.11(a) clearly shows the tradeoff between the outage due to aggregate interference and the outage due to the unavailability of channels. Increasing the number of available channels increases the spectrum opportunities for the FAPs and decreases the outage probability due to the unavailability of channels. Hence, the femtocells can be more conservative to mitigate the aggregate interference. Fig. 5.11(b) shows that due to the higher transmission power of the

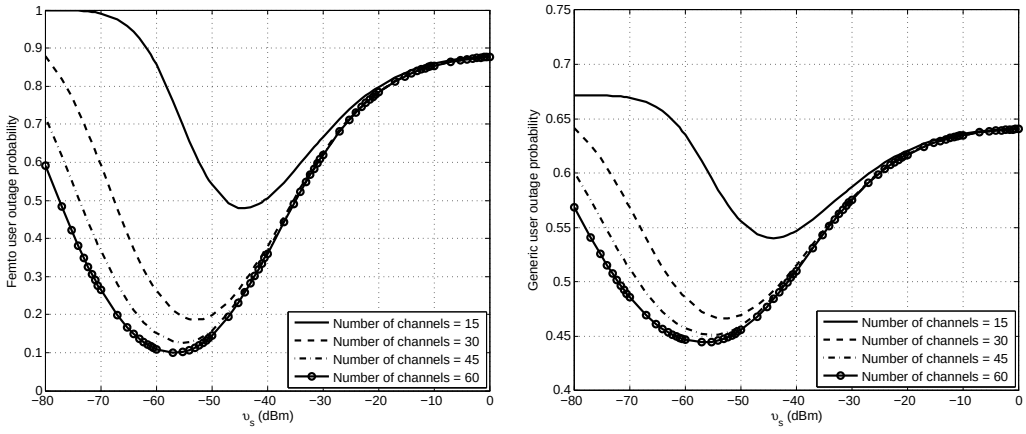

(a) (b)

Figure 5.11: The effects of the number of channels and the spectrum sensing threshold on the outage probability (for $P_b/P_a = 50$, $\mathcal{A}/\mathcal{B} = 2$, $\beta = 2$, and $\mathcal{U} = 2(\mathcal{A} + \mathcal{B})$).

macro BSs and the higher association probability of the users to the macro BSs, the femto-tier network performance does not have a strong impact on the overall outage probability. However, in a heavily deployed FAP scenario, the effect of the performance of the femto users on the overall outage performance will be prominent (as shown in Fig. 5.9).

Effects of Relative Transmission Power and Spectrum Sensing Threshold on Outage Probability

In Fig. 5.12, the transmission power of the macro BSs is increased while the transmission power of the FAPs is kept constant. The figure shows that the optimal spectrum sensing threshold is almost the same despite increasing transmission power of the macro BSs. This is because the higher the transmission power of the macro BSs w.r.t. the FAPs' transmission power, the larger will be the *macro SSR* to stabilize the aggregate interference while the *femto SSR* remains the same. An increased

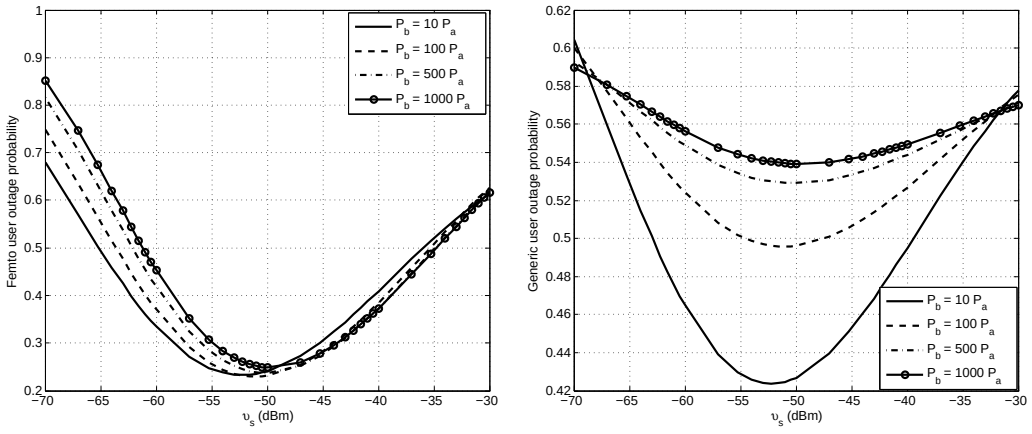

(a) (b)

Figure 5.12: The effects of the relative transmission power of macro BSs to FAPs and the spectrum sensing threshold on the outage probability (for $|\mathbf{S}| = 25$, $\mathcal{A}/\mathcal{B} = 2$, $\beta = 2$, and $\mathcal{U} = 2(\mathcal{A} + \mathcal{B})$).

macro SSR implies a higher number of macro BSs in the *macro SSR*. However, due to the sequential assignment of the channels in the macro BSs, increasing the number of BSs within the *macro SSR* does not highly affect the availability of channels, and hence, does not affect the opportunistic spectrum access probability for FAPs. The factor that highly affects the opportunistic spectrum access probability for FAPs is the *femto SSR*.

Fig. 5.12(b) shows that increasing the transmission power of the macro BSs decreases the impact of the femto users on the total outage probability. This is because, increasing the transmission power of the macro BSs offloads more users from the femto tier to the macro tier, hence, decreases the weight of the femto users' performance in the total network performance.

In Fig. 5.12, keeping in mind that the transmission power of the FAPs is kept constant, some insightful observations can be obtained from the intersection of curves. Fig. 5.12(a) shows that the curves reverse their order at approximately -50 dBm.

That is, in the range from -70 dBm to -50 dBm, the femto user performance is enhanced by decreasing the macro BSs' transmission power. On the other hand, in the range from -70 dBm to -50 dBm, the femto user performance is degraded by decreasing the macro BSs' transmission power. This behavior can be interpreted by looking into the offloading effect on the network performance. In the range from -70 dBm to -50 dBm the cognitive FAPs are too conservative and the *macro SSR* is large. Increasing the transmission power of the macro BSs not only increases the *macro SSR*, but also offloads users from the femto network tier to the macro network tier which increases the load of users per macro BSs. Hence, increases the channel consumed by the macro network tier and decreases the opportunistic channel access probability. On the other hand, in the range -50 dBm to -30 dBm, the FAPs are too aggressive in accessing the spectrum which results in a degraded SINR performance. Although decreasing the transmission power of the macro BSs decreases the *macro SSR* which should increase the opportunistic spectrum access, it also offloads users to the femto network tier and increase the number of active FAPs which degrade the SINR performance even more. The two crossing points in Fig. 5.12(b) can be interpreted in the same manner. That is, when the FAPs' outage performance is better than the macro BS outage performance, decreasing the macro BSs' transmission power offloads users to the femto network tier and enhance the overall network performance and vice versa.

As seen in Fig. 5.12, offloading control can be utilized to optimize the network performance. For instance, in a congested macro network scenario where the number of users per macro BS is relatively high, FAPs will experience degraded opportunistic spectrum access probability. At this point, offloading may be utilized to increase the FAPs' opportunistic spectrum access probability. For instance, increasing the relative

transmission power of FAPs, or increasing their relative intensity (i.e., deploying more FAPs) with the proper manipulation of the spectrum sensing threshold will offload users from the macro network tier to the femto network tier while maintaining the SINR performance. Hence, the load of each macro BS decreases, which decreases the number of channels used within each macro BS and creates spectrum opportunities for the FAPs, and consequently, increases their opportunistic channel access probability.

5.8 Chapter Summary

We have provided a framework for modeling and analysis of two-tier cellular networks with cognitive femtocells. We have shown that cognition is an important feature that can boost up the overall network performance. The performance gain due to cognition depends on the network operating parameters. The results have shown that the spectrum sensing threshold is a critical parameter which should be tuned carefully. We have observed that the correct choice of the spectrum sensing threshold can decrease the outage probability by 60% for the femtocell users. In general, more users are associated to macro BSs due to the high transmission power of the macro BSs. More efficient offloading for the users from the macro-tier to the femto-tier can be achieved by increasing the intensity of the FAPs. We have observed that a 10 dB gain of the transmission power of the macro BSs over that of femto access points can be compensated by increasing the intensity of the FAPs by 5 dB. The results have also showed that it can be quite misleading to look into the overall outage performance as it does not convey the performance of the femtocell users and it is recommended to explicitly account for the outage probability of femtocell users in order to optimize the spectrum sensing threshold.

In this chapter, I used the sequential channel assignment assumption at the MBSs

to develop the modeling paradigm for a two tier cellular network with cognitive FAPs. In the next chapter I analyze the effects of different channel assignment techniques at the MBSs on the opportunistic channel access of the FAPs to show the motivation behind the sequential channel assignment assumption. We also show in the next chapter that implementing cognition at the FAP significantly improves the performance of the macro users.

Chapter 6

Channel Assignment Techniques in Two-tier Cellular Networks with Cognitive Femtocells

As discussed in the previous chapter, cognitive femtocells using opportunistic spectrum access (OSA) are envisioned to be a key technology for future generation multi-tier cellular wireless networks. In a multi-tier cellular network with universal frequency reuse, macrocell users may suffer performance degradation due to inter-tier interference caused by closed-access femtocells. On the other hand, when the traffic load served by the macro network tier is high, the OSA performance of the femtocells will be poor. However, similar to that for the macrocell users, the quality-of-service (QoS) performance of the femtocell users needs to be guaranteed. Therefore, efficient channel sharing mechanisms need to be developed for macrocell and femtocell users. In this chapter, I use tools from stochastic geometry to inspect two extremal downlink channel assignment techniques, namely, the random channel assignment (RCA) and the sequential channel assignment (SCA) techniques in the macro tier in order to

accommodate the overlaid cognitive femtocells with an acceptable OSA performance. We show that, for downlink transmission, while the RCA scheme offers low intra-tier interference for macro users, it results in a degraded OSA performance (in terms of probability of successful channel access) for the femtocells. On the other hand, the SCA scheme enhances the OSA performance of the femtocells at the expense of increased intra-tier interference for macro users. To quantify the performance gain achieved due to OSA by the femtocells for these two channel assignment schemes, I compare the coverage probability of a generic macro user when the femtocells are cognitive and when the femtocells aggressively use the spectrum.

6.1 Introduction

In the context of cellular networks, overlaying the macro base stations (MBSs) with femtocells is a key technique to increase the spectral efficiency and network capacity. In a two-tier network adopting universal frequency reuse for macrocells and femtocells, macro users' performance is expected to deteriorate due to high cross-tier interference from closed-access femtocells. Therefore, efficient channel assignment and sharing mechanisms will be required. Since centralized control of spectrum access and interference management is infeasible (in terms of complexity, delay, and scalability), opportunistic spectrum assess (OSA) via cognition (e.g., spectrum sensing) is highly desirable for the femtocells [109]. However, cognitive femtocells may suffer from deteriorated spectrum access performance when the traffic load in the macro network tier is high. Note that, since both the macrocell and femtocell users are licensed users, there should be some performance guarantee for users in both network tiers. This can be achieved by using efficient techniques for channel assignment at the macro tier and OSA at the femtocell tier.

In this chapter, I investigate the effect of channel assignment techniques in the macro network tier on the OSA performance of the cognitive femtocells. For a two-tier cellular network with cognitive femtocells, I consider two channel assignment schemes at the MBSs, namely, the random channel assignment (RCA) scheme and the sequential channel assignment (SCA) scheme. In the RCA scheme, each MBS, independent of the other MBSs, randomly and uniformly chooses one channel for each of its associated users such that no two users associated to the same MBS are assigned the same channel. The main motivation for considering the RCA scheme is that there is no loss in generality in assuming uniform distribution for the channel selection. That is, if each MBS follows a channel quality index (CQI) based assignment (i.e., based on the channel gain between the MBS and the user) to exploit the multiuser diversity in the macrocells and all the channel gains are identically distributed, then, for a generic user at a generic time instant, each of the channels will have the same probability to be the channel with the highest CQI. However, the RCA scheme may degrade the OSA performance for femtocell users due to the fewer spectrum opportunities. On the contrary, the SCA scheme is a conservative channel assignment scheme which minimizes the number of unique channels accessed by the MBSs to maximize the probability of successful channel access (or OSA probability) for the cognitive femtocells. In the SCA scheme, the available channels have a specific order and each MBS assigns the channels to its associated users in a sequential manner. However, SCA will increase the intra-tier interference for the macrocell users.

We quantify the user performance in the macro network tier if the femtocells use OSA under the two channel assignment techniques. The performance metric for the macro users is the coverage probability in the downlink, which is defined as the probability that the signal-to-interference-plus-noise-ratio (SINR) exceeds the

threshold defined for correct signal reception. For the femtocells, I analyze the OSA probability for the two channel assignment techniques by the MBSs.

6.2 System Model and Assumption

6.2.1 Network Model

The MBSs are spatially distributed according to the homogeneous PPP $\mathbf{\Psi}_b = \{b_i; i = 1, 2, 3, \dots\}$ with intensity $\mathcal{B}$, where b_i is the location of the i^{th} MBS. Each MBS b is assumed to serve a random number of users (denoted by $\mathcal{N}_b$) with a mean directly proportional to its coverage range. It was shown in **Lemma 5.5.1** that if the macro users are assumed to be spatially distributed according to a homogenous PPP with intensity $\mathcal{U}_b$, the probability mass function (*pmf*) of the number of users served by a generic MBS b is given equation (5.4). The FAPs are spatially distributed according to an independent homogeneous PPP $\mathbf{\Psi}_a = \{a_i; i = 1, 2, 3, ...\}$ with intensity $\mathcal{A}$, where a_i denotes the location of the i^{th} FAP.

The access policy of the coexisting femtocells (i.e., open access and closed access) is independent of their locations, and a fraction p_c ($0 \leq p_c \leq 1$) of all the femtocells employ the closed access policy. Therefore, the closed access femtocells constitute a PPP with intensity $\mathcal{A}_c = p_c\mathcal{A}$, and the open access femtocells constitute a PPP with intensity $\mathcal{A}_o = (1 - p_c)\mathcal{A}$. It is assumed that all the femtocells are active and each of them has at least one associated user.

We assume that each user is associated to the base station (i.e., a MBS or a FAP) that provides the highest received signal strength (RSS) [58, 76] among all the MBSs and open access FAPs, and all other base stations using the same channel are considered as interference sources. Both the network tiers share the same set of

channels[1] $\mathbf{S}$. All MBSs transmit with the same power P_b, all FAPs transmit with the same power P_a, and a saturation condition is assumed for all the base stations for downlink transmission.

6.2.2 Radio Channel Model

A general power-law path loss model is considered. The signal power decays at the rate $r^{-\eta}$ with the propagation distance r, where η is the path-loss exponent. The channel (power) gains between a generic location $x \in \mathbb{R}^2$ and the MBS b_i and the FAP a_i are denoted by $h_{b_i}(x)$ and $h_{a_i}(x)$, respectively. All the channel gains are assumed to be independent from each other, independent from the spatial locations, and are identically distributed (i.i.d.). Hence, for the brevity of exposition, hereafter, the spatial index x is dropped. For analysis, only Rayleigh fading environment is assumed[2], hence, the channel gains h_{b_i} and h_{a_i} are exponentially distributed with means $\frac{1}{\mu_b}$ and $\frac{1}{\mu_a}$, respectively. A receiver is said to be covered if the SINR at the receiver is greater than a certain threshold β.

6.2.3 Channel Allocation in the Macro Tier

Both network tiers share the same set of available channels denoted by $\mathbf{S}$. We will denote by $\mathbf{S}_{b_i} \subseteq \mathbf{S}$ the set of channels selected by the MBS b_i for its associated users. In the RCA scheme, each MBS randomly and uniformly chooses a channel $s_j \in \mathbf{S}$ for each associated user such that no two users are assigned the same channel. Note that, since all channel gains are assumed to be i.i.d., there is no loss in generality if I assume a uniform distribution for the channel assignment. For instance, if the channels are assigned based on the channel gain realization and there is no preference from

[1] A channel can be, for example, one or multiple resource blocks (RB) in LTE-Advanced systems.
[2] Techniques to generalize the model for general fading environment are discussed in Sec. 2.3.

one channel to another, the channel selection in a generic time instant is uniformly distributed. For the SCA scheme, I assume that the channels have a specific order known to all MBSs in the network and each MBS assigns the channels to its associated users in a sequential manner (i.e., channel s_j is assigned before channel s_{j+1}).

6.2.4 Opportunistic Spectrum Access by femtocells

All of the FAPs are cognitive and access the channels opportunistically. That is, an FAP $a_i \in \mathbf{\Psi}_a$ accesses a channel $s_j \in \mathbf{S}$ if the received power from any MBS $b_k \in \mathbf{\Psi}_b$ at the FAP a_i is greater than the sensing threshold υ_s. Let $\mathbf{N}_{a_i} = \left\{b_j \mid P_b h_{b_j} \left\|a_i - b_j\right\|^{-\eta}\right\}$ denote the set of neighboring MBSs to the FAP a_i (i.e., the set of MBSs in which the transmit power of each of them received at a_i is greater that the sensing threshold υ_s), then the FAP a_i would not reuse any channel used by an MBS $b_j \in \mathbf{N}_{a_i}$.

The spectrum sensing threshold υ_s is a design parameter for the FAPs. Decreasing (increasing) υ_s increases (decreases) the sensitivity of the cognitive FAPs to the transmission from MBSs in the spatial domain and results in a low (high) cross-tier interference but conservative (aggressive) spatial frequency reuse. From a geometric perspective, υ_s defines a spectrum sensing region (SSR) around each FAP where no channel can be reused if it is used by an MBS within that region. Note that the spectrum sensing region is a random shaped region which is dynamically varying according to the channel gain realizations. Following **Lemma 5.5.2**, $|\mathbf{N}_a| \sim Poisson(\varphi_a)$, and $\varphi_a = \pi \mathcal{B} \left(\frac{P_b}{\mu_b \upsilon_s}\right)^{\frac{2}{\eta}} \Gamma(1 + \frac{2}{\eta})$, where $|.|$ denotes the set cardinality.

Note that a non-cognitive FAP can be considered as a special case of a cognitive FAP with $\mathbf{N}_a = \phi$. Perfect spectrum sensing is assumed for all FAPs. Each cognitive FAP uses all the channels that are not used by its neighbor MBSs. That is, let $\mathbf{S}_{a_i}$ be the set of channels used by the FAP a_i at a generic time instant, then, the set of

channels used by a generic FAP a_i is given by $\mathbf{S}_{a_i} = \mathbf{S} \setminus \left\{ \bigcup_{b_i \in \mathbf{N}_{a_i}} \mathbf{S}_{b_i} \right\}$.

6.3 Opportunistic Spectrum Access Probability for Cognitive FAPs

Since the FAPs are cognitive, the number of channels available for each FAP is a random variable with a mean proportional to the sensing threshold but inversely proportional to the mean number of users served by each MBS. This is because the lower the sensing threshold, the higher the number of neighbor MBSs which leads to a higher number of channels used by those MBSs. Furthermore, since each MBS assigns orthogonal channels for its associated users, the higher the number of users associated to the MBSs, the higher the number of channel used per MBS. In this section, I aim at deriving the distribution of the number of free channels for a generic FAP. For an FAP a_i, a free channel refers to a channel which is not used by any of the MBSs within the SSR of a_i (i.e., not used by an MBS $b_j \in \mathbf{N}_{a_i}$).

6.3.1 OSA Probability for the RCA Scheme

In the RCA scheme, each MBS randomly and uniformly chooses one channel for each of its associated users such that no two users associated to the same MBS are assigned the same channel. The number of channels used within the SSR of a generic FAP s is given by $K_u = \left| \bigcup_{b_i \in \mathbf{N}_s} \mathbf{S}_{b_i} \right|$. Note that $K_u \neq \sum_{b_i \in \mathbf{N}_a} |\mathbf{S}_{b_i}|$ because each MBS is independently choosing the channels for its associated users from the finite set of channels $\mathbf{S}$, and hence, ties may occur. The random variable K_u is not indexed by the spatial location of the test FAP because, by Slivnyak's theorem [6, 8], all FAPs will have the same distribution for the number of used channels within their SSRs.

The *pmf* of the number of channels used within the SSR of a generic FAP can be obtained from the following lemma:

Lemma 6.3.1. *Let* $|\mathbf{S}|$ *be the total number of available channels. Then, the* pmf *of the number of channels* K_u *used within the SSR of a generic FAP located at* $s \in \mathbb{R}^2$ *is given by:*

$$\mathbb{P}\{K_u = k\} = \mathbf{1}_{\{k=0\}}\mathbb{P}\{|\mathbf{N}_a| = 0\} + \sum_{n=1}^{\infty} \mathbb{P}\{|\mathbf{N}_a| = n\}\, \mathcal{P}_n(k), \quad 0 \leq k \leq |\mathbf{S}| \tag{6.1}$$

where $\mathcal{P}_n(k) = \sum_{t=0}^{k} \mathcal{P}_{n-1}(t) \sum_{p=k-t}^{k} \mathbb{P}\{\mathcal{N}_b = p\}\, \mathrm{Bi}\left(p, p-(k-t), \frac{t}{|\mathbf{S}|}\right)$, *where* $\mathrm{Bi}(x, y, z) = \binom{x}{y} (z)^y (1-z)^{(x-y)}$ *and* $\mathcal{P}_1(t) = \mathbb{P}\{\mathcal{N}_b = t\}$.

Proof. See **Appendix C**. □

Note that the *pmf* of K_u cannot be found in a closed form due to the high complexity introduced by the random number of ties (i.e., the probability that two MBSs choose the same channel). From **Lemma 6.3.1**, to calculate the probability that there are k channels used within the SSR of a generic FAP (i.e., $\mathbb{P}\{K_u = k\}$), all possible realizations of $|\mathbf{N}_a|$ in the SSR of the FAP should be considered and all the combinations and permutations that lead to the usage of k unique channels for every realized value of $\mathbf{N}_a$ should be accounted for. However, the probability that $K_u = k$ can still be obtained with an approximation error less than ϵ by terminating the summation in (6.1) at n_{max}, where n_{max} is chosen such that $\mathbb{P}\{|\mathbf{N}_a| \geq n_{max}\} \leq \epsilon$. The *pmf* of the number of free channels (K_f) within the SSR of a generic FAP is given by $\mathbb{P}\{K_f = k\} = \mathbb{P}\{K_u = |\mathbf{S}| - k\}$.

To obtain the interference statistics on a given channel, I calculate the intensity of network entities using that channel. The probability that a generic MBS accesses a certain channel depends on the distribution of the number of users associated to that

MBS. Hence, the probability that a generic MBS accesses a generic channel $s_k \in \mathbf{S}$ is given by

$$\begin{aligned}\kappa_b^{(k)} &= \mathbb{P}\left\{s_k \in \mathbf{S}_{b_i}\right\} \\ &= \sum_{n=1}^{|\mathbf{S}|} \frac{n}{|\mathbf{S}|} \mathbb{P}\left\{|\mathbf{S}_{b_i}| = n\right\} + \sum_{n=|\mathbf{S}|+1}^{\infty} \mathbb{P}\left\{|\mathbf{S}_{b_i}| = n\right\} \\ &= 1 - \sum_{n=0}^{|\mathbf{S}|} \left(1 - \frac{n}{|\mathbf{S}|}\right) \mathbb{P}\left\{|\mathbf{S}_{b_i}| = n\right\}. \end{aligned} \tag{6.2}$$

Note that, due to the orthogonal channel assignment for the users associated with each MBS, $|\mathbf{S}_{b_i}| \overset{(d)}{=} \mathcal{N}_b$, where $(\overset{(d)}{=})$ denotes the equality in distribution. Since each MBS independently chooses the set of channels for its operation, the MBSs using the same channel s_k form a PPP with intensity $\mathcal{B}_I = \kappa_b^{(k)}\mathcal{B}$. Equation (6.2) shows that all channels have the same probability for being used by all of the MBSs. Given that an MBS b_i is using channel s_k, I will consider the worst case scenario and assume that all non-neighbor FAPs $\{a_i \in \Psi_a : b_i \notin \mathbf{N}_{a_i}\}$ will be using that channel.

6.3.2 OSA Probability for the SCA Scheme

The SCA scheme is a distributed channel assignment scheme where the channels have a specific order known to all MBSs. In this scheme, each MBS assigns the channels to its users in a sequential manner (i.e., channel s_i is assigned before channel s_{i+1}), and hence, ties between assigned channels in different MBSs occur with probability one. Therefore, the number of channels used K_u within the SSR of a generic FAPs a_i is equal to the number of channels used by the MBS with the highest number of associated users $K_u = \max_j(\left|\mathbf{S}_{b_j}\right|)$, $\forall b_j \in \mathbf{N}_{a_i}$. Due to the simple relation between the number of used channels in the SSR of a test FAP and the number of channels used

by each MBS within that SSR, the distribution of the free channels within the SSR of a generic FAP can be obtained in a simple form. From **Lemma 5.5.3**, the *pmf* of K_u for a generic FAP in the SCA scheme is obtained by:

$$\begin{aligned}\mathbb{P}\left\{K_f = k\right\} &= e^{-\varphi_a\left(1-\sum_{t=0}^{|\mathbf{S}|-k}\mathbf{P}\{\mathcal{N}_b=t\}\right)\mathbf{1}_{\{k>0\}}} \\ &- \mathbf{1}_{\{k<|\mathbf{S}|\}}e^{-\varphi_a\left(1-\sum_{t=0}^{|\mathbf{S}|-k-1}\mathbf{P}\{\mathcal{N}_b=t\}\right)}, 0 \leq k \leq |\mathbf{S}|\,. \end{aligned} \tag{6.3}$$

Different from the RCA, the channel allocation in the SCA is deterministic and the probability of using a certain channel depends on the index of that channel. That is, the channels $s_1, s_2, .., s_n$ will be used with probability one by all MBSs having n or more associated users. Hence, the probability that a MBS is accessing a generic channel $s_k \in \mathbf{S}$ is given by

$$\kappa_b^{(k)} = 1 - \sum_{t=0}^{k-1}\mathbb{P}\left\{\mathcal{N}_b = t\right\}. \tag{6.4}$$

Hence, the MBS using the same channel $s_k \in \mathbf{S}$ is a PPP with intensity $\mathcal{B}_I = \kappa_b^{(k)}\mathcal{B}$. Equation (6.4) shows that each channel has a different probability to be accessed by the MBSs (i.e., $\kappa_b^{(i)} < \kappa_b^{(j)}$ for $i > j$). Hence, each channel has different intensities of MBSs using it and the interference statistics is a function of the channel index. For the FAPs, I will also consider the worst case scenario as in Sec. 6.3.1.

6.4 Coverage Probability for the Macro Users

In this section, I derive the coverage probability of a generic macro user for each channel assignment scheme. Note that for the SCA scheme, since the interference statistics varies with the channels index, I will calculate the coverage probability on the channel with the lowest index to insure that the channel with highest interference

satisfies the performance guarantee. A generic macro user $u \in \mathbb{R}^2$ will be covered on a given channel if the SINR on that channel is above the threshold β. Let r_b be the random distance between a generic macro user and his serving MBS, then the user coverage probability can be given by:

$$\begin{aligned}\mathbb{P}\left\{\text{SINR} > \beta\right\} &= \mathbb{P}\left\{\frac{P_b h_b r_b^{-\eta}}{\sigma^2 + \mathcal{I}_{mm} + \mathcal{I}_{cm} + \mathcal{I}_{om}} > \beta\right\} \\ &= \mathbb{P}\left\{h_b > \frac{\beta r_b^{\eta}}{P_b}\left(\sigma^2 + \mathcal{I}_{mm} + \mathcal{I}_{cm} + \mathcal{I}_{om}\right)\right\} \\ &\overset{(i)}{=} \int_0^{\infty} 2\pi r \mathcal{B} e^{-\pi\mathcal{B}r^2 - \frac{\sigma^2 \mu_b \beta r^{\eta}}{P_a}} \mathcal{L}_{\mathcal{I}_{mm}}\left(\frac{\beta\mu_b r^{\eta}}{P_b}\right) \\ &\qquad \mathcal{L}_{\mathcal{I}_{om}}\left(\frac{\beta\mu_b r^{\eta}}{P_b}\right) \mathcal{L}_{\mathcal{I}_{cm}}\left(\frac{\beta\mu_b r^{\eta}}{P_b}\right) dr \end{aligned} \tag{6.5}$$

where $\mathcal{L}_X(.)$ denotes the Laplace transform of the *pdf* of the random variable X, $\mathcal{I}_{mm}$, $\mathcal{I}_{om}$, and $\mathcal{I}_{cm}$ are the random variables denoting the aggregate interference from the MBSs, the open access FAPs, and the closed access FAPs, respectively. Note that (i) follows from the exponential distribution of h_b, the definition of the Laplace transform, and integrating over the *pdf* of r_b, $f_{r_b}(r) = 2\pi\mathcal{B}re^{-\pi\mathcal{B}r^2}$, $r \geq 0$ [12, 54, 58, 76]. The Laplace transform of the aggregate interference for each point process can be obtained from **Lemma 5.6.1**. For $\eta = 4$, **Lemma 5.6.1** reduces to (see **Appendix B.5**)

$$\mathcal{L}_I(t) = e^{-\pi\lambda\sqrt{\frac{Pt}{\mu}}\arctan\left(\frac{\sqrt{\frac{Pt}{\mu}}}{r_e^2}\right)}. \tag{6.6}$$

For non-cognitive closed-access FAPs, there is no exclusion distance (i.e., $r_e = 0$) and the Laplace transform of the *pdf* of the aggregate interference is obtained in the form

$$\mathcal{L}_{\mathcal{I}_{cm}}\left(\frac{\beta\mu_b r^{\eta}}{P_b}\right) = e^{-\frac{\pi^2}{2}\mathcal{A}_c r^2\sqrt{\frac{\beta P_a \mu_b}{P_b \mu_a}}}. \tag{6.7}$$

For non-cognitive open-access FAPs, based of the association criterion, there should

not be an interferer closer than $r_e = \left(\frac{P_a \mu_b}{P_b \mu_a}\right)^{\frac{1}{\eta}} r_b$ [58,76]. Hence, the Laplace transform of the *pdf* of the aggregate interference is obtained in the form

$$\mathcal{L}_{\mathcal{I}_{om}}\left(\frac{\beta \mu_b r^\eta}{P_b}\right) = e^{-\pi \mathcal{A}_o r^2 \sqrt{\frac{\beta P_a \mu_b}{P_b \mu_a}} \arctan\left(\sqrt{\beta}\right)}. \tag{6.8}$$

For MBSs, based of the association criterion, there should not be an interferer closer than $r_e = r_b$. Hence, the Laplace transform of the *pdf* of the aggregate interference is obtained in the form

$$\mathcal{L}_{\mathcal{I}_{mm}}\left(\frac{\beta \mu_b r^\eta}{P_b}\right) = e^{-\pi \mathcal{B}_I r^2 \sqrt{\beta} \arctan\left(\sqrt{\beta}\right)}. \tag{6.9}$$

where $\mathcal{B}_I = \kappa_b^{(k)} \mathcal{B}$ is obtained based on the channel assignment scheme. For cognitive FAPs (both closed access and open access), on average the exclusion region around a generic macro user is calculated as $r_e = \left(\frac{P_b}{\mu_b \upsilon_s}\right)^{\frac{1}{\eta}} - r_b$, and hence, the Laplace transform of the *pdf* of the aggregate interference from the entire set of FAPs is obtained in the form

$$\mathcal{L}_{\mathcal{I}_{sm}}\left(\frac{\beta \mu_b r^\eta}{P_b}\right) = e^{-\pi \mathcal{A} r^2 \sqrt{\frac{\beta P_a \mu_b}{P_b \mu_a}} \arctan\left(\frac{r^2 \sqrt{\frac{\beta P_a \mu_b}{P_b \mu_a}}}{\sqrt{\frac{P_b}{\mu_b \upsilon_s}} - r}\right)}. \tag{6.10}$$

Substituting back in (6.5), for interference-limited networks (i.e., ignoring noise), the coverage probability for a generic macro user with non-cognitive FAPs is given by:

$$\begin{aligned}\mathbb{P}\left\{\text{SINR} > \beta\right\} = \mathcal{B}\Bigg(\mathcal{B} + \frac{\pi}{2}\mathcal{A}_c \sqrt{\frac{\beta P_a \mu_b}{P_b \mu_a}} + \\ \mathcal{A}_o \sqrt{\frac{\beta P_a \mu_b}{P_b \mu_a}} \arctan\left(\sqrt{\beta}\right) + \mathcal{B}_I \sqrt{\beta} \arctan\left(\sqrt{\beta}\right)\Bigg)^{-1}\end{aligned} \tag{6.11}$$

and the coverage probability for a generic macro user with cognitive FAPs is given

by:

$$\mathbb{P}\left\{\text{SINR} > \beta\right\} = \int_0^\infty 2\pi r\mathcal{B} \exp\Big\{-\pi\mathcal{B}r^2 - \pi\mathcal{B}_I r^2\sqrt{\beta} \arctan\left(\sqrt{\beta}\right) - \pi\mathcal{A}r^2\sqrt{\frac{\beta P_a \mu_b}{P_b \mu_a}} \arctan\left(\frac{r^2\sqrt{\frac{\beta P_a \mu_b}{P_b \mu_a}}}{\sqrt{\frac{P_b}{\mu_b \upsilon_a}} - r}\right)\Big\} dr. \tag{6.12}$$

6.5 Numerical Results and Discussions

6.5.1 Numerical Results

For the numerical evaluations (using Matlab), I choose $P_b = 5$ W, $P_a = 20$ dBm, $\mathcal{B} = 1$ MBS/km^2, $\mathcal{A} = 25$ FAP/km^2, $\lambda_b = 10$ macro user/km^2, $p_c = 0.5$, $|\mathbf{S}| = 30$ channels, all the channel gains to have unit mean (i.e., $\frac{1}{\mu_a} = \frac{1}{\mu_b} = 1$), $\epsilon = 10^{-10}$, and $\eta = 4$. The effect of noise is ignored (i.e., the network is interference-limited) [54].

Fig. 6.1 shows the coverage probability of a generic macro user vs. spectrum sensing threshold υ_s and the SINR threshold β. The figure demonstrates the performance gain due to OSA by the femtocells. When the FAPs are not cognitive, the interference from the femtocells dominates and the two channel assignment techniques in the MBSs have approximately similar performance. On the other hand, when the FAPs are cognitive, the intra-tier interference is the performance limiting factor and the RCA technique always outperforms the SCA technique. Fig. 6.1(a) shows that there is a critical sensing threshold value (-90 dBm in my case) after which the coverage probability saturates. On the other hand, when the sensing threshold is too high, the FAPs become aggressive in accessing the spectrum and match the performance of the non-cognitive FAPs.

Fig. 6.2 shows that independent random channel assignment highly degrades the OSA probability for the FAPs. Fig. 6.2(a) shows the *pmf* of K_f for a generic FAP

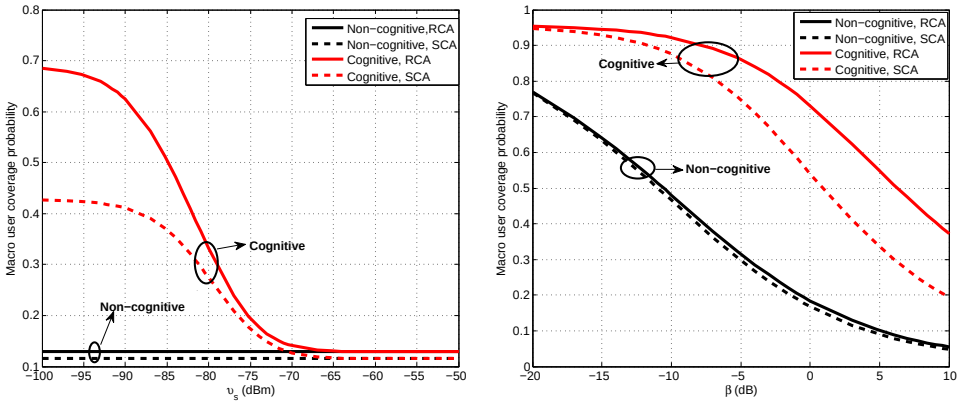

(a) (b)

Figure 6.1: (a) Macro user coverage probability vs. spectrum sensing threshold (υ_s) at $\beta = 0$ dB, (b) Macro user coverage probability vs. SINR threshold defined for correct reception (β) at ($\upsilon_s = -90$ dBm).

at $\upsilon_s = -90$ dBm. The figure shows that if the MBSs are using RCA, a generic FAP will not find any channel to access with probability 31%. The figure also shows that the probability that a generic FAP accesses a higher number of channels under the SCA scheme is quite larger than that of the RCA scheme. Fig. 6.2(b) shows the probability that $K_f \geq n$ vs. the sensing threshold υ_s for different values of n. Note that $n = 1$ shows the OSA probability for the FAPs. The figure shows that the sensitivity of the OSA probability to the sensing threshold under the RCA scheme is much higher than under the SCA scheme. Moreover, it shows that the SCA scheme offers much higher OSA probability compared to that by the RCA scheme.

6.5.2 Discussions

The developed model, for the two extremes of the channel assignment techniques, is capable of capturing the effect of tradeoffs offered by splitting the spectrum into two subsets $\mathbf{S}_r$ and $\mathbf{S}_s$. The subset of channels $\mathbf{S}_r$ will be assigned by the MBSs based

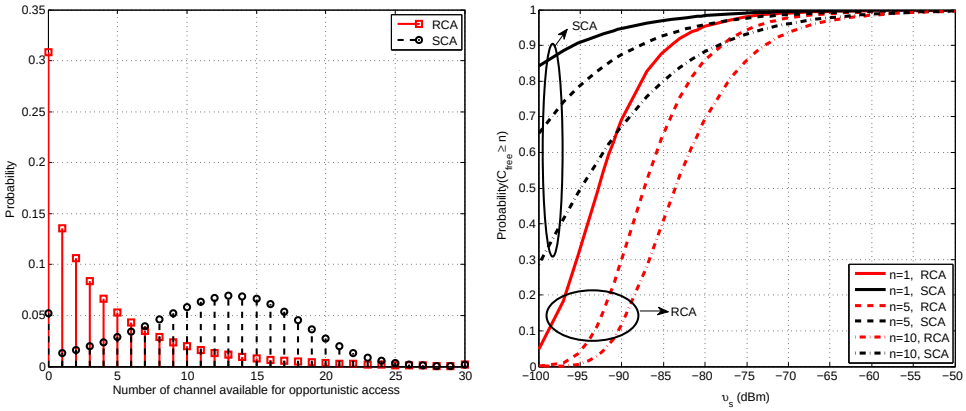

(a) (b)

Figure 6.2: (a) The *pmf* of the number of available channels for OSA for a generic FAP at ($\upsilon_s = -90$ dBm), (b) The probability of having n or more available channels for OSA by generic FAP (i.e., $\mathbb{P}\{K_f \geq n\}$) at ($\upsilon_s = -90$ dBm).

on the CQI to exploit the multiuser diversity, while the subset of channels $\mathbf{S}_s$ will be assigned using the SCA if the MBSs has consumed all the channels in $\mathbf{S}_r$. Optimal splitting of the channels will insure that lightly loaded MBSs (i.e., $|\mathcal{N}_b| < |\mathbf{S}_s|$) avoid massive intra-tier interference while achieving an acceptable OSA performance for the FAPs. In that case, the lightly loaded MBSs will constitute a PPP with intensity $\mathbb{P}\{|\mathcal{N}_b| < |\mathbf{S}_s|\}\mathcal{B}$ and the corresponding analysis will follow the RCA scheme. On the other hand, heavily loaded MBSs will constitute an independent PPP with intensity $(1 - \mathbb{P}\{|\mathcal{N}_b| < |\mathbf{S}_s|\})\mathcal{B}$ and the analysis will follow the SCA scheme. Note that the total interference for a generic user will be the summation of the aggregate interference from the two PPPs.

The load served by the macro tier has a significant effect on the OSA of the FAP. That is, the higher the user population served by the MBSs, the higher the number of channels used by the MBSs which deteriorate the OSA performance of the femtocells. Therefore, offloading users to the FAPs [58, 76] is a potential solution to enhance the

OSA performance of femtocells.

6.6 Chapter Summary

We have used stochastic geometry tools to develop a paradigm that captures the effect of two channel assignment techniques at the macro tier on both the macro users' coverage probability and the opportunistic spectrum access performance of cognitive femtocells. The results have shown that, although the coverage probability of the macro users is always higher under random channel assignment at the macro tier, conservative channel assignment techniques can enhance the spectrum access performance of the femtocells.

To this end, I have applied stochastic geometry analysis for downlink cellular networks. The next chapter presents the stochastic geometry analysis for the uplink case.

Chapter 7

Uplink Transmissions in Multi-tier Cellular Networks

In this chapter, I exploit tools from stochastic geometry to develop a tractable uplink model for multi-tier cellular wireless networks with truncated channel inversion power control. The analysis accounts for per user equipment (UE) power control as well as the maximum power limitations for UEs. My model gives simple expressions for the outage probability and spectral efficiency which characterize the network performance in terms of the design parameters. In particular, the model reveals a transfer point in the uplink system behavior that depends on the tuple: BS intensity (λ), maximum transmit power of UEs (P_u), and power control cutoff threshold ρ_o. More specifically, when P_u is a tight operational constraint with respect to [w.r.t.] λ and ρ_o, the uplink performance highly depends on the values of λ and ρ_o. In contrast, when P_u is a non-binding operational constraint w.r.t. λ and ρ_o, the uplink performance becomes independent of λ and ρ_o.

7.1 Introduction

There have been significant developments in the stochastic geometry modeling of cellular wireless networks. However, most of the available literature focuses on modeling and analysis of downlink transmissions due to its relative simplicity. As shown in Chapter 5, in a multi-tier cellular network, if the users associate to the BSs in the downlink based on their average received signal strength, the average useful signal power received at each user equipment (UE) from its corresponding BS will be strictly greater than the average interference power from any individual interfering BS. Therefore, power control is not crucial[1] for the network operation, and hence, power control is ignored in most of the stochastic geometry models on downlink cellular networks and it is generally assumed that all the BSs in the same tier transmit with equal power [5,12,54,63,65,67,74–77]. In contrast, uplink analysis is quite more involved due to the following reasons:

- **Per user power control:** in the uplink, due to the random cell sizes, an interfering UE in a neighboring cell can be much closer to a BS than its tagged UE (cf. Fig. 7.1). Therefore, power control per UE is crucial for basic uplink operation in order to mitigate the inter-cell interference. As will be shown later, per UE power control introduces a new source of randomness to the uplink system model which makes the uplink analysis more involved.

- **Correlation among interferers:** orthogonal channel assignment per BS ensures no channel reuse in the same Voronoi cell. That is, given that a UE is transmitting in the uplink on a certain channel, this channel cannot be reused

[1]Indeed power control is important in downlink to enhance the network performance (see [120]) but not crucial for the basic network operation due to the inherent interference protection introduced by the association criterion.

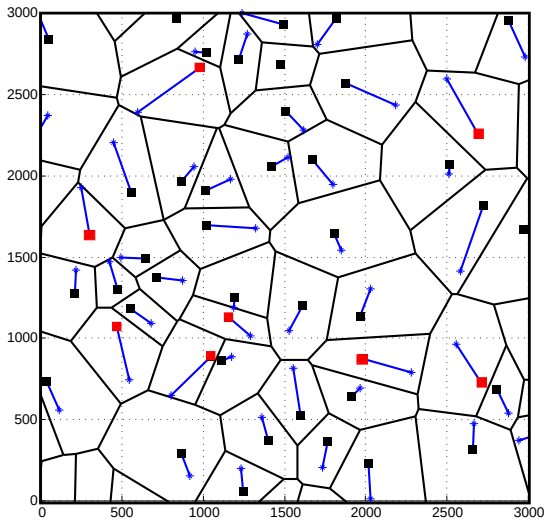

Figure 7.1: Uplink network model representing the UEs served per channel, where the BSs are represented by squares, the UEs are represented by stars, and the lines denote the UEs' association. BSs having an interfering UE closer than their tagged UE are highlighted in red.

within the coverage of its serving BS, and hence, the locations of the UEs using the same uplink channel are correlated.

7.1.1 Related Work

Compared to the downlink, only few efforts were invested to understand and model the uplink transmissions in cellular networks. Uplink modeling has been done in an ad hoc manner where different works in the literature made different assumptions based on the problem in hand. For instance, [69] derived the uplink network capacity region for a two-tier cellular network consisting of macro BSs (MBSs) modeled via the hexagonal grid, femto access points (FAPs) modeled via PPP, and UEs modeled via an independent PPP. Due to the small coverage radius of the FAPs, in [69], the interference seen from all uplink UEs associated with the same FAP was approximated by an isotropic point source of interference with the worst-case sum transmit powers

of the FAP UEs (i.e., power control was ignored). [68] investigated the spectrum sharing between a cellular network uplink and a mobile ad hoc network. In [68], the service areas of all BSs were approximated by circles and power control was ignored. Note that the assumption of circular coverage areas for the BSs eliminates the aforementioned interference problem in the uplink where an interfering UE can be much closer to a BS than the tagged UE which communicates to that BS. Therefore, under the assumption of circular coverage area, power control can be ignored.

In [121], the authors modeled uplink transmission with fractional channel inversion power control in a single-tier cellular network. However, for analytical tractability and to avoid the singularity at the origin imposed by the unbounded path-loss model [5], the authors in [121] approximated the entire network model and assumed that the Voronoi cells are divided w.r.t. the users (rather than with respect to (w.r.t.) the BSs) and each user has her own serving BS randomly located in her Voronoi cell. In [122], the authors modeled uplink UEs with channel inversion power control. However, the authors assumed that the tagged UE is uniformly distributed in the tagged BS's coverage which is approximated by a circle having the radius $\frac{1}{\sqrt{\pi\lambda}}$, where λ is the BS intensity[2]. Each of the available stochastic geometry models [68, 69, 121, 122] approximates the system model in a different way to simplify the analysis and none of them accounts for the maximum transmit power of the UEs.

7.1.2 Motivation and Contribution

Motivated by the lack of any rigorous model that characterizes the uplink transmission in cellular networks, I present a tractable model for uplink analysis to help understand uplink system performance in both single and multi-tier cellular networks. The

[2]More discussions on the work presented in [121, 122] will be provided in Sec. 7.5.

proposed model accounts for the maximum transmit power of the UEs. We aim at providing a unified uplink modeling framework for multi-tier cellular networks to fill in the gap between the well-understood downlink performance and the lagging uplink analysis. For an organized exposition, I first develop the baseline uplink paradigm for a single-tier cellular network. Then, I show that the developed single-tier uplink analysis is flexible and can be easily generalized to multi-tier cellular networks.

The contributions of this work can be summarized in the following points:

- We present a tractable framework for uplink modeling and analysis in a Poisson cellular network. The model is general and extends to multi-tier cellular networks. The model accounts for limited transmit power of the UEs, per UE power control, and cutoff threshold for the power control.

- Simple closed-form equations are derived for the outage probability and simple forms with only one numerical integral are derived for the spectral efficiency.

- We discuss the tradeoffs introduced by the cutoff threshold and the maximum transmit power and show that there exists an optimal cutoff threshold for the power control that minimizes the outage probability and power consumption (i.e., transmit power) of the UEs.

- We characterize the uplink performance and show the commonalities and differences between the downlink and uplink performances in cellular networks. In particular, I show the existence of a transfer point in the uplink system performance which depends on the tuple (λ, P_u, ρ_o), where λ is the BS intensity, P_u is the maximum transmit power of a UE, and ρ_o is the average received power required at the serving BS. That is, when the relative values of λ, P_u, and ρ_o lead to a binding maximum transmit power constraint for the uplink operation,

the uplink operation is quite different from the downlink operation and depends on both the cutoff threshold and the BS intensity. In contrast, when the relative values of λ, P_u, and ρ_o lead to a non-binding maximum transmit power constraint for the uplink operation (i.e., transmissions are not constrained by the maximum transmit power), the uplink operation becomes analogous to the downlink operation (i.e., becomes independent of the BS intensity and cutoff threshold).

7.2 System Model and Assumptions

7.2.1 Network Model

We consider an independent K-tier Poisson cellular network. That is, the BSs of each tier are spatially distributed in $\mathbb{R}^2$ according to an independent homogenous PPP $\mathbf{\Psi}_k = \{b_i; i = 1, 2, 3, ...\}$, $k \in \{1, 2, 3, ..., K\}$ with intensity λ_k, where $b_i \in \mathbf{\Psi}_k$ is the location of the i^{th} BS in the k^{th} tier. The users' equipments (UEs) are spatially distributed in $\mathbb{R}^2$ according to an independent PPP $\mathbf{\Phi} = \{u_i; i = 1, 2, 3, ...\}$ with intensity $\mathcal{U}$. It is assumed that the intensity of the UEs is high enough such that each BS will have at least one user served per channel and that UEs have data to transmit in the uplink (i.e., saturation conditions are assumed). The BSs in each tier k have equal receiver sensitivity $\rho_{min}^{(k)}$, however, two BSs from different tiers do not necessarily have the same receiver sensitivity. For successful uplink communication, it is required that the received signal power at the BS is greater than the receiver sensitivity. Therefore, each of the UEs associated to tier k controls its transmit power such that the average signal received at the corresponding serving BS is equal to the threshold $\rho_o^{(k)}$, where $\rho_o^{(k)} > \rho_{min}^{(k)}$.

It is assumed that all the UEs have the same maximum transmit power of P_u. Due to the maximum transmit power constraint P_u, for uplink communications, the UEs use truncated channel inversion power control where the transmitters compensate for the path-loss to keep the average received signal power equal to the threshold $\rho_o^{(k)}$ [91, Chapter 4]. That is, an uplink connection is established between a UE and its serving BS if and only if the transmit power required for the path-loss inversion is less than P_u. Otherwise, the UE does not transmit and goes into an outage (denoted hereafter as *truncation outage*) due to the insufficient transmit power.

It is worth mentioning that the truncated channel inversion power control mechanism is a realistic power control scheme for code-division multiple access (CDMA) networks to eliminate the near-far effect. Moreover, for orthogonal frequency-division multiple access (OFDMA) networks, it has been shown in [123] that if the edge users (i.e., users with insufficient power to compensate for their channel inversions) are allowed to transmit with their maximum power, the interference in the system increases significantly. Consequently, the entire network performance is deteriorated without much improvement in the cell edge user performance. Hence, in this chapter I consider the truncated channel inversion power control with the cutoff threshold $\rho_o^{(k)}$, where the cutoff threshold $\rho_o^{(k)}$ is a network design parameter that highly impacts the system behavior. As will be shown later, the relative values of the BS intensity, P_u, and $\rho_o^{(k)}$ control the tradeoff between transmit power efficiency, signal-to-interference-plus-noise-ratio (SINR), and truncation outage (i.e., outage due to insufficient transmit power).

Fig. 7.2 shows the network model for different values of ρ_o for a single-tier cellular network. As shown in Fig. 7.2(a) if the value of ρ_o is relatively high (i.e., relative to λ and P_u), not all the UEs can compensate for the path-loss inversion and the cell

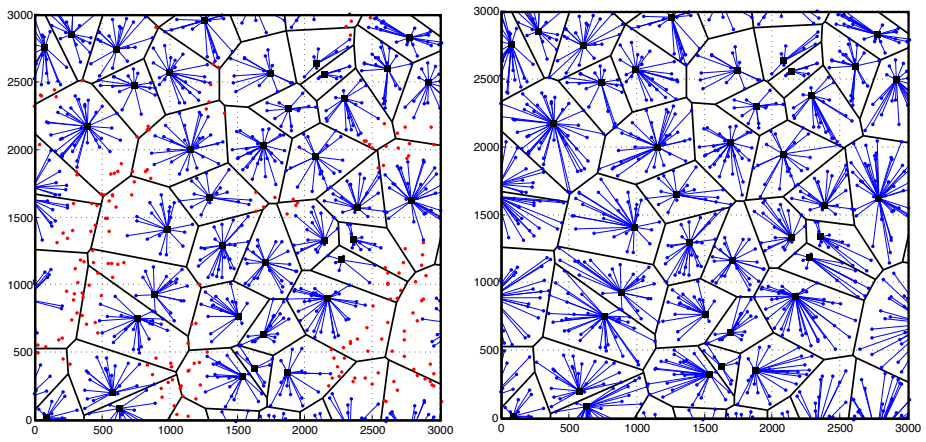

(a) (b)

Figure 7.2: Network model showing the served users on all channels in $[0, 3000]^2$ m^2; the black squares represent the BSs, the blue dots represent the active UEs, the blue lines denote the UEs' associations, and the red dots are the inactive UEs due to the insufficient transmit power. The simulation parameters are $\lambda = 5$ BS/km^2, $\mathcal{U} = 100$ UE/km^2, and (a) $\rho_o = -70$ dBm, (b) $\rho_o = -90$ dBm.

edge UEs suffer from *truncation outage*. In contrast, Fig. 7.2(b) shows that if the value of ρ_o is relatively low (or equivalently, the BSs are dense enough and/or the maximum transmit power is high enough), all of the UEs can compensate for the path-loss inversion and none of the UEs suffers from truncation outage. Hereafter, I will denote the scenario in Fig. 7.2(a) as the uplink operation under binding maximum transmit power constraint and the scenario in Fig. 7.2(b) as the uplink operation under non-binding maximum transmit power constraint. Universal frequency reuse is used within each tier and across different tiers. Within a network tier, there is no intra-cell interference. That is, in a network tier, each BS assigns a unique channel to each of its associated UEs.

7.2.2 Radio Channel Model

A general power-law path-loss model is considered in which the signal power decays at the rate $r^{-\eta}$ with the propagation distance r, where η is the path-loss exponent. For simplicity, it is assumed that all BSs in all tiers share the same path-loss exponent η. The case where each network tier has its own path-loss exponent η_k will be discussed in Sec. 7.4. The channel (power) gain between two generic locations $x, y \in \mathbb{R}^2$ is denoted by $h(x, y)$. All the channel gains are assumed to be independent of each other, independent of the spatial locations, symmetric, and are identically distributed (i.i.d.). Therefore, for the brevity of exposition, hereafter, the spatial indices x, y are dropped. For analysis, only Rayleigh fading (i.e., technique #1 in Sec. 2.3) environment is assumed[3], hence, the channel power gain h is assumed to be exponentially distributed with unit mean. An SINR model is considered where a message can be successfully decoded at the tagged BS in tier k if and only if the SINR of the useful signal is greater than a certain threshold β_k. If the SINR at the tagged BS does not exceed the threshold β_k, the link experiences an outage (hereafter referred to as SINR *outage*).

7.2.3 Criterion for Uplink Association

Without loss of generality, all BSs in all tiers are assumed to have an open access policy[4], and hence, all UEs can associate with all BSs. The UEs are assumed to associate to the BSs according to their average link quality. That is, a generic UE u associates with its nearest BS (i.e., b_i if $\|u - b_i\| < \min_{m_j \in \{\mathbf{\Psi}_k \setminus b_i\}} \|u - m_j\|$, $\forall k$), where $\|.\|$ denotes the Euclidean norm. It is worth mentioning that, in a multi-tier network, due to the heterogeneous transmit powers of the BSs in different network tiers, the

[3]Techniques to relax the Rayleigh fading assumption to general fading channels is discussed in Sec. 2.3.

[4]Closed access policy can be easily captured by thinning the PPP representing the complete set of BSs in the association analysis and simple modifications in the interference analysis [77].

downlink association regions of the BSs form a *weighted Voronoi* tessellation [54, 76]. In contrast, in the uplink, the homogenous transmit powers of the UEs result in association regions in the form of a *Voronoi* tessellation. Therefore, the uplink association is different from the downlink association in multi-tier cellular networks [124]. That is, the UE might not be associated to the same BS in the uplink and the downlink. Note that the LTE-A standard defines the coordinated multi-point (COMP) transmission to allow flexible and different uplink and downlink association [125, Chapter 13].

7.2.4 Modeling Methodology

The SINR is a very important parameter in wireless networks that affects many performance metrics such as outage, rate, delay, and energy efficiency. We characterize the SINR by driving its cumulative distribution function (*cdf*) [5]. Due to the randomized network topology, the distances between the UEs and their serving BSs are random. Therefore, the transmit powers of the UEs are random (due to the truncated channel inversion power control).

We will first characterize the transmit power of active UEs (i.e., users not in truncation outage) by deriving its probability density function (*pdf*) and moments. Then, I derive the *cdf* of SINR. We first develop the modeling paradigm for single-tier cellular networks. Then, I show that the developed modeling paradigm for single-tier cellular networks can be naturally extended to multi-tier networks.

7.3 Uplink Modeling in a Single-tier Cellular Network

In this section, I develop the baseline uplink modeling framework for a single-tier cellular network. For the sake of an organized presentation, I further divide this

section into two subsections, namely, transmit power analysis and SINR analysis.

7.3.1 Transmit Power Analysis

Due to the random network topology and the use of truncated channel inversion power control, each UE will transmit with a different power to invert the path-loss towards its serving BS. In this section, I derive the distribution and the moments of the transmit power of a generic UE. Fig. 7.2 shows the uplink association for a single-tier cellular network for different values of the cutoff threshold ρ_o. As shown in Fig. 7.2(a), due to the truncated channel inversion power control, not all of the UEs can communicate in the uplink when the cutoff threshold is relatively high (i.e., relative to P_u and λ). That is, the UEs located at a distance greater than $\left(\frac{P_u}{\rho_o}\right)^{\frac{1}{\eta}}$ from their nearest BS are unable to communicate in the uplink due the insufficient transmit power. Therefore, the complete set of UEs is divided into two non-overlapping subsets, namely, the subset of *active* UEs and the subset of *inactive* UEs. The inactive UEs do not transmit and experience outage due to insufficient transmit power. The distribution for the transmit power of a generic active UE is obtained from the following lemma.

Lemma 7.3.1. *In a single-tier Poisson cellular network with truncated channel inversion power control with the cutoff threshold ρ_o, the* pdf *of the transmit power of a generic active UE in the uplink is given by*

$$f_P(x) = \frac{2\pi\lambda x^{\frac{2}{\eta}-1} e^{-\pi\lambda\left(\frac{x}{\rho_o}\right)^{\frac{2}{\eta}}}}{\eta\rho_o^{\frac{2}{\eta}}\left(1-e^{-\pi\lambda\left(\frac{P_u}{\rho_o}\right)^{\frac{2}{\eta}}}\right)}, 0 \leq x \leq P_u.$$

The moments of the transmit power can be obtained as

$$\mathbb{E}\left[P^{\alpha}\right] = \frac{\rho_o^{\alpha}\gamma\left(\frac{\alpha\eta}{2}+1, \pi\lambda\left(\frac{P_u}{\rho_o}\right)^{\frac{2}{\eta}}\right)}{(\pi\lambda)^{\frac{\alpha\eta}{2}}\left(1-e^{-\pi\lambda\left(\frac{P_u}{\rho_o}\right)^{\frac{2}{\eta}}}\right)} \tag{7.1}$$

where $\gamma(a,b) = \int_0^b t^{a-1}e^{-t}dt$ *is the lower incomplete gamma function.*

Proof. See **Appendix D.1**. □

Lemma 7.3.1 shows that the smaller the cutoff threshold ρ_o, the lower the power consumption (i.e., transmit power) of the UEs. That is, when the maximum transmit power is unlimited (i.e., $\lim_{P_u\to\infty}\mathbb{E}\left[P^{\alpha}\right] = \frac{\rho_o^{\alpha}\Gamma\left(\frac{\alpha\eta}{2}+1\right)}{(\pi\lambda)^{\frac{\alpha\eta}{2}}}$, where $\Gamma(.)$ is the gamma function), the expected transmit power linearly increases with ρ_o. This is because as ρ_o increases the UEs are required to transmit at a higher power which increases the power consumption in the UEs. **Lemma 7.3.1** also shows that the average transmit power decreases with λ. That is, as the BS intensity increases, the distance between a generic UE and the corresponding serving BS decreases, and hence, a lower transmit power is required to invert the path-loss. The truncation outage probability (i.e., the probability that a UE experiences outage due to the insufficient power) is given by

$$\mathcal{O}_p = e^{-\pi\lambda\left(\frac{P_u}{\rho_o}\right)^{\frac{2}{\eta}}} \tag{7.2}$$

which is decreasing in ρ_o. From **Lemma 7.3.1** and equation (7.2) it appears that the lower the cutoff threshold, the better is the network performance in terms of truncation outage probability and power consumption. However, as will be discussed later, a low ρ_o may highly deteriorate the SINR outage and spectral efficiency, and hence, ρ_o introduces a tradeoff for the network performance. Equation (7.2) shows

that the truncation outage probability exponentially decreases with increasing BS intensity.

7.3.2 SINR *Analysis*

In this section I derive the SINR *outage* probability for active UEs (i.e., users not in truncation outage). Note that the inactive UEs do not transmit any power and are in truncation outage due to the insufficient transmit power. Without any loss in generality, the SINR analysis is conducted on a tagged BS located at the origin. According to Slivnyak's theorem [8], conditioning on having a BS at the origin does not change the statistical properties of the coexisting PPPs. Hence, the analysis holds for a generic BS located at a generic location. For the tagged active UE operating on a tagged channel, the SINR experienced at the BS located at the origin can be written as

$$\mathrm{SINR} = \frac{\rho_o h_o}{\sigma^2 + \underbrace{\sum_{u_i \in \tilde{\mathbf{\Phi}}} P_i h_i \left\| u_i \right\|^{-\eta_d}}_{\mathcal{I}}} \tag{7.3}$$

where the useful signal power is equal to $\rho_o h_o$ due to the truncated channel inversion power control, σ^2 is the noise power, and the random variable $\mathcal{I}$ denotes the aggregate interference at the tagged BS from the uplink transmissions by other active UEs on the tagged channel. Note that $\mathcal{I}$ is not identified with the channel index because all channels have i.i.d. interference. The SINR outage probability can be calculated as

$$\begin{aligned} \mathbb{P}\left\{\mathrm{SINR} \leq \beta\right\} &= \mathbb{P}\left\{\rho_o h_o \leq \beta\left(\sigma^2 + \mathcal{I}\right)\right\} \\ &= \mathbb{E}\left[1 - \exp\left\{-\frac{\beta}{\rho_o}\left(\sigma^2 + \mathcal{I}\right)\right\}\right] \\ &= 1 - \exp\left\{-\frac{\beta}{\rho_o}\sigma^2\right\} \mathcal{L}_{\mathcal{I}}\left(\frac{\beta}{\rho_o}\right) \end{aligned} \tag{7.4}$$

where the expectation in the second line of (7.4) is w.r.t. $\mathcal{I}$, and $\mathcal{L}_{\mathcal{I}}(.)$ denotes the Laplace transform (LT) of the *pdf* of the random variable $\mathcal{I}$[5].

As discussed in Sec. 7.1, in the uplink, the interfering UEs do not constitute a PPP due to the correlations among them. The correlation among the UEs is due to the unique channel assignment per user in each BS. Hence, the interfering UEs are better modeled using a Strauss processes (i.e., soft-core processes) to capture the pairwise correlations among the locations of the active UEs per channel. Unfortunately, Strauss processes are not analytically tractable [5, 8], and hence, an exact expression for the LT of the aggregate interference cannot be obtained. For this reason, I will approximate the locations of the interfering UEs with a PPP of the same intensity. Note that this approximation only partially ignores the correlations introduced by the system model because the correlation with the tagged BS and the tagged UE is captured by the model. It is worth mentioning that the PPP assumption for the interference sources has been widely exploited in the literature (even with the hard core point processes which introduce stronger pairwise correlation between points) and has been proved to be accurate if the correlation among the interfering nodes and the tagged receiver is captured [40, 45, 49, 121, 122]. The accuracy of this assumption is also validated in this results section via simulations. Exploiting the PPP approximation for the set of interfering UEs in the uplink, the outage probability for a generic active UE can be given by the following theorem.

Theorem 7.3.1. *In a single-tier Poisson cellular network with truncated channel inversion power control with the cutoff threshold ρ_o, in the uplink, the* SINR *outage*

[5]With a slight abuse of terminology, I will denote the LT of the *pdf* of a random variable X by the LT of X.

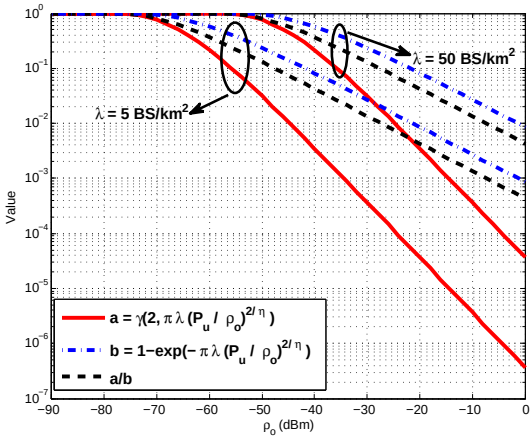

Figure 7.3: The behavior of $\frac{\gamma(2,\pi\lambda\left(\frac{P_u}{\rho_o}\right)^{\frac{2}{\eta}})}{\left(1-\exp(-\pi\lambda\left(\frac{P_u}{\rho_o}\right)^{\frac{2}{\eta}})\right)}$ for $P_u = 1$ and $\eta = 4$.

probability for a generic active UE is given by

$$\mathcal{O}_s = 1 - \exp\left\{-\frac{\beta\sigma^2}{\rho_o} - \frac{2\beta^{\frac{2}{\eta}}\gamma\left(2, \pi\lambda\left(\frac{P_u}{\rho_o}\right)^{\frac{2}{\eta}}\right)}{\left(1 - e^{-\pi\lambda\left(\frac{P_u}{\rho_o}\right)^{\frac{2}{\eta}}}\right)} \int_{\beta^{\frac{-1}{\eta}}}^{\infty} \frac{y}{y^\eta + 1} dy\right\}. \tag{7.5}$$

Proof. See **Appendix D.2**. □

Generally, it can be shown that the SINR outage $\mathcal{O}_s$ is non-increasing in ρ_o (c.f. 7.3). Recalling (from Sec. 7.3.1) that both the truncation outage and the average transmit power are non-decreasing in ρ_o, it is concluded that ρ_o introduces a tradeoff in the system performance as will be shown in the numerical results.

The SINR statistics also controls the average uplink spectral efficiency obtained via Shannon's formula. The average uplink spectral efficiency can be obtained from the following theorem.

Theorem 7.3.2. *In a single-tier Poisson cellular network with truncated channel*

inversion power control with the cutoff threshold ρ_o, in the uplink, the average spectral efficiency for active UEs is given by

$$\mathcal{R} = \int_0^\infty \frac{1}{x+1} \exp\left\{ -\frac{x\sigma^2}{\rho_o} - \frac{2x^{\frac{2}{\eta}}\gamma\left(2, \pi\lambda\left(\frac{P_u}{\rho_o}\right)^{\frac{2}{\eta}}\right)}{\left(1 - e^{-\pi\lambda\left(\frac{P_u}{\rho_o}\right)^{\frac{2}{\eta}}}\right)} \int_{x^{\frac{-1}{\eta}}}^\infty \frac{y}{y^\eta + 1} dy \right\} dx. \tag{7.6}$$

Proof. See **Appendix D.3**. □

Equation (7.6) incorporates the tradeoff between ρ_o and spectral efficiency. The spectral efficiency and the SINR outage improve with increasing ρ_o, however, increasing ρ_o deteriorates the truncation outage probability and increases the power consumption of the UEs. In the following, I show some interesting special cases that help understanding the uplink system performance.

Special case 1 (Infinite P_u)

The case of infinite maximum transmit power P_u is of particular interest because it captures the scenario where the transmit power is not a binding constraint for the uplink communication (cf. Fig.7.2(b)). In other words, the BSs are dense enough (with respect to the required cutoff threshold) such that the distance between a generic UE and its serving BS is relatively small, and hence, the transmit power will be less than the maximum value P_u almost surely (i.e., P_u is a non-binding operational constraint). In the analysis, the case of non-binding transmit power can be captured by setting $P_u = \infty$. In this case, the SINR is given by

$$\mathcal{O}_s = 1 - \exp\left\{ -\frac{\beta\sigma^2}{\rho_o} - 2\beta^{\frac{2}{\eta}} \int_{\beta^{\frac{-1}{\eta}}}^\infty \frac{y}{y^\eta + 1} dy \right\} \tag{7.7}$$

and the spectral efficiency reduces to

$$\mathcal{R} = \int_0^\infty \frac{\exp\left\{-\frac{x\sigma^2}{\rho_o} - 2x^{\frac{2}{\eta}} \int_{x^{\frac{-1}{\eta}}}^\infty \frac{y}{y^\eta+1} dy\right\}}{x+1} dx. \tag{7.8}$$

Equations (7.7) and (7.8) show that when the transmit power is not a binding constraint, the SINR outage and the average spectral efficiency in a single-tier cellular network are independent of the BS intensity. This result is in compliance with the results in [12] and it can be concluded that both the uplink performance (in case of non-binding maximum transmit power constraint) and the downlink performance, in terms of SINR outage and average spectral efficiency, are independent of the BS intensity.

It is quite insightful to see that the SINR outage probability and the average spectral efficiency are independent of the intensity of the BSs. That is, when the maximum transmit power P_u is not a binding operational constraint for the UEs, increasing the intensity (number) of the BSs neither degrades nor improves the SINR outage probability and the average spectral efficiency within the cell. For the uplink, this behavior can be explained as follows: since each BS will be serving one user per channel, as the intensity of the BSs increases, the intensity of the interfering UEs increases; however, the average distance between a UE and its serving BS decreases which decreases the transmit power required to maintain the received signal power at ρ_o. Hence, the increased intensity of interfering UEs is compensated by the decreased transmit power per interfering UE, and the SINR statistics does not change if $\frac{\rho_o}{\sigma^2}$ is kept constant, and vice versa. Therefore, the coverage probability and the average spectral efficiency in the uplink and downlink can only be improved through interference management techniques such as frequency reuse [61], interference cancellation [126], multiple-input-multiple-output (MIMO) antennas [73], interference

avoidance via cognition [78], or multi-cell cooperation [127]. Although these results are only valid for the PPP network model, they are insightful because they reflect the worst-case network performance. More specifically, deploying more BSs, in the worst case, will not degrade the SINR statistics.

Special case 2 ($\eta = 4$)

The integral in (7.5) can be found in closed form for integer values of η. For instance, if $\eta = 4$, the SINR outage probability reduces to the following closed form:

$$\mathcal{O}_s = 1 - \exp\left\{ -\frac{\beta\sigma^2}{\rho_o} - \frac{\sqrt{\beta}\gamma\left(2, \pi\lambda\sqrt{\frac{P_u}{\rho_o}}\right)}{\left(1 - e^{-\pi\lambda\sqrt{\frac{P_u}{\rho_o}}}\right)} \arctan(\sqrt{\beta}) \right\} \tag{7.9}$$

and the spectral efficiency reduces to the following:

$$\mathcal{R} = \int_0^\infty \frac{\exp\left\{ -\frac{x\sigma^2}{\rho_o} - \frac{\sqrt{x}\gamma\left(2, \pi\lambda\sqrt{\frac{P_u}{\rho_o}}\right)}{\left(1 - e^{-\pi\lambda\sqrt{\frac{P_u}{\rho_o}}}\right)} \arctan(\sqrt{x}) \right\}}{x+1} dx. \tag{7.10}$$

Special case 3 ($\eta = 4$, infinite P_u, interference-limited scenario)

In the interference-limited case, ρ_o is assumed to be large enough such that $\frac{\beta\sigma^2}{\rho_o} << \mathcal{I}$ and hence noise can be ignored. In this case, the SINR outage reduces to the following simple closed form:

$$\mathcal{O}_s = 1 - \exp\left\{ -\sqrt{\beta} \arctan(\sqrt{\beta}) \right\} \tag{7.11}$$

and the spectral efficiency reduces to

$$\mathcal{R} = \int_0^\infty \frac{\exp\left\{-\sqrt{x}\arctan(\sqrt{x})\right\}}{x+1} dx. \tag{7.12}$$

Equations (7.11) and (7.12) give expressions for the outage probability and average rate in their simplest forms. These equations clearly show that when P_u is not a binding constraint and the interference is much larger than the noise, both the SINR outage and the spectral efficiency are independent of the cutoff threshold as well as the BS intensity.

7.4 Uplink Modeling in Multi-tier Cellular Networks

In this section, I show that the developed baseline model for uplink transmission in single-tier cellular networks can be extended for uplink transmission in multi-tier cellular networks. First, I present the analysis for multi-tier cellular networks with common path-loss exponent. Then, I will show and comment on the case with different path-loss exponents in the different tiers.

7.4.1 Common Path-loss Exponent

The developed model naturally captures multi-tier cellular networks with different intensities λ_k and different cutoff thresholds $\rho_o^{(k)}$ for the different tiers but with a common path-loss exponent η. In this case, the distribution of the transmit power for the active UEs is obtained from the following lemma.

Lemma 7.4.1. *In a K-tier Poisson cellular network with a common path-loss exponent η and a truncated channel inversion power control where each tier has the BS intensity of λ_k and the cutoff threshold $\rho_o^{(k)}$, the distribution of the transmit power of*

the active UEs in the uplink in the j^{th} tier is given by

$$f_{P_j}(x) = \frac{2\pi\Lambda x^{\frac{2}{\eta}-1} e^{-\pi\Lambda\left(\frac{x}{\rho_o^{(j)}}\right)^{\frac{2}{\eta}}}}{\eta(\rho_o^{(j)})^{\frac{2}{\eta}}\left(1 - e^{-\pi\Lambda\left(\frac{P_u}{\rho_o^{(j)}}\right)^{\frac{2}{\eta}}}\right)}, 0 \leq x \leq P_u$$

where $\Lambda = \sum_{k=1}^{K} \lambda_k$. The moments of the transmit power of a UE in the j^{th} tier can be obtained as

$$\mathbb{E}\left[P_j^{\alpha}\right] = \frac{(\rho_o^{(j)})^{\alpha}\gamma\left(\frac{\alpha\eta}{2}+1, \pi\Lambda\left(\frac{P_u}{\rho_o^{(j)}}\right)^{\frac{2}{\eta}}\right)}{(\pi\Lambda)^{\frac{\alpha\eta}{2}}\left(1 - e^{-\pi\Lambda\left(\frac{P_u}{\rho_o^{(j)}}\right)^{\frac{2}{\eta}}}\right)}. \tag{7.13}$$

Proof. Since the UEs associate to the BSs based on the average uplink link quality, following the superposition theorem of the PPP [8], the association regions for the BSs form a Voronoi tessellation for a PPP with intensity Λ. Note that, for the uplink in a multi-tier network, the association regions form a Voronoi tessellation rather than a weighted Voronoi tessellation due to the homogenous transmit powers of the UEs. The rest of the proof follows the same steps as in **Appendix D.1**. □

The truncation outage probability at the j^{th} tier is given by

$$\mathcal{O}_p^{(j)} = e^{-\pi\Lambda\left(\frac{P_u}{\rho_o^{(j)}}\right)^{\frac{2}{\eta}}}. \tag{7.14}$$

Without loss of generality, let SINR_j be the SINR experienced by a tagged BS in the j^{th} tier and the BS is located at the origin. By Slivnyak's theorem, the analysis holds for any BS in the j^{th} tier. Let each tier has its own SINR threshold β_k, then, following (7.4), the SINR outage in the j^{th} tier can be expressed as

$$\mathbb{P}\left\{\mathrm{SINR_j} \leq \beta_j\right\} = \mathbb{E}\left[1 - \exp\left\{-\frac{\beta_j}{\rho_o^{(j)}}\left(\sigma^2 + \sum_{k=1}^{K}\mathcal{I}_k\right)\right\}\right]$$
$$= 1 - \exp\left\{-\frac{\beta_j}{\rho_o^{(j)}}\sigma^2\right\}\prod_{k=1}^{K}\mathcal{L}_{\mathcal{I}_k}\left(\frac{\beta_j}{\rho_o^{(j)}}\right) \tag{7.15}$$

where $\mathcal{I}_k$ is the aggregate interference from the k^{th} tier, and the second line of equation (7.15) follows from the independence of $\mathcal{I}_k$ and $\mathcal{I}_i$ $\forall i \neq k$. Note that $\mathcal{I}_j$ represents the co-tier interference and $\mathcal{I}_k$ for $k \neq j$ represents the cross-tier interference. As discussed in the single-tier case, the interfering UEs do not constitute a PPP. Hence, for analytical tractability, similar to the single-tier case, I approximate the interfering UEs in each tier with a PPP. The SINR outage for a generic active UE in the j^{th} tier is then given by the following theorem.

Theorem 7.4.1. *In a K-tier Poisson cellular network with a common path-loss exponent η and truncated channel inversion power control where each tier has BS intensity λ_k and cutoff threshold $\rho_o^{(k)}$, in the uplink, the* SINR *outage probability for a generic active UE in the j^{th} tier is given by*

$$\mathcal{O}_s^{(j)} = 1 - \exp\left\{-\frac{\beta_j\sigma^2}{\rho_o^{(j)}} - \sum_{k=1}^{K}\left(\frac{\beta_j(\rho_o^{(k)})}{\rho_o^{(j)}}\right)^{\frac{2}{\eta}}\frac{2\lambda_k\gamma\left(2, \pi\Lambda\left(\frac{P_u}{\rho_o^{(k)}}\right)^{\frac{2}{\eta}}\right)}{\Lambda\left(1 - e^{-\pi\Lambda\left(\frac{P_u}{\rho_o^{(k)}}\right)^{\frac{2}{\eta}}}\right)}\int_{\left(\frac{\beta_j\rho_o^{(k)}}{\rho_o^{(j)}}\right)^{\frac{-1}{\eta}}}^{\infty}\frac{y}{y^\eta + 1}dy\right\}. \tag{7.16}$$

Proof. See **Appendix D.3**. □

The SINR outage in (7.16) reduces to the single-tier case given in (7.5), but with

intensity Λ, when all tiers have the same cutoff threshold ρ_o despite of their different intensities. The spectral efficiency in the multi-tier case can be obtained from the following theorem.

Theorem 7.4.2. *In a K-tier Poisson cellular network with a common path-loss exponent η and truncated channel inversion power control where each tier has BS intensity λ_k and cutoff threshold $\rho_o^{(k)}$, in the uplink, the average spectral efficiency for active UEs in the j^{th} tier is given by*

$$\mathcal{R}_j = \int_0^\infty \frac{\exp\left\{ -\frac{x\sigma^2}{\rho_o^{(j)}} - \sum_{k=1}^K \left(\frac{x\rho_o^{(k)}}{\rho_o^{(j)}}\right)^{\frac{2}{\eta}} \frac{2\lambda_k \gamma\left(2, \pi\Lambda\left(\frac{P_u}{\rho_o^{(k)}}\right)^{\frac{2}{\eta}}\right)}{\Lambda\left(1-e^{-\pi\Lambda\left(\frac{P_u}{\rho_o^{(k)}}\right)^{\frac{2}{\eta}}}\right)} \int_{\left(\frac{x\rho_o^{(k)}}{\rho_o^{(j)}}\right)^{\frac{-1}{\eta}}}^\infty \frac{y}{y^\eta+1} dy \right\}}{x+1} dx. \tag{7.17}$$

Proof. The proof is similar to the one in **Appendix D.3**. □

For brevity, I consider only one special case. For infinite P_u, interference-limited network scenario, and $\eta = 4$, the SINR outage and average spectral efficiency in the uplink in the j^{th} tier reduce to the following:

$$\mathcal{O}_s^{(j)} = 1 - \exp\left\{ -\sum_{k=1}^K \frac{\lambda_k}{\Lambda} \sqrt{\frac{\beta_j \rho_o^{(k)}}{\rho_o^{(j)}}} \arctan\left(\sqrt{\frac{\beta_j \rho_o^{(k)}}{\rho_o^{(j)}}}\right) \right\} \tag{7.18}$$

$$\mathcal{R}_j = \int_0^\infty \frac{\exp\left\{ -\sum_{k=1}^K \frac{\lambda_k}{\Lambda} \sqrt{\frac{x\rho_o^{(k)}}{\rho_o^{(j)}}} \arctan\left(\sqrt{\frac{x\rho_o^{(k)}}{\rho_o^{(j)}}}\right) \right\}}{x+1} dx. \tag{7.19}$$

Equations (7.18) and (7.19) show that, in general, the SINR outage probability and spectral efficiency in a certain tier depend on the relative cutoff thresholds and the relative BS intensities. The SINR outage probability and spectral efficiency improve as the cutoff threshold in the target tier increases and the cutoff thresholds in the other tiers and/or the BS intensities in the other tiers decrease. This is because, a higher cutoff threshold in the target tier increases the useful signal power and lower cutoff thresholds and/or lower BS intensities in the other tiers reduce the cross-tier interference.

Theorems 7.4.1 and **7.4.2** show an important difference between multi-tier and single-tier cellular networks. That is, regardless of the maximum transmit power value P_u (i.e., binding or non-binding maximum transmit power constraint), the SINR outage probability and spectral efficiency in multi-tier cellular networks depend on the relative values of the cutoff thresholds and the relative BS intensities. However, note that if all the tiers have the same cutoff threshold, regardless of the relative BSs intensities, (7.18) and (7.19) reduce to (7.11) and (7.12), respectively. Hence, the multi-tier cellular network can be reduced to a single-tier with intensity Λ and both the SINR outage probability and the average spectral efficiency become independent of the BS intensities in the different tiers if P_u in non-binding.

7.4.2 Different Path-loss Exponents

In the previous section, it has been shown that when all network tiers share the same path-loss exponent, the association of the UEs does not change from that in the single-tier cellular networks. That is, the association regions of the BSs will form a Voronoi tessellation. On the other hand, if different tiers have different path-loss exponents, the association of UEs in the multi-tier case deviates from that in the

single-tier case where the association regions of the BSs form a weighted Voronoi tessellation. That is, the BSs in tiers with lower path-loss exponents will have larger service areas than BSs in tiers with higher path-loss exponents. The transmit power in a multi-tier cellular network with different path-loss exponents can be characterized by the following lemma.

Lemma 7.4.2. *In a K-tier Poisson cellular network with truncated channel inversion power control where each tier has BS intensity λ_k, cutoff threshold $\rho_o^{(k)}$, and path-loss exponent η_k, the* pmf *of the transmit power of the active UEs in the uplink in the j^{th} tier is given by*

$$f_{P_j}(x) = \frac{\sum_{k=1}^{K} \frac{2\pi\lambda_k x^{\frac{2}{\eta_k}-1}}{\eta_k (\rho_o^{(j)})^{\frac{2}{\eta_k}}}}{1 - e^{-\sum_{b=1}^{K} \pi\lambda_b \left(\frac{P_u}{\rho_o^{(j)}}\right)^{\frac{2}{\eta_b}}}} e^{-\sum_{a=1}^{K} \pi\lambda_a \left(\frac{x}{\rho_o^{(j)}}\right)^{\frac{2}{\eta_a}}}. \tag{7.20}$$

The moments of the transmit power of a UE in the k^{th} tier can be obtained as

$$\mathbb{E}\left[P_j^{\alpha}\right] = \int_0^{P_u} \frac{\sum_{k=1}^{K} \frac{2\pi\lambda_k x^{\frac{2}{\eta_k}+\alpha-1}}{\eta_k (\rho_o^{(j)})^{\frac{2}{\eta_k}}}}{1 - e^{-\sum_{b=1}^{K} \pi\lambda_b \left(\frac{P_u}{\rho_o^{(j)}}\right)^{\frac{2}{\eta_b}}}} e^{-\sum_{a=1}^{K} \pi\lambda_a \left(\frac{x}{\rho_o^{(j)}}\right)^{\frac{2}{\eta_a}}}. \tag{7.21}$$

Proof. See **Appendix D.5**. □

The truncation outage probability in the uplink for a UE at the j^{th} tier is given by

$$\mathcal{O}_p^{(j)} = e^{-\sum_{k=1}^{K} \pi\lambda_k \left(\frac{P_u}{\rho_o^{(k)}}\right)^{\frac{2}{\eta_k}}}. \tag{7.22}$$

Lemma 7.4.2 shows that the moments of the transmit power of the UEs cannot be obtained in closed form due to the complications introduced by the different path-loss exponents. Note that, since the transmit power appears in the LT of the interference

as $\mathbb{E}[P_k^{\frac{2}{\eta_k}}]$, the calculations of outage probability and spectral efficiency do not require obtaining the moments of the transmit power in closed forms. It can be shown that, for a common path-loss exponent, **Lemma 7.4.2** reduces to **Lemma 7.4.1**. Similar to the previous cases, the interfering UEs do not constitute a PPP. Therefore, for analytical tractability, I will approximate the locations of the interfering UEs by a PPP. The SINR outage in multi-tier cellular networks with different path-loss exponents can be characterized by the following theorem.

Theorem 7.4.3. *In a K-tier Poisson cellular network with truncated channel inversion power control where each tier has BS intensity λ_k, cutoff threshold $\rho_o^{(k)}$, and path-loss exponent η_k, the* SINR *outage probability in the uplink for a generic active UE in the j^{th} tier is given by*

$$\mathcal{O}_s^{(j)} = 1 - \exp\left\{ -\frac{\beta_j \sigma^2}{\rho_o^{(j)}} - \sum_{k=1}^{K} 2\pi\lambda_k \left(\frac{\beta_j}{\rho_o^{(j)}}\right)^{\frac{2}{\eta_j}} \mathbb{E}_{P_k}\left[P_k^{\frac{2}{\eta_j}}\right] \int_{\left(\frac{\beta_j \rho_o^{(k)}}{\rho_o^{(j)}}\right)}^{\infty} \frac{y}{y^{\eta_j}+1} dy \right\}. \quad (7.23)$$

Proof. See **Appendix D.6**. □

The spectral efficiency can be characterized via the following theorem.

Theorem 7.4.4. *In a K-tier Poisson cellular network with truncated channel inversion power control where each tier has the BS intensity λ_k, cutoff threshold $\rho_o^{(k)}$, and path-loss exponent η_k, the average spectral efficiency in the uplink for active UEs in the j^{th} tier is given by*

$$\mathcal{R}_j = \int_0^{\infty} \frac{1}{x+1} \exp\left\{ -\frac{\beta_j \sigma^2}{\rho_o^{(j)}} - \sum_{k=1}^{K} 2\pi\lambda_k \left(\frac{x}{\rho_o^{(j)}}\right)^{\frac{2}{\eta_j}} \mathbb{E}_{P_k}\left[P_k^{\frac{2}{\eta_k}}\right] \int_{\left(\frac{x\rho_o^{(k)}}{\rho_o^{(j)}}\right)}^{\infty} \frac{y}{y^{\eta_j}+1} dy \right\} dx. \quad (7.24)$$

Proof. The proof is similar to the one in **Appendix D.3**. □

Due to the complicated expressions for the moments of the transmit power as given in **Lemma 7.4.2**, **Theorems 7.4.3** and **7.4.4** do not give simple formulas for the SINR outage and spectral efficiency. However, **Theorems 7.4.3** and **7.4.4** do give general formulas that reduce to all of the previously presented special cases. Note that without simple expressions, significant insights may not be extracted from the results obtained in **Theorems 7.4.3** and **7.4.4** and **Lemma 7.4.2** for multi-tier networks with different path-loss exponents. In contrast, with a common path-loss exponent, **Theorems 7.4.3** and **7.4.4** and **Lemma 7.4.2** simplify to **Theorems 7.4.1** and **7.4.2** and **Lemma 7.4.1**, respectively. The main conclusion from this section is that the developed paradigm is general and flexible to capture different practical system parameters.

7.5 Results and Discussions

7.5.1 Results

In this section, I validate my model against simulations and present some numerical results for a single-tier cellular network (or equivalently, a multi-tier cellular network with common cutoff threshold ρ_o and path-loss exponent η). Unless otherwise stated, I set the BS intensity to $\lambda = 2$ BSs/km^2, the maximum transmit power $P_u = 1$ W, the receiver sensitivity $\rho_{min} = -90$ dBm, the cutoff threshold $\rho = -70$ dBm, the SINR threshold $\beta = 1$, $\sigma^2 = -90$ dBm, and the number of channels $S = 1$.

First, I validate my model against simulation results obtained for a Poisson cellular network and compare it with the circular approximation of the target BS coverage as used in [68, 122]. The reason for the model validation is that the derived *cdf* of the SINR assumes that the set of active UEs constitutes a PPP. This assumption partially

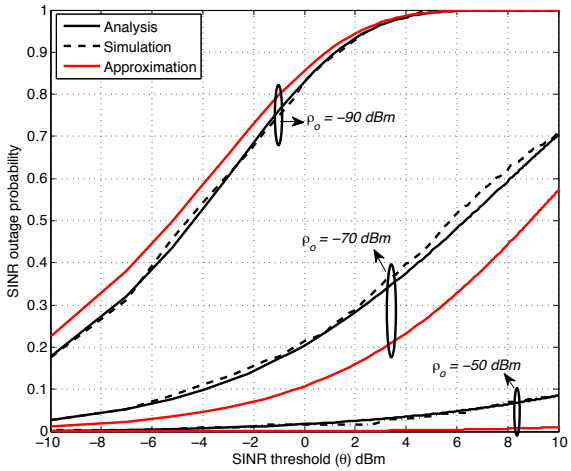

Figure 7.4: The *cdf* of the SINR for $\lambda = 2$ BS/km^2 and $|\mathbf{S}| = 1$.

ignores the correlation among the simultaneously active UEs on the same channel. That is, given that a UE is transmitting on a tagged channel, all other active UEs should be outside the Voronoi cell of its serving BS. Note that my model partially ignores these correlations because the correlation with the tagged BS is captured by the fact that the average received interference power from any interfering UE is less than the cutoff threshold ρ_o (cf. **Facts** #1–#3 in **Appendix D.2**).

Fig. 7.4 shows that the derived model accurately captures the SINR outage. The figure also shows that approximating the coverage area of the tagged BS with a circle with the radius $\frac{1}{\sqrt{\pi\lambda}}$ underestimates the outage at $\rho_o \leq -70$ dBm and overestimates the outage at $\rho_o = -90$ dBm. The reason is that at low cutoff threshold ρ_o, the interference exclusion region around each BS is large (cf. **Fact** #2 in **Appendix D.2**), and hence, the radius $\frac{1}{\sqrt{\pi\lambda}}$ estimates a more aggressive interference. On the other hand, for high cutoff threshold ρ_o, the interference exclusion region around the tagged BS is small, and hence, the radius $\frac{1}{\sqrt{\pi\lambda}}$ estimates a more conservative interference.

Fig. 7.5 shows the tradeoff introduced by ρ_o on the total outage probability $\mathcal{O}_t = \mathcal{O}_p + (1-\mathcal{O}_p)\mathcal{O}_s$. As shown in the figure, ρ_o tunes the tradeoff between the two outage

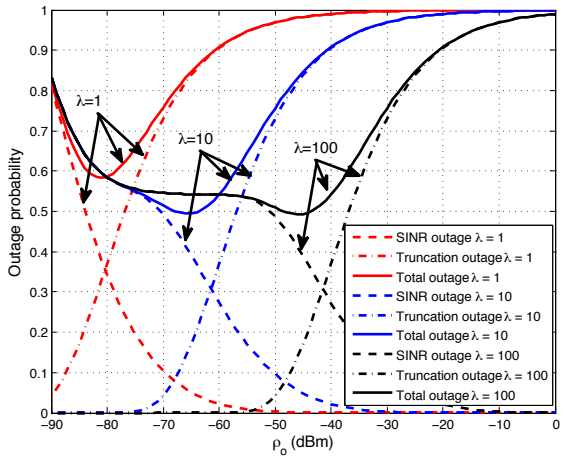

Figure 7.5: Total outage probability for $\beta = 1$ and $|\mathbf{S}| = 1$.

probabilities and there exists an optimal cutoff threshold ρ_o^* that minimizes the total outage probability. That is, at lower values of ρ_o, the SINR outage dominates the outage probability. On the other hand, at high values of ρ_o, the truncation outage dominates the outage probability. The figure shows the two regions of operation for the uplink, namely, when P_u is a binding constraint and when P_u is a non-binding constraint. Note that P_u becomes binding when the truncation outage probability is not zero. For small values of ρ_o, P_u induces a non-binding constraint, and hence, for relatively high BS intensity (e.g., $\lambda = 10$ and $\lambda = 100$) the SINR outage is independent (i.e., the two curves for $\lambda = 10$ and $\lambda = 100$ coincides) of the BS intensity (which reinforces case #1 in Sec. 7.3.2). Note that when ρ_o is comparable to the noise power σ^2, the SINR outage depends on ρ_o. However, when ρ_o is much greater the noise and P_u is non-binding, the SINR outage is independent of both the cutoff threshold ρ_o and BS intensity (case #3 in Sec. 7.3.2). In contrast, for high values of ρ_o, P_u becomes a binding constraint and the SINR outage depends on both the BS intensity and cutoff threshold.

To show the two regions of operation for the uplink more clearly, I plot Fig. 7.6

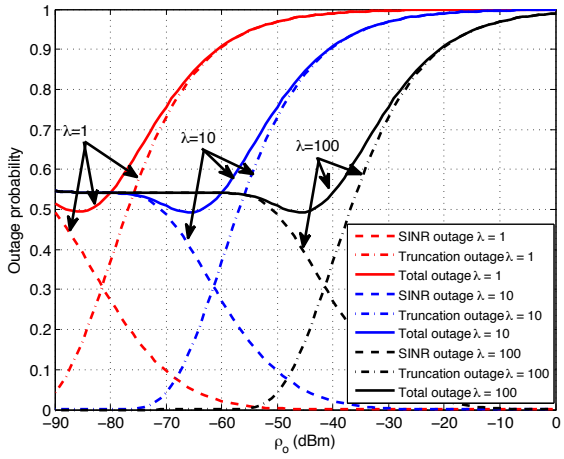

Figure 7.6: Total outage probability for $\sigma^2 = -110$ dBm, $\beta = 1$, and $|\mathbf{S}| = 1$.

with a negligible noise power value of $\sigma^2 = -110$ dBm. This figure shows that when P_u is non-binding (i.e., the truncation outage probability is almost zero), the SINR outage is completely independent of both the cutoff threshold ρ_o and BS intensity (case #3 in Sec. 7.3.2). Note that the independence w.r.t. the BS intensity can be seen from the coincidence of the curves for $\lambda = 10$ and $\lambda = 100$ as long as P_u is non-binding for both intensities (i.e., the truncation outage is equal to zero). In contrast, when P_u becomes binding (i.e., the truncation outage is not zero), the SINR outage is highly affected by both the BS intensity and cutoff threshold (case #2 in Sec. 7.3.2).

Fig. 7.7 shows the tradeoff introduced by ρ_o on the effective spectral efficiency defined as $(1 - \mathcal{O}_p)\mathcal{R}$. The effective spectral efficiency captures the average spectral efficiency for active users (i.e., users with no truncation outage). As shown in the figure, when P_u is a non-binding constraint (i.e., for $\rho_o \leq -75$ with $\lambda = 10$ and $\rho_o \leq -55$ with $\lambda = 100$ [cf. Fig. 7.5]), the effective spectral efficiency is independent of the BS intensity. Note that the effective spectral efficiency depends on ρ_o when P_u induces a non-binding constraint due to the relatively (i.e., relative to ρ_o) high noise power (case #1 in Sec. 7.3.2). However, for $\lambda = 100$ the effective spectral efficiency is

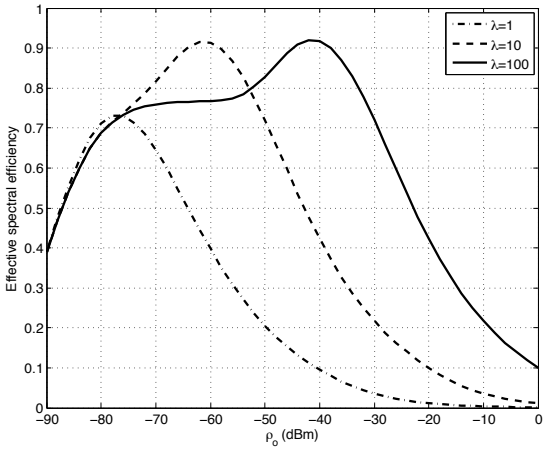

Figure 7.7: Effective spectral efficiency $\sigma^2 = -90$ dBm and $|\mathbf{S}| = 1$.

independent of the cutoff threshold in the range of $-70 \leq \rho_o \leq -55$ dBm because P_u induces a non-binding constraint and the noise power is negligible w.r.t. the value of ρ_o (case #3 in Sec. 7.3.2). On the other hand, when P_u becomes a binding constraint, the effective spectral efficiency depends on both the BS intensity and cutoff threshold. This figure also shows the existence of an optimal cutoff threshold ρ_o^* which maximizes the effective spectral efficiency.

To show the tradeoff introduced by ρ_o on the effective spectral efficiency more clearly, I plot Fig. 7.8 for negligible noise power $\sigma^2 = -110$ dBm. This figure shows that when P_u induces a non-binding constraint, the effective spectral efficiency is completely independent of the BS intensity and cutoff threshold. On the other hand, when P_u induces a binding constraint, the effective spectral efficiency depends on both the BS intensity and the cutoff threshold.

Fig. 7.9 shows the average transmit power of the UEs vs. the cutoff threshold ρ_o. As the cutoff threshold ρ_o increases, the UEs are required to transmit at higher powers to invert their path-loss and maintain a high threshold ρ_o at their serving BSs. Therefore, the average transmit power is non-decreasing in ρ_o. Note that the average

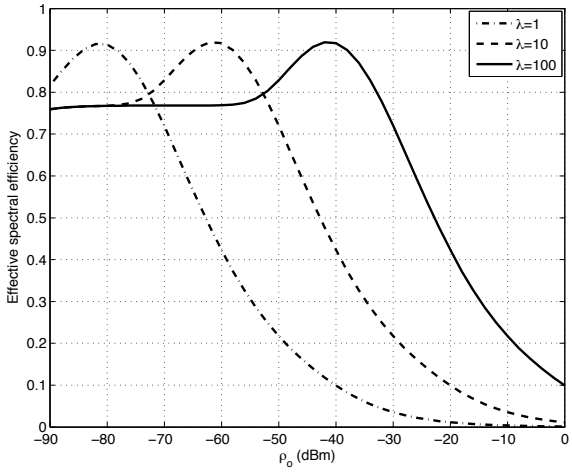

Figure 7.8: Effective spectral efficiency for $\sigma^2 = -110$ dBm, $\frac{\mathcal{U}}{\lambda} = 50$, and $|\mathbf{S}| = 1$.

transmit power saturates at $\lim_{\rho_o \to \infty} \mathbb{E}[P] = \frac{P_u}{3}$.

7.5.2 Discussions

In the light of the proposed uplink framework and the results provided in [12, 54], I highlight the commonalities and differences between the uplink and downlink transmission performances. The criticality of the power control is the first main difference between the uplink and downlink transmission performances. While power control enhances the downlink transmission performance, it is not crucial for the basic network operation due to the inherent interference protection provided by the user association policy. On the other hand, power control is essential for the case of uplink operation to mitigate severe interference caused by the arbitrary close interfering UEs (cf. Fig. 7.1).

The second difference between the uplink and downlink operation is the maximum transmit power constraint for the UEs. For a single-tier cellular network, the relative values of λ, P_u, and ρ_o may lead to a binding maximum transmit power constraint for

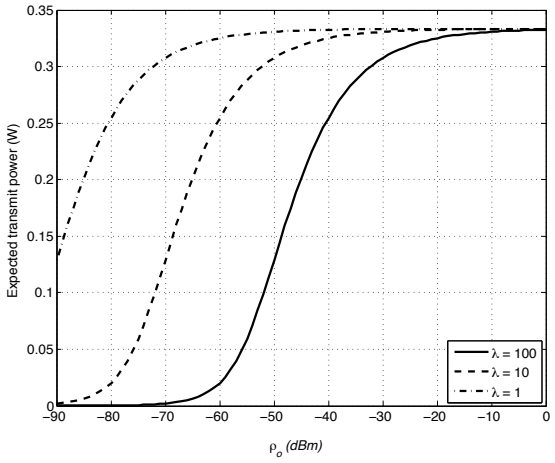

Figure 7.9: Expected transmit power in the uplink.

the uplink operation. In this case, the uplink performance is highly affected by the intensity of the BSs as well as the cutoff threshold for power control. On the other hand, when the relative values of λ, P_u, and ρ_o lead to an uplink operation under non-binding maximum transmit power constraint, the uplink transmission performance is analogous to the downlink transmission performance. More specifically, the uplink network can be transformed into an equivalent network where all UEs have a constant transmit power of $E\left[P^{\frac{2}{\eta}}\right]$ (see (D.2)). Hence, the uplink performance is the same as the downlink performance with BS transmit power of $E\left[P^{\frac{2}{\eta}}\right]$ and a constant downlink distance of $\left(\frac{E[P^{\frac{2}{\eta}}]}{\rho_o}\right)^{\frac{1}{\eta}}$. Therefore, as discussed in [12] in the context of downlink performance, the presented results also show that the SINR outage and spectral efficiency performances for the uplink communication in a single-tier cellular network with a loose maximum transmit power constraint are independent of the BS intensity. Therefore, in the worst case (because of the PPP assumption), deploying more BSs will not affect the SINR statistics in either the uplink or the downlink.

For multi-tier cellular networks, regardless of whether P_u is binding or not, the

uplink performance depends on the relative cutoff thresholds and relative BS intensities in the network tiers. However, if all of the tiers share a common cutoff threshold, the uplink performance becomes independent of the relative BS intensities in the case of a loose maximum transmit power constraint. In this case, as discussed in [54] in the context of downlink communication, the presented results show that the SINR outage and the spectral efficiency performances for uplink communications in a multi-tier cellular network with a common cutoff threshold, a common path-loss exponent, and a loose maximum transmit power constraint, are independent of the BS intensity. Therefore, in the worst case (because of the PPP assumption), deploying more BSs or more tiers will not affect the SINR statistics in either the uplink or the downlink.

Another important difference between the uplink and the downlink is the UE association. The heterogeneity in the downlink transmit powers of BSs in a multi-tier cellular network leads to a coverage in the form of a weighted Voronoi tessellation. On the other hand, in the uplink, the homogeneity of the transmit powers of the UEs leads to a coverage in the form of Voronoi tessellation in a multi-tier cellular network with a common path-loss exponent. The simple association in the uplink highly simplifies the analysis in the case of multi-tier cellular network. It is worth mentioning that if the different tiers have different path-loss exponents, the uplink association regions will follow a weighted Voronoi tessellation. However, the association in the downlink is still different from the association in the uplink due to the homogeneous transmit powers of the UEs in the latter case and the heterogeneous transmit powers of the BSs in the former case.

In addition to its practicality, the channel inversion power control with the cutoff threshold highly facilitates the analysis in this work and leads to simple expressions for the outage probability and rate. However, the presented analysis can be con-

sidered as a special case of the fractional channel inversion power control (i.e., full inversion) and cannot be used to capture the fractional channel inversion power control. Nevertheless, the presented analysis provides design insights and helps understanding the uplink system behavior. In addition, in contrast to fractional channel inversion power control, the channel inversion power control with the cutoff threshold results in a location independent outage probability and average rate for active users (i.e., homogenous performance for all active users.). The fractional channel inversion power control imposes a location dependent performance for the active users. Furthermore, the fractional channel inversion power control highly complicates the system model, and hence, necessitates more approximations as in [121] in order to maintain the tractability. Although [121] provided a mathematically elegant technique to deal with uplink cellular networks with fractional channel inversion power control, the results reveal that the model provided in [121] will not be accurate when considering the maximum transmit power constraint for the UEs and the UEs operate in a binding maximum transmit power scenario. This is because, in [121] the system model was approximated and it was assumed that the Voronoi cells are realized w.r.t. the users not the BSs. In other words, the uplink system model was converted to an equivalent downlink (i.e., the users are treated as BSs) which, as I have shown here, is inaccurate if P_u is a binding operational constraint. Moreover, the model presented in [121] resulted in relatively more complex expression for the outage probability[6].

7.6 Chapter Summary

We have introduced a novel modeling approach for uplink transmission in Poisson cellular networks with truncated channel inversion power control. The model assumes

[6]Note that, the expressions presented in [121] for the outage probability and rate do not reduce to the expression presented in this work due to the system model approximation used in [121].

a practical system model and accounts for power control, maximum transmit power of the UEs, and cutoff threshold for the power control. The developed modeling approach is general and captures the uplink performance of multi-tier cellular networks. The results show that the cutoff threshold introduces tradeoffs in the system performance and there exists an optimal cutoff threshold that minimizes the outage probability. When multiple outage optimal cutoff thresholds exist, the minimum cutoff threshold minimizes the average power consumption of the users. Closed-form simple expressions for the outage probability and simple forms with one numerical integral for the spectral efficiency have been obtained.

We have characterized the uplink performance and showed the existence of a transfer point for the uplink operation which depends on the relative values of the BS intensity, the maximum transmit power of the UEs, and the cutoff threshold for power control. When the BSs are dense enough such that the maximum transmit power is not a binding constraint to establish an uplink connection with the nearest BS, the SINR outage and the spectral efficiency are independent of the BS intensity. Since the maximum transmit power P_u is, in general, not a binding constraint in dense cellular networks, deploying more tiers and more BSs may decrease the power consumption for UEs, improve the spatial frequency reuse and system capacity, but will neither improve nor deteriorate the SINR outage probability and spectral efficiency. Hence, the SINR outage probability and the spectral efficiency in the uplink and downlink could only be improved via interference management/avoidance techniques.

In the next chapter, I conclude the work done in this thesis and highlight some future directions.

Chapter 8

Conclusion and Future Direction

8.1 Conclusion

Stochastic geometry is the only mathematical technique available that provides a rigorous analytical approach to the modeling, analysis, and design of networks with random topologies. While it is extremely powerful when applied to networks modeled as PPPs with Rayleigh fading, leading to short and general closed-form expressions, generalizing the network models diminishes its tractability. That said, it has been shown that stochastic geometry modeling helps understanding the effects of the fundamental design parameters on the system behavior. Furthermore, I exploited stochastic geometry models to optimize the network design. For instance, in Chapter 3, I used stochastic geometry to study the effect of CSMA MAC protocol on the SINR and to optimize the spectrum sensing threshold to maximize the transmission capacity. In Chapter 4, stochastic geometry was utilized to develop a spectrum efficient design paradigm to increase the coexistence capability of IEEE 801.15.4 in the crowded ISM band. In Chapters 5 and 6, for a two-tier downlink cellular network, I have studied the effect of opportunistic spectrum access via cognition on the performance of both

the macro users and femto users. We have also developed a paradigm to optimize the spectrum sensing threshold of the cognitive femto-access points. Finally, in Chapter 7, for uplink multi-tier cellular networks, I have revealed a transition point in the system behavior that depends on the system parameters. Furthermore, I have shown that when the transmit power of the UEs are not a binding constraint for the uplink operations, the SIR statistics do not depend on the intensity of the BSs or the cutoff threshold of the power control.

8.2 Future Research Direction

There are two main research directions for stochastic geometry modeling. The first direction is to go beyond the coverage probability and the performance metrics based only on the Shannon's formula. For instance, if the queuing dynamics can be incorporated in the analysis, useful performance metrics such as the transmission delay can be obtained. Another future direction is to adopt point processes that capture the characteristics of wireless networks with more accuracy and thus provide better modeling approaches. A detailed discussion on these potential research directions is provided below.

8.2.1 Adapting New Point Processes

Although spatial randomness in the topology is an intrinsic characteristic of both large-scale ad hoc networks and cellular networks, sophisticated distributed MAC protocols in ad hoc networks as well as sophisticated planning and interference management protocols in cellular networks bring some structure to the network topology. That is, the independence assumption for the positions of simultaneously active transmitters is not realistic. Hence, the repulsive point processes such as the Matérn HCPP

provide more realistic and accurate modeling for wireless networks.

For instance, for cellular networks, [13] examined four point processes to find which of them better models the spatial distribution of Bss in an actual cellular network, namely, the PPP, the HCPP, the Strauss process (SP), and the perturbed triangular lattice. The Strauss process belongs to the general class of Gibbs processes, which first appeared in statistical physics [8, Sec. 3.6]. It captures the pairwise interactions between nearby BSs by making it less likely that two BSs are located close to each other, i.e., Strauss processes are *soft-core* processes. The authors in [13] showed that, compared to the PPP, the three non-Poisson models can model the spatial locations of the deployed BSs more accurately. The Gibbs processes were also used in [128]. The authors compared the spatial characteristics of two actual cellular deployments in a coastal city and sprawling landlocked city to the spatial characteristics of the PPP, the hexagonal grid as well as to the Gibbs models, and it was shown that the Gibbs model, in particular the so-called *Geyer saturation process*, better captures (i.e., better than both the PPP and the hexagonal grid models) the spatial characteristics of the actual cellular deployments. However, the main problem with Gibbs processes is that they are not analytically tractable [8, Sec. 3.6].

The tractability issue of the Gibbs processes makes the HCPP of special interest. The HCPP is relatively more tractable than the Gibbs process and has been frequently used for modeling ad hoc networks and the existing results may facilitate its application in the context of cellular networks. However, as show in Chapter 3, the HCPP suffer for the intensity underestimation flaw which aggravates with the intensity and/or the SSR. Furthermore, the derivation of the distribution of the distance between a generic location and the nearest point in the HCPP is still an open problem. Note that the distribution of this distance is crucial if the HCPP is used

to model a cellular network because this distance refers to the distance between a user and her serving network entity. An approximate expression for this distance was derived in [41]. Another challenge for the HCPP is to obtain an expression for the probability generating functional in order to obtain the LT of the interference associated with a HCPP. This problem is reported in [40, 49] and in Chapters 3 and 5 in this thesis. One interesting future direction is to address the challenges of the HCPP and extend the existing results in the literature for more accurate modeling of wireless networks.

In [88, 89], an asymptotic approach for the outage characterization of wireless networks with general node distribution and general fading was presented. This includes the PPP, HCPP, clustered PPs, and grid models as special cases, and permits arbitrary MAC schemes. However, the results are restricted to the high-SIR case. In [129], the method of factorial moment expansion [130] was used to characterize and approximate interference in networks with general spatial distribution of nodes. The proposed model has a high potential for more accurate modeling of wireless networks and presents a clear tradeoff between the accuracy and complexity of the obtained expressions. The initiatives proposed in [88, 89, 128, 129] open the road for discovering new stochastic geometry tools for more accurate, flexible, and general modeling of wireless networks.

8.2.2 Performance Metrics Beyond Coverage and Rate

Coverage probability and average rate are the key performance indicators (KPIs) for most of the stochastic geometry models available in the literature. Therefore, another interesting future direction is to go beyond these KPIs and incorporate the queueing dynamics into the stochastic geometry models. Note that most of the work in the

literature assumes saturation conditions for the traffic. That is, the buffers of all network elements are always full, which might not be true and will provide a pessimistic view of the aggregate interference as well as some other performance metrics (e.g., spectrum access probability in cognitive and CSMA networks). Moreover, no insights regarding the packet delays can be obtained since the queuing dynamics are ignored. The commonly used saturation conditions were relaxed in [44, 131, 132] for ad hoc networks. However, to the best of my knowledge, there has not been any work that incorporates the queueing dynamics into the stochastic geometry models for cellular networks. [44] proposed a three-dimensional PPP to model the traffic flow for the coexisting network nodes in a CSMA network. The locations of the network nodes were modeled via a two-dimensional PPP while the traffic arrivals were modeled via a one-dimensional PPP. However, [44] only modeled the outage probability and no insights on the packet delay performance was given. In [131], the stability and delay performances were analyzed for nodes with infinite queues in a PPP ad hoc network with one and two classes of nodes. In [132], the authors calculated bounds on the end-to-end delay, the optimum hop lengths, and the number of hops in a TDMA/ALOHA multi-hop network in the presence of a PPP field of interferers.

Bibliography

[1] D. Stoyan, W. S. Kendall, and J. Mecke, *Stochastic Geometry and its Applications*. John Wiley & Sons, 1995.

[2] A. J. Baddeley, "Spatial Point Processes and their Applications," in *Lecture Notes in Mathematics: Stochastic Geometry*, Springer Verlag , Berlin Heidelberg, 2007, pp. 1–75.

[3] M. Haenggi, J. G. Andrews, F. Baccelli, O. Dousse, and M. Franceschetti, "Stochastic Geometry and Random Graphs for the Analysis and Design of Wireless Networks," *IEEE Journal on Selected Areas of Communications*, Sept. 2009.

[4] P. Cardieri, "Modeling Interference in Wireless Ad Hoc Networks," *IEEE Communications Surveys & Tutorials*, vol.12, no. 4, pp. 551–572, Fourth Quarter 2010.

[5] H. ElSawy, E. Hossain, and M. Haenggi, "Stochastic Geometry for Modeling, Analysis, and Design of Multi-tier and Cognitive Cellular Wireless Networks: A Survey," *IEEE Communications Surveys and Tutorials*, vol. 15, pp. 996–1019, July 2013

[6] M. Haenggi and R. Ganti, *Interference in Large Wireless Networks*, in *Foundations and Trends in Networking*, NOW Publishers, 2008, vol. 3, no. 2, pp. 127–248.

[7] S. Weber and J. G. Andrews, *Transmission Capacity of Wireless Networks* in *Foundations and Trends in Networking*, NOW Publishers, February 2012.

[8] M. Haenggi, *Stochastic Geometry for Wireless Networks*. Cambridge University Press, 2012.

[9] F. Baccelli and B. Blaszczyszyn, *Stochastic Geometry and Wireless Networks* in *Foundations and Trends in Networking*, Volume 1, Now Publishers, 2009.

[10] F. Baccelli and B. Blaszczyszyn, *Stochastic Geometry and Wireless Networks* in *Foundations and Trends in Networking*, Volume 2, NOW Publishers, 2009.

[11] J. Xu, J. Zhang, and J. G. Andrews, "On the Accuracy of the Wyner Model in Cellular Networks," *IEEE Transactions on Wireless Communications*, vol. 10, no. 9, pp. 3098–3109, September 2011.

[12] J. Andrews, F. Baccelli, and R. Ganti, "A Tractable Approach to Coverage and Rate in Cellular Networks," *IEEE Transactions on Communications*, vol. 59, no. 11, pp. 3122–3134 November 2011.

[13] A. Guo and M. Haenggi, "Spatial Stochastic Models and Metrics for the Structure of Base Stations in Cellular Networks," *IEEE Transactions on Wireless Communications*, accepted.

[14] L. Fu, S. C. Liew, and J. Huang, "Effective Carrier Sensing in CSMA Networks under Cumulative Interference," *IEEE Transactions on Mobile Computing*, vol. 12, no. 4, pp.748–760, April 2013.

[15] T. Lin and J.C. Hou, "Interplay of Spatial Reuse and SINR-determined Data Rates in CSMA/CA-Based, Multi-Hop, Multi-Rate Wireless Networks," in *Proc.*

26th IEEE International Conference on Computer Communications (INFOCOM'07), pp. 803–811, May 2007.

[16] T. Yang, G. Mao, and W. Zhang, "Connectivity of Large-Scale CSMA Networks," *IEEE Transactions on Wireless Communications*, vol. 11, no. 6, pp. 2266–2275, June 2012.

[17] L. Kleinrock and J. A. Silvester, "Optimum Transmission Radii for Packet Radio Networks or Why Six is a Magic Number," in Conference Record: National Telecommunication Conference, December 1978, pp. 4.3.1-4.3.5.

[18] T. Hou and V. Li, "Transmission Range Control in Multihop Packet Radio Networks," *IEEE Transactions on Communications*, vol. 34, no. 1, pp. 38–44, January 1986.

[19] R. Mathar and J. Mattfeldt, "On the Distribution of Cumulated Interference Power in Rayleigh Fading Channels," *Wireless Networks*, vol. 1, pp. 31–36, February 1995.

[20] S. Weber, J. G. Andrews and N. Jindal, "The Effect of Fading, Channel Inversion and Threshold Scheduling on Ad Hoc Networks," *IEEE Transactions on Information Theory*, vol. 53, no. 11, pp. 4127–4149, November 2007.

[21] S. Weber, X. Yang, J. G. Andrews, and G. de Veciana, "Transmission Capacity of Wireless Ad hoc Networks with Outage Constraints," *IEEE Transactions on Information Theory*, vol. 51, no. 12, pp. 4091–4102, December 2005.

[22] S. Weber, J. Andrews, X. Yang, and G. de Veciana, "Transmission Capacity of Wireless Ad Hoc Networks with Successive Interference Cancellation," *IEEE Transactions on Information Theory*, vol. 53, no. 8, pp. 2799–2814, August 2007.

[23] N. Jindal, S. Weber and J. G. Andrews, "Fractional Power Control for Decentralized Wireless Networks," *IEEE Transactions on Wireless Communications*, vol. 7, no. 12, pp. 5482–5492, December 2008.

[24] A. M. Hunter, J. G. Andrews and S. P. Weber, "Transmission Capacity of Ad Hoc Networks with Spatial Diversity," *IEEE Transactions on Wireless Communications*, vol. 7, no. 12, pp. 5058–71, December 2008.

[25] J. Venkataraman, M. Haenggi, and O. Collins, "Shot Noise Models for Outage and Throughput Analyses in Wireless Ad Hoc Networks," in Proc. of *IEEE Military Commun. Conf. (MILCOM'06)*, Washington, DC, USA, October 2006.

[26] S. Weber, J. G. Andrews, and N. Jindal, "An Overview of the Transmission Capacity of Wireless Networks," *IEEE Transactions on Communications*, vol. 58, no. 12, December 2010.

[27] J. Venkataraman, M. Haenggi, and O. Collins, "Shot Noise Models for the Dual Problems of Cooperative Coverage and Outage in Random Networks," in *Proc. 44th Annual Allerton Conf. Commun., Control, and Comput. (Allerton'06)*, Monticello, IL, USA, September 2006.

[28] E. S. Sousa, "Optimum Transmission Range in a Direct-sequence Spread Spectrum Multihop Packet Radio Network," *IEEE Journal on Selected Areas in Communications*, vol. 8, no. 5, pp. 762–771, 1990.

[29] M. Souryal, B. Vojcic and R. Pickholtz, "Ad hoc, Multihop CDMA Networks with Route Diversity in a Rayleigh Fading Channel," in *Proc. IEEE Military Commun. Conf. (MILCOM'01)* pp. 1003–1007, October 2001.

[30] H. Inaltekin, S. B. Wicker, M. Chiang, and H. V. Poor, "On Unbounded Path-loss Models: Effects of Singularity on Wireless Network Performance," *IEEE Journal on Selected Areas in Communications*, pp. 1078–1092, 2009.

[31] M. Z. Win, P. C. Pinto, and L. A. Shepp, "A Mathematical Theory of Network Interference and Its Applications," in *Proceedings of the IEEE*, vol. 97, no. 2, pp. 205–230, 2009.

[32] F. Baccelli, B. Blaszczyszyn, and P. Mühlethaler, "Stochastic Analysis of Spatial and Opportunistic ALOHA," *IEEE Journal on Selected Areas in Communications*, vol. 27, no. 7, pp. 1105–1119, September 2009.

[33] X. Zhang and M. Haenggi, "Random Power Control in Poisson Networks," *IEEE Transactions on Communications*, vol. 60, pp. 2602–2611, Sept. 2012.

[34] X. Zhang and M. Haenggi, "Delay-optimal Power Control Policies," *IEEE Transactions on Wireless Communications*, vol. 11, pp. 3518–3527, Oct. 2012.

[35] Z. Gong and M. Haenggi, "Interference and Outage in Mobile Random Networks: Expectation, Distribution, and Correlation," *IEEE Transactions on Mobile Computing*, 2012. Accepted.

[36] M. Haenggi, "On Distances in Uniformly Random Networks," *IEEE Transactions on Information Theory*, vol. 51, pp. 3584–3586, October 2005.

[37] S. Srinivasa and M. Haenggi, "Modeling Interference in Finite Uniformly Random Networks," in *International Workshop on Information Theory for Sensor Networks (WITS 2007)*, Santa Fe, NM, June 2007.

[38] S. Srinivasa and M. Haenggi, "Distance Distributions in Finite Uniformly Random Networks: Theory and Applications," *IEEE Transactions on Vehicular Technology*, vol. 59, pp. 940–949, February 2010.

[39] R. K. Ganti and M. Haenggi, "Interference and Outage in Clustered Wireless Ad Hoc Networks," *IEEE Transactions on Information Theory*, vol. 55, pp. 4067–4086, September 2009.

[40] H. Nguyen, F. Baccelli, and D. Kofman, "A Stochastic Geometry Analysis of Dense IEEE 802.11 Networks," in *Proc. 26th IEEE International Conference on Computer Communications (INFOCOM'07)*, May 2007, pp. 1199–1207.

[41] G. Alfano, M. Garetto, and E. Leonardi, "New Insights into the Stochastic Geometry Analysis of Dense CSMA Networks," in *Proc. 30th Annual IEEE International Conference on Computer Communications (INFOCOM'11)*, April 2011, pp. 2642–2650.

[42] Y. Kim, F. Baccelli, and G. de Veciana, "Spatial Reuse and Fairness of Mobile Ad-hoc Networks with Channel-aware CSMA Protocols," in *Proc. 17th Workshop on Spatial Stochastic Models for Wireless Networks*, May 2011.

[43] A. Hasan and J. G. Andrews, "The Guard Zone in Wireless Ad hoc Networks," *IEEE Transactions on Wireless Communications*, vol. 4, no. 3, pp. 897–906, March 2007.

[44] M. Kaynia, N. Jindal, and G. Oien, "Improving the Performance of Wireless Ad hoc Networks through MAC Layer Design," *IEEE Transactions on Wireless Communications*, vol. 10, no. 1, pp. 240–252, January 2011.

[45] H. ElSawy and E. Hossain, "A Modified Hard Core Point Process for Analysis of Random CSMA Wireless Networks in General Fading Environments," *IEEE Transactions on Communications*, accepted.

[46] H. ElSawy, E. Hossain, and S. Camorlinga, "Spectrum-efficient Multi-channel Design for Coexisting IEEE 802.15.4 Networks: A Stochastic Geometry Approach," submitted to the *IEEE Transactions on Mobile Computing*.

[47] H. ElSawy, E. Hossain, and S. Camorlinga, "Multi-channel Design for Random CSMA Wireless Networks: Stochastic Geometry Approach," in Proc. *IEEE Int. Conference on Communications (ICC'13)*, Budapest, Hungary, 9-13 June, 2013.

[48] P. Mühlethaler and A. Najid, "Throughput Optimization of a Multihop CSMA Mobile Ad hoc Network," INRIA, Research Report 4928, September 2003.

[49] M. Haenggi, "Mean Interference in Hard-core Wireless Networks," *IEEE Communications Letters*, vol. 15, pp. 792–794, August 2011.

[50] H. ElSawy and E. Hossain, "Modeling Random CSMA Wireless Networks in General Fading Environments," in *Proc. IEEE Int. Conf. on Communications (ICC 2012)*, Ottawa, Canada, 10-15 June 2012.

[51] H. ElSawy, E. Hossain, and S. Camorlinga, "Characterizing Random CSMA Wireless Networks: A Stochastic Geometry Approach," in *Proc. IEEE Int. Conf. on Communications (ICC 2012)*, Ottawa, Canada, 10-15 June 2012.

[52] F. Baccelli, M. Klein, M. Lebourges, and S. Zuyev, "Stochastic Geometry and Architecture of Communication Networks," *Journal of Telecommunication Systems*, vol. 7, no. 1, pp. 209–227, 1997.

[53] T. X. Brown, "Cellular Performance Bounds via Shotgun Cellular Systems," *IEEE Journal on Selected Areas in Communications*, vol. 18, no. 11, Nov. 2000, pp. 2443–2455.

[54] H. Dhillon, R. Ganti, F. Baccelli, and J. Andrews, "Modeling and Analysis of K-Tier Downlink Heterogeneous Cellular Networks," *IEEE Journal on Sel. Areas in Comm.*, vol. 30, no. 3, pp. 550–560, April 2012.

[55] S. Singh, H. S. Dhillon, and J. G. Andrews, "Offloading in Heterogeneous Networks: Modeling, Analysis, and Design Insights," *IEEE Transactions on Wireless Communications*, accepted.

[56] H. Dhillon, T. Novlan, J. Andrews, "Coverage Probability of Uplink Cellular Networks," in *Proc. IEEE Global Communications Conference (Globecom 2012)*, 3-7 December, Anaheim, CA, USA, 2012.

[57] H. S. Dhillon, R. K. Ganti and J. G. Andrews, "Load-Aware Modeling and Analysis of Heterogeneous Cellular Networks", *IEEE Transactions on Wireless Communications*, vol. 12, no. 4, April 2013.

[58] H. Jo, Y. Sang, P. Xia, and J. Andrews, "Outage Probability for Heterogeneous Cellular Networks with Biased Cell Association," in *Proc. IEEE Global Communications Conference (Globecom 2011)*, 5-9 December, Houston, TX, USA, 2011.

[59] H. Jo, Y. Sang, P. Xia, and J. Andrews, "Heterogeneous Cellular Networks With Flexible Cell Association: A Comprehensive Downlink SINR Analysis," *IEEE Transactions on Wireless Communications*, vol. 11, no. 9, pp. 3484–3495, October 2012.

[60] H. ElSawy, E. Hossain, and S. Camorlinga, "Offloading Techniques in Two-tier Femtocell Networks," in *Proc. IEEE Int. Conference on Communications (ICC'13)*, Budapest, Hungary, 9-13 June 2013.

[61] T. Novlan, R. Ganti, A. Ghosh, and J. Andrews, "Analytical Evaluation of Fractional Frequency Reuse for OFDMA Cellular Networks," *IEEE Transactions on Wireless Communications*, vol. 10, no. 12, pp. 4294–4305, December 2011.

[62] T. Novlan, R. Ganti, A. Ghosh, and J. Andrews, "Analytical Evaluation of Fractional Frequency Reuse for Heterogeneous Cellular Networks," *IEEE Transactions on Communications*, vol. 60, no. 7, pp. 2029–2039, July 2012.

[63] D. Cao, S. Zhou, and Z. Niu, "Optimal Base Station Density for Energy-efficient Heterogeneous Cellular Networks," in *Proc. IEEE Int. Conf. on Communications (ICC 2012)*, Ottawa, Canada, 10-15 June 2012.

[64] Y. Zhong and W. Zhang, "Downlink Analysis of Multi-channel Hybrid Access Two-tier Networks," in *Proc. IEEE Int. Conf. on Communications (ICC 2012)*, Ottawa, Canada, 10-15 June 2012.

[65] S. Mukherjee, "Distribution of Downlink SINR in Heterogeneous Cellular Networks," *IEEE Journal on Sel. Areas in Comm.*, vol. 30, no. 3, pp. 575–585, April 2012.

[66] V. Chandrasekhar and J. Andrews, "Spectrum Allocation in Tiered Cellular Networks," *IEEE Transactions on Communications*, vol. 57, no. 10, pp. 3059–3068, October 2009.

[67] W. Cheung, T. Quek, and M. Kountouris, "Throughput Optimization, Spectrum Allocation, and Access Control in Two-tier Femtocell Networks," *IEEE Journal on Sel. Areas in Comm.*, vol. 30, no. 3, pp. 561–574, April 2012.

[68] K. Huang, V. Lau, and Y. Chen, "Spectrum Sharing between Cellular and Mobile Ad Hoc Networks: Transmission-capacity Tradeoff," *IEEE Journal on Sel. Areas in Comm.*, vol. 27, no. 7, pp. 1256–1266, September 2009.

[69] V. Chandrasekhar and J. Andrews, "Uplink Capacity and Interference Avoidance for Two-tier Femtocell Networks," *IEEE Transactions on Wireless Communications*, vol. 8, no. 7, pp. 3498–3509, July 2009.

[70] P. Pinto, A. Giorgetti, M. Win, and M. Chiani, "A Stochastic Geometry Approach to Coexistence in Heterogeneous Wireless Networks," *IEEE Journal on Sel. Areas in Comm.*, vol. 27, no. 7, pp. 1268–1282, September 2009.

[71] A. Guidotti, M. Di Renzo, G. Corazza, and F. Santucci, "Simplified Expression of the Average Rate of Cellular Networks Using Stochastic Geometry," in *Proc. IEEE Int. Conf. on Communications (ICC 2012)*, Ottawa, Canada, 10-15 June 2012.

[72] R. W. Heath, M. Kountouris, "Modeling heterogeneous network interference," in *Proc. Information Theory and Applications Workshop (ITA)*, pp.17–22, 5-10 Feb. 2012

[73] H. Dhillon, M. Kountouris, J. Andrews, "Downlink Coverage Probability in MIMO HetNets," in *Proc.* 46^{th} *Annual Asilomar Conference on Signals, Systems, and Computers*, 4-7 November, Pacific Grove, CA, USA, 2012.

[74] R. W. Heath, M. Kountouris, and T. Bai, "Modeling Heterogeneous Network Interference With Using Poisson Point Processes," submitted to *IEEE Trans. on Signal Processing*, July 2012. Available Online: (http://arxiv.org/abs/1207.2041).

[75] C. Lima, M. Bennis, and M. Latva-aho, "Coordination Mechanisms for Self-Organizing Femtocells in Two-Tier Coexistence Scenarios," *IEEE Transactions on Wireless Communications*, vol. 11, no. 6, pp. 2212–2223, June 2012.

[76] H. ElSawy and E. Hossain, "Two-Tier HetNets with Cognitive Femtocells: Downlink Performance Modeling and Analysis in a Multi-Channel Environment," *IEEE Transactions on Mobile Computing*, accepted.

[77] H. ElSawy and E. Hossain, "On Cognitive Small Cells in Two-tier Heterogeneous Networks," in *Proc.* 9^{th} *Workshop on Spatial Stochastic Models for Wireless Networks (SpaSWiN 2013)*, Tsukuba Science City, Japan, May 13-17, 2013.

[78] H. ElSawy, E. Hossain, and D. I. Kim, "HetNets with Cognitive Small Cells: User Offloading and Distributed Channel Allocation Techniques," *IEEE Communications Magazine*, Special Issue on "Heterogeneous and Small Cell Networks (HetSNets)," vol. 51, no. 6, pp. 28–36, June 2013.

[79] H. ElSawy and E. Hossain, "Channel Assignment and Opportunistic Spectrum Access in Two-tier Cellular Networks with Cognitive Small Cells," submitted to *IEEE Global Communications Conference (Globecom 2013)*, Atlanta, GA, USA, 9-13 December 2013.

[80] M. Khoshkholgh, K. Navaie, and H. Yanikomeroglu, "Outage Performance of the Primary Service in Spectrum Sharing Networks," *IEEE Transactions on Mobile Computing*, accepted, 2012.

[81] A. Ghasemi and E. Sousa, "Interference Aggregation in Spectrum Sensing Cognitive Wireless Networks," *IEEE J. on Sel. Topics in Signal Processing*, vol. 2, no. 1, pp. 41–56, February 2008.

[82] C.-H. Lee and M. Haenggi, "Interference and Outage in Poisson Cognitive Networks," *IEEE Transactions on Wireless Communications*, vol. 11, pp. 1392–1401, April 2012.

[83] A. Rabbachin, T. Q. S. Quek, H. Shin, and M. Z. Win, "Cognitive Network Interference," *IEEE Journal on Sel. Areas in Comm.*, vol. 29, no. 2, pp. 480–493, February 2011.

[84] T. Nguyen and F. Baccelli, "A Probabilistic Model of Carrier Sensing Based Cognitive Radio," in *Proc. IEEE Symposium on New Frontiers in Dynamic Spectrum Access Networks*, pp. 1–12, April 2010.

[85] T. Nguyen and F. Baccelli, "Stochastic Modeling of Carrier Sensing Based Cognitive Radio Networks," in *Proc. 8th International Symposium on Modeling and Optimization in Mobile, Ad Hoc and Wireless Networks (WiOpt)*, pp. 472–480, June 2010.

[86] J. Møller, M. L. Huber, and R. L. Wolpert, "Perfect Simulation and Moment Properties for the Matérn Type III Process," *Stochastic Processes and Their Applications*, vol. 120, no. 11, November 2010, pp. 2142–2158.

[87] M. L. Huber and R. L. Wolpert, "Likelihood Based Inference for Matérn Type III Repulsive Point Processes," *Advances in Applied Probability*, vol. 41, no. 4, 2009, pp. 958–977.

[88] R. K. Ganti, J. G. Andrews, and M. Haenggi, "High-SIR Transmission Capacity of Wireless Networks with General Fading and Node Distribution," *IEEE Transactions on Information Theory*, vol. 57, pp. 3100–3116, May 2011.

[89] R. Giacomelli, R. K. Ganti, and M. Haenggi, "Outage Probability of General Ad Hoc Networks in the High-reliability Regime," *IEEE/ACM Transactions on Networking*, vol. 19, pp. 1151–1163, August 2011.

[90] P. Brémaud, *Mathematical Principles of Signal Processing: Fourier and Wavelet Analysis*. Springer, 2002.

[91] A. Goldsmith, *Wireless Communications*. Cambridge University Press, 2005.

[92] F. Baccelli, J. Li, T. Richardson, S. Shakkottai, S. Subramanian, and X. Wu, "On Optimizing CSMA for Wide Area Ad Hoc Networks," in *Proc. IEEE Int. Symp. on Modeling and Optimization in Mobile, Ad Hoc and Wireless Networks (WiOpt)*, pp. 354–359, 9-13 May 2011.

[93] A. Ghasemi and E. S. Sousa, "Fundamental Limits of Spectrum-sharing in Fading Environments," *IEEE Transactions on Wireless Communications*, vol. 6, no. 2, pp. 649–658, February 2007.

[94] IEEE Std 802.15.4-2003, Part 15.4, "Wireless Medium Access Control (MAC) and Physical Layer (PHY) Specification for Low Rate Wireless Personal Area Networks (LR-WPANs)," IEEE, December 2003.

[95] A. Elahi and A. Gschwender, *ZigBee Wireless Sensor and Control Network*. ISBN: 978-0-13-713485-4, Prentice Hall, 2010.

[96] A. Sikora and V. F. Groza, "Coexistence of IEEE802.15.4 with other Systems in the 2.4 GHz ISM Band," in *Proc. IEEE Instrumentation and Measurement Technology Conference (IMTC'05)*, vol. 3, pp. 1786–1791, 16-19 May 2005.

[97] S. Shin, H. Park, S. Choi, and W. Kwon, "Packet Error Rate Analysis of ZigBee under WLAN and Bluetooth Interferences," *IEEE Transactions on Wireless Communications*, vol. 6, no. 8, pp. 2825–2830, August 2007.

[98] M. Petrova, W. Lili, P. Mahonen, and J. Riihijarvi, "Interference Measurements on Performance Degradation Between Colocated IEEE 802.11g/n and IEEE 802.15.4 networks," in *Proc. IEEE Sixth Int. Conf. on Networking (ICN '07)*, April 2007.

[99] J. Huang, G. Xing, G. Zhou, and R. Zhou, "Beyond Co-existence: Exploiting WiFi White Space for ZigBee Performance Assurance," in *Proc. 18th IEEE Int. Conf. on Network Protocols (ICNP 2010)* pp.305–314, 5-8 October 2010

[100] H. ElSawy, E. Hossain, and S. Camorlinga, "A Distributed Spectrum Sharing Method for Improving Coexistence of IEEE 802.15.4 Networks," in *Proc. IEEE Global Communications Conference (Globecom 2011)*, 5-9 December, Houston, TX, USA, 2011.

[101] T. Kim, J. Ha, and S. Choi, "Improving Spectral and Temporal Efficiency of Collocated IEEE 802.15.4 LR-WPANs," *IEEE Transactions on Mobile Computing*, vol. 8, no. 12, pp. 1596–1609, December 2009.

[102] T. Kim, H. Lim, and J. Hou, "Improving Spatial Reuse through Tuning Transmit Power, Carrier Sense Threshold, and Data Rate in Multihop Wireless Net-

works," in *Proc. IEEE international conference on Mobile Computing and networking (MobiCom)*, September 2006.

[103] S. B. Lowen and M. C. Teich, "Power-law Shot Noise," *IEEE Transactions on Information Theory*, vol. 36, no. 6, pp. 1302–1318, 1990.

[104] D. Williamson and D. Shmoys, *The Design of Approximation Algorithms*. Cambridge University Press, 2011.

[105] H. Ma, R. Vijayakumar, S. Roy, and J. Zhu, "Optimizing 802.11 Wireless Mesh Networks Based on Physical Carrier Sensing," *IEEE Transactions on Networking*, vol. 17, no. 5, pp. 1550–1563, October 2009.

[106] J. Mo, H. -S. W. So, and J. Walrand, "Comparison of Multichannel MAC Protocols," *IEEE Transactions on Mobile Computing*, vol. 7, no. 1, pp. 50–65, January 2008.

[107] V. Bhandari and N. Vaidya, "Scheduling in Multi-channel Wireless Networks," in *Proc. IEEE International Conference on Distributed Computing and Networking (ICDCN)*, Kolkata, India, January 2010.

[108] Y. Shobowale and K. A. Hamdi, "A Unified Model for Interference Analysis in Unlicensed Frequency Bands," *IEEE Transactions on Wireless Communications*, vol. 8 no. 8, pp. 4004–4013, August 2009.

[109] S. Cheng, S. Lien, F. hu, and K. Chen, "On Exploiting Cognitive Radio to Mitigate Interference in Macro/Femto Heterogeneous Networks," *IEEE Wireless Commun. Mag*, vol. 18, no. 3, pp. 40–47, June 2011.

[110] J. Andrews, H. Claussen, M. Dohler, S. Rangan, and M. Reed, "Femtocells: Past, Present, and Future," *IEEE Journal on Sel. Areas in Comm.*, vol, 30 no. 3 pp. 497–508, April 2012.

[111] S. Nai and T. Quek, "Coexistence in Two-tier Femtocell Networks: Cognition and Optimization," in Proc. of *IEEE Int. Conf. Computing, Networking, and Commun.*, Maui, HA, January 2012, pp. 655–659.

[112] K. Gilhousen, I. Jacobs, R. Padovani, A. J. Viterbi, L. Weaver, and C. Wheatley, "On the Capacity of a Cellular CDMA System," *IEEE Trans. on Veh. Technology*, vol. 40, no. 2, pp. 303–312, May 1991.

[113] Y. Li, M. Macucha, E. Sousa, T. Sato, and M. Nanri, "Cognitive Interference Management in 3G Femtocells," in Proc. of *IEEE 20th Int. Symp. on Personal, Indoor and Mobile Radio Communications (PIMRC 2009)*, 13-16 September, Tokyo, Japan, 2009

[114] S. Lien, C. Tseng, K. Chen, and C. Su, "Cognitive Radio Resource Management for QoS Guarantees in Autonomous Femtocell Networks," in Proc. of *IEEE Int. Conf. on Communications (ICC 2010)*, 23-27 May, Cape Town, South Africa, 2010

[115] I. Demirdogen, I. Guvenc, and H. Arslan, "Capacity of Closed-Access Femtocells Networks with Dynamic Spectrum Reuse," in Proc. of *IEEE 21st Int. Symp. on Personal, Indoor and Mobile Radio Communications (PIMRC 2010)*, 26-29 September, Istanbul, Turkey, 2010

[116] R. Urgaonkar and M. Neely, "Opportunistic Cooperation in Cognitive Femtocell Networks," *IEEE Journal on Sel. Areas in Comm.*, vol. 30, no. 3, pp. 607–616, April 2012.

[117] A. Okabe, B. Boots, and K. Sugihara, *Spatial Tessellations: Concepts and Applications of Voronoi Diagrams*. John Wiley, 1992.

[118] K. Hamdi, "A Useful Lemma for Capacity Analysis of Fading Interference Channels," *IEEE Transactions on Communications*, vol. 58, no. 2, pp. 411–416, February 2010.

[119] B. Blaszczyszyn, M. K. Karray, and H.-P. Keeler, "Using Poisson Processes to Model Lattice Cellular Networks," in *Proc. 32th Annual IEEE International Conference on Computer Communications (INFOCOM'13)*, Turin, Italy, April 14-19, 2013.

[120] M. Chiang, P. Hande, T. Lan, and C. W. Tanet, "Power Control in Wireless Cellular Networks," in Foundations and Trends in Networking. NOW Publishers, April 2008.

[121] T. Novlan, H. Dhillon, and J. G. Andrews, "Analytical Modeling of Uplink Cellular Networks," *IEEE Transactions on Wireless Communications*, accepted.

[122] X. Lin, J. G. Andrews and A. Ghosh, "A Comprehensive Framework for Device-to-Device Communications in Cellular Networks," submitted to *IEEE Journal on Selected Areas of Communications*, May 2013, Available at: http://users.ece.utexas.edu/∼jandrews/publications.php.

[123] H. Tabassum, F. Yilmaz, Z. Dawy, and M. Alouini, "A Statistical Model of Uplink Inter-cell Interference with Slow and Fast Power Control Mechanisms," *IEEE Transactions on Communications*, accepted.

[124] J. G. Andrews, "Seven Ways that HetNets are a Cellular Paradigm Shift," *IEEE Communications Magazine*, vol. 51, no. 3, pp. 136–144, March 2013.

[125] H. Holma, A. Toskala, *LTE Advanced: 3GPP Solution for IMT Advanced*. Wiley, 2012.

[126] M. Wildemeersch, T. Q. S. Quek, M. Kountouris, and C. H. Slump, "Successive Interference Cancellation in Uplink Cellular Networks," in *Proc. IEEE International Workshop on Signal Processing Advances for Wireless Communications (SPAWC)*, Darmstadt, Germany, June 2013.

[127] N. Saquib, E. Hossain, L. B. Le, and D. I. Kim, "Interference Management in OFDMA Femtocell Networks: Issues and Approaches," *IEEE Wireless Communications*, vol. 19, no. 3, pp. 86–95, June 2012.

[128] D. Taylor, H. Dhillon, T. Novlan, and J. Andrews, "Pairwise Interaction Processes for Modeling Cellular Network Topology," in *Proc. IEEE Global Communications Conference (Globecom 2012)*, 3-7 December, Anaheim, CA, USA, 2012.

[129] R. Ganti, F. Baccelli, and J. Andrews, "Series Expansion for Interference in Wireless Networks," *IEEE Transactions on Information Theory*, vol. 58, no. 4, pp. 2194–2205, April 2012.

[130] B. Blaszczyszyn, "Factorial Moment Expansion for Stochastic Systems," *Stochastic Processes and Their Applications*. vol. 56, no. 2, pp. 321–335, 1995.

[131] K. Stamatiou and M. Haenggi, "Random-Access Poisson Networks: Stability and Delay," *IEEE Communications Letters*, vol. 14, pp. 1035-1037, November 2010.

[132] K. Stamatiou and M. Haenggi, "Delay Characterization of Multihop Transmission in a Poisson Field of Interference," *IEEE/ACM Transactions on Networking*, accepted.

Appendix A

A.1 Deriving the distribution of $|\mathbf{N}|$

Let $\mathbf{N}_{x_i} = \{x_j \in \mathbf{\Psi}_T \setminus x_i | A h_j \|x_i - x_j\|^{-\eta} \geq \upsilon\}$ be the set of neighbor nodes to a generic transmitter x_i, where $h_j = h(x_i, x_j)$, where h_j are i.i.d corresponding to channel gain between a transmitter $x_j \in \mathbf{\Psi}_T$ and the test transmitter x_i, and $h_j \sim Gamma(m, k)$. We are interested to calculate the *pmf* of the number of neighbors $|\mathbf{N}_{x_i}|$. Without loss of generality, I will condition on having x_i at the origin (Slivnyak's theorem [1]). For notational simplicity, hereafter I will use $\mathbf{N}$ to denote $\mathbf{N}_{x_i}$ (i.e., index x_i is dropped) because, by Slivnyak's theorem, the results hold for any generic $x_i \in \mathbf{\Psi}_T$. A node $x_j \in \mathbf{\Psi}_T$ is a neighbor to $x_i = (0, 0)$ if and only if $A h_j \|x_j\|^{-\eta} \geq \upsilon_s$. Due to the random variable h_j, I cannot determine a regular shaped region that contains the neighbors set $\mathbf{N}$. However, if I limit my observation area to $\mathbf{B}_{x_i}(r_d)$ (where r_d sufficiently large), I can characterize $\mathbf{N}$ very accurately.

Let $\tilde{\mathbf{N}} = \mathbf{N} \cap \mathbf{B}_{x_i}(r_d)$ denote the set of neighbors of x_i within the observation area $\mathbf{B}_{x_i}(r_d)$. Due to the infinite support range of the gamma distribution, $\tilde{\mathbf{N}} \subseteq \mathbf{N}$. However, if r_d is sufficiently large, for any realization of the point process, the probability that $|\tilde{\mathbf{N}}| < |\mathbf{N}|$ will be negligible (i.e., $\mathbb{P}\left\{\frac{P_t A h_j}{\|x_j\|^{\eta}} \geq \upsilon_s | \, \|x_j\| > r_d\right\} \approx 0$). One way to choose r_d is to use a small number $\epsilon = 10^{-6}$ and then choose r_d such that

$r_d = \left(\frac{P_t A}{\upsilon_s}\bar{F}_h^{-1}(\epsilon)\right)^{1/\eta}$. Let $\mathcal{P}_{\upsilon_s} = \mathbb{P}\{Ah_j \left\|x_j\right\|^{-\eta} \geq \upsilon_s\}$ be the probability that a generic node $x_j \in \{\mathbf{\Psi}_T \cap \mathbf{B}_{x_i}(r_d)\}$ is a neighbor to $x_i = (0,0)$. Let $P_k = \frac{(\lambda\pi r_d^2)^k e^{-\lambda\pi r_d^2}}{k!} = \frac{\mathcal{N}e^{-\mathcal{N}^k}}{k!}$, then the *pmf* of $\tilde{\mathbf{N}}$ is given by:

$$\begin{aligned}
\mathbb{P}\{|\tilde{\mathbf{N}}| = n\} &= \sum_{k=n}^{\infty} P_k \binom{k}{n} \mathcal{P}_{\upsilon_s}^n (1-\mathcal{P}_{\upsilon_s})^{k-n} \\
&= \frac{\mathcal{P}_{\upsilon_s}^n e^{-\mathcal{N}}}{n!} \sum_{k=n}^{\infty} \frac{\mathcal{N}^k}{k-n!} (1-\mathcal{P}_{\upsilon_s})^{k-n} \\
&= \frac{(\mathcal{N}\mathcal{P}_{\upsilon_s})^n e^{-\mathcal{N}}}{n!} \sum_{m=0}^{\infty} \frac{(1-\mathcal{P}_{\upsilon_s})\mathcal{N}^m}{m!} \\
&= \frac{(\mathcal{N}\mathcal{P}_{\upsilon_s})^n e^{-\mathcal{N}\mathcal{P}_{\upsilon_s}}}{n!}
\end{aligned} \tag{A.1}$$

where $\binom{k}{n}\mathcal{P}_{\upsilon_s}^n(1-\mathcal{P}_{\upsilon_s})^{k-n}$ in the first equality means that out of the k coexisting nodes in $\mathbf{B}_{x_i}(r_d)$, only n of them satisfy the neighborhood requirement (i.e., have sufficiently high channel gain to keep the received power at x_i greater than the carrier-sensing threshold υ_s). Equation (A.1) shows that $|\tilde{\mathbf{N}}|$ has a Poisson distribution with the mean $\mathcal{N}\mathcal{P}_{\upsilon}$.

The probability $\mathcal{P}_{\upsilon}$ is the *neighborhood success probability* between $x_i = (0,0)$ and $x_j \in \mathbf{\Psi}_T \cap \mathbf{B}_{x_i}(r_d)$. Let the random variable z denote the random distance between point $x_i = (0,0)$ and any other point existing in $\mathbf{B}_{x_i}(r_d)$. The probability $\mathcal{P}_{\upsilon}$ is governed by a relation between two random variables, namely, the random channel gain (h) and the random distance (z) between the two points. Following the PPP definition, the locations of the points are independent and uniformly distributed across the area of interest. Using this fact, the distribution of the random distance z can be obtained as $f_z(z) = \frac{2z}{r_d^2}$, $0 \leq z \leq r_d$ [28].

First, I condition on the distance between the two nodes under consideration (i.e., conditioning on that $\|x_j\| = r$) to obtain the expression for their *neighborhood*

success probability, which is in fact the complementary *cdf* of the channel gain (i.e., $1-F_g(\frac{\upsilon_s r^\eta}{P_t A})$). Then, removing the condition on the random distance, the unconditional *neighborhood success probability* is obtained as follows:

$$\mathcal{P}_{\upsilon_s} = \int_0^{r_d} \frac{2z}{r_d^2} \left(1 - F_h\left(\frac{\upsilon_s z^\eta}{P_t A}\right)\right) dz = \int_0^{r_d} \frac{2z}{r_d^2} \frac{\Gamma_u(k, \frac{\upsilon_s z^\eta}{s P_t A})}{\Gamma(k)} dz. \tag{A.2}$$

Now I will perform an **exact analysis** for the distribution of $|\mathbf{N}|$. We will condition on having the test transmitter at the origin (i.e., $x_i = (0,0)$), and by using Slivnyak's theorem, the results will hold for a generic FAPs [1]. A transmitter $x_j \in \mathbf{\Psi}_T$ is inside the neighborhood domain of x_i if and only if $\{A h_j \left\|x_j\right\|^{-\eta} > \upsilon_s\}$, where h_j are i.i.d. indicating the random channel gain (small scale fading) associated with each transmitter x_j (note that h_j is also independent from the location x_j). Hence, the random variable $|\mathbf{N}|$ can be expressed as a sum of indicator functions as follows:

$$|\mathbf{N}| = \sum_{x_j \in \mathbf{\Psi}_T \setminus x_i} \mathbb{1}\{A h_j \left\|x_j\right\|^{-\eta} > \upsilon_s\}. \tag{A.3}$$

Since the distribution of a random variable is uniquely characterized by its moment generating function, I will derive the moment generating function of $|\mathbf{N}|$ to infer its

distribution. The moment generating function of $|\mathbf{N}|$ can be expressed as

$$\begin{aligned}
\mathbb{E}\left[e^{t|\mathbf{N}|}\right] &= \mathbb{E}\left[e^{t\sum\limits_{x_j\in\Psi_T}\mathbb{1}\{Ah_j\|x_j\|^{-\eta}>\upsilon_s\}}\right] \\
&= \mathbb{E}_{\Psi}\left[\prod_{x_j\in\Psi_T}\mathbb{E}_{h_j}\left[e^{\mathbb{1}\{Ah_j\|x_j\|^{-\eta}>\upsilon_s\}}\right]\right] \\
&\overset{(i)}{=} \exp\left\{-\mathbb{E}_h\left[\int_0^{2\pi}\int_0^{\left(\frac{Ah}{\upsilon_s}\right)^{\frac{1}{\eta}}}(1-e^t)\lambda r dr d\theta\right\}\right] \\
&\overset{(ii)}{=} \exp\left\{-\int_{-\infty}^{\infty}\pi\lambda_T\left(\frac{Ah}{\upsilon_s}\right)^{\frac{2}{\eta}}(1-e^t)f_h(h)dh\right\} \\
&= \exp\left\{-\int_0^{\infty}\pi\lambda_T\left(\frac{Ah}{\upsilon_s}\right)^{\frac{2}{\eta}}(1-e^t)\frac{h^{k-1}e^{-x/s}}{s^k\upsilon(k)}dh\right\} \\
&= \exp\left\{(e^t-1)\pi\lambda_T\left(\frac{As}{\upsilon_s}\right)^{\frac{2}{\eta}}\frac{\Gamma(k+\frac{2}{\eta})}{\upsilon(k)}\right\} \qquad \text{(A.4)}
\end{aligned}$$

where $\mathbb{E}_{\mathbf{\Psi}_T}[.]$ is the expectation w.r.t. the point process $\mathbf{\Psi}_T$ and $\mathbb{E}_{h_j}[.]$ is the expectation w.r.t. the channel gain h_j. The equality in (i) is due to the probability generating functional of the PPP and switching the order of the integration and the expectation [6]. Differentiating (A.4) and equating to zero, the first moment of $|\mathbf{N}|$ is obtained as $\mathbb{E}[|\mathbf{N}|] = \pi\lambda_T\left(\frac{As}{\upsilon_s}\right)^{\frac{2}{\eta}}\upsilon(1+\frac{2}{\eta})$. Hence, the moment generating function of $|\mathbf{N}|$ is in the form $\mathbb{E}\left[e^{t|N|}\right] = \exp\left\{(e^t-1)\mathbb{E}[|\mathbf{N}|]\right\}$ which is the moment generating function of the Poisson distribution. Note that from (ii), since $(\eta > 2)$, the only condition required to hold in order to have a finite mean number of nodes (i.e., finite mean for $|\mathbf{N}|$) is to have the finite first moment for g.

Fig. 1 shows the effect of the bounding approach on my model. To see the rate of decay of ϵ with the distance r I plot Fig. 3.9(a). The figure shows that the value of r_d which gives $\epsilon = 10^{-6}$ will be different for different fading and path-loss conditions. However, the probability to have a neighbor transmitter beyond r_d decays

very rapidly. To show that the bounding approach used in the analysis is exact, I compare the exact and the approximated probability mass functions (*pmf*s) of the number of transmitters in the neighborhood domain of a generic transmitter. We observe in Fig. 3.9(b) that the *pmf* obtained via the bounding approach matches exactly with the actual *pmf*.

A.2 Analysis for (a) and (b) in P_{in} and P_{out}

Both (a) in P_{in} and (b) in P_{out} have the following form:

$$P = \frac{ye^{-(x+y)}}{x}\left(\underbrace{\sum_{n=1}^{\infty}\frac{x^{n+1}}{(n+1)!}\sum_{t=1}^{\infty}\left(\frac{1}{n+t+1}\right)\frac{y^{t-1}}{(t-1)!}}_{S}\right)$$

where $x = \mathcal{N}\mathcal{P}_v$, $y = \mathcal{N}\mathcal{P}_v^*(1-\mathcal{P}_v)$ for (a) in P_{in}, while $y = \mathcal{N}\mathcal{P}_v^{**}$ for (b) in P_{out}. Then

$$
\begin{aligned}
S &= \sum_{n=1}^{\infty} \frac{x^{n+1}}{(n+1)!} \sum_{t=1}^{\infty} \left(\frac{1}{n+t+1} \right) \frac{y^{t-1}}{(t-1)!} \\
&= \sum_{t=1}^{\infty} \frac{y^{t-1}}{(t-1)!} \sum_{n=1}^{\infty} \left(\frac{1}{n+t+1} \right) \frac{x^{n+1}}{(n+1)!} \\
&= \sum_{t=1}^{\infty} \frac{y^{t-1}}{(t-1)!} \left(\frac{-x}{t+1} + \frac{e^x \left(\sum_{m=0}^{t} (-1)^m x^{t-m} \frac{(t-1)!}{(t-m-1)!} \right) + (-1)^t (t-1)!}{x^t} - \frac{1}{t} \right) \\
&= (-x) \sum_{t=1}^{\infty} \frac{y^{t-1}}{(t+1)(t-1)!} + \frac{e^x}{y} \sum_{t=1}^{\infty} \sum_{m=0}^{t-1} \frac{(-1)^m x^{t-m-1} \left(\frac{y}{x}\right)^t}{(t-m-1)!} \\
&+ \frac{1}{y} \sum_{t=1}^{\infty} \left(\frac{-y}{x} \right)^t - \frac{1}{y} \sum_{t=1}^{\infty} \frac{y^t}{t!} \\
&= \frac{x\left(-1 - e^y(y-1)\right)}{y^2} + \frac{e^x}{y} \sum_{t=1}^{\infty} \sum_{m=0}^{t-1} \frac{(-1)^m x^{t-m-1} \left(\frac{y}{x}\right)^t}{(t-m-1)!} - \frac{1}{x+y} - \frac{(e^y-1)}{y} \\
&= \frac{x\left(-1 - e^y(y-1)\right)}{y^2} + \frac{e^{x+y}}{x+y} - \frac{1}{x+y} - \frac{e^y-1}{y} \\
&= \frac{e^{x+y}-1}{x+y} + \frac{(y-x)(1-e^y) - xye^y}{y^2}.
\end{aligned}
$$

Substituting back in P I have

$$
\begin{aligned}
P &= \frac{ye^{-(x+y)}}{x} \left(\frac{e^{x+y}-1}{x+y} + \frac{(y-x)(1-e^y) - xye^y}{y^2} \right) \\
&= \frac{y\left(1-e^{-(x+y)}\right)}{x(x+y)} + e^{-x} \left(\frac{(y-x)(e^{-y}-1)}{xy} - 1 \right).
\end{aligned}
$$

A.3 The distribution of the random distance w

In this section, the distribution of the random distance (w) between two of x_i's neighbors (as shown in Fig. A.1) is calculated. As both x_L and x_j are neighbors of the

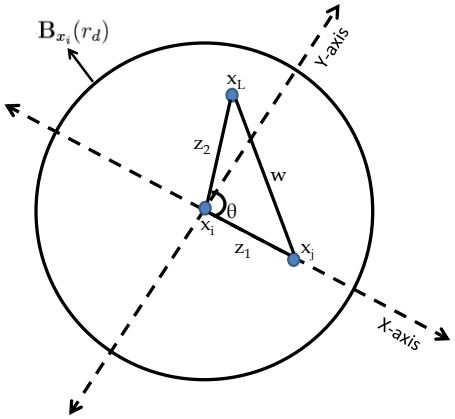

Figure A.1: The distribution of x_i's potential neighbors around x_L given that x_i and x_L are neighbors.

point x_i, both random distances z_1 and z_2 have the same distribution $f_z(z) = \frac{2z}{r_d^2}$, where $0 \leq z \leq r_d$, and the angle θ is uniformly distributed with the *pdf*, $f_\theta(\theta) = \frac{1}{\pi}$, where $0 \leq \theta \leq \pi$. In order to tackle this problem, I will convert the coordinate system from the polar coordinates to the Cartesian coordinates. Let x_i be the origin of the Cartesian coordinate and z_1 lie on the positive side of the x-axis such that the point x_j will always be on the positive side of the y-axis. Then, x_j will always have the coordinates $(a_1, 0)$, where $a_1 = \|x_i - x_j\|$ is a random variable which has the same distribution of z_1 given by $f_{a_1} = \frac{2a_1}{r_d^2}$, $0 \leq a_1 \leq r_d$. The point x_L will have the coordinates (a_2, b_2), where $a_2 = z_2 \cos(\theta)$ and $b_2 = z_2 \sin(\theta)$. We can obtain the joint distribution of the two random variables a_2 and b_2 using the fact that the elementary probability of an event in a differential area is independent of the coordinate system. Therefore, I have

$$
\begin{aligned}
f_{a_2b_2}(a_2,b_2)da_2db_2 &= f_{z_2}(z_2)f_\theta(\theta)dz_2d\theta \\
f_{a_2b_2}(a_2,b_2)z_2dz_2d\theta &= \frac{2z_2}{r_d^2}\frac{1}{\pi}dz_2d\theta \\
f_{a_2b_2}(a_2,b_2) = \frac{2}{\pi r_d^2}, &\qquad \begin{cases} -r_d \le a_2 \le r_d \\ 0 \le b_2 \le r_d \\ 0 \le a_2^2 + b_2^2 \le r_d^2 \end{cases}
\end{aligned} \tag{A.5}
$$

The random distance w can be calculated as $w^2 = (a_2 - a_1)^2 + b_2^2$. Let $u = b_2$ and $\mathrm{v} = a_1$. Then I have $a_2 = \mathrm{v} \pm \sqrt{w^2 - u^2}$. The Jacobian can be written as

$$
J = \begin{vmatrix} \frac{\partial a_2}{\partial w} & \frac{\partial a_2}{\partial u} & \frac{\partial a_2}{\partial \mathrm{v}} \\ \frac{\partial b_2}{\partial w} & \frac{\partial b_2}{\partial u} & \frac{\partial b_2}{\partial \mathrm{v}} \\ \frac{\partial a_1}{\partial w} & \frac{\partial a_1}{\partial u} & \frac{\partial a_1}{\partial \mathrm{v}} \end{vmatrix} = \begin{vmatrix} \frac{w}{\sqrt{w^2-u^2}} & \frac{-u}{\sqrt{w^2-u^2}} & 1 \\ 0 & 1 & 0 \\ 0 & 0 & 1 \end{vmatrix} = \frac{w}{\sqrt{w^2-u^2}}. \tag{A.6}
$$

Then the joint *pdf* of w, u, and v is given by

$$
f_{wu\mathrm{v}}(w,u,\mathrm{v}) = \frac{4}{\pi r_d^4}\frac{w\mathrm{v}}{\sqrt{w^2-u^2}}, \qquad \begin{cases} 0 \le u \le r_d \\ 0 \le \mathrm{v} \le r_d \\ -r_d \le \left(\mathrm{v} \pm \sqrt{w^2-u^2}\right) \le r_d \\ 0 \le \left(\mathrm{v} \pm \sqrt{w^2-u^2}\right)^2 + u^2 \le r_d^2. \end{cases} \tag{A.7}
$$

Although, in general, obtaining the marginal *pdf* from the joint *pdf* is straightforward, it is very tedious in this particular case. Therefore, the deviation of the marginal *pdf* of w is not shown here. After the proper integration of the joint *pdf* and

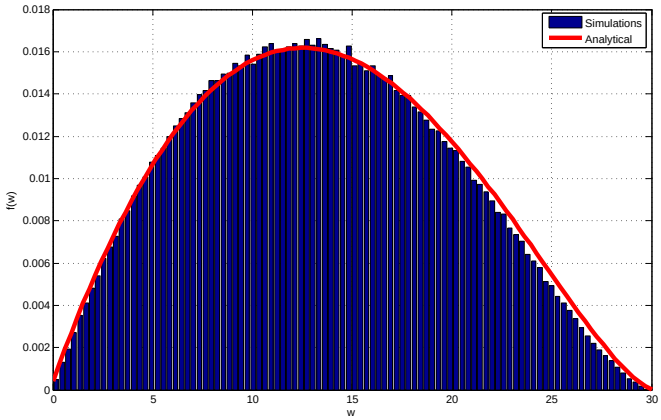

Figure A.2: The distribution of the random distance w.

several manipulation, the marginal *pdf* of w is given by

$$f_w(w) = \frac{2w}{r_d^2} - \frac{w^2\sqrt{(2r_d)^2 - w^2}}{\pi r_d^4} - \frac{4w}{\pi r_d^2}\sin^{-1}\left(\frac{w}{2r_d}\right), \qquad 0 \leq w \leq 2r_d. \tag{A.8}$$

Fig. A.2 shows that the analytical *pdf* obtained in (A.8) accurately matches the histogram obtained from simulations.

A.4 The distribution of the random distance l

In this section, I derive the distribution of the random distance (l) between the point x_L and any of its neighbors which coexist in the random area $A_r(z)$ (the diagonally shaded region in Fig. A.3(a)). For the sake of analytical tractability, I approximate the problem of finding the random distance l when the other points coexist in the area $A_r(z)$ by including the two areas B and C to $A_r(z)$. Hence, the problem reduces to finding the distribution of the random distance l between x_L and its neighbor which coexist in the random annulus sector $\widetilde{A}_r(z) = A_r(z) + B + C$ as shown in Fig. A.3(b). The same approximation was used in [44] to calculate the area of the random distance $A_r(z)$. Although this approximation was not explicitly sated in [44], the authors integrated the sector's angle over the inner and outer radii to calculate the area of $A_r(z)$. This means that they approximated the area of the random area $A_r(z)$ with the area of an annular sector as assumed in this paper. The validity of this assumptions is proved via simulations in Fig. A.4.

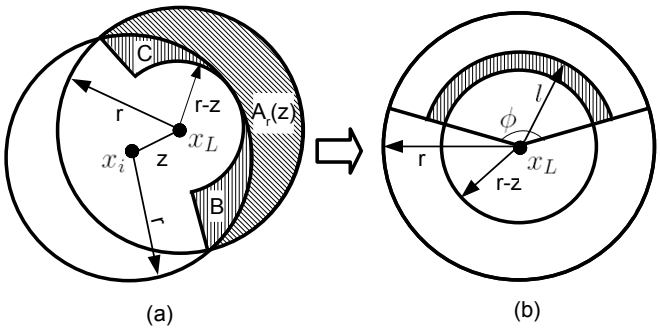

Figure A.3: Approximating the problem to obtain the *pdf* of the random distance l: (a) the problem before approximation, (b) the approximated problem.

Conditioning on z, the *cdf* of the random distance l can be written as

$$Pr\{x \leq l|z\} = \frac{\phi \int_{r-z}^{l} x dx}{\phi \int_{r-z}^{r} x dx} = \frac{l^2 - (r-z)^2}{r^2 - (r-z)^2} = \frac{l^2 - (r-z)^2}{z(2r-z)}. \tag{A.9}$$

Then differentiating with respect to l the conditional *pdf* if l is given as $f_{l|z}(l) = \frac{2l}{z(2r-z)}$.

Multiplying by the *pdf* of the random distance z, the joint *pdf* of l and z is given by

$$f_{l,z}(l,z) = \frac{2l}{z(2r-z)} \frac{2z}{r^2} = \frac{4l}{r^2(2r-z)}, \qquad 0 \leq z \leq r, (r-z) \leq l \leq r. \tag{A.10}$$

Finally, integrating over z I get the marginal *pdf* of the random distance l as

$$f_l(l) = \int_{r-z}^{r} \frac{4l}{r^2(2r-z)} = \frac{4l}{r^2} \ln\left(\frac{r+l}{r}\right), \qquad 0 < l < r. \tag{A.11}$$

Fig. A.4 shows that the analytical *pdf* obtained in (A.11) accurately matches the histogram obtained from simulations.

A.5 The distribution of the random distance v

In this appendix, I calculate the distribution of the random distance v. The random distance v is the distance is between a node in the vulnerability circle of the receiver R_{x_i} and the transmitter x_i. The transmitter x_i is always located at distance R form its receiver in a random direction. To derive the distribution of the random distance v, I will convert the coordinate system from the polar coordinates to the Cartesian coordinates. Let R_{x_i} always be my origin and x_i lie on the positive side of the x-axis. Then x_i will have the coordinates $(R, 0)$ while x_j will have the coordinates (x, y).

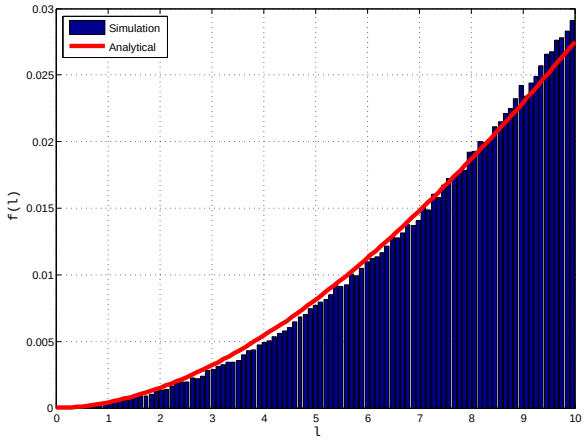

Figure A.4: The distribution of the random distance l.

Since the elementary probability of an event in a differential area is independent of the coordinate system, I have

$$
\begin{aligned}
f_{xy}(x,y)dxdy &= f_z(z)f_\theta(\theta)dzd\theta \\
f_{xy}(x,y)zdzd\theta &= \frac{2z}{r_{\text{vul}}^2}\frac{1}{\pi}dzd\theta \\
f_{xy}(x,y) &= \frac{2}{\pi r_{\text{vul}}^2}, \begin{cases} -r_{\text{vul}} \le x \le r_{\text{vul}} \\ 0 \le y \le r_{\text{vul}} \\ 0 \le x^2+y^2 \le r_{\text{vul}}^2. \end{cases}
\end{aligned} \tag{A.12}
$$

The random distance v can be calculated as $\mathrm{v}^2 = (x_2 - R)^2 + y_2^2$. Let $u = x_2$, then I have $y = \sqrt{\mathrm{v}^2 - (u-R)^2}$. The Jacobian can be written as

$$J = \begin{vmatrix} \frac{\partial y}{\partial \mathrm{v}} & \frac{\partial y}{\partial u} \\ \frac{\partial x}{\partial \mathrm{v}} & \frac{\partial x}{\partial u} \end{vmatrix} = \begin{vmatrix} \frac{\mathrm{v}}{\sqrt{\mathrm{v}^2-(u-R)^2}} & \frac{-u}{\sqrt{\mathrm{v}^2-(u-R)^2}} \\ 0 & 1 \end{vmatrix} = \frac{\mathrm{v}}{\sqrt{\mathrm{v}^2-(u-R)^2}}. \tag{A.13}$$

Then the joint *pdf* of v and u is given by

$$f_{\mathrm{v}u}(\mathrm{v},u) = \frac{2}{\pi r_{\mathrm{vul}}^2} \frac{\mathrm{v}}{\sqrt{\mathrm{v}^2-(u-R)^2}}, \qquad \begin{cases} -r_{\mathrm{vul}} \le u \le r_{\mathrm{vul}} \\ 0 \le \sqrt{\mathrm{v}^2-(u-R)^2} \le r_{\mathrm{vul}} \\ 0 \le \mathrm{v}^2 - (u-R)^2 + u^2 \le r_{\mathrm{vul}}^2. \end{cases} \tag{A.14}$$

The marginal *pdf* of v is given by

$$f_{\mathrm{v}}(\mathrm{v}) = \begin{cases} \int_{-\mathrm{v}+R}^{\mathrm{v}+R} \frac{2}{\pi r_{\mathrm{vul}}^2} \frac{\mathrm{v}}{\sqrt{\mathrm{v}^2-(u-R)^2}}, & 0 \le \mathrm{v} \le (r_{\mathrm{vul}} - R) \\ \int_{-\mathrm{v}+R}^{\frac{r^2+R^2-\mathrm{v}^2}{2R}} \frac{2}{\pi r_{\mathrm{vul}}^2} \frac{\mathrm{v}}{\sqrt{\mathrm{v}^2-(u-R)^2}}, & (r_{\mathrm{vul}} - R) < \mathrm{v} \le (r_{\mathrm{vul}} + R) \end{cases} \tag{A.15}$$

which can be expressed as

$$f_{\mathrm{v}}(\mathrm{v}) = \begin{cases} \frac{2\mathrm{v}}{r_{\mathrm{vul}}^2}, & 0 \le \mathrm{v} \le (r_{\mathrm{vul}} - R) \\ \frac{\mathrm{v}}{r_{\mathrm{vul}}^2} - \frac{2\mathrm{v}}{\pi r_{\mathrm{vul}}^2} \sin^{-1}\left(\frac{\mathrm{v}^2+R^2-r_{\mathrm{vul}}^2}{2\mathrm{v}R}\right), & (r_{\mathrm{vul}} - R) < \mathrm{v} \le (r_{\mathrm{vul}} + R). \end{cases} \tag{A.16}$$

Fig. A.5 shows that the analytical *pdf* obtained in (A.16) accurately matches the histogram obtained from simulations.

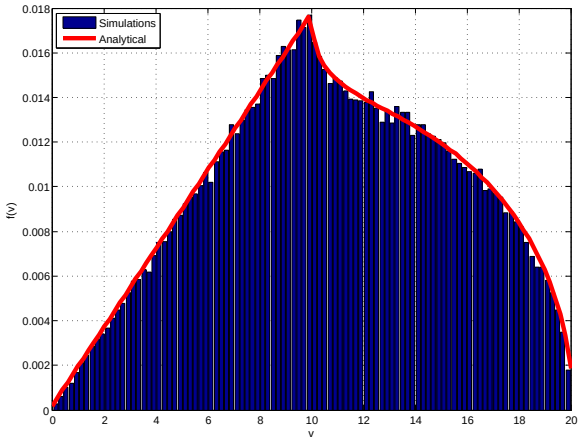

Figure A.5: The distribution of the random distance v.

Appendix B

B.1 Derivation of *pdf*s for the Random variables $R_{a/b}$ and $h_{a/b}$

The *cdf* of the distance $R_a = \min_i(\|a_i\|)$, $\forall a_i \in \mathbf{\Psi}$ can be easily derived from the PPP null probability as follows:

$$F_{R_a}(r) = \mathbb{P}\{R_a \leq r\} = 1 - e^{-\mathcal{A}\pi r^2}, \qquad r > 0. \tag{B.1}$$

Differentiating the *cdf* of R_a, the *pdf* of R_a is obtained as

$$f_{R_a}(r) = \frac{dF_{R_a}(r)}{dr} = 2\pi\mathcal{A}re^{-\mathcal{A}\pi r^2}, \qquad r > 0. \tag{B.2}$$

Similarly, the *pdf* of R_b is obtained as

$$f_{R_b}(r) = 2\pi\mathcal{B}re^{-\mathcal{B}\pi r^2}, \qquad r > 0. \tag{B.3}$$

Let $R_{a/b} = \left(\frac{R_a}{R_b}\right)^{\eta}$, then the *cdf* of $R_{a/b}$ can be written as

$$\begin{aligned} F_{R_{a/b}}(r) = \mathbb{P}\left\{R_{a/b} < r\right\} &= \mathbb{P}\left\{\left(\frac{R_a}{R_b}\right)^{\eta} < r\right\} \\ &= \int F_{R_a}(r^{\frac{1}{\eta}} R_b) f_{R_b}(R_b) dR_b \\ &= \int_0^{\infty} (1 - e^{-\pi \mathcal{A} r^{\frac{2}{\eta}} R_b^2}) 2\pi \mathcal{B} R_b e^{-\pi \mathcal{B} R_b^2} dR_b \\ &= 1 - \int_0^{\infty} 2\pi \mathcal{B} R_b e^{-\pi R_b^2 (r^{\frac{2}{\eta}} \mathcal{A} + \mathcal{B})} dR_b \\ &= 1 - \frac{\mathcal{B}}{r^{\frac{2}{\eta}} \mathcal{A} + \mathcal{B}}, \qquad 0 \leq r \leq \infty. \end{aligned} \tag{B.4}$$

Differentiating the *cdf* of $R_{a/b}$, the *pdf* of $R_{a/b}$ is obtained as

$$f_{R_{a/b}}(r) = \frac{2 r^{\frac{2}{\eta} - 1} \mathcal{A} \mathcal{B}}{\eta \left(r^{\frac{2}{\eta}} \mathcal{A} + \mathcal{B}\right)^2}, \qquad 0 \leq r \leq \infty. \tag{B.5}$$

Let $h_{a/b} = \frac{h_{a_i}}{h_{b_i}}$, then the *cdf* of $h_{a/b}$ is given by

$$\begin{aligned} F_{h_{a/b}}(h) = \mathbb{P}\left\{h_{a/b} < h\right\} &= \mathbb{P}\left\{\frac{h_a}{h_b} < h\right\} \\ &= \int F_{h_a}(h h_b) f_{h_b}(h_b) dh_b \\ &= \int_0^{\infty} (1 - e^{-h h_b \mu_a}) \mu_b e^{-h_b \mu_b} dh_b \\ &= 1 - \frac{\mu_b}{h \mu_a + \mu_b}, \qquad 0 \leq h \leq \infty. \end{aligned} \tag{B.6}$$

Differentiating the *cdf* of $h_{a/b}$, the *pdf* of $h_{a/b}$ is obtained as

$$f_{h_{a/b}}(h) = \frac{\mu_a \mu_b}{(h \mu_a + \mu_b)^2}, \qquad 0 \leq h \leq \infty. \tag{B.7}$$

B.2 Proof of Lemma 5.5.1

Conditioning on a Voronoi cell area V, the number of macro users N_{v} in that Voronoi cell is a Poisson random variable with the probability mass function (*pmf*) given by

$$\mathbb{P}\{N_{\mathrm{v}} = n\} = \frac{(\mathcal{U}_b V)^n e^{-\mathcal{U}_b V}}{n!}. \tag{B.8}$$

Note that in (B.8) I account only for macro users by considering $\mathcal{U}_b$. The Voronoi cell area V is a random variable that is accurately approximated by the gamma distribution $f_{\mathrm{v}}(v) \approx \frac{(\mathcal{B}c)^c v^{c-1} e^{-c\mathcal{B}v}}{\Gamma(c)}$, $0 \leq v < \infty$, where $c = 3.575$ is a constant defined for the Voronoi tessellation in the $\mathbb{R}^2$ [63, 117]. Therefore, the unconditional *pmf* of N_{v} is given by

$$\begin{aligned}
f_{N_{\mathrm{v}}}(n) &= \int_0^\infty \frac{(\mathcal{U}_b v)^n e^{-\mathcal{U}_b v}}{n!} f_V(v) da \\
f_{N_{\mathrm{v}}}(n) &= \frac{(\mathcal{U}_b)^n}{n!} \int_0^\infty v^n e^{-\mathcal{U}_b v} \frac{(\mathcal{B}c)^c v^{c-1} e^{-c\mathcal{B}v}}{\Gamma(c)} da \\
&= \frac{(\mathcal{U}_b)^n (\mathcal{B}c)^c}{(n)!\Gamma(c)} \int_0^\infty v^{n+c-1} e^{-v(c\mathcal{B}+\mathcal{U}_b)} dv \\
&\overset{\text{(i)}}{=} \frac{(\mathcal{U}_b)^n (\mathcal{B}c)^c}{(n)!\Gamma(c)} \frac{\Gamma(n+c)}{(c\mathcal{B}+\mathcal{U}_b)^{n+c}} \underbrace{\int_0^\infty \frac{(c\mathcal{B}+\mathcal{U}_b)^{n+c}}{\Gamma(n+c)} v^{n+c-1} e^{-v(c\mathcal{B}+\mathcal{U}_b)} dv}_{C} \\
&= \frac{\Gamma(n+c)}{\Gamma(n+1)\Gamma(c)} \frac{(\mathcal{U}_b)^n (\mathcal{B}c)^c}{(c\mathcal{B}+\mathcal{U}_b)^{n+c}}
\end{aligned}$$

where the integration $C = 1$ in (i) because it is an integration of a gamma *pdf* over its entire support domain. We will denote the *cdf* of N_{v} by $F_{N_{\mathrm{v}}}(k)$ and it is given by

$$F_{N_{\mathrm{v}}}(k) = \sum_{n=0}^{k} \frac{\Gamma(n+c)}{\Gamma(n+1)\Gamma(c)} \frac{(\mathcal{U}_b)^n (\mathcal{B}c)^c}{(c\mathcal{B}+\mathcal{U}_b)^{n+c}}, \quad 0 \leq k < \infty. \tag{B.9}$$

B.3 Proof of Lemma 5.5.2

Without loss in generality I will condition of having the test FAP at the origin, by Slivnyak's theorem, the results will hold for a generic FAP [8]. A macro BS $b_i \in \mathbf{\Psi}_b$ is inside the *macro* SSR of the test FAP located at the origin if and only if $\{P_b h_{b_i} \|b_i\|^{-\eta} > \upsilon_s\}$. Hence, the random variable $\mathcal{N}_b$ can be expressed as a sum of indicator functions as

$$\mathcal{N}_b = \sum_{b_i \in \mathbf{\Psi}_b} \mathbb{1}\{P_b h_{b_i} \|b_i\|^{-\eta} > \upsilon_s\}. \tag{B.10}$$

Since the distribution of a random variable is uniquely characterized by its moment generating function (*mgf*), I will derive the *mgf* of $\mathcal{N}_b$ to infer its distribution. The *mgf* of $\mathcal{N}_b$ can be expressed as

$$\begin{aligned}
\mathbb{E}\left[e^{t\mathcal{N}_b}\right] &= \mathbb{E}\left[e^{t\sum\limits_{b_i \in \mathbf{\Psi}_b} \mathbb{1}\{P_b h_{b_i} \|b_i\|^{-\eta} > \upsilon_s\}}\right] \\
&= \mathbb{E}_{\Psi_b}\left[\prod_{b_i \in \mathbf{\Psi}_b} \mathbb{E}_{h_{b_i}}\left[e^{t\mathbb{1}\{P_b h_{b_i} \|b_i\|^{-\eta} > \upsilon_s\}}\right]\right] \\
&\overset{\text{(iii)}}{=} \exp\left\{-\mathbb{E}_{h_b}\left[\int_0^{2\pi}\int_0^{\left(\frac{P_b h_b}{\upsilon_s}\right)^{\frac{1}{\eta}}} (1-e^t)\mathcal{B} r dr d\theta\right]\right\} \\
&= \exp\left\{-\int_0^{\infty} \mathcal{B}\pi\left(\frac{P_b h_b}{\upsilon_s}\right)^{\frac{2}{\eta}} (1-e^t)\mu_b e^{-\mu_b h_b} dh_b\right\} \\
&= \exp\left\{-(1-e^t)\pi\mathcal{B}\left(\frac{P_b}{\mu_b \upsilon_s}\right)^{\frac{2}{\eta}} \Gamma(1+\frac{2}{\eta})\right\}
\end{aligned} \tag{B.11}$$

where $\mathbb{E}_{\mathbf{\Psi}_b}[.]$ is the expectation w.r.t. the point process $\mathbf{\Psi}_b$ and $\mathbb{E}_{h_{b_i}}[.]$ is the expec-

tation w.r.t. the channel gain h_{b_i}. The equality (iii) is by the probability generating functional of the PPP and switching the order of the integration and the expectation [6, 12]. Differentiating (B.11) and equating with zero, the first moment of $\mathcal{N}_b$ is obtained as $\mathbb{E}[\mathcal{N}_b] = \pi\mathcal{B}\left(\frac{P_b}{\mu_b \upsilon_s}\right)^{\frac{2}{\eta}} \Gamma(1+\frac{2}{\eta})$. Hence, the moment generating function of $\mathcal{N}_b$ is in the form $\mathbb{E}\left[e^{t\mathcal{N}_b}\right] = \exp\left\{(e^t-1)\mathbb{E}[\mathcal{N}_b]\right\}$ which is the moment generating function of the Poisson distribution.

B.4 Proof of Lemma 5.5.3

Due to the sequential assignment of the channels, conditioning on the number of BSs in the *macro* SSR to be $\mathcal{N}_b$, the number of occupied channels is equal to the number of users in the most congested BS (i.e., the BS with the highest number of associated users). Since each BS $b_i \in \mathbf{\Psi}_b$ has N_{v_i} users[1], I have

$$\mathbb{P}\left\{K_u \leq k\right\} = \mathbb{P}\left\{\max_{i=1,2,\ldots,\mathcal{N}_b}(N_{\mathrm{v}_i}) \leq k\right\} = \left(F_{N_{\mathrm{v}}}(k)\right)^{\mathcal{N}_b}. \tag{B.12}$$

According to the theory of total probability, I have

$$\begin{aligned}\mathbb{P}\left\{K_u \leq k\right\} &= \sum_{j=0}^{\infty} \mathbb{P}\left\{\mathcal{N}_b = j\right\} \mathbb{P}\left\{\max_{i=1,2,\ldots,j}(N_{v_i}) \leq k\right\} \\ &= \sum_{j=0}^{\infty} \frac{(\varphi_b)^j e^{-\varphi_b}}{j!} \left(F_{N_{\mathrm{v}}}(k)\right)^j \\ &= e^{-\varphi_b(1-F_{N_{\mathrm{v}}}(k))}. \end{aligned} \tag{B.13}$$

[1]The random variables N_{v_i} are i.i.d. and follow the distribution of N_{v}.

B.5 Reduction of Lemma 5.6.1 for $\eta = 4$

For $\eta = 4$, I have

$$\begin{aligned}
\mathbb{E}_h\left[(Ph)^{\frac{2}{\eta}}\gamma\left(1-\frac{2}{\eta}, sPhr_s^{-\eta}\right)\right] &= \int_0^\infty (Ph)^{\frac{1}{2}}\gamma\left(1-\frac{1}{2}, sPhr_s^{-4}\right)\mu e^{-\mu h}dh \\
&= \int_0^\infty \mu(Ph)^{\frac{1}{2}}\int_0^{sPr_s^{-4}}(uh)^{-\frac{1}{2}}e^{-uh}hdue^{-\mu h}dh \\
&= \int_0^{sPr_s^{-4}}\frac{\sqrt{P}\mu(u)^{-\frac{1}{2}}}{(u+\mu)^2}du \\
&= \sqrt{P}\mu\left[\frac{r_s^{-2}\sqrt{Ps}}{\mu(\mu+sPr_s^{-4})}+\frac{1}{2\mu}\left(\frac{2}{\sqrt{\mu}}\arctan\left(\frac{\sqrt{Ps}r_s^{-2}}{\sqrt{\mu}}\right)\right)\right] \\
&= \frac{r_s^2P\sqrt{s}}{(\mu r_s^4+Ps)}+\frac{\sqrt{P}}{\sqrt{\mu}}\left(\frac{\pi}{2}-\arctan\left(\frac{r_s^2\sqrt{\mu}}{\sqrt{Ps}}\right)\right). \qquad \text{(B.14)}
\end{aligned}$$

Appendix C

C.1 Proof of Lemma 6.3.1

We will derive the distribution of the number of channels used within the SSR of a generic SBS by induction. Conditioning on having 2 MBSs in the SSR of the FAP $s \in \Psi_a$, the probability that there are k channels used in the SSR is given by:

$$\mathbb{P}\left\{K_u = k \mid |\mathbf{S}_{b_1}| = t, t \leq k, |\mathbf{N}_a| = 2\right\} = \sum_{p=k-t}^{k} \mathbb{P}\left\{|\mathbf{S}_{b_2}| = p\right\} \binom{p}{p-(k-t)} \left(\frac{t}{|\mathbf{S}|}\right)^{p-(k-t)} \left(1 - \frac{t}{|\mathbf{S}|}\right)^{(k-t)}.$$

Unconditioned on the number of channels used within the MBS b_1, I have

$$\mathbb{P}\left\{K_u = k \mid |\mathbf{N}_a| = 2\right\} = \sum_{t=0}^{k} \mathbb{P}\left\{|\mathbf{S}_{b_1}| = t\right\} \sum_{p=k-t}^{k} \mathbb{P}\left\{|\mathbf{S}_{b_2}| = p\right\} \binom{p}{p-(k-t)} \left(\frac{t}{|\mathbf{S}|}\right)^{p-(k-t)} \left(1 - \frac{t}{|\mathbf{S}|}\right)^{(k-t)} = \mathcal{P}_2(k).$$

Similarly, conditioning that there are 3 MBSs within the SSR of the test SBS, the probability that there are k channels used in the SSR is given by:

$$\mathbb{P}\left\{K_u = k \mid |\mathbf{S}_{b_1} \cup \mathbf{S}_{b_2}| = t, t \leq k, |\mathbf{N}_a| = 3\right\} = \sum_{p=k-t}^{k} \mathbb{P}\left\{|\mathbf{S}_{b_3}| = p\right\} \binom{p}{p-(k-t)} \left(\frac{t}{|\mathbf{S}|}\right)^{p-(k-t)} \left(1 - \frac{t}{|\mathbf{S}|}\right)^{(k-t)}.$$

Unconditioned on the number of channels used within the MBSs b_1 and b_2, I have

$$\mathbb{P}\left\{K_u = k | \, |\mathbf{N}_a| = 3\right\} = \sum_{t=0}^{k} \mathcal{P}_2(t) \sum_{p=k-t}^{k} \mathbb{P}\left\{|\mathbf{S}_{b_3}| = p\right\} \binom{p}{p-(k-t)} \left(\frac{t}{|\mathbf{S}|}\right)^{p-(k-t)} \left(1 - \frac{t}{|\mathbf{S}|}\right)^{(k-t)} = \mathcal{P}_3(k).$$

By induction and deconditioning on $|\mathbf{N}_a|$, **Lemma 6.3.1** can be obtained.

Appendix D

D.1 Proof of Lemma 7.3.1

For a generic UE u, let $r_o = \min_{b_i \in \mathbf{\Psi}} \|u - b_i\|$. The uplink distance r_o has the Rayleigh distribution $f_{r_o}(r) = 2\pi\lambda r e^{-\pi\lambda r^2}$, $0 \leq r \leq \infty$ [8,12]. The transmit power for a generic UE is given by $P = \rho_o r_o^{\eta}$ such that $0 \leq P \leq P_u$. Therefore, the *pdf* of P is given by

$$\begin{aligned} f_P(x) &= \frac{2\pi\lambda x^{\frac{2}{\eta}-1} e^{-\pi\lambda\left(\frac{x}{\rho_o}\right)^{\frac{2}{\eta}}}}{\eta\rho_o^{\frac{2}{\eta}} \int_0^{P_u} \frac{2\pi\lambda}{\eta\rho_o^{\frac{2}{\eta}}} y^{\frac{2}{\eta}-1} e^{-\pi\lambda\left(\frac{y}{\rho_o}\right)^{\frac{2}{\eta}}} dy} \\ &= \frac{2\pi\lambda x^{\frac{2}{\eta}-1} e^{-\pi\lambda\left(\frac{x}{\rho_o}\right)^{\frac{2}{\eta}}}}{\eta\rho_o^{\frac{2}{\eta}} \left(1 - e^{-\pi\lambda\left(\frac{P_u}{\rho_o}\right)^{\frac{2}{\eta}}}\right)}, 0 \leq x \leq P_u. \end{aligned}$$

Note that the *pdf* of P is normalized due to the truncated channel inversion power control. The α^{th} moment of P is given by $\int_0^{P_u} x^{\alpha} f_P(x) dx$ and the lemma is obtained.

D.2 Proof of Theorem 7.3.1

For the interference experienced by a cellular uplink, I find the Laplace Transform (LT) of the aggregate interference at a tagged BS located at the origin. Note that orthogonal channel assignment per BS brings correlations among the locations of the

interfering UEs as well as with the location of the tagged BS, which highly complicates the analysis. The derivation here is based on the three facts and a key assumption listed below:

- **Fact** #1: the average useful signal received at any BS is equal to the cutoff threshold ρ_o.
- **Fact** #2: the average interference received from any single interfering UE is strictly less than ρ_o.
- **Fact** #3: at any time instant each BS will have a single user served per channel, and hence, the intensity of interfering UEs on each channel is λ.
- **Key assumption**: the interfering UEs constitute a PPP.

Note that **Fact** #1 and **Fact** #2 are a direct consequence of the association policy and power control, while **Fact** #3 is because each BS assigns a unique channel for each of its associated users. Hence, the aggregate interference received at the tagged BS can be written as

$$\mathcal{I} = \sum_{u_i \in \tilde{\mathbf{\Phi}} \setminus \{o\}} \mathbb{1}\left(P_i \left\|u_i\right\|^{-\eta} < \rho_o\right) P_i h_i \left\|u_i\right\|^{-\eta} \tag{D.1}$$

where $\tilde{\mathbf{\Psi}}$ is a PPP with intensity λ representing the interfering UEs, and $\mathbb{1}(.)$ is the indicator function which takes the value 1 if the statement (.) is true and zero otherwise. Note that the indicator function in (D.1) captures the correlation between the interfering UEs and the tagged BS. The LT of the aggregate interference from the

interfering UEs received at the tagged BS is obtained as

$$\begin{aligned}
\mathcal{L}_{\mathcal{I}}(s) &= \mathbb{E}\left[e^{-s\mathcal{I}}\right] \\
&= \mathbb{E}\left[e^{-s\sum\limits_{u_i\in\tilde{\mathbf{\Phi}}\setminus\{o\}}\mathbb{1}\left(P_i\|u_i\|^{-\eta}<\rho_o\right)P_ih_i\|u_i\|^{-\eta}}\right] \\
&\overset{(i)}{=} \mathbb{E}_{\tilde{\mathbf{\Phi}}}\left[\prod_{u_i\in\tilde{\mathbf{\Phi}}\setminus\{o\}}\mathbb{E}_{P_i,h_i}\left[e^{-s\mathbb{1}\left(\|u_i\|>\left(\frac{P_i}{\rho_o}\right)^{\frac{1}{\eta}}\right)P_ih_i\|u_i\|^{-\eta}}\right]\right] \\
&\overset{(ii)}{=} \exp\left(-2\pi\lambda\int_{\left(\frac{P}{\rho_o}\right)^{\frac{1}{\eta}}}^{\infty}\mathbb{E}_{P,h}\left[\left(1-e^{-sPhx^{-\eta}}\right)\right]xdx\right) \\
&\overset{(iii)}{=} \exp\left(-2\pi\lambda\int_{\left(\frac{P}{\rho_o}\right)^{\frac{1}{\eta}}}^{\infty}\mathbb{E}_{P}\left[\left(1-\frac{1}{1+sPx^{-\eta}}\right)\right]xdx\right) \\
&= \exp\left(-2\pi\lambda\int_{\left(\frac{P}{\rho_o}\right)^{\frac{1}{\eta}}}^{\infty}\mathbb{E}_{P}\left[\frac{sPx}{x^{\eta}+sP}\right]dx\right) \\
&\overset{(iv)}{=} \exp\left(-2\pi\lambda s^{\frac{2}{\eta}}\mathbb{E}_P\left[P^{\frac{2}{\eta}}\right]\int_{(s\rho_o)^{\frac{-1}{\eta}}}^{\infty}\frac{y}{y^{\eta}+1}dy\right)
\end{aligned} \tag{D.2}$$

where $\mathbb{E}_x[.]$ is the expectation with respect to the random variable x, (i) follows from independence between $\tilde{\mathbf{\Phi}}$, P, and h, (ii) follows for the probability generation functional of the PPP [8], (iii) follows from the LT of h, and (iv) follows by changing the variables $y = \frac{x}{(SP)^{\frac{1}{\eta}}}$. The theorem is obtained be substituting (D.2) in (2.5) for $s = \frac{\beta}{\rho_o}$ and substituting the value of $\mathbb{E}[P^{\frac{2}{\eta}}]$ from **Lemma 4.5.1**.

D.3 Proof of Theorem 7.3.2

Since the SINR is a strictly positive random variable, the average spectral efficiency can be obtained as

$$\begin{aligned}
\mathcal{R} &= \mathbb{E}[\ln(1+\mathrm{SINR})] \\
&= \int_0^\infty \mathbb{P}\left\{\ln(1+\mathrm{SINR}) > t\right\} dt \\
&= \int_0^\infty \mathbb{P}\left\{\mathrm{SINR} > \left(e^t-1\right)\right\} dt \\
&\overset{(v)}{=} \int_0^\infty e^{-\frac{\left(e^t-1\right)\sigma^2}{\rho_o}} \mathcal{L}_{\mathcal{I}}\left(\frac{(e^t-1)}{\rho_o}\right) dt \\
&\overset{(vi)}{=} \int_0^\infty \frac{1}{x+1} e^{-\frac{x\sigma^2}{\rho_o}} \mathcal{L}_{\mathcal{I}}\left(\frac{x}{\rho_0}\right) dx
\end{aligned} \tag{D.3}$$

where (v) follows from (7.4), and (vi) is obtained by changing the variables $x = (e^t - 1)$. The theorem is obtained by substituting the value of $\mathcal{L}_{\mathcal{I}}(s)$ from (D.2) in (D.3) for $s = \frac{x}{\rho_o}$ and substituting the value of $\mathbb{E}[P^{\frac{2}{\eta}}]$ from **Lemma 4.5.1**.

D.4 Proof of Theorem 7.4.1

For the interference experienced by a cellular uplink from UEs in tier j, I find the LT of the aggregate interference at a tagged BS located at the origin. Similar to **Appendix D.2**, this proof is based on the 3 facts and a key assumption listed below:

- **Fact** #1: the average useful signal received at any BS in the j^{th} tier is equal to the cutoff threshold $\rho_o^{(j)}$.
- **Fact** #2: the average interference received from any single interfering UE in the k^{th} tier is strictly less than $\rho_o^{(k)}$.
- **Fact** #3: at any time instant each BS in tier k will have a single user served per channel, and hence, the intensity of interfering UEs from the k^{th} tier on each channel is λ_k.

- **Key assumption**: the interfering UEs from the k^{th} tier constitute a PPP with intensity λ_k.

Hence, the aggregate interference from UEs in tier k received at the tagged BS can be written as

$$\mathcal{I}_k = \sum_{u_i \in \tilde{\mathbf{\Phi}}_k \setminus \{o\}} \mathbb{1}\left(P_{ki} \left\|u_i\right\|^{-\eta} < \rho_o^{(k)}\right) P_{ki} h_i \left\|u_i\right\|^{-\eta} \tag{D.4}$$

where $\tilde{\mathbf{\Psi}}_k$ is a PPP with intensity λ_k representing the interfering UEs. Note that the indicator function in (D.4) captures the correlation among the locations of the interfering UEs and the location of the tagged BS. The LT of the aggregate interference from UEs in tier k received at the tagged BS in tier j is obtained as

$$\begin{aligned}
\mathcal{L}_{\mathcal{I}_k}(s) &= \mathbb{E}\left[e^{-s \sum\limits_{u_i \in \tilde{\mathbf{\Phi}}_k \setminus \{o\}} \mathbb{1}\left(P_{ki}\|u_i\|^{-\eta} < \rho_o^{(k)}\right) P_{ki} h_i \|u_i\|^{-\eta}}\right] \\
&= \exp\left(-2\pi_k \lambda_k \int_{\left(\frac{P_k}{\rho_o^{(k)}}\right)^{\frac{1}{\eta}}}^{\infty} \mathbb{E}_{P_k,h}\left[\left(1 - e^{-sP_k h x^{-\eta}}\right)\right] x dx\right) \\
&= \exp\left(-2\pi_k \lambda_k \int_{\left(\frac{P_k}{\rho_o^{(k)}}\right)^{\frac{1}{\eta}}}^{\infty} \mathbb{E}_{P_k}\left[\frac{sP_k x}{x^\eta + sP_k}\right] dx\right) \\
&= \exp\left(-2\pi_k \lambda_k s^{\frac{2}{\eta}} \mathbb{E}_{P_k}\left[P_k^{\frac{2}{\eta}}\right] \int_{(s\rho_o^{(k)})^{\frac{-1}{\eta}}}^{\infty} \frac{y}{y^\eta + 1} dy\right).
\end{aligned} \tag{D.5}$$

The theorem is obtained by substituting (D.5) in (7.5) for $s = \frac{\beta}{\rho_o^{(j)}}$ and substituting the value of $\mathbb{E}[P_k^{\frac{2}{\eta}}]$ from **Lemma 4.5.2**.

D.5 Proof of Lemma 7.4.2

Let $r_k = \min\limits_{b_i \in \mathbf{\Psi}_k} (\|u - b_i\|)$ be the distance from a UE to its nearest BSs from each of the coexisting tiers. Then, $f_{r_k}(r) = 2\pi\lambda_k r e^{-\pi\lambda_k r^2}$, $0 \leq r \leq \infty$. Since a UE connects

to the BS with the best link quality, then given that a generic UE u is connected to a generic BS from the j^{th} tier, I have $r_j^{\eta_j} \leq r_k^{\eta_k}\ \forall k,\ k \neq j$. Using this fact, I can write $r_j^{\eta_j} = \min_k(r_k^{\eta_k})$, and hence, the transmit power of a generic UE connected to a generic BS in the j^{th} tier is given by $P_j = \rho_o^{(j)} \min_k(r_k^{\eta_k})$ such that $0 \leq P_j \leq P_u$. Hence, the *cdf* of the transmit power can be written as

$$F_{P_j}(x) = \frac{1 - e^{-\sum_{k=1}^{K} \pi \lambda_k \left(\frac{x}{\rho_o^{(j)}}\right)^{\frac{2}{\eta_k}}}}{1 - e^{-\sum_{b=1}^{K} \pi \lambda_b \left(\frac{P_u}{\rho_o^{(j)}}\right)^{\frac{2}{\eta_b}}}} \tag{D.6}$$

and the *pdf* of the transmit power is given by

$$f_{P_j}(x) = \frac{\sum_{k=1}^{K} \frac{2\pi\lambda_k x^{\frac{2}{\eta_k}-1}}{\eta_k (\rho_o^{(j)})^{\frac{2}{\eta_k}}}}{1 - e^{-\sum_{b=1}^{K} \pi \lambda_b \left(\frac{P_u}{\rho_o^{(j)}}\right)^{\frac{2}{\eta_b}}}} e^{-\sum_{a=1}^{K} \pi \lambda_a \left(\frac{x}{\rho_o^{(j)}}\right)^{\frac{2}{\eta_a}}}. \tag{D.7}$$

The α^{th} moment of P_k cannot be obtained in closed from except for a common path-loss exponent η.

D.6 Proof of Theorem 7.4.3

This proof is based on the 3 facts and key assumption listed in **Appendix D.4**. The aggregate interference from UEs in tier k received at the tagged BS from tier j can be written as

$$\mathcal{I}_k = \sum_{u_i \in \tilde{\mathbf{\Phi}}_k \setminus \{o\}} \mathbb{1}\left(P_{ki} \left\|u_i\right\|^{-\eta_j} < \rho_o^{(k)}\right) P_{ki} h_i \left\|u_i\right\|^{-\eta_j}. \tag{D.8}$$

Note that, although the path-loss exponents are different, as long as the UEs associate based on the link quality, (D.8) will hold ture. Similar to **Appendix D.4**, after some

mathematical manipulations, the theorem can be proved.